

# **The development of gene therapy for Niemann-Pick Type C disease**

*Michael Hughes*

**Thesis submitted for the degree of Doctor of Philosophy  
University College London**

Department of Pharmacology  
UCL School of Pharmacy  
29-39 Brunswick Square  
London  
WC1N 1AX

February 25, 2017

I, Michael Hughes confirm that the work presented in this thesis is my own. Where information has been derived from other sources, I confirm that this has been indicated in the thesis.

---

# Abstract

Niemann-Pick Type C (NP-C) is a lysosomal storage disorder with neurological and visceral pathology, for which there is currently no major disease modifying treatment. Loss of NPC1 function, a late endosomal transmembrane protein, leads to systemic intracellular lipid accumulation. The subsequent premature death is usually associated with neurological manifestations, such as neurodegeneration and neuroinflammation. This project focuses on the development and preclinical evaluation of gene therapy for NP-C in a mouse model using an adeno-associated viral (AAV) vector. The vector would be capable of delivering and expressing human *NPCI* in the mouse brain and providing therapeutic benefit.

AAV vectors exhibit efficient and widespread gene delivery throughout the brain, however their limited packaging capacity can be a constraint for larger genes. In this project extensive construct modifications were carried out to incorporate the relatively large *NPCI* cDNA into a functional AAV serotype 9 vector, where *NPCI* is controlled by a constitutively active neuronal promoter. Initial *in vivo* testing demonstrated successful NPC1 over-expression in administered mouse brains, compared to endogenous NPC1 levels in unadministered controls. No indications of toxicity were observed as a result of exogenous NPC1 overexpression *in vivo*. A series of preclinical proof of concept survival studies were subsequently carried out on the *Npc1*<sup>-/-</sup> model, where newborn *Npc1*<sup>-/-</sup> mice were administered with  $4.6 \times 10^9$  vector genomes of AAV9-NPC1 via intracerebroventricular injections. Treated *Npc1*<sup>-/-</sup> mice exhibited an increased lifespan (median survival - 116.5 days) compared to untreated *Npc1*<sup>-/-</sup> mice (median survival - 75.5 days). Low dose treated mice exhibited permanent normalisation of locomotor function and significant neuronal rescue in all brain regions analysed. A subsequent study with a 65-fold dose increase resulted in an additional significant extension of lifespan, along with improved weight maintenance. Combined, these results demonstrate the potential

beneficial use of gene therapy for NP-C and support the further development of this approach.

# Acknowledgements

I would like to thank Dr. Ahad Rahim for giving me the opportunity to do my PhD in his group, as well as his guidance and support throughout the last few years. My thanks also go out to everyone in the Rahim lab, particularly Giulia and Sam for all their invaluable help. I also thank Dr. Simon Waddington for his advice and valuable input, along with everyone from the Waddington lab. I would also like to thank everyone from Prof. Fran Platt's group in Oxford, who helped me throughout this project. A special shout-out needs to go to Dave Smith for his endurance, persistence and expertise with the animal work. I also thank Nuria Martin and Julie Tordo for their help with teaching me how to work with AAV.

I would really like to thank all my colleagues from the 6<sup>th</sup> floor who have made my time at the UCL School of Pharmacy so enjoyable and unforgettable.

I would also importantly like to thank the Niemann-Pick family and charity associations, especially 'Asociación Neimann Pick de Fuenlabrada' and 'NPUK'. Although small, they work incredibly hard to give support to patients and facilitate research, including this project.

Finally, my love goes out to my parents for their support and encouragement, as well as giving me the opportunities to get where I am today.

# Publications

Hughes, M. P., Smith, D. A., Morris, L., Colaco, A., Huebecker, M., Tordo, J., Palomar, N., Henckaerts, E., Waddington, S. N., Platt, F. M. & Rahim A. A. 2017. Low dose gene therapy improves lifespan, locomotor function and pathology in a mouse of Niemann-Pick Type C disease. *Mol Ther.* (Submitted and under review)

Rocha-Ferreira, E., Rudge, B., Hughes, M. P., Rahim, A. A., Hristova, M. & Robertson, N. J. 2016. Immediate Remote Ischemic Postconditioning Reduces Brain Nitrotyrosine Formation in a Piglet Asphyxia Model. *Oxid Med Cell Longev* 2016, 5763743.

Karda, R., Buckley, S. M., Mattar, C. N., Ng, J., Massaro, G., Hughes, M. P., Kurian, M. A., Baruteau, J., Gissen, P., Chan, J. K., Bacchelli, C., Waddington, S. N. & Rahim, A. A. 2014. Perinatal systemic gene delivery using adeno-associated viral vectors. *Front Mol Neurosci* 7, 89.

# Table of Contents

<b>Abstract</b>	<b>3</b>
<b>Acknowledgements</b>	<b>5</b>
<b>Publications</b>	<b>6</b>
<b>List of Figures</b>	<b>12</b>
<b>List of Tables</b>	<b>16</b>
<b>Abbreviations</b>	<b>17</b>
<b>1 Introduction</b>	<b>20</b>
1.1 Lysosomal Storage Disorders	21
1.2 Niemann-Pick Diseases	29
1.3 Niemann-Pick Type C Disease	30
1.3.1 NP-C Epidemiology	31
1.3.2 NP-C Proteins	31
1.3.3 NP-C Lipid storage	34
1.3.4 NP-C Pathology	37
1.3.5 Clinical Presentation of NP-C	40
1.3.6 NP-C Diagnosis	44
1.3.7 Therapeutic Options for NP-C	46
1.3.8 NP-C Animal Models	49
1.4 Gene Therapy	50

1.5 Viral Vectors	51
1.5.1 Adenoviral vectors	52
1.5.2 Lentiviral and retroviral vectors	54
1.5.3 Adeno-associated viral vectors	56
1.6 Non-viral gene delivery systems	62
1.7 Gene therapy for lysosomal storage disorders	63
1.7.1 Gene delivery to the CNS	69
1.8 Gene therapy for Niemann-Pick Type C disease	73
1.9 Aims: Rationale and Significance	75
<b>2 Materials and Methods</b>	<b>77</b>
2.1 AAV vector construct design	77
2.2 Cloning	78
2.2.1 Bacterial transformation	78
2.2.2 Plasmid amplification and purification	78
2.2.3 Polymerase Chain Reaction	81
2.2.4 Restriction enzyme digest	82
2.2.5 DNA electrophoresis	82
2.2.6 DNA extraction	83
2.2.7 Ligation	83
2.2.8 DNA sequencing	84
2.3 Tissue Culture	84
2.3.1 Culture of cell lines	84
2.3.2 Cell culture passaging	84
2.3.3 Transfection	85
2.3.4 <i>In vitro</i> protein expression analysis	85
2.4 Virus Production	87
2.4.1 Lentiviral vector preparation	87
2.4.2 Lentiviral vector titration	88

2.4.3	AAV vector preparation	88
2.4.4	AAV vector titration	91
2.5	<i>In vivo</i> experiments	93
2.5.1	Animals	93
2.5.2	Vector administration	93
2.5.3	Drug administration	94
2.5.4	Behavioural analysis – Rearing	94
2.5.5	Behavioural analysis – Tremor	95
2.5.6	Behavioural analysis – Gait	95
2.5.7	Tissue harvest	95
2.6	Expression Analysis	96
2.6.1	Double gelatine coating of slides	96
2.6.2	Immunohistochemistry	96
2.6.3	Quantitative analysis of immunohistochemical staining	99
2.6.4	Immunofluorescence and scanning confocal microscopy	99
2.6.5	Brain section histology	100
2.6.6	Stereology	101
2.6.7	Western blotting of tissue protein extract	102
2.7	Biochemical glycosphingolipid analysis	102
2.8	Statistical Analysis	103
<b>3</b>	<b>Development of a functional and efficient hNPC1 viral vector</b>	<b>104</b>
3.1	Introduction	104
3.2	Chapter Aims	105
3.3	Vector Study	105
3.4	Incorporating hNPC1 into an rAAV construct	111
3.5	Introduction of SV40pA signal sequence	115
3.6	Synthesis of eGFP reporter construct	117
3.7	<i>In vitro</i> testing confirms functional hNPC1 and eGFP constructs	119

3.8 No elevation in NPC1 following codon optimisation of hNPC1 cDNA _____	121
3.9 Successful production of oversized AAV2/9-hNPC1 viral vector _____	122
3.10 AAV2/9-eGFP viral vector production _____	124
3.11 Overexpression of NPC1 following low dose AAV9-hNPC1 administration ____	125
3.12 Dose dependent increase of eGFP expression following AAV9-eGFP administration _____	128
3.13 Neuronal tropism of AAV9-hNPC1 vector _____	130
3.14 No toxicity associated to supraphysiological levels of NPC1 following AAV9- hNPC1 administration _____	135
3.15 Summary _____	137
<b>4 Preclinical low dose AAV9-hNPC1 study in the <i>Npc1</i><sup>-/-</sup> mouse model ____</b>	<b>138</b>
4.1 Introduction _____	138
4.2 Chapter aims _____	139
4.3 Extension of lifespan in <i>Npc1</i> <sup>-/-</sup> mice following low dose AAV9-hNPC1 treatment	140
4.4 Improved weight gain in <i>Npc1</i> <sup>-/-</sup> mice treated with low dose AAV9-hNPC1 _____	141
4.5 Normalisation of neurological, locomotor and coordination symptoms in <i>Npc1</i> <sup>-/-</sup> mice following low dose AAV9-hNPC1 treatment _____	144
4.6 Summary _____	150
<b>5 Analysis of neurodegeneration and neuropathology following low dose AAV9-hNPC1 treatment _____</b>	<b>151</b>
5.1 Introduction _____	151
5.2 Chapter Aims _____	151
5.3 Low dose AAV9-hNPC1 treatment ameliorates neurodegeneration in <i>Npc1</i> <sup>-/-</sup> mice	152
5.4 Limited amelioration of inflammatory response in <i>Npc1</i> <sup>-/-</sup> mice following low dose AAV9-hNPC1 administration _____	158

5.5 Gene therapy ameliorates increase of lysosomal staining in <i>Npc1</i> <sup>-/-</sup> mice	162
5.6 Low dose gene therapy results in redistribution of lipids in <i>Npc1</i> <sup>-/-</sup> mice	164
5.7 Summary	167
<b>6 Ongoing high dose AAV9-hNPC1 study</b>	<b>169</b>
6.1 High dose AAV9-hNPC1 survival study	169
6.2 No toxicity associated with high dose AAV9-hNPC1 administration	170
6.3 Enhanced survival and weight of <i>Npc1</i> <sup>-/-</sup> mice following high dose AAV9-hNPC1 treatment	172
6.4 Early indications of locomotor normalisation following administration of high dose AAV9-hNPC1	174
6.5 Completion of high dose ICV AAV9-hNPC1 study	176
<b>7 Discussion</b>	<b>178</b>
7.1 Overview	178
7.2 AAV construct for optimised expression of larger transgenes	180
7.3 Suitability of AAV9-hNPC1 for NP-C disease	183
7.4 Therapeutic efficacy of AAV9-hNPC1	186
7.5 Limitations	192
7.6 AAV9-hNPC1 and competing NP-C therapies	195
7.7 Future Work	201
7.8 Conclusion	203
<b>8 Supplementary Data</b>	<b>205</b>
<b>References</b>	<b>210</b>

# List of Figures

- Figure 1:** Mechanisms of neuropathology in lysosomal storage disorders. \_\_\_\_\_ 25
- Figure 2:** NPC1 structure and proposed pathway of cholesterol binding \_\_\_\_\_ 33
- Figure 3:** Sphingolipid structure and degradation pathway in the late endosomes/lysosomes of cells. \_\_\_\_\_ 36
- Figure 4:** Presentations of Niemann-Pick Type C disease \_\_\_\_\_ 42
- Figure 5:** Illustrations of the HIV-1 viral genome and recombinant lentiviral vector genome. \_\_\_\_\_ 55
- Figure 6:** Illustrations of wild-type AAV genome and rAAV vector genome. \_\_\_\_ 60
- Figure 7:** Representative diagram of triple transfection in HEK293T cells, resulting in AAV2/9 vector production. \_\_\_\_\_ 89
- Figure 8:** Image of completed iodixanol gradient in ultracentrifuge tube prior to centrifugation. \_\_\_\_\_ 90
- Figure 9:** Illustration of injection sites (red arrows) used for P0/1 neonatal bilateral ICV administration. \_\_\_\_\_ 94
- Figure 10:** Example of cells identified as neurons for neuronal quantification \_\_\_\_ 102
- Figure 11:** Vector study comparing eGFP expression in mouse brains following P0 bilateral intracerebroventricular administration of gene delivery vectors. \_\_\_\_\_ 107

<b>Figure 12:</b> Lentiviral vector transduction of neuroblasts in the rostral migratory stream. _____	110
<b>Figure 13:</b> Summary of <i>hNPC1</i> cDNA integration into a rAAV construct to produce <i>pAAV.hSynI.hNPC1.hGHpA</i> . _____	114
<b>Figure 14:</b> Summary of SV40pA signal sequence integration to produce <i>pAAV.hSynI.hNPC1.SV40pA</i> . _____	116
<b>Figure 15:</b> Summary of <i>hNPC1</i> replacement with <i>eGFP</i> reporter gene to produce <i>pAAV.hSynI.eGFP.SV40pA</i> . _____	118
<b>Figure 16:</b> <i>In vitro</i> <i>hNPC1</i> and <i>eGFP</i> expression. _____	120
<b>Figure 17:</b> <i>In vitro</i> testing of codon optimised <i>hNPC1O</i> cDNA in HEK-293T cells. _____	122
<b>Figure 18:</b> AAV2/9-SynI- <i>hNPC1</i> -SV40pA titration and vector genome analysis.	123
<b>Figure 19:</b> AAV2/9-SynI- <i>eGFP</i> -SV40pA titration _____	125
<b>Figure 20:</b> <i>hNPC1</i> expression to supraphysiological levels in various brain regions following low dose AAV9- <i>hNPC1</i> administration to neonatal wild-type mice. __	127
<b>Figure 21:</b> Widespread <i>eGFP</i> expression following low and high dose AAV9- <i>eGFP</i> administration to neonatal wild-type mice. _____	129
<b>Figure 22:</b> Neuronal overexpression of <i>hNPC1</i> protein following AAV9- <i>hNPC1</i> administration. _____	131
<b>Figure 23:</b> Glial cells do not exhibit overexpression of <i>hNPC1</i> protein following AAV9- <i>hNPC1</i> administration. _____	133
<b>Figure 24:</b> Lysosomal localisation of <i>hNPC1</i> protein following AAV9- <i>hNPC1</i> administration. _____	134

- Figure 25:** No astrocyte- or microglia-mediated immune response, as a result of hNPC1 overexpression in wild-type mice. \_\_\_\_\_ 136
- Figure 26:** Efficacy of low dose gene therapy and competing therapies on the lifespan of *Npc1*<sup>-/-</sup> mice. \_\_\_\_\_ 141
- Figure 27:** Improvement in weight loss in *Npc1*<sup>-/-</sup> mice following low dose AAV9-hNPC1 treatment. \_\_\_\_\_ 143
- Figure 28:** Permanent normalisation of rearing count in *Npc1*<sup>-/-</sup> mice following low dose AAV9-hNPC1 treatment. \_\_\_\_\_ 145
- Figure 29:** Permanent normalisation of high frequency tremor in *Npc1*<sup>-/-</sup> mice following low dose AAV9-hNPC1 treatment. \_\_\_\_\_ 147
- Figure 30:** Permanent normalisation or significant improvement in the gait of *Npc1*<sup>-/-</sup> mice following low dose AAV9-hNPC1 administration. \_\_\_\_\_ 149
- Figure 31:** Amelioration of neurodegeneration in AAV9-hNPC1 treated *Npc1*<sup>-/-</sup> mice. \_\_\_\_\_ 154
- Figure 32:** Amelioration of Purkinje cells loss in the cerebellum of *Npc1*<sup>-/-</sup> mice following low dose AAV9-hNPC1 treatment. \_\_\_\_\_ 156
- Figure 33:** Limited amelioration of microglial activation in end-stage *Npc1*<sup>-/-</sup> mice following low dose AAV9-hNPC1 treatment. \_\_\_\_\_ 159
- Figure 34:** Limited amelioration of astrogliosis in end-stage *Npc1*<sup>-/-</sup> treated with low dose AAV9-hNPC1. \_\_\_\_\_ 161
- Figure 35:** Regional reduction of increased LAMP1 staining in end-stage *Npc1*<sup>-/-</sup> mice following low dose AAV9-hNPC1 treatment. \_\_\_\_\_ 163

- Figure 36:** Redistribution of positive unesterified cholesterol filipin staining in the cortex and thalamus of *Npc1*<sup>-/-</sup> mice following low dose AAV9-hNPC1 treatment. \_\_\_\_\_ 165
- Figure 37:** Glycosphingolipid quantification of brain and liver tissue lysates from *Npc1*<sup>-/-</sup> mice following low dose AAV9-hNPC1 treatment. \_\_\_\_\_ 166
- Figure 38:** No neurological toxicity resulting from high dose AAV9-hNPC1 administration \_\_\_\_\_ 171
- Figure 39:** High dose AAV9-hNPC1 treatment further enhances survival of *Npc1*<sup>-/-</sup> mice. \_\_\_\_\_ 173
- Figure 40:** Sustained weight improvement in *Npc1*<sup>-/-</sup> mice following high dose AAV9-hNPC1 treatment. \_\_\_\_\_ 174
- Figure 41:** Correction of rearing activity in high and low dose AAV9-hNPC1 treated *Npc1*<sup>-/-</sup> mice. \_\_\_\_\_ 175
- Figure 42:** Summary of average survival data of *Npc1*<sup>-/-</sup> mice in recent NP-C gene therapy studies. \_\_\_\_\_ 199

# List of Tables

<b>Table 1:</b> Summary of major lysosomal storage disorders, their defective proteins and neurological disease involvement. _____	23
<b>Table 2:</b> Summary of the characteristics of the most commonly used viral vectors for gene therapy. _____	52
<b>Table 3:</b> Summary of principle characteristics for AAV serotypes 1 - 9. _____	58
<b>Table 4:</b> Completed and ongoing clinical trials using gene therapy for the treatment of lysosomal storage disorders. _____	68
<b>Table 5:</b> Plasmids used in this study _____	80
<b>Table 6:</b> List of oligonucleotides used in this study _____	82
<b>Table 7:</b> List of antibodies used for IHC in this study _____	98
<b>Table 8:</b> List of antibodies used for IF in this study _____	100
<b>Table 9:</b> Animal cohorts of preclinical low dose AAV9-hNPC1 study. _____	139
<b>Table 10:</b> List of animal cohorts compared throughout this study. _____	170

# Abbreviations

AAV	adeno-associated virus
ANOVA	analysis of variance
ASM	acid sphingomyelinase
BBB	blood-brain barrier
bp	base pair
BSA	bovine serum albumin
CAV-2	Canine Adenovirus Type 2
CD68	cluster of differentiation 68
cDNA	complementary DNA
CNS	central nervous system
CSF	cerebrospinal fluid
DAB	3,3'- diaminobenzidine
DAPI	4',6-diamidino-2-phenylindole
dH <sub>2</sub> O	deionised water
DMEM	Dulbecco's modified Eagle's medium
DNA	deoxyribonucleic acid
dNTPs	deoxynucleotide triphosphates
EDTA	ethylenediaminetetraacetic acid
eGFP	enhanced green fluorescent protein
ER	endoplasmic reticulum
EU	European Union
FBS	fetal bovine serum
GC	genome copies
GFAP	glial fibrillary acidic protein
GSL	glycosphingolipid
HEK	human embryonic kidney
hGHpA	human growth hormone polyadenylation signal

HP- $\beta$ -CD	2-hydroxypropyl- $\beta$ -cyclodextrin
HSD	honest significant difference
ICV	intracerebroventricular
IF	immunofluorescence
IHC	immunohistochemistry
IT	intrathecal
ITR	inverted terminal repeat
Kb	kilobase
LAMP1	lysosomal-associated membrane protein 1
LB	lysogeny broth
LTR	long terminal repeat
MPS	Mucopolysaccharidoses
NP-A	Niemann-Pick Type A
NP-B	Niemann-Pick Type B
NP-C	Niemann-Pick Type C
ns	non-significant
PBS	phosphate buffered saline
PCR	polymerase chain reaction
PEI	polyethylenimine
rAAV	recombinant AAV
RIPA	radioimmunoprecipitation assay buffer
RNA	ribonucleic acid
S.D.	standard deviation
S1BF	somatosensory barrelfield cortex
SDS	sodium dodecyl sulfate
Sim	Simple cerebellar lobule
SNR	substantia nigra pars reticulata
SV40pA	simian virus 40 polyadenylation signal
TAE	tris-acetate-ethylenediaminetetraacetic acid
TBS	Tris-buffered saline
UV	ultraviolet
vg	viral genomes
vp	viral particles

VPM/VPL	ventral posterior medial and lateral nuclei of the thalamus
VSGP	vertical supranuclear gaze palsy
VSV-G	Vesicular-stomatitis virus G-protein
w/v	weight/volume
WPRE	Woodchuck hepatitis virus posttranscriptional regulatory element

# 1 Introduction

Niemann-Pick Type C disease is one of over 70 genetically distinct lysosomal storage disorders. In 95% of cases the disease is caused by a loss of function mutation in the *NPCI* gene, which results in the abnormal accumulation of lipids in cellular late endosomal and lysosomal compartments (Vanier, 2010). Although there are a small number of treatment options that have shown therapeutic efficacy in Niemann-Pick Type C animal models, there is currently no major disease modifying or curative treatment available for patients. Due to their monogenic nature and the potential benefit of cross-correction in the majority of cases, lysosomal storage disorders have been identified as attractive candidates for gene therapy. Combined with advances in viral vector technology, significant progress in the development of gene therapy for a number of lysosomal storage disorders has resulted in a series of currently ongoing clinical trials (Biffi, 2016). However, the development of these promising trials was thought to not be easily applicable to Niemann-Pick Type C disease, due to notable additional challenges relating to the defective gene and protein.

The aim of this introductory chapter is to provide a background on lysosomal storage disorders and Niemann-Pick Type C disease, investigating pathology, clinical presentations, currently available treatment options and available animal models. Gene therapy, viral vectors and gene delivery to the central nervous system are also introduced. Finally, the rationale behind the approach taken and the aims of this project are presented.

## 1.1 Lysosomal Storage Disorders

Lysosomal storage disorders are a heterogeneous group of inherited diseases, usually characterised by the accumulation of macromolecules, resulting in cellular dysfunction, cell degeneration and ultimately premature death (**Table 1**). Although these disorders are individually classified as rare diseases, their combined frequency is estimated at 1 in 7,500 live-born infants (Meikle et al., 1999). The accumulative frequency may be higher, if mis- or un-diagnosed patient numbers are also taken into account (Platt et al., 2012). Due to the critical importance and near-ubiquitous nature of lysosomes throughout the body, dysfunction of lysosomal proteins leads to multi-system cellular dysfunction, oxidative stress, abnormal autophagy and impaired organ function (Bellettato and Scarpa, 2010). Visceral pathology is normally characterised by enlargement of the liver and spleen, but cardiac disease, haematological, pulmonary and skeletal dysfunction are also common (Parenti et al., 2015). Classical lysosomal storage disorder pathology is usually associated with degeneration of the central nervous system. The critical importance of normal lysosomal function is further highlighted by the presentation of severe neurodegeneration in approximately 60% of all lysosomal storage disorders (Cox and Cachon-Gonzalez, 2012). In combination, neurodegenerative lysosomal storage disorders account for the most common cause of childhood neurodegeneration (Lloyd-Evans and Haslett, 2016), resulting in a substantial strain to both families and health care systems (Pastores, 2010).

Disease type	Neurological involvement?	Defective enzyme or protein
<b>Sphingolipidoses</b>		
Fabry disease	Y	$\alpha$ -Galactosidase A
Farber lipogranulomatosis	N	Ceramidase
Gaucher disease type I	N	$\beta$ -Glucosidase
Gaucher disease types II and III	Y	Saposin-C activator
Niemann–Pick disease types A and B	Y	Sphingomyelinase
GM1-gangliosidosis: infantile, juvenile and adult variants	Y	$\beta$ -Galactosidase
GM2-gangliosidosis (Sandhoff): infantile and juvenile	Y	$\beta$ -Hexosaminidase A and B
GM2-gangliosidosis (Tay–Sachs): infantile, juvenile and adult variants	Y	$\beta$ -Hexosaminidase A
GM2-gangliosidosis (GM2-activator deficiency)	Y	GM2-activator protein
GM3-gangliosidosis	Y	GM3 synthase
Metachromatic leukodystrophy (late infantile, juvenile and adult)	Y	Arylsulphatase A
Sphingolipid-activator deficiency	Y	Sphingolipid activator
<b>Mucopolysaccharidoses</b>		
MPS I (Scheie, Hurler–Scheie and Hurler disease)	Y	$\alpha$ -Iduronidase
MPS II (Hunter)	Y	Iduronidase-2-sulphatase
MPS IIIA (Sanfilippo A)	Y	Heparan N-sulphatase (sulphamidase)
MPS IIIB (Sanfilippo B)	Y	N-acetyl- $\alpha$ -glucosaminidase
MPS IIIC (Sanfilippo C)	Y	Acetyl-CoA; $\alpha$ -glucosamide N-acetyltransferase
MPS IIID (Sanfilippo D)	Y	N-acetylglucosamine-6-sulphatase
MPS IVA (Morquio syndrome A)	Y	N-acetylgalactosamine-6-sulphate sulphatase
MPS IVB (Morquio syndrome B)	N	$\beta$ -Galactosidase
MPS VI (Maroteaux–Lamy)	Y	N-acetylgalactosamine-4-sulphatase (arylsulphatase B)
MPS VII (Sly disease)	Y	$\beta$ -Glucuronidase
MPS IX	Y	Hyaluronidase
<b>Glycogen storage disease</b>		
Pompe (glycogen storage disease type II)	Y	$\alpha$ -Glucosidase
<b>Oligosaccharidoses</b>		
$\alpha$ -Mannosidosis	Y	$\alpha$ -Mannosidase
$\beta$ -Mannosidosis	Y	$\beta$ -Mannosidase
Fucosidosis	Y	$\alpha$ -Fucosidase
Aspartylglucosaminuria	Y	Aspartylglucosaminidase
Schindler disease	Y	$\alpha$ -N-acetylgalactosaminidase

Sialidosis	Y	$\alpha$ -Neuraminidase
Galactosialidosis	Y	Lysosomal protective protein
Mucopolysaccharidosis II (I-cell disease); mucopolysaccharidosis III	Y	Urine diphosphate-N-acetylglucosamine; lysosomal enzyme N-acetylglucosaminyl-1- phosphotransferase
<b>Integral membrane protein disorders</b>		
Cystinosis	N	Cystinosis
Danon disease	Y	Lysosome-associated membrane protein 2
Action myoclonus–renal failure syndrome	N	Lysosome membrane protein 2
Salla disease	Y	Sialin
Niemann–Pick disease type C1	Y	NPC1 , NPC2
Mucopolysaccharidosis IV	Y	Mucopolysaccharin
<b>Neuronal ceroid lipofuscinoses</b>		
CLN1	Y	Palmitoyl-protein thioesterase-1
CLN2	Y	Serine protease
CLN3	Y	CLN3 protein
CLN4	Y	DnaJ homologue subfamily C member 5
CLN5	Y	Protein CLN5
CLN6	Y	Protein CLN6
CLN7	Y	Major facilitator superfamily domain-containing protein 8
CLN8	Y	Protein CLN8
CLN10	Y	Cathepsin D
CLN11	Y	Progranulin
CLN12	Y	Unknown
CLN13	Y	Cathepsin F
CLN14	Y	Potassium channel tetramerization domain- containing protein 7
<b>Additional disease types</b>		
Multiple sulphatase deficiency	Y	Sulphatase-modifying factor 2
Niemann–Pick disease type C2	Y	NPC2
Wolman disease (infantile); cholesteryl ester storage disease	N	Lysosomal acid lipase
Galactosialidosis	Y	Cathepsin A

**Table 1: Summary of major lysosomal storage disorders, their defective proteins and neurological disease involvement.**

Abbreviations: MPS, mucopolysaccharidosis; NPC1, Niemann–Pick disease type C1 protein; NPC2, Niemann–Pick disease type C2 protein. Adapted from (Boustany, 2013).

Although pathology and symptoms are often shared between different lysosomal storage disorders, they are individually genetically distinct (**Table 1** and **Figure 3A**). The majority of disorders are caused by mutations to genes encoding soluble lysosomal enzymes localised to within the lumen of late endosomal/lysosomal compartments (Cox and Cachon-Gonzalez, 2012), with their loss of function mostly resulting in the accumulation of a specific enzyme substrate. However, other proteins necessary for lysosomal function can also be the source of lysosomal storage disorders, such as integral membrane proteins, transporter proteins and activator proteins (Parenti et al., 2015). In comparison, these disorders generally result in the accumulation of various primary and secondary macromolecules. The complex nature of non-enzymatic disorders is associated with the lack of knowledge on the exact function of these proteins (Lloyd-Evans and Platt, 2010). Primary accumulation of the specific substrate or target macromolecule can also lead to secondary lipid accumulation or impairment of lysosomal pathways, further contributing to the pathology and complexity of lysosomal storage disorders (Walkley and Vanier, 2009, Prinetti et al., 2011). A wide range of lipid macromolecules accumulate within lysosomes in lysosomal storage disorders, depending on the specific disorder and dysfunctional lysosomal protein. However, these lipids can be broadly classified into major lysosomal storage disease categories of: glycosaminoglycan (Coutinho et al., 2012), sphingolipid (Platt, 2014), lipofuscin (Jolly et al., 1993) and cholesterol accumulation (Lloyd-Evans and Platt, 2010).

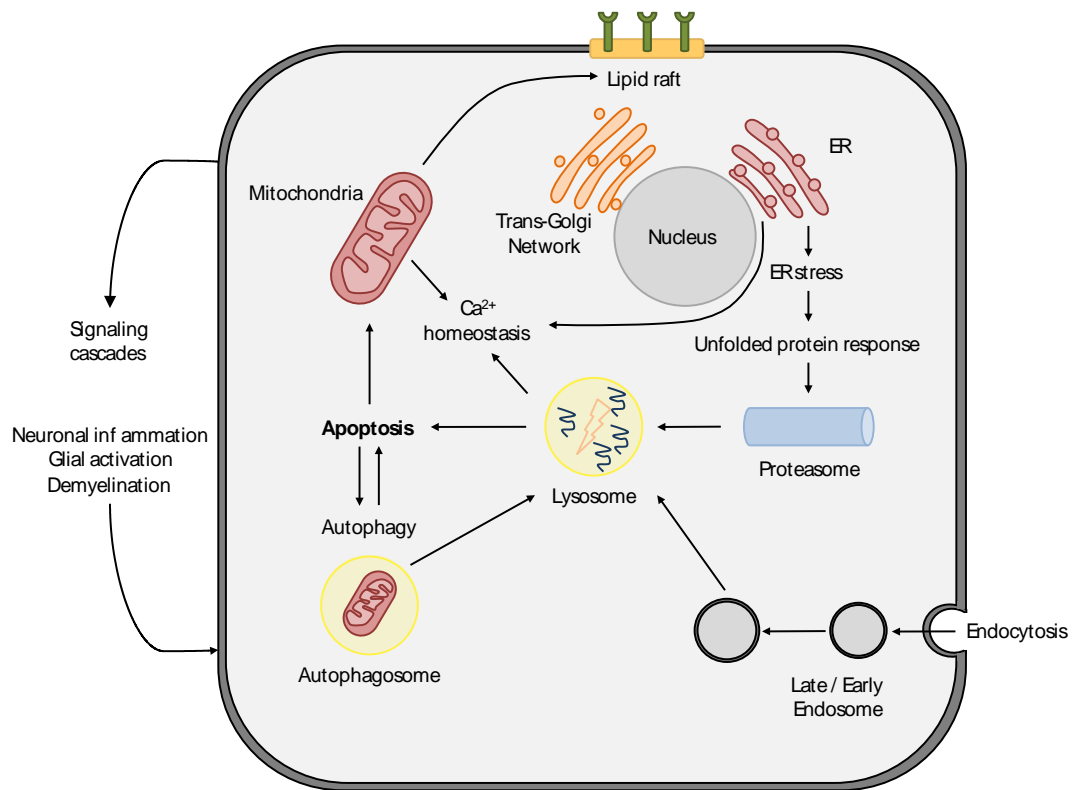


**Figure 1: Mechanisms of neuropathology in lysosomal storage disorders.**

Summary of the range of potential intra- and inter-cellular mechanisms affected in lysosomal storage disorders, ultimately leading to cell damage and death.

The complex nature of lysosomal storage diseases is reflected by their complex pathophysiology, as a number of diverse lysosomal and cellular mechanisms have been identified to potentially contribute towards disease pathology (**Figure 1**). One example is the lysosomal pH imbalance, observed in a range of lysosomal storage disorders, such as Gaucher disease (Sillence, 2013), mucopolysaccharidoses (Pereira et al., 2010) and most neuronal ceroid lipofuscinoses (Holopainen et al., 2001). The maintenance of lysosomal pH within the range of 4-5 is critical for normal lysosomal function, including lysosomal hydrolase maturation, phago-lysosome fusion, vesicle maturation, neurotransmitter loading into synaptic vesicles and autophagy (Schultz et al., 2011, Lloyd-Evans and Haslett, 2016).

Autophagy is a highly conserved self-degradative process regulated by over 30 proteins (Nakatogawa et al., 2009), crucial for development, energy conservation and clearance of both damaged organelles and intracellular pathogens (Glick et al., 2010). Induced by cellular stress or starvation stimuli, macroautophagy results in the formation of autophagosomes containing damaged cytoplasmic contents, which

subsequently undergo fusion with lysosomes, thereby releasing lysosomal hydrolases for autolysosomal degradation (Xie and Klionsky, 2007). Impaired autophagy has previously been linked to cellular damage and neurodegeneration (Komatsu et al., 2006, Hara et al., 2006), which are also observed in lysosomal storage disorders. Studies in various neurodegenerative and lysosomal storage disorder animal models, including neuronal ceroid lipofuscinoses (Cao et al., 2006), Pompe disease (Fukuda et al., 2006) and Niemann-Pick Type C disease (Pacheco et al., 2007), have confirmed impairment of macroautophagy and autophagic flux. These lysosomal storage disorder associated autophagy impairments have also been reported to result in significant mitochondrial dysfunction (Settembre et al., 2008), and lack of mitophagy mediated mitochondrial quality control (Kim et al., 2007). Cellular damage, apoptosis and inflammation may therefore be enhanced by the accumulation of reactive oxygen species and free radicals produced by dysfunctional mitochondria (Platt et al., 2012).

Dysregulation of intracellular  $\text{Ca}^{2+}$  homeostasis has been observed in a range of lysosomal storage disorders (Lloyd-Evans et al., 2010).  $\text{Ca}^{2+}$  is utilised as an intracellular signalling molecule, by creating a  $\text{Ca}^{2+}$  concentration gradient from high concentration in organelles to low concentrations in the cytosol. Release of  $\text{Ca}^{2+}$  from intracellular stores such as lysosomes, mitochondria and the endoplasmic reticulum can activate various inducible mechanisms from transcription to vesicular fusion and exocytosis (Lloyd-Evans and Haslett, 2016). However, in many lysosomal storage disorders, intracellular  $\text{Ca}^{2+}$  stores fail to buffer these higher concentrations of cytosolic  $\text{Ca}^{2+}$ , resulting in sustained  $\text{Ca}^{2+}$  elevation (Lloyd-Evans and Platt, 2011). Prolonged cytosolic  $\text{Ca}^{2+}$  elevation can result in mitochondria-mediated apoptosis (Sano et al., 2009) and neuronal excitotoxicity, whereby nitric oxide synthesis results in the generation of free radicals and ultimately apoptosis (Lewen et al., 2000).

Other potential sources of lysosomal storage disorder pathology include the activation of cell-death signalling, such as the over activation of Toll-like receptor 4 via high glycosaminoglycan levels in mucopolysaccharidoses (Simonaro et al., 2010), alteration of intracellular lipid content and lipid raft stoichiometry (Persaud-Sawin and Boustany, 2005), prolonged inflammation (DiRosario et al., 2009) or

over-activation of the unfolded protein response, which results in stress to the endoplasmic reticulum and apoptosis (Tessitore et al., 2004).

Although neurological pathology is common in most lysosomal storage disorders, the extent, severity and specific brain regions presenting neurodegeneration can differ. In the classical presentation of neuropathology in lysosomal storage disorders, neurodegeneration and inflammation will initially develop in specific brain regions, such as the cerebellum, thalamus or hippocampus, which will then ultimately advance to the rest of the brain (Platt et al., 2012). The initial susceptibility of certain brain regions during neurodegeneration progression is due to the combination of several factors. Certain neuronal populations appear more vulnerable to the accumulation of storage material, demonstrated by the commonly observed early degeneration of Purkinje neurons in the cerebellum of brains with lysosomal storage disorders (Walkley et al., 2010). The rates at which certain macromolecules are synthesised and utilised is dependent on the neuronal subtype, and as a result the detrimental effects of primary or secondary accumulation of individual storage materials can also differ between neuronal populations. Most lysosomal storage disorders also result in neuroinflammation through activation of the innate immunity in the central nervous system, which can further contribute towards neuropathology, exemplified by the neurotoxic effects of astrogliosis (Vitner et al., 2010).

Although lysosomal storage disorders may share a range of fundamental characteristics, their age of clinical onset and resulting symptoms can vary greatly between individual disorders, or even within the same disorder depending on the relative mutation severity. Combined with the specific biochemistry and types of cell populations accumulating the stored material, the spectrum of neurological and visceral symptoms can be broad (Platt et al., 2012). Although in certain severe cases newborns can exhibit symptoms, the majority of lysosomal storage disorders develop deficiencies commencing from early to late infancy (Wraith, 2002). Adult-onset disease variants have also been observed, however associated disease progression is often less acute (Nixon et al., 2008). As a result of the wide clinical symptom spectrum comparable to many other metabolic disorders and the relative rarity of the individual disorders, correct and rapid diagnosis can be challenging. Definitive lysosomal storage disorder diagnosis in most cases has to be confirmed through

specialised biochemical testing, such as lysosomal enzymatic assays or through genetic testing (Filocamo and Morrone, 2011).

The development of therapies for lysosomal storage disorders has progressed significantly in the last 25 years, as before treatment was mainly limited to palliative therapy, although this approach is still required for certain disorder groups (Parenti et al., 2015). Most current approaches focus on improving or stabilising the activity of the defective enzyme or regulating its upstream substrates. Enzyme replacement therapy, whereby a functional recombinant version of the defective protein is administered to patients, is now a standard form of care for many lysosomal storage disorders (Desnick and Schuchman, 2012). However, its use is restricted to soluble lysosomal proteins and has a limited bioavailability in the central nervous system, due to the inability of the majority of recombinant protein to cross the blood-brain barrier. Additionally, manufacturing costs of the specific recombinant proteins and the need for continual repeated administration results in a substantial burden for national health systems and individual families (Wyatt et al., 2012).

Lysosomal storage disorders are often caused by missense mutations, resulting in a disruption to the three-dimensional structure and folding of the encoded protein, ultimately leading to protein degradation, endoplasmic reticulum (ER) retention, mistrafficking or protein dysfunction (Parenti et al., 2014). Pharmacological chaperones bind to these proteins, with the aim of improving protein folding and stability, leading to enhanced trafficking and protein activity (Valenzano et al., 2011). A combination therapy of the  $\alpha$ -galactosidase A stabilising pharmacological chaperone 1-deoxygalactonojirimycin (migalastat hydrochloride) and recombinant  $\alpha$ -galactosidase A enzyme replacement therapy has been demonstrated to be particularly effective in Fabry disease (Benjamin et al., 2012).

Other potential therapies include bone marrow transplantation, substrate reduction therapy and gene therapy, which will be discussed later in more detail. Although remarkable advancements in lysosomal storage disorder treatment have been made, many disorders lack any effective and specialised treatment options. Where treatment may be possible, the delivery to critical yet isolated tissues, immunological

resistance, timing of diagnosis and access to the costly therapy still remain significant challenges (Boustany, 2013).

## 1.2 Niemann-Pick Diseases

Niemann-Pick diseases are a subgroup of lysosomal storage disorders first described by Albert Niemann and Ludwig Pick in the early 20<sup>th</sup> century (Pentchev, 2004). These can be further categorised by their respective lysosomal protein deficiency. Niemann-Pick Type A (NP-A) and B (NP-B) are caused by the loss of acid sphingomyelinase (ASM) function, whereas Type C1 and C2 result from the loss of either NPC1 or NPC2 function (Vanier, 2013).

The autosomal recessive lipid storage diseases Niemann-Pick Type A and B result from loss of function mutations to the *SMPDI* gene, which encodes the lysosomal hydrolase acid sphingomyelinase (ASM). The form and severity of the disease depends on the type of *SMPDI* mutation and to date more than 120 disease causing mutations have been identified (Schuchman and Wasserstein, 2015). ASM deficiency is classified as a rare genetic disorder, with a prevalence of approximately 1 in 100,000 (Poupetova et al., 2010), however this may be an underrepresentation due to the difficulties associated with a correct clinical diagnosis of the milder NP-B disease. The extent of ASM deficiency differs between the two types, with Type A patients producing little to no functional ASM activity (<1%), whereas Type B patients retain a certain level of ASM activity (~10%) (Schultz et al., 2016). ASM catalyses the breakdown of sphingomyelin to phosphocholine and ceramide, and as a result ASM deficiency leads to the primary accumulation of sphingomyelin in patients with NP-A and NP-B disease (Wasserstein and Schuchman, 1993). Sphingomyelin is a sphingolipid that forms a major component of the cellular plasma membrane and axon insulating myelin sheath (Quinn, 2014). A potential additional source of pathology along with storage material accumulation may result from abnormalities in the plasma membrane and myelin sheath, which in turn can cause secondary affects to receptor function, transport mechanisms and cell signalling

pathways (Schuchman and Wasserstein, 2015). Moderate secondary storage of cholesterol, gangliosides, glucocerebroside and lactosylceramide has also been observed, similar to the multi-lipid accumulation in Niemann-Pick Type C disease, suggesting an overlap of disease mechanisms. Foam cells, characterised as large lipid-laden cells, have been observed in the visceral organs of patients with ASM deficiency, particularly within the liver, spleen, lung and bone marrow (Wasserstein and Schuchman, 2015). The clinical disease presentation differs between Types A and B, where patients with NP-A exhibit severe hepatosplenomegaly from the first months of life. Progressive neurological pathology commences from 6 months of age, characterised by hypotonia, ataxia and spasticity, with premature death occurring before 3 years of age (Vanier, 2013). In comparison, NP-B does not show any neurological involvement, however patients do exhibit variable degrees of chronic hepatosplenomegaly from late infancy and most survive until late adulthood (McGovern et al., 2008).

Symptomatic management currently remains the standard care for patients with Niemann-Pick Types A and B. Bone marrow transplantation in Type A patients showed moderate visceral efficacy, however no neurological therapeutic effects were observed and secondary complications associated to the procedure were severe (Victor et al., 2003). Patients with the non-neuropathic Type B disease should be ideal targets for enzyme replacement therapy and a recently completed phase I clinical trial demonstrated the safety of this treatment (Wasserstein et al., 2015).

### **1.3 Niemann-Pick Type C Disease**

Niemann-Pick Type C disease (NP-C) is an atypical autosomal recessive lysosomal storage disorder, which can be further subcategorised into Niemann-Pick Type C1 (NP-C1) or C2 (NP-C2) disease, depending on either NPC1 or NPC2 lysosomal protein deficiency. NP-C disease is characterised by the accumulation of multiple storage materials, resulting in neurovisceral symptoms. The following sections aim

to give a detailed overview of NP-C epidemiology, pathology, clinical presentation, diagnosis, available therapies and animal models.

### 1.3.1 NP-C Epidemiology

As with other lysosomal storage disorders, NP-C is classified as a rare disease. The actual prevalence of NP-C has been difficult to determine, due to the previously discussed challenges demonstrated by most lysosomal storage disorders, such as relative disease rareness, broad clinical spectrum and difficulty of diagnosis. The current clinical incidence is estimated at approximately 1 in every 100,000 live births (Vanier, 2010), however this is likely an underestimation. A recent study evaluating data from massive parallel exome sequencing data sets for damaging mutations to NP-C causing genes predicted a combined frequency of 1 in every 89,000 births, with a rate of 1:92,000 for NP-C1 and 1:2,860,000 for NP-C2 (Wassif et al., 2016). The authors also reported that when damaging mutations expected to cause protein dysfunction but not classical NP-C disease were taken into account, the frequency may be as high as 1:19,000 – 1:36,000. These cases may represent milder or atypical versions of the disease often described in older-onset patients, which are most likely misdiagnosed. NP-C occurrence is pan-ethnic, with two genetic isolates described in Spanish Americans in South Colorado and French Arcadians in Nova Scotia, which were previously misclassified as Niemann-Pick Type D patients (Wenger et al., 1977).

### 1.3.2 NP-C Proteins

NP-C is caused by mutations to either of two genes, *NPC1* or *NPC2*, resulting in NP-C1 and NP-C2 disease respectively. Approximately 95% of NP-C cases are attributed to mutations in the *NPC1* gene, whereas until 2010 only 30 cases of NP-C have been officially recorded due to mutations in the *NPC2* gene (Vanier, 2010). The two proteins encoded by these genes are involved in late endosomal/lysosomal lipid trafficking, as opposed to metabolite catabolism observed in the majority of lysosomal storage disorders. *NPC1* encodes a large 1,278 amino acid transmembrane

glycoprotein, shown to predominantly localise within late endosomal compartments, with only transient lysosomal interactions (Higgins et al., 1999, Neufeld et al., 1999). Analysis of NPC1 transmembrane domains revealed the presence of a sterol-sensing domain, a highly conserved region of five transmembrane segments proposed to be involved in the response to sterols in the lipid bilayer (Kuwabara and Labouesse, 2002) (**Figure 2A**). Although the exact function and mechanism of this domain has remained unclear, its activity is crucial for NPC1 function (Watari et al., 1999, Ohgami et al., 2004, Millard et al., 2005). The recent publication of a detailed NPC1 crystal structure led to the proposal that NPC1's sterol sensing domain acts as a cavity for docking of individual cholesterol molecules, where the cavity is accessible from both the lipid bilayer and lysosome lumen (Li et al., 2016). This would allow the movement of cholesterol from the endosomal/lysosomal lumen to within the luminal leaflet of the lipid bilayer. The luminal N-terminal domain of NPC1 has also crucially been shown to bind cholesterol (Kwon et al., 2009) and is attached to the rest of the NPC1 protein via a long flexible proline-rich bridge (Infante et al., 2008a).

In comparison, the *NPC2* gene encodes the smaller 132 amino acid soluble NPC2 protein, found within the lumen of late endosomes and lysosomes (Storch and Xu, 2009). NPC2 is also thought to be involved in the trafficking of cholesterol (Naureckiene et al., 2000), as 1:1 stoichiometric binding of cholesterol with a cholesterol-binding site within the NPC2 protein has been observed (Friedland et al., 2003). Previous studies have shown that the correct function of both NPC1 and NPC2 is necessary for the escape of cholesterol from within late endosomal/lysosomal compartments, with the affinity of cholesterol binding and dissociation to NPC1 greatly enhanced by the presence of NPC2 (Infante et al., 2008b).

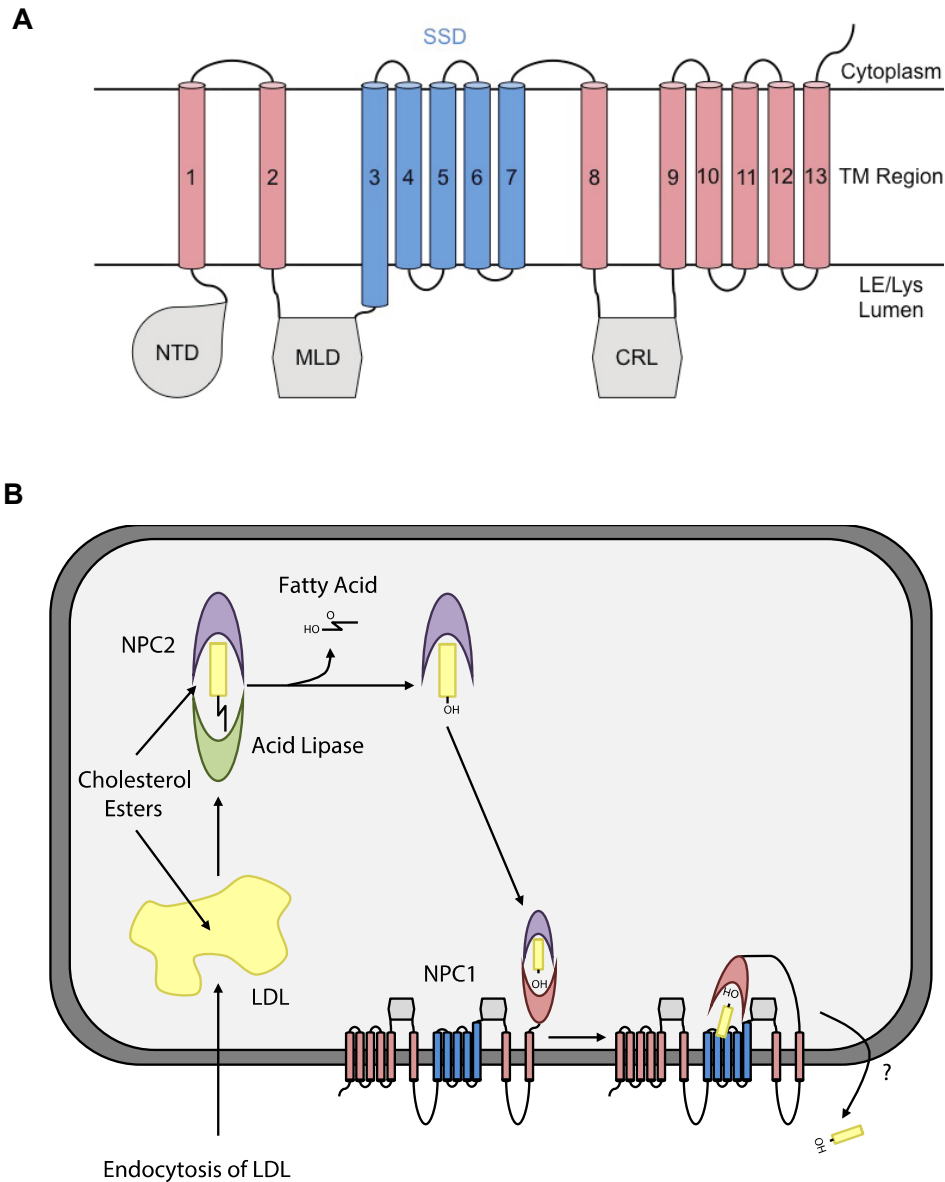


**Figure 2: NPC1 structure and proposed pathway of cholesterol binding**

- (A) Secondary structure schematic of NPC1 in relation to the late endosomal/lysosomal membrane, showing 13 transmembrane domains (1-13). NTD, N-terminal domain; MLD, middle luminal domain; SSD, sterol-sensing domain; CRL, Cysteine-rich loop (Lloyd-Evans and Platt, 2010, Li et al., 2016).
- (B) Suggested model of NPC2 and NPC1 mediated cholesterol transport in late endosomes/lysosomes. Cholesterol esters released from endocytosed low-density lipoprotein complexes are hydrolysed by acid lipase to produce unesterified cholesterol, which is subsequently bound by the soluble luminal protein NPC2. NPC2 transfers unesterified cholesterol to NPC1 at the N-terminal domain, resulting in a conformational change in NPC1 structure, giving unesterified cholesterol access to the transmembrane sterol-sensing domain. Unesterified cholesterol subsequently escapes the late endosomal/lysosomal by an unknown mechanism for downstream use (Kwon et al., 2009).

Although the exact and complete mechanism for late endosomal/lysosomal cholesterol egress via NPC1 and NPC2 is still currently unknown, the combination of structural and biochemical studies have led to the proposal of a cholesterol transport chain (**Figure 2B**). Due to its poor solubility in water, cholesterol is distributed throughout the body in the form of cholesterol esters that are packaged into lipoproteins (Brown and Goldstein, 1986). These lipoproteins are absorbed by cells for downstream use via the cholesterol uptake pathway, to which both NPC1 and NPC2 are crucial (Carstea et al., 1997). Endocytosis of these lipoproteins results in their transportation to late endosomes and lysosomes, where cholesterol is liberated via lipolysis by the lysosomal acid lipase enzyme (Goldstein et al., 1975). Luminal free unesterified cholesterol subsequently binds to the cholesterol-binding site of NPC2, with its hydroxyl group exposed (Xu et al., 2007). NPC2 bound cholesterol is then docked and transferred to a pocket in the N-terminal domain of NPC1, that has been shown to bind cholesterol in the opposite orientation to NPC2, with its hydrophobic side chain exposed (Kwon et al., 2009). Reorientation of the flexible proline-rich bridge connecting the N-terminal domain and the rest of NPC1 may then allow the movement of cholesterol to within the sterol-sensing domain cavity, which gives access to the late endosomal/lysosomal bilayer. As the hydrophobic side chain remains exposed, the deposited cholesterol could escape via the membrane pocket's lateral opening, releasing cholesterol into the luminal leaflet of the endosomal/lysosomal bilayer (Li et al., 2016). The embedded cholesterol must subsequently be flipped to the cytoplasmic leaflet of the late endosomal/lysosomal leaflet by an unknown mechanism, for subsequent downstream delivery to other intracellular membranes, such as the endoplasmic reticulum, recycling endosomes and mitochondria (Ikonen, 2008).

### 1.3.3 NP-C Lipid storage

Although NP-C is often characterised as a cholesterol storage disorder, NPC1 or NPC2 deficiency results in the storage of multiple lipid species within late endosomal/lysosomal compartments of cells throughout almost all tissues. Early studies revealed moderate levels of sphingomyelin storage, compared to the levels seen in ASM deficient NP-A and NP-B patients, leading to the denomination

Niemann-Pick Type C (Spence and Callahan, 1989). However, an extensive accumulation of unesterified cholesterol, multiple glycosphingolipids and sphingosine has also been shown (Lloyd-Evans et al., 2008), with the ratio of cholesterol to sphingomyelin significantly higher in NP-C than in NP-A or NP-B patients (Fan et al., 2013, Vanier, 2015). This indicated towards a different developmental pattern between the disease groups, where sphingomyelin accumulation was a secondary result of primary storage (Walkley and Vanier, 2009).

Interestingly, differences in the ratio of individual lipid species accumulation within this multi-lipid storage disease has also been demonstrated between visceral organs and the central nervous system, in both patients and an NP-C mouse model (Vanier, 2015) (**Figure 3B**). In the peripheral tissues such as the liver and spleen of patients, NP-C leads to the major accumulation of unesterified cholesterol, sphingomyelin and sphingosine, with significant elevations of several glycosphingolipids also observed, including glucosylceramide, lactosylceramide, globotriaosylceramide and gangliosides GM2 and GM3 (Rodriguez-Lafrasse et al., 1994, Walkley and Vanier, 2009). The NP-C mouse model demonstrates similar visceral storage profiles, however in contrast to human patients, higher levels of lipid accumulation occur in the liver than in the spleen (Goldin et al., 1992, Sleat et al., 2004, Fan et al., 2013). In comparison, brains exhibit extreme levels of glycosphingolipid accumulation, including gangliosides GM3 and GM2, and to a lesser extent glucosylceramide, lactosylceramide and gangliotriaosylceramide in both patients (Tjiong et al., 1973, Vanier, 1999) and the NP-C mouse model (Sleat et al., 2004, Fan et al., 2013) (**Figure 3B**). Interestingly, no changes in overall brain cholesterol or sphingomyelin levels have been observed (Vanier, 1999), however histochemical analysis has revealed positive cholesterol accumulation in neurones of the NP-C mouse (Zervas et al., 2001a), suggesting a redistribution of intracellular cholesterol. The brain is the most cholesterol-rich organ, with the majority of cholesterol being contained in the myelin sheaths formed by oligodendrocytes. Most brain cholesterol is synthesised locally via *de novo* synthesis in the ER, independent of NPC1/2 function (Zhang and Liu, 2015). However, relatively small amounts of cholesterol uptake have been reported in neurons via glial delivery, which would require NPC1/2 functionality and may explain the low level neuronal cholesterol accumulation (Vance, 2012).

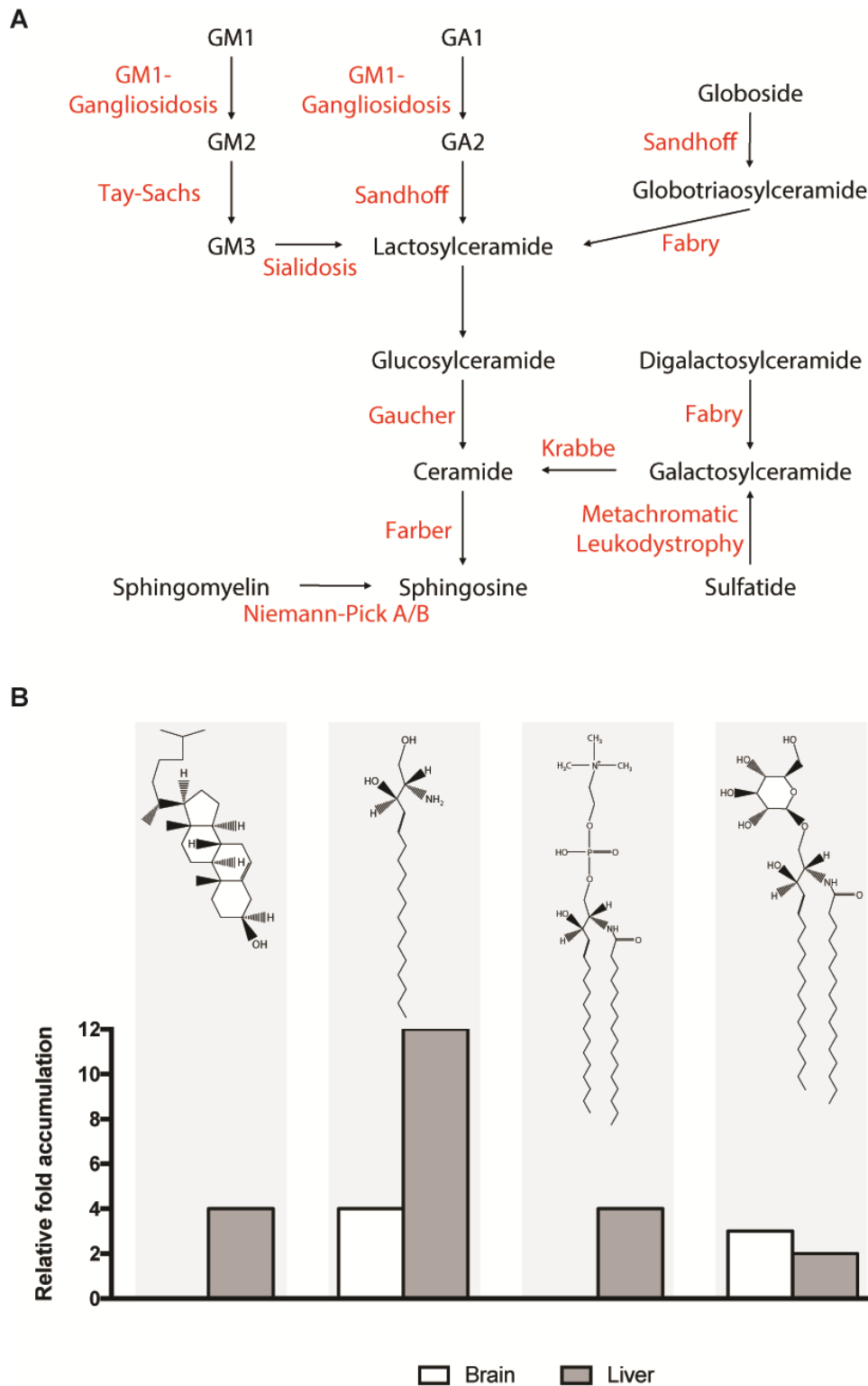


**Figure 3: Sphingolipid structure and degradation pathway in the late endosomes/lysosomes of cells.**

- (A) Graphical representation of the catabolic pathway of selected sphingolipids within the late endosomes/lysosomes of cells. The individual proteins and activator proteins required for each degradation step and their respective diseases are also presented.
- (B) Graphical representation of the structure of lipids that accumulate in the brain and liver of *Npc1*<sup>-/-</sup> mice (Lloyd-Evans and Platt, 2010).

The identification of the primary offending metabolite in NP-C still remains unanswered (Lloyd-Evans and Platt, 2010). While NPC1 and NPC2 have been demonstrated to bind cholesterol, NPC1 has still not been shown to function as a direct cholesterol transporter. NPC1 may also act as a cholesterol-regulated protein, where NPC1 transports other cargo in response to, or in combination, with cholesterol. This function would be consistent with other proteins containing a sterol-sensing domain (Infante et al., 2008a), while NPC1's sterol sensing domain would allow cholesterol sensing in both the late endosomal/lysosomal lumen and inner luminal leaflet. Other factors suggesting that cholesterol is not the primary offending metabolite in NP-C include: (1) lysosomal accumulation of cholesterol has been observed in other disorders despite the normal function of NPC1, (2) no clinical benefit of cholesterol lowering therapies to NP-C patients and (3) the only currently licenced drug in the European Union (EU) for NP-C disease is miglustat, which does not affect cholesterol levels (Lloyd-Evans and Platt, 2010). Lloyd-Evans and Platt have extensively covered cases for and against several other individual lipid species being the primary offending metabolite, however its identification and role in pathology remains unclear (Lloyd-Evans and Platt, 2010).

#### **1.3.4 NP-C Pathology**

Common to the majority of lysosomal storage disorders, the exact or combination of processes resulting in cellular damage and ultimately degeneration are not known in NP-C, however a range of potential NP-C specific pathology mechanisms have been identified and proposed.

The previously discussed link between abnormal intracellular calcium homeostasis and lysosomal storage disorders has also been made in Niemann-Pick Type C disease. In contrast to other disorders, NPC1-mutant cells demonstrated normal  $\text{Ca}^{2+}$  concentrations within the endoplasmic reticulum and mitochondria, however significantly lower levels of  $\text{Ca}^{2+}$  were observed in late endosomal/lysosomal compartments (Lloyd-Evans et al., 2008). The release of calcium from these acidic compartments is crucial for endocytic fusion and transport events (Piper and Luzio, 2004, Morgan et al., 2011), with this dysfunction thought to lead to the additional

multi-lipid accumulation observed in NPC1-mutant cells. Although NP-C is often considered primarily a cholesterol storage disease, the accumulation of sphingosine was identified as the initiating storage metabolite during altered calcium homeostasis, resulting in secondary cholesterol and sphingolipid storage via endocytic dysfunction (Lloyd-Evans et al., 2008).

The block in late endosome and lysosome fusion and secondary lipid storage observed in NP-C mutant cells (Goldman and Krise, 2010) may also have a profound effect on cellular metabolic stress and autophagy. As endocytic and autophagic pathways are crucial for the maintenance of intracellular metabolic homeostasis (Platt et al., 2012), the loss in the release of lipid species from endolysosomes and autolysosomes necessary for downstream metabolic pathways may result in cellular metabolic stress (Walkley, 2007). This effect may be particularly significant in NPC1 or NPC2 deficient cells, due to the wide range of lipids that accumulate and become trapped in late endosomal/lysosomal compartments (Platt et al., 2012). Cholesterol and sphingomyelin demonstrate a particularly strong interaction, as these two lipids will normally co-localise in cells (Quinn, 2013). Together they stabilize bilayers and form lipid rafts, which are major sites of cell signalling activity (Skocaj et al., 2014). Interestingly, the loss of NPC2 function has been reported to result in the specific impairment of lysosome reformation, which should result in a similar pathological consequence as endocytic dysfunction (Goldman and Krise, 2010). Metabolic stress and starvation are stimuli for enhanced autophagy, where the fusion of late endosomes and lysosomes with autophagosomes are crucial steps resulting in cargo degradation within autophagy. However, NPC1-mutant cells demonstrated impairment of autophagy-specific traffic needed for amphisome and autolysosome formation (Sarkar et al., 2013). Additionally, the degradation of autolysosomal cargoes has also shown to be impaired in NPC1-mutant cells, with the reduction in autophagic flux due to the presence of accumulated storage material (Cologna et al., 2014). Interestingly, the autophagic pathway was also shown to further exacerbate lipid storage by representing an additional source of stored cholesterol in lysosomes, thereby creating a positive feedback loop.

The central nervous system is particularly sensitive to oxidative stress damage, due to the high concentration of polyunsaturated fatty acids available for peroxisomal

oxidation, high amounts of oxygen consumed during energy production and low concentrations of antioxidants (Vazquez et al., 2012). The extent of oxidative stress damage in NP-C pathology is unknown, however oxidative stress has been observed in the brain and livers of NP-C mice (Smith et al., 2009). Additionally, cholesterol oxidation products known as oxysterols have been detected in the plasma of NP-C patients (Porter et al., 2010) and NP-C patients exhibit decreased antioxidant defence capability (Fu et al., 2010). The likely driving force behind oxidative damage in NP-C cells could be the dysfunction of mitochondria, as their dysfunction is a central part of many neurodegenerative disorders (Vazquez et al., 2012). Various studies have reported high levels of cholesterol within mitochondria of NP-C cells, which resulted in changes to the mitochondrial organisational network, abnormal mitochondrial morphology and impaired mitochondrial function, characterised by altered composition of the respiratory chain complex, reduction in cellular ATP concentrations and increased respiration (Yu et al., 2005, Charman et al., 2010, Wos et al., 2016). A further source of reactive oxygen species is the dysfunctional peroxisome (Bonekamp et al., 2009) and the impairment of fatty acid oxidation within peroxisomes has also been reported as an early indication of disease progression in the NPC1 mouse model (Schedin et al., 1997). Interestingly, peroxisomal disorders result in the storage of gangliosides within cells and may form a link with other lysosomal storage disorders including NP-C, where these gangliosides are observed as secondary storage metabolites (Platt et al., 2012). Other additional sources of oxidative stress include high concentrations of copper (Barnham and Bush, 2008), which was been reported to accumulate in the liver, bile and plasma of NP-C mice (Vazquez et al., 2011), and decreased bioavailability of the antioxidant vitamin E, which also accumulates in the lysosomes of NP-C mutant cells and is normally particularly abundant in the cerebellum (Vazquez et al., 2012).

As with other lysosomal storage disorders, the prolonged activation of the innate immune system and resulting inflammation may represent an additional possible source of pathology (Platt et al., 2016). However, studies have pointed towards cell autonomous neurodegeneration, resulting in the proposal of neuroinflammation as a secondary result of neurodegeneration, rather than a primary cause (Lopez and Scott, 2013). Additionally, complement has been shown to not be involved in NP-C neuropathology (Lopez et al., 2012). While innate immune activation may not be a

major source of pathogenesis, anti-inflammatory therapies demonstrated therapeutic efficacy and significant extension in the lifespan of NP-C mice (Smith et al., 2009), indicating that neuroinflammation may play a role in disease enhancement (Platt et al., 2016).

Further reported sources of possible pathology include up-regulation of genes associated with death receptor signalling, resulting in the induction of apoptosis in the brains of the NP-C mouse model (Wu et al., 2005), necroptosis (Cougoux et al., 2016), altered transition metal homeostasis (Hung et al., 2014) and impaired neurosteroid synthesis (Griffin et al., 2004).

### **1.3.5 Clinical Presentation of NP-C**

The clinical presentation of Niemann-Pick Type C is extremely heterogenous and complex, as the age of disease onset, average lifespan and symptoms can vary greatly (Vanier, 2010). As with the majority of other lysosomal storage disorders, NP-C is generally classified as a neurovisceral condition, however the extent of either visceral or neurological pathology development and timing of the respective disease manifestations can also differ. Visceral pathology has been reported to be absent in approximately 15% of all diagnosed patients, with an absence of 50% in adult-onset patients (Vanier, 2013). Visceral pathology severity increases with earlier disease onset, however there is no apparent link between timing of visceral disease onset and subsequent neurological pathology development. The strongest indicator of NP-C visceral pathology is isolated splenomegaly or in combination with hepatomegaly (Wijburg et al., 2012), which is observed in the majority of NP-C patients (Patterson et al., 2012). However, the degree of splenomegaly has no correlation with neurological disease severity or stage of overall disease progression (Mengel et al., 2013). Hepatomegaly is usually isolated to younger patients, developing simultaneously to splenomegaly (Sevin et al., 2007), while in extreme early-onset cases cholestatic jaundice and hepatopathy leading to liver failure have been observed (Kelly et al., 1993). Other visceral NP-C symptoms include lung disease and thrombocytopenia, however their occurrence is limited (Mengel et al., 2013).

In comparison, the neurological manifestations of NP-C are even more diverse and occur in all patients, apart from severe perinatal cases where patients die before neurological disease progression. The development of ataxia is typical in NP-C patients and is linked to the degeneration of Purkinje cells in the cerebellum (Sarna et al., 2003, Walterfang et al., 2013). Ataxia in NP-C patients is classified as a 'slow ataxia' when compared to other non-NP-C ataxia patients, resulting in slow movements, impaired gait and general clumsiness (Mengel et al., 2013). Progressive ataxia will usually develop after dystonia, with the delay between manifestations correlating to disease progression. Dystonia, a neurological movement disorder observed in the majority of NP-C patients, is due to neuropathology in the basal ganglia and cerebellum, which results in excessive involuntary muscle contraction (Walterfang et al., 2013). The specific combination of ataxia and dystonia is a clear sign of NP-C (Wraith et al., 2014), however they can present individually, often resulting in misdiagnosis. A result of this combination is the development of dysarthria, where impaired coordination of the motor-speech system leads to irregular slurring of speech (Ogawa et al., 2010). Dysphagia is a common symptom in NP-C patients (Patterson et al., 2012), with impaired brainstem and cortical function ultimately causing swallowing difficulties (Ertekin and Aydogdu, 2003). A major implication of dysphagia is the correlation with aspiration pneumonia, which is a common cause of death in NP-C patients (Walterfang et al., 2012). One of the earliest neurological manifestations can be the development of hypotonia, characterised by weakness, low muscle tone and abnormal reflexes (Mengel et al., 2013). Additionally, the early onset of hypotonia correlates to a more progressive infantile version of NP-C (Wijburg et al., 2012). The early development of vertical supranuclear gaze palsy (VSGP) in patients is a strong indicator for neurological NP-C pathology and is present in approximately 65% of cases (Salsano et al., 2012). VSGP is characterised by a deficit in voluntary and reflexive vertical saccadic movements of the eyes, due to a lesion above the cranial motor nerve nuclei. Subsequent impairment of horizontal saccades correlates to progressive neurodegeneration and disease progression (Solomon et al., 2005). Other common neurological manifestations include partial or general seizures, cataplexy, high frequency hearing loss and delayed developmental milestones (Mengel et al., 2013).

Neurological manifestations are accompanied by progressive psychiatric symptoms in NP-C patients. Gradual cognitive decline has been observed in most NP-C patients and is characterised by the delay in cognitive development in younger-onset patients and impaired executive functioning, memory loss and cognitive slowing in older-onset patients, which may be misinterpreted as other more common neurodegenerative disorders, such as Alzheimer's disease (Mengel et al., 2013). Psychosis with a visual hallucinatory phenotype has also been reported to present in older-onset patients (Nia, 2014).

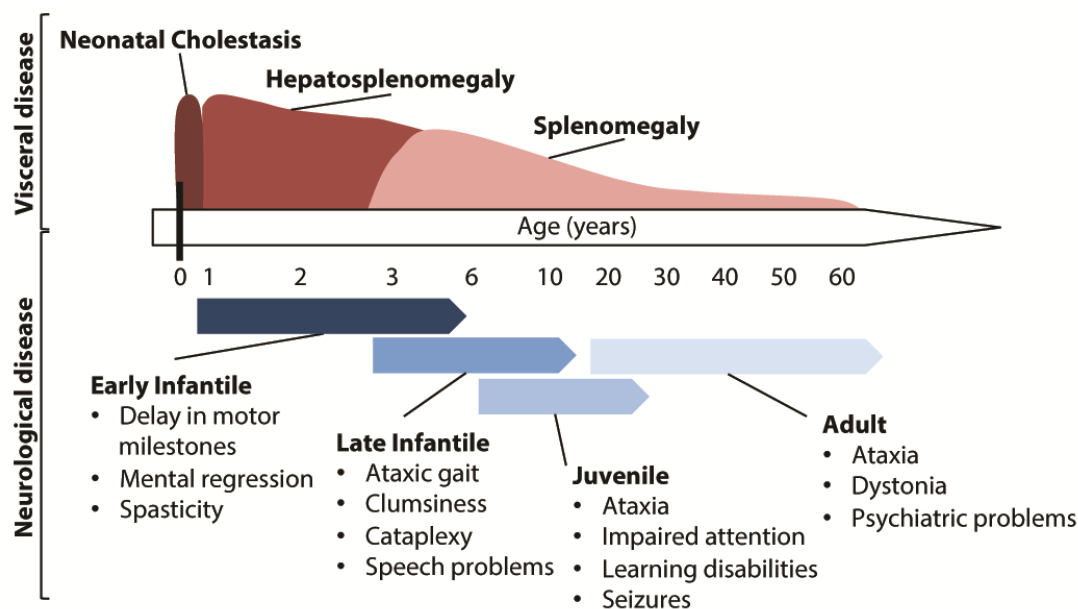


**Figure 4: Presentations of Niemann-Pick Type C disease**

Graphical representation of the common types of NP-C with their associated neurovisceral symptoms, depending on age of neurological pathology onset (Vanier, 2015).

Due to the extremely heterogeneous clinical presentations of NP-C disease, patients are categorised by NP-C types based on the age of neurological symptoms onset (**Figure 4**), regardless of prior visceral symptoms, apart from severe perinatal cases where death is caused by visceral pathology presumably before neurological disease progression (Vanier, 2010).

Perinatal presentation of NP-C is characterised by severe visceral pathology in the form of cholestatic liver disease and progressive hepatosplenomegaly. The majority of patients with this severe acute neonatal cholestatic form will die by 6 months of age (Vanier et al., 1988). Unlike all other forms, no neurological manifestations are observed during the neonatal period.

The early infantile period (2 months – 2 years) is usually characterised by delayed motor development and central hypotonia from the age of 1 year and patients will often fail to learn to walk. Disease progression results in impaired motor skills, mental regression, spasticity and intention tremor, with death usually occurring before 5 years of age (Vanier, 2010). Visceral NP-C disease is mainly limited to splenomegaly or hepatosplenomegaly and occurs before neurological manifestations in the first months of life.

NP-C patients with the late infantile type NP-C (2 – 6 years) present with early splenomegaly or hepatosplenomegaly, which may go undiagnosed. Subsequent neuropathology is associated with ataxic gait and clumsiness at the age of 3 to 5 years. Disease progression can result in cataplexy, impaired mental development, seizures, dysphagia, dysarthria and increased spasticity, with death usually occurring before 12 years of age.

The juvenile form of NP-C is the most common form of the disease and onset occurs from 6 to 15 years of age. Late infantile and juvenile forms are often combined under the heading childhood onset NP-C (Patterson, 1993). Moderate splenomegaly is frequent and may have commenced from the neonatal period, yet remained undetected. Neurological onset is characterised by writing difficulties, impaired attention and VSGP. As the disease progresses, patients exhibit learning disabilities, cataplexy, dysarthria, seizures, dysphagia and ataxia. The lifespan of patients with the juvenile form of NP-C is extremely varied, with patients often surviving until 25-30 years of age (Group et al., 2009).

The final form of NP-C is adult onset, occurring after 15 years of age. Visceral pathology in the form of splenomegaly appears rare at the time of diagnosis (Fensom et al., 1999), however previous visceral pathology cannot be ruled out. The diagnosis

of this form of NP-C is likely to be underestimated, due to a characteristically slow disease progression and large spectrum of neurological symptoms similar to the juvenile form (Vanier, 2010). VSGP is common along with cerebellar ataxia, dysarthria, cognitive decline and psychiatric disorders including psychosis, paranoia and visual hallucinations.

### 1.3.6 NP-C Diagnosis

As previously discussed, the correct and timely diagnosis of NP-C can be challenging and as a result the incidence of this disease is most likely underrated (**Section 1.3.1**). Although significant advancements in the understanding of NP-C genetics and biochemistry, laboratory testing has remained complex, expensive and localised to specialist centres (Vanier et al., 2016). Combined with a broad disease manifestation spectrum and limited disease awareness, the time between disease onset, diagnosis and subsequent treatment can be substantial (Group et al., 2009). Early diagnosis is particularly important, as treatments will be more effective the earlier in disease progression they are given. Initial steps towards diagnosis are the gathering and analysis of clinical history, where certain combinations of visceral, neurological and psychiatric symptoms can point specifically towards NP-C. To aid in this effort the screening tool 'NP-C Suspicion Index' was developed (Wijburg et al., 2012), however overlapping symptoms and heterogeneity of disease manifestations and onset can complicate this process.

Current laboratory techniques utilised for NP-C fall into 3 major categories: lipid accumulation testing, biochemical markers and genetic testing. Until recently the filipin test was regarded as the standard assay for NP-C diagnosis, where the fluorescent polyene macrolide filipin is applied to patient fibroblasts, causing the fluorescent staining of accumulated unesterified cholesterol (Pentchev et al., 1985). Strong perinuclear staining is visible in 80% - 85% of NP-C patients, with the remaining patients exhibiting either an intermediate staining profile or no filipin staining, which will normally be followed by complementary *NPC1* and *NPC2* gene sequencing for further clarification (Vanier and Latour, 2015). Additionally, certain heterozygotes, compound heterozygotes, ASM deficient patients and patients with

other disorders associated with secondary impaired cholesterol egress such as Smith-Lemli-Opitz syndrome (Platt et al., 2014) and Tangier disease (Sechi et al., 2014) have been shown to demonstrate abnormal filipin patterns (Vanier et al., 2016).

The timing, cost and specialist knowledge required for filipin testing demonstrates the need for a high-throughput, cost-effective and specific biomarker analysis screen for NP-C. A further beneficial use of NP-C specific biomarkers would be their potential use in the tracking of treatment efficacy during preclinical animal studies and clinical trials. Two of the currently most promising biomarkers for NP-C are plasma oxysterols and bile acid metabolites. As previously discussed (**Section 1.3.4**), the increase in oxidative stress in NP-C affected cells leads to elevated reactive oxygen species levels and a subsequent accumulation in abnormal oxysterol concentration, which has also been demonstrated by mass spectrometry in NP-C patients (Porter et al., 2010, Jiang et al., 2011). However, a certain number of confirmed NP-C patients have also shown non-significant levels of oxysterol elevation, and patients with other disorders including NP-A and NP-B have also exhibited elevated plasma oxysterol levels (Klinke et al., 2015). Bile acid metabolites represent another possible biomarker for NP-C patients, as they were identified at high concentrations in patient urine (Alvelius et al., 2001), thought to be due to the utilisation of different bile acid synthesis pathways in NP-C patients. While this assay is less prone to artefacts compared to oxysterol analysis and can be applied to dry blood spots as well as plasma, it may not be able differentiate between ASM-deficient and NP-C patients (Vanier et al., 2016).

Finally genetic testing of the *NPC1* and *NPC2* genes via Sanger sequencing is usually carried out for confirmation of NP-C diagnosis, in combination with biomarker or filipin testing (Patterson et al., 2012). However, advancements in availability, cost and throughput capacity of next-generation sequencing and whole exome sequencing techniques will result in increased routine genetic screening potential and is currently recommended for all patients (McKay Bounford and Gissen, 2014).

### 1.3.7 Therapeutic Options for NP-C

As with many lysosomal storage disorders, there is currently no cure for NP-C, but a range of therapies have shown therapeutic efficacy in stabilising or slowing disease progression, in either preclinical NP-C animal model studies or in clinical trials.

The rationale behind substrate reduction therapy is the inhibition of the biosynthesis of compounds that accumulate in specific lysosomal storage disorders, which will subsequently result in a decrease in storage material (Radin, 1996). *N*-butyldeoxynojirimycin (miglustat, Zavesca®) is a small water-soluble imino-sugar that reversibly inhibits glucosylceramide synthase, the primary enzyme in glycosphingolipid synthesis (Platt et al., 1994). Miglustat can be administered orally, has a half-life of 7 hours and can readily cross the blood-brain barrier, allowing treatment of neurological pathology (European Medicines Agency, 2016). Although miglustat was initially approved for the treatment of Type I Gaucher disease (Cox et al., 2000), it has also shown beneficial effects in NP-C animal models by reducing storage material and significantly slowing neurodegeneration and disease progression (Zervas et al., 2001b, Lachmann et al., 2004, te Vruchte et al., 2004, Stein et al., 2012). Several clinical trials involving NP-C patients have subsequently been carried out (Patterson et al., 2007, Patterson et al., 2010, Wraith et al., 2010), as well as multicentre observational retrospective cohort studies (Pineda et al., 2009). Generally, miglustat treatment resulted in the deceleration or stabilisation of key individual neurological manifestations after 6 - 12 months of treatment, including improvements in ambulation, manipulation, language and swallowing (Walterfang et al., 2012, Lyseng-Williamson, 2014). Benefits of miglustat were also generally better in patients with older onset of neurological manifestations, especially when administration was started in the early stages of disease progression (Santos-Lozano et al., 2015, Papandreou and Gissen, 2016). The use of miglustat has subsequently been approved for the treatment of neurological manifestations in both paediatric and adult NP-C patients in a number of countries including the EU, Australia, Brazil, Canada, Japan, Russia, Switzerland and South Korea, however the Food and Drug Administration have not approved its use in the USA. The main side effects of miglustat treatment are primarily tolerability issues relating to gastrointestinal affects, such as diarrhoea, flatulence, abdominal pain, nausea and vomiting. 80% of

patients present these side effects accompanied by mild to moderate weight loss in the first 6 months of treatment, which then decreased to 50 - 60% (Remenova et al., 2015). These gastrointestinal effects are attributed to suboptimal hydrolysis of carbohydrates and osmotic diarrhoea, due to the inhibition of intestinal disaccharidase enzymes (Belmatoug et al., 2011, Papandreou and Gissen, 2016). The most common cause of miglustat treatment discontinuation is due to these gastrointestinal side effects (Belmatoug et al., 2011, Lyseng-Williamson, 2014).

A recent promising candidate for NP-C treatment is the starch derivative 2-hydroxypropyl- $\beta$ -cyclodextrin (HP- $\beta$ -CD). Cyclodextrins are a group of oligosaccharides that form a cone-like structure with a hydrophobic core and hydrophilic exterior, allowing the formation of water-soluble complexes with otherwise hydrophobic compounds (Pitha et al., 1988). It was initially given as an excipient with allopregnanolone to *Npc1*<sup>-/-</sup> mice (Griffin et al., 2004), however it was later identified that the beneficial effects of decelerated neurodegeneration and reduced lipid storage were mainly due to HP- $\beta$ -CD (Davidson et al., 2009, Liu et al., 2009). HP- $\beta$ -CD is thought to bind unesterified cholesterol that accumulates in late endosomes/lysosomes of NP-C cells and facilitate its egress (Rosenbaum et al., 2010), however the exact mechanism by which HP- $\beta$ -CD affects cholesterol trafficking and neurodegeneration is unknown. It has been proven that HP- $\beta$ -CD does not cross the blood-brain barrier efficiently (Pontikis et al., 2013) and as a result is most effective in decelerating neurological disease progression when administered directly into the cerebrospinal fluid (Vance and Karten, 2014, Vite et al., 2015). Systemic delivery via subcutaneous or intravenous administration of HP- $\beta$ -CD resulted in amelioration of visceral liver pathology in the feline model of NP-C, however the higher doses necessary to affect neurological pathology resulted in pulmonary toxicity (Vite et al., 2015). Although HP- $\beta$ -CD demonstrates a moderate half-life, the lack of movement across the blood-brain barrier results in the need for delivery to the cerebrospinal fluid via lumbar puncture or ommaya reservoir every one to two weeks. Continual invasive administration is accompanied by a side effect of high frequency hearing loss due to ototoxicity (Ward et al., 2010, Matsuo et al., 2013, Maarup et al., 2015). Analysis of HP- $\beta$ -CD treatment efficacy and safety in NP-C patients until now has been limited to individual cases (Matsuo et al., 2013, Maarup et al., 2015), however clinical trials with intrathecal delivery (Phase I

ClinicalTrials.gov Identifier: NCT01747135, Phase II/III ClinicalTrials.gov Identifier: NCT02534844) and intravenous delivery (Phase I ClinicalTrials.gov Identifier: NCT02939547, Phase I/II ClinicalTrials.gov Identifier: NCT02912793) are currently underway.

As a high amount of NP-C cases are caused by mutations causing NPC1 misfolding and subsequent degradation, the use of chaperone protein based therapy may be beneficial to NP-C patients. The small molecular drug arimoclomol induces expression of molecular chaperones from the heat shock protein 70 family, thought to be involved in cellular protein repair pathways, thereby protecting pathologically challenged cells (Muchowski and Wacker, 2005). These molecular chaperones have also been linked to the folding and activity of NPC1 (Nakasone et al., 2014), and their upregulation via arimoclomol has subsequently shown efficacy in reducing lipid accumulation in NPC1 deficient cells (Kirkegaard et al., 2010) and moderate amelioration in both visceral and neurological pathology in the *Npc1*<sup>-/-</sup> mouse model (Kirkegaard et al., 2016). An observational study in NP-C patients is currently underway, which is being followed by a phase II/III clinical trial (ClinicalTrials.gov Identifier: NCT02612129).

Histone deacetylase inhibitors represent another potential proteostatic therapy for NP-C. Histone deacetylase enzymes are involved in a number of cellular processes by influencing transcription regulation and have previously been used for various brain and neurodegenerative disorders (Kazantsev and Thompson, 2008, Haberland et al., 2009). The orally available histone deacetylase inhibitor, vorinostat, has shown to ameliorate cholesterol homeostasis in NP-C patient cells and a phase I/II clinical trial is currently in progress (ClinicalTrials.gov Identifier: NCT02124083).

Other treatment options that have shown promise for NP-C include: acetyl-DL-leucine, a natural amino acid derivative, previously shown to have a beneficial effect in patients with cerebellar ataxia (Strupp et al., 2013) and recently several NP-C patients (Bremova et al., 2015), and curcumin, the active ingredient of turmeric, which has been shown to normalise Ca<sup>2+</sup> homeostasis and lipid storage in *Npc1*<sup>-/-</sup> mice, leading to a significant increase in the survival of *Npc1*<sup>-/-</sup> mice (Lloyd-Evans et al., 2008).

### 1.3.8 NP-C Animal Models

Animal models are crucial tools used for understanding disease biology and therapeutic testing. Due to the highly conserved nature of the *NPC1* gene (Blom et al., 2003), a variety of NP-C models from yeast to cats have been characterised or developed for analysis. The most commonly used and well-characterised NP-C model is the *Npc1<sup>nih</sup>* mouse (BALB/cNctr-*Npc1<sup>min</sup>*/J, referred throughout this study as *Npc1<sup>-/-</sup>* mouse) (Pentchev et al., 1980). Genetic analysis of these mice revealed a large spontaneous frameshift mutation, via an insertion of 1,100bp and deletion of 800bp from the *Npc1* gene, ultimately knocking out the majority of the *Npc1* gene (Loftus et al., 1997). This mutation results in minimal expression of truncated *Npc1* mRNA and no measurable levels of murine NPC1 expression in the *Npc1<sup>-/-</sup>* mouse model (Elrick et al., 2010). The *Npc1<sup>-/-</sup>* mouse model recapitulates many of the neuropathological features of human NP-C disease, with a rapid disease progression suggesting late infantile or juvenile form of NP-C disease. *Npc1<sup>-/-</sup>* mice exhibit no apparent symptoms until 4 weeks of age, however initial locomotor and behavioural deficits develop from 5 weeks of age. Disease progress is characterised by impaired gait, noticeable tremor and significant loss in weight from 7 - 10 weeks of age and death occurs from 10 - 12 weeks of age (Smith et al., 2009). Human neuropathology is also mirrored on the cellular level, with severe neurodegeneration and neuroinflammation, particularly in the cortex, thalamus, substantia nigra and the cerebellum (Elrick et al., 2010, Pressey et al., 2012). Accumulation of cholesterol and glycosphingolipids comparable to the human form of NP-C has been reported in the *Npc1<sup>-/-</sup>* mouse, with extreme elevation of sphingoid bases, ceramide and GM2 gangliosides in the liver, compared to sphingoid bases and GM2 and GM3 gangliosides in the brain (Pentchev et al., 1980, Fan et al., 2013).

Recently other variant NP-C mouse models have been created or identified in an attempt to reflect other forms of the disease, such as the C57BL/6J-*Npc1<sup>-/-</sup>*, where the transferring of the BALB/c *Npc1<sup>nih</sup>* mutation to a C57BL/6 background resulted in a more severe form of the disease, particularly in the viscera (Parra et al., 2011). As a high amount of NP-C cases occur due to missense mutations in the *NPC1* gene (Carstea et al., 1997, Bauer et al., 2002, Park et al., 2003), several NP-C mouse models with common missense mutations have been created (Maue et al., 2012,

Praggastis et al., 2015). These mutations result in misfolding of the NPC1 protein, rather than a complete loss of NPC1 expression, allowing the testing of proteostatic therapies such as chaperone therapy or histone deacetylase inhibition (Praggastis et al., 2015). These models are characterised by slower disease progression, comparable to later onset forms of NP-C. A range of studies has also been carried out in conditional *Npc1* mutant mice, with the aim of analysing the effect of NPC1 loss in specific cell populations or organ compartments. These studies have led to the conclusion of cell autonomous neurodegeneration, where expression of NPC1 in neurons was critical for cell survival and isolated NPC1 expression in glial cells demonstrated no or minimal effect on neurodegeneration (Ko et al., 2005, Elrick et al., 2010, Lopez et al., 2011, Yu et al., 2011).

A feline model of NP-C has also been characterised (Lowenthal et al., 1990, Brown et al., 1994), which is the result of a spontaneous missense mutation (2864G-C) (Somers et al., 2003) to *Npc1*, leading to neurovisceral pathology and lipid accumulation comparable to human NP-C (Vite et al., 2008). Other available NP-C models include yeast (Malathi et al., 2004), *Caenorhabditis elegans* (Sym et al., 2000), *Drosophila melanogaster* (Huang et al., 2005) and zebrafish (Schwend et al., 2011).

## 1.4 Gene Therapy

Gene therapy is defined by the European Medicines Agency as a therapy generally consisting of a vector or delivery system containing a genetic construct. This construct may be engineered to express a specific sequence or protein responsible for the regulation, repair, addition or deletion of a genetic sequence. Additionally, the therapeutic, prophylactic or diagnostic effects relate directly to either the recombinant nucleic acid sequence or to the protein product of the genetic construct. Recent rapid advances and successes in the field of nucleic acid delivery have attracted substantial scientific and commercial interest. The potential use of gene therapy is vast, from genetic disorders such as haemophilia or lysosomal storage

disorders, acquired diseases such as cancer or neurodegenerative disorders, to use in vaccinations (Del Pozo-Rodriguez et al., 2016). Over 1,800 ongoing or completed gene therapy clinical trials have been approved and while the majority focus on cancer therapy, the second largest disease group is monogenic disorders (Wirth et al., 2013, Abedia.com, 2017). Monogenic disorders are in theory ideal candidates for gene therapy, as the delivery and subsequent expression of the single defective gene will result in the treatment of the disease. Successes have been fuelled by improvements in our understanding of the defective mechanisms and pathology of these disorders, combined with advances in genetic engineering and virology. Gene delivery is achieved by the use of a vector system, categorised as either viral or non-viral, where the aim is efficient gene delivery to the correct site of action, while also minimising potential adverse effects. The following sections aim to introduce the field of viral vector mediated gene therapy and the use of viral vectors for the treatment of neurovisceral lysosomal storage disorders, including its potential use for Niemann-Pick Type C.

## 1.5 Viral Vectors

Viruses naturally represent appealing tools for gene delivery as they have evolved to efficiently deliver their genes in the form of either ribonucleic acid (RNA) or deoxyribonucleic acid (DNA) into mammalian cells. Viruses can differ by their viral particle structure, genome structure and composition, replication cycle and method of immune system evasion. Depending on the virus, the ultimate aim of infection may also differ, from hijacking host cell machinery for replication, killing the host cell in the process, such as with adenoviruses or herpes simplex viruses, to laying dormant in cells by integrating into the host genome, such as with adeno-associated viruses or lentiviruses. As viruses are ultimately pathogenic agents, their use for gene delivery requires their attenuation to be safely used in clinical applications. The results are known as recombinant viral vectors, where pathogenic and viral sequences unnecessary for viral vector transduction are removed, allowing the replacement with a therapeutic expression cassette. Despite the large number of viral families only a

small number of viruses have been extensively characterised and utilised for gene delivery. Currently, the most commonly used viral vectors are adenoviral, retroviral or lentiviral and adeno-associated viral vectors, each with their own advantages and disadvantages depending on the gene therapy target and requirement (**Table 2**). The efficiency of viral vectors is reflected by the fact that over 70% of all gene delivery vectors in gene therapy clinical trials are viral vector based (Ginn et al., 2013, Abedia.com, 2017). Early setbacks in the field of viral vector mediated gene therapy have forced the advancement in understanding the risks, characteristics and capabilities of viral vector gene delivery. These lessons have led to a series of successful and clinically promising clinical trials and commercialisation of the first viral vector gene therapy product.

Vector	Adenoviral	$\gamma$ -Retroviral	Lentiviral	Adeno-associated viral
Family	<i>Adenoviridae</i>	<i>Retroviridae</i>	<i>Retroviridae</i>	<i>Parvoviridae</i>
Particle size (nm)	70 - 120	100	100	20 - 25
Genome	dsDNA	RNA	RNA	ssDNA
Packaging capacity (kb)	8 - 10	7 - 8	7 - 9	4.7
Vector yield (vp/ml)	$1 \times 10^{12}$	$1 \times 10^9$	$1 \times 10^9$	$1 \times 10^{13}$
Chromosomal integration ?	No	Yes	Yes	Minimal
Infects post-mitotic cells?	Yes	No	Yes	Yes
Immunogenicity	High	Low	Low	Low
Insertional mutagenesis risk	None	High	Medium	Low

**Table 2: Summary of the characteristics of the most commonly used viral vectors for gene therapy.**

Adapted from (Choudhury et al., 2016).

### 1.5.1 Adenoviral vectors

In terms of the overall number of clinical trials, adenovirus based vectors have been the most widely used viral vectors, with a total of 23% of trials until 2012 utilising adenoviral vectors (Ginn et al., 2013). Adenoviruses are a family of non-enveloped

viruses with a relatively large, linear and double stranded DNA genome, which is packaged inside an icosahedral nucleocapsid. With over 57 distinct serotypes, adenoviruses have a wide range of tropism with the ability to infect an extensive range of organisms, often characterised by moderate to severe pathogenicity (Arnberg, 2012). Adenoviral vectors have been a popular choice as certain serotypes such as hAd2 and hAd5 are well characterised, they do not integrate into the host genome (Harui et al., 1999), are easily purified to high titres, can transduce a wide variety of both dividing and non-dividing cells and have a packaging capacity of up to 37 kilobase (kb) (Bett et al., 1993). Studies directly delivering adenoviral vectors to the brain also demonstrated promising long-term transduction in both neurons and glial cell populations (Akli et al., 1993, Davidson et al., 1993, Barcia et al., 2007). A major limitation associated with adenoviral administration *in vivo* is their capsid immunoreactivity, shown to be a result of their strong activation of host innate immune system (Appledorn et al., 2008, Tian et al., 2009). Additionally, due to the ubiquitous nature of wild-type adenoviral infections within populations, pre-existing neutralising antibodies can be a major obstacle and risk (Burgert et al., 2002). Although this antigenicity may be beneficial for adenoviral vector use as an immunogenic adjuvant, the high doses required for *in vivo* delivery can result in extreme inflammation and cytotoxicity. These dangers were demonstrated in an extreme case, where administration of an adenoviral vector for the treatment of ornithine transcarbamylase deficiency resulted in the death of a patient (Marshall, 1999). Additionally, these host immune responses can often result in transient transgene expression *in vivo* (Stein et al., 1998, Yang et al., 1996).

While adenoviral vectors remain popular for use in certain situations, such as cancer therapy, the development of new strategies limiting the extent of immunogenicity for direct gene delivery *in vivo* is crucial (Sheridan, 2011). Examples of such approaches include development of ‘guttled’ helper-dependent adenoviral vectors that lack all viral genes (Palmer and Ng, 2005), and the identification of alternative serotype-based vectors shown to evade pre-existing immunity. Canine adenovirus serotype 2 (CAV-2) is a promising alternative adenovirus serotype that has shown non-significant levels of pre-existing neutralising antibodies in 98% of samples from a randomised cohort and also does not show cross-reactivity with ubiquitously present human adenovirus neutralising antibodies (Kremer et al., 2000). CAV-2 vectors have

also been reported to reduce innate immunoreactivity, compared to human Ad5 vectors (Soudais et al., 2004). The potential use of CAV-2 for the treatment of Niemann-Pick Type C1 via direct cerebrospinal fluid administration is evaluated in this study.

## 1.5.2 Lentiviral and retroviral vectors

Lentiviruses and  $\gamma$ -retroviruses are part of the *Retroviridae* family, where a linear single stranded RNA genome (**Figure 5A**) is packaged into an isometric capsid surrounded by a spherical envelope consisting of a combination of glycosylated viral proteins (Burns et al., 1993, Tang et al., 1999). Following entry into a cell, the RNA genome is translated to produce viral reverse transcriptase and integrase proteins, which combine to synthesis double stranded DNA copies of the RNA viral genome that is subsequently integrated into the host genome. On the one hand, this stable integration into the host genome can be of great advantage, as integration leads to long-term expression in both the originally transduced cell and any resulting progeny. *Ex vivo* gene therapy modification of hematopoietic stem cells with retroviral and lentiviral vectors utilises this system for therapeutic effect (Cavazzana-Calvo et al., 2000, Aiuti et al., 2013, Biffi et al., 2013). On the other hand, integration events can also result in insertional mutagenesis by disrupting or upregulating host genes. Where these two viruses differ is their preferred sites of integration and their ability to transduce dividing and non-dividing cells (Matrai et al., 2010).  $\gamma$ -retroviral vectors are only capable of transducing and integrating into dividing cells and their integration has been shown to preferentially target active genes and regional hotspots, specifically within a 5-kilobase pair window either side of the transcription start site (Schroder et al., 2002, Schwarzwaelder et al., 2007). The potential extreme dangers of such integration were demonstrated by the development of a leukaemia-like disorder in 4 patients administered with  $\gamma$ -retroviral based vectors for the treatment of X-linked severe combined immune deficiency (Hacein-Bey-Abina et al., 2003, Hacein-Bey-Abina et al., 2008). Analysis showed that these leukaemia-like disorders were the result of uncontrolled clonal T cell proliferation, due to integration events near proto-oncogenes *LMO2* and *BM11*.

In comparison, lentiviral vectors are capable of transducing both dividing and non-dividing cells, and while integration into the host genome does occur, they demonstrate a relatively randomised integration preference (Schroder et al., 2002, Montini et al., 2006). Although lentiviral integration events are still more likely to occur around actively transcribed areas, they have been reported to not show any preference for integration in the immediate proximity of transcription start sites. Additionally the development of self-inactivating vectors has further reduced the potential side effects of insertion (Miyoshi et al., 1998, Zufferey et al., 1998). In self-inactivating vectors a deletion in the 3' lentiviral long terminal repeat (LTR region) results in the loss of intrinsic LTR promoter activity, which previously may have interfered with host gene regulation (**Figure 5B**). This modification also demonstrated a reduction of vector genomic RNA generation in host cell and viral insert silencing *in vivo*. While the risk of insertional mutagenesis remains present with integrating lentiviral vectors, the statistical probability of such events are significantly reduced, as demonstrated by their common and therapeutic use in *ex vivo* clinical trials and *in vivo* preclinical studies (Biffi, 2016). Recently, integrase-defective non-integrating lentiviral vectors have been designed, which eliminate the danger for insertional mutagenesis at the potential cost of stable long-term transgene expression (Vargas et al., 2004, Yanez-Munoz et al., 2006).

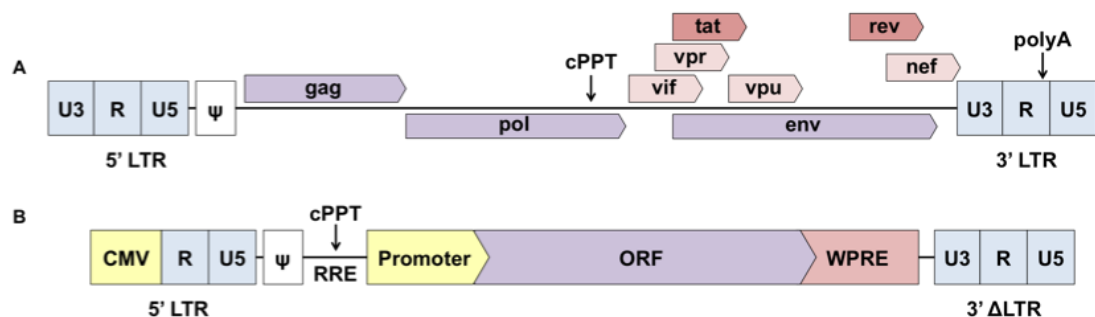


**Figure 5: Illustrations of the HIV-1 viral genome and recombinant lentiviral vector genome.**

- (A) Illustration of HIV-1 (lentiviral) genome organisation with all proviral-coding sequences.
- (B) Illustration of a current generation self-inactivating recombinant lentiviral vector, with LTR modifications, crucial cis-acting elements and inserted transgene cassette. ORF, open reading frame; WPRE, woodchuck hepatitis virus post-transcriptional regulatory element; polyA, polyadenylation signal sequence.

Current generation non-replicating lentiviral vectors are based on the HIV-1 virus, but have been extensively modified for optimal transgene expression and safety, by the removal of specific viral genome sequences associated with pathogenicity. This includes the removal of lentiviral genes essential for replication (*pol*), capsid production (*gag*) and envelope packaging (*env*), along with a combination of accessory genes (*vpu*, *vif*, *vpr*, *nef* and *tat*). The resulting vector backbone only contains the modified 5' and 3' LTR, and packaging signal element ( $\Psi$ ) as remaining HIV-1 elements, with a moderate packaging capacity of 11kb (Kumar et al., 2001). These vectors can only replicate and produce fully functioning viral particles in the presence of these removed genes, which are provided in *trans* to cells during viral vector production. The viral envelope plays a crucial role in the tropism and transduction efficiency of lentiviral vectors. One of the most widely used lentiviral envelope is pseudotyped and contains the *gag* sequence from the completely independent vesicular-stomatitis virus. The resulting lentiviral pseudotyped vesicular-stomatitis virus G-protein (VSV-G) envelope produces a combination of broad tissue and cell tropism following *in vivo* administration, while also allowing high viral titre purification during vector production (Burns et al., 1993, Mochizuki et al., 1998, Sena-Esteves et al., 2004). During this study the potential use of a VSV-G pseudotyped self-inactivating lentiviral vector for NP-C therapy is evaluated following *in vivo* administration directly into the cerebrospinal fluid.

### 1.5.3 Adeno-associated viral vectors

Adeno-associated virus (AAV) was originally identified as a contaminant during a laboratory production of adenovirus (Atchison et al., 1965) and has been subsequently classified as part of the *Parvoviridae* family, a family that is characterised by their relatively small and simplistic nature. Within the *Parvoviridae* family, AAV belong to the genus *Dependoparvovirus*, which for replication and virion production are dependent on a co-infection with a helper virus, such as adenovirus or herpesvirus (Casto et al., 1967, Buller et al., 1981). In the absence of a helper virus, wild-type AAV may remain quiescent by site specific integration at a targeted locus on human chromosome 19 (Kotin et al., 1992). No human pathology has been reported to be associated with AAV infection (Dismuke et al., 2013).

AAVs contain a relatively small 4.7kb single stranded (ss) DNA genome, which is packaged within an icosahedral, non-enveloped capsid. The wild-type AAV genome structure contains two 145bp short inverted terminal repeat (ITR) sequences at the 5' and 3' ends of the viral genome, which flank the two multi-cistronic coding regions *rep* and *cap* (Koczot et al., 1973). Base-pairing between the palindromic regions in AAV ITRs results in a T-shaped secondary structure, which is crucial for both AAV origin of replication and conversion of viral ssDNA genome into double-stranded (ds) DNA necessary for viral gene for expression (Weitzman and Linden, 2011). The *rep* gene encodes a group of 4 Rep proteins (Rep78, Rep68, Rep52 and Rep40), which are expressed via alternative promoters and as splice variants (Qiu and Pintel, 2008). The Rep proteins are involved in viral genome replication, integration and genome packaging into readily synthesised empty capsids (Surosky et al., 1997, King et al., 2001). Both the sense and antisense ssDNA strands of the replicated viral genome are packaged into separate virions with identical efficiency (Berns and Adler, 1972). The *cap* gene encodes AAV capsid proteins VP1, VP2 and VP3 (Becerra et al., 1988), together with a group of other viral proteins that traffic and assemble these capsid proteins during capsid synthesis (Naumer et al., 2012). The final icosahedral capsid consists of 60 copies of the three AAV capsid proteins VP1:VP2:VP3 in a 1:1:10 ratio, with variations to the VP3 protein structure thought to determine AAV receptor usage and viral serotype (Weitzman and Linden, 2011) (**Table 3**).

Serotype	Origin	Primary receptor	Co-receptor	Capsid homology to AAV2 (%)	NAbs in humans (%)
AAV1	NHP	$\alpha$ 2,3/ $\alpha$ 2,6 N-linked SA	?	83	67
AAV2	Human	HSPG	HGFR, LamR, FGFR-1, Integrin	100	72
AAV3	NHP	HSPG	FGFR-1, integrin, HGFR, LamR	88	?
AAV4	NHP	$\alpha$ 2,3/ $\alpha$ 2,3 O-linked SA	?	60	?
AAV5	Human	$\alpha$ 2,3/ $\alpha$ 2,3 N-linked SA	PDGFR	57	40
AAV6	Human	$\alpha$ 2,3/ $\alpha$ 2,6 N-linked SA, SA/HSPG	EGFR	83	46
AAV7	NHP	?	?	82	?
AAV8	NHP	?	LamR	83	38
AAV9	Human	N-linked Galactose	LamR	82	47

**Table 3: Summary of principle characteristics for AAV serotypes 1 - 9.**

NHP, non-human primate; ?, unknown; HGFR; hepatocyte growth factor receptor; LamR, laminin receptor; FGFR1, fibroblast growth factor receptor 1; HSPG, heparin sulphate proteoglycan; EGFR, epidermal growth factor receptor; PDGFR, platelet-derived growth factor receptor; NAb, neutralising antibodies. Adapted from (Lisowski et al., 2015) and (Saraiva et al., 2016).

The ubiquitous nature of AAV in humans is demonstrated by the identification of 12 natural serotypes and over 100 distinct AAV isolates from human or non-human primate origins (Gao et al., 2004). These 12 serotypes, defined by motifs in the capsid proteins that can be identified by specific neutralising antibodies, share between 51% and 99% identity in capsid amino acid sequence (Lisowski et al., 2014) (**Table 3**) and the general organisation of the viral genome is also maintained. The variation in the structure of exposed regions of the viral capsid proteins defines the interaction with the principal AAV receptors (**Table 3**) and intracellular trafficking pathways, which are central to viral tropism (Gao et al., 2003, Nonnenmacher and

Weber, 2012). Following cell surface receptor binding, the successful infection of AAV depends on a series of steps including endocytosis, escape from endosomal/lysosomal compartments, translocation to the nucleus and viral capsid uncoating, whereby the ssDNA genome is released for complementary strand synthesis and ultimately transcription from the now dsDNA viral genome (Weitzman and Linden, 2011, Balakrishnan and Jayandharan, 2014). Characterisation studies of these naturally occurring AAV variants have demonstrated extremely diverse organ, tissue and cell tropism (White et al., 2011, Asokan et al., 2012).

The relatively simplistic structure of the wild-type AAV genome facilitated the production of recombinant AAV (rAAV) gene delivery vectors (**Figure 6**) (Daya and Berns, 2008). This is accomplished by the removal of viral coding sequences *rep* and *cap*, and replacing them with a desired expression cassette. Only the flanking ITRs remain from the original genome, as they contain the *cis*-acting sequences required for vector genome replication and packaging. Despite the removal of all viral genes, the packaging capacity of rAAV vectors remains extremely limited, as an expression cassette containing the minimum of a promoter, transgene and polyadenylation signal sequence together with flanking ITRs should not exceed the wild-type AAV genome length of 4.7kb to avoid packaging or truncation problems. The resulting viral vectors are non-replicating, so to achieve the necessary replication during vector production, the *rep* and *cap* genes are provided in *trans* together with other necessary adenoviral helper functions. As these vectors lack the viral Rep proteins necessary for host genome integration, the viral genome persists in an extra-chromosomal episomal form (Nakai et al., 2001). Insertional mutagenesis risk is therefore thought to be minimal, although these episomal vector genomes may be lost over time in actively replicating cell populations (Cunningham et al., 2008). Recent studies have reported that a small yet significant percentage of rAAV vector genomes can still achieve integration into the host genome, demonstrated by integration events within the liver of rAAV administered animals being associated with an increased occurrence of hepatocellular carcinoma (Donsante et al., 2007, Chandler et al., 2015). The potential seriousness of this risk in human patients currently remains unclear, however this factor should be taken into consideration, especially with higher dose administration.

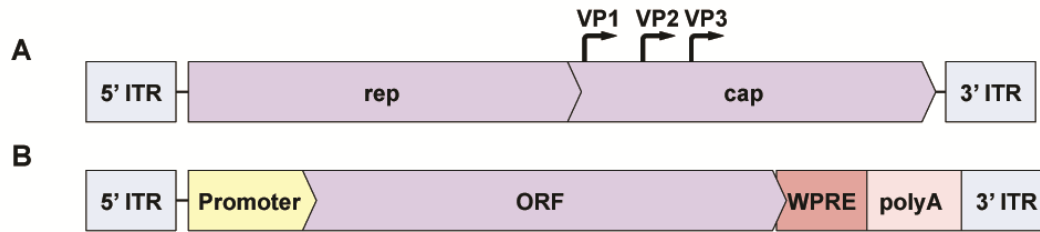


**Figure 6: Illustrations of wild-type AAV genome and rAAV vector genome.**

- (A) Illustration of wild-type AAV genome organisation with all proviral coding sequences. Arrows depict start of VP1, VP2 and VP3 open reading frames.
- (B) Illustration of current recombinant AAV vector, with crucial *cis*-acting inverted terminal repeat (ITR) regions flanking inserted transgene cassette. ORF, open reading frame; WPRE, woodchuck hepatitis virus post-transcriptional regulatory element; polyA, polyadenylation signal sequence.

The development of recombinant AAV vectors has allowed the cross-packaging of rAAV vector genomes into different AAV capsids, thereby creating pseudo-serotyped rAAV vectors (Rabinowitz et al., 2002). As capsid structure is a major factor in AAV tropism, the use or modification of different capsids can greatly benefit vector efficiency. This process has led to the AAV vector toolkit metaphor, where different rAAV vectors can be chosen for their specific tropism or properties, depending on organ, tissue or cell target (Asokan et al., 2012). The availability of capsids for selection is rapidly increasing, due to both continual isolation of naturally occurring AAV variants and the creation of engineered capsids. Capsid engineering in particular is thought to show promise for increased clinical benefit, as vectors can be tailored by rational design or directed evolution to specifically address the relevant aim or challenge. This can result in enhanced vector efficiency and specificity, thereby reducing both the administration dose necessary for clinical benefit and potential dose-related toxicity.

The combination of a lack in AAV associated pathogenicity, low integration rate, ability to purify rAAV at a high titer and wide vector tropism, has led to the emergence of rAAV vectors as extremely promising and extensively used viral vectors for *in vivo* gene delivery, in both preclinical studies (Mingozzi and High, 2011) and clinical trials (Ginn et al., 2013, Lisowski et al., 2015). In some successfully regarded recent trials, the use of rAAV resulted in the treatment of 3 distinct genetic disorders, including retinal degenerative disease Leber congenital amaurosis with rAAV2 (Maguire et al., 2008), blood clotting disorder haemophilia B

with rAAV2/8 (Nathwani et al., 2011) and lipoprotein lipase deficiency with rAAV1 (Stroes et al., 2008, Gaudet et al., 2013), which became the product Glybera, the first EU authorised and commercially available gene therapy treatment.

Although rAAV are non-pathogenic and show low immune activation compared to other viral vectors (Zaiss et al., 2002), certain clinical trial results have revealed potential immune challenges and how they affect transgene expression efficiency. As demonstrated in a phase I/II dose escalation study for haemophilia B, rAAV2 administration only resulted in transient expression of Factor IX for approximately 6 weeks (Manno et al., 2006). Further analysis revealed loss of expression was due to a capsid-specific CD8<sup>+</sup> T-cell response in transduced hepatocytes in a dose dependent manner (Mingozzi et al., 2007), which was mirrored by several other trials (Brantly et al., 2009, Mingozzi et al., 2009). This response may be a result of either pre-existing immunity in the form of neutralising antibodies or vector-induced cellular and humoral immunity (Hareendran et al., 2013). Natural exposure to wild-type AAVs lead to the generation of anti-AAV antibodies, with sero-positivity levels varying depending on the prevalence of certain serotypes (**Table 3**). Studies have also suggested possible cross-reactivity between closely related serotypes in terms of structural capsid homology (Calcedo et al., 2009). Relative titers of individual pre-existing neutralising antibodies can correlate with levels of transgene expression following rAAV administration (Manno et al., 2006). Interestingly for paediatric diseases, such as early infantile NP-C, comparative analysis of AAV2 and AAV8 neutralising antibody titers in humans revealed that titers were lowest from 7-11 months of age and increased significantly at adolescence (Calcedo et al., 2011). In comparison, adaptive immune responses to AAV can be targeted against either the viral capsid or against the protein being expressed from the vector. As part of vector internalisation, degradation of the viral capsid reveals antigenic peptides that can activate adaptive immunity via cross-presentation to major histocompatibility complex I molecules (Li et al., 2013). Targeting and presentation of epitopes within the viral vector encoded protein has also been shown to influence CD8<sup>+</sup> T-cell reactivity (Li et al., 2009).

The success or failure of a clinical trial and therapeutic efficacy may be affected by these factors, which has subsequently led to the development of strategies to avoid

immune responses against AAV vectors. Pre-screening of patients for the presence of neutralising antibodies is carried out for all trials, however this can lead to the exclusion of significant numbers of patients, which is especially problematic in rare diseases where patient numbers are limited. Transient immune-suppression of patients has been proposed as a potential approach (Adriouch et al., 2011, Sack et al., 2014), which may even allow secondary AAV administration (McIntosh et al., 2012). During the haemophilia B clinical trial, asymptomatic elevations in AAV capsid-induced aminotransferase levels following rAAV2/8 administration in two patients were controlled by a short course of glucocorticoids, without any apparent loss in transgene expression (Nathwani et al., 2011). The targeted delivery of vectors to immune-privileged sites, such as the eye, brain and to a certain extent the liver can also reduce potential adaptive immune response (Maguire et al., 2008, Breous et al., 2009, LeWitt et al., 2011). Tissue or cell specific promoters have also been used to reduce expression of the transgene to the specific target, thereby reducing antigen presentation for adaptive immunity (Ziegler et al., 2004, Nathwani et al., 2006). Finally modification or shielding of neutralising antibody epitopes on the viral capsid have also shown promise in reducing possible immune response, however this may affect vector tropism (Hareendran et al., 2013).

## 1.6 Non-viral gene delivery systems

Despite the recent successes in viral vector mediated gene therapy, the development of non-viral gene delivery systems remains attractive, due to their relatively simple and cheap production process, combined with a low safety profile. Additionally, there is no limitation to the size of genetic material that can be encapsulated and delivered. However, the major problem with current non-viral gene delivery systems is their extremely limited transfection efficacy *in vivo*. Despite these disadvantages, advances in efficiency, specificity and gene expression have resulted in an increase in the number of non-viral gene delivery systems entering clinical trials (Ramamoorth and Narvekar, 2015). The simplest form of a non-viral gene delivery approach is the use of naked DNA or RNA via physical methods, such as

electroporation, sonoporation or ballistic DNA. However, these methods are associated with poor transfection efficiency, rapid degradation and possible tissue damage. Other approaches use chemical carrier vectors to protect the nucleic acid cargo and promote gene delivery. These include inorganic particles, such as calcium phosphate and silica (Al-Dosari and Gao, 2009), and biodegradable compounds, such as lipid based, polymer based and peptide based vectors (Jin et al., 2014).

Lipid nanoparticles have recently become popular, due to their composition of physiological lipids that are already approved in pharmaceutical preparation for human use, complex stability and solvent-free production techniques (Del Pozo-Rodriguez et al., 2016). Hundreds of lipids have been developed, however they share a common structure of a positively charged hydrophilic head and a hydrophobic tail. Together with DNA or RNA, these lipid nanoparticles form compact lipoplexes and protect the cargo, as the positively charged head binds to the negatively charged nucleic acid. These lipoplexes then interact with negatively charged cell membrane proteins to induce cellular uptake (Rehman et al., 2013). The structure and ratio of lipids to nucleic acids determines the stability, toxicity and potential release of cargo upon endocytosis. Assuming uptake into the cell, these lipoplexes must overcome significant barriers in terms of endosomal escape, intracellular trafficking and access to the nucleus for transgene expression to occur. Recent studies with lipoplex-mediated gene delivery have demonstrated early indications of potential *in vivo* transfection efficacy, following direct administration at the target area in mouse models of retinal degeneration (Apaolaza et al., 2015) and neuroblastoma tumour (Tagalakakis et al., 2011). Despite the current lack of efficiency demonstrated by these non-viral vectors *in vivo*, a novel non-viral cationic lipid nanoparticle complex was evaluated in this study, in the context of direct cerebrospinal fluid administration.

## 1.7 Gene therapy for lysosomal storage disorders

Lysosomal storage disorders are generally considered as favourable candidates for gene therapy, due to a number of factors. Firstly, lysosomal storage disorders are

monogenic by nature, therefore the efficient delivery and expression of only a single gene should be necessary for treatment. This has also resulted in the development or identification of a wide range of animal models that accurately mimic human lysosomal storage disease pathology and progression, allowing critical preclinical gene therapy evaluation. Secondly, relatively minimal amelioration in the level of functional lysosomal enzymes beta-hexosaminidase A and arylsulfatase A (from 1 - 10%) has been shown to have significant therapeutic benefit on disease progression (Leinekugel et al., 1992). Patient data further supports this theory, as more severe infantile forms of lysosomal storage diseases generally demonstrate extremely low levels of enzyme activity (<1%), compared to the higher levels of enzyme activity (< 10%) exhibited in milder adult onset forms (Polten et al., 1991, Mechtler et al., 2012). The final factor is the mechanism of cross-correction therapy, whereby functional extracellular lysosomal protein secreted by transduced cells can be absorbed and subsequently trafficked to late endosomes and lysosomes in other cells, directly at their site of action (Fratantoni et al., 1968). The same principle is taken advantage of by enzyme replacement therapy, which is currently used for significant therapeutic effect in several lysosomal storage disorders. Therefore, although the hallmark of lysosomal storage disorders is the ubiquitous accumulation of storage material, the treatment of relatively small amounts of cells in certain organs or tissues could result in widespread benefits. These targeted tissues or organs could act as factories for functional lysosomal protein, which is subsequently released and delivered to diseased tissues and cells. Examples of the use of this mechanism are liver-directed gene delivery, resulting in distribution via the bloodstream following *in vivo* administration, or the *ex vivo* treatment of hematopoietic stem cells, which are then replanted back into patients and the subsequent differentiated cells containing the functional protein can be delivered directly to multiple organs (Biffi, 2016).

However, the mechanism of cross-correction is limited to soluble lysosomal enzymes found within the lumen of late endosomes/lysosomes. This is due to the process that endogenously synthesised lysosomal enzymes undergo for delivery to acidic compartments (Kaplan et al., 1977). The correct trafficking of lysosomal enzymes requires a series of post-translational modifications and protein-protein interactions (Kornfeld, 1992). After glycosylation in the endoplasmic reticulum, newly

synthesised lysosomal enzymes are phosphorylated in the Golgi apparatus at the 6 position of the terminal mannose residues (mannose-6-phosphate). Within the Golgi apparatus at standard physiological pH, mannose-6-phosphate receptors subsequently bind these phosphorylated lysosomal enzymes. These enzyme-receptor complexes are then trafficked to late endosomes/lysosomes, where the decrease in pH results in their dissociation, thereby releasing the protein into the late endosomal/lysosomal lumen for maturation. The isolated mannose-6-phosphate receptors are then either trafficked back to the Golgi apparatus for recycling or to the plasma membrane. A small portion of lysosomal enzyme has been shown to escape endosomal sorting and is subsequently sent to the cell membrane for exocytosis, resulting in its release into the extracellular space. Free mannose-6-phosphate receptors on the plasma membrane of cells can bind extracellular lysosomal proteins, which subsequently undergo endocytosis leading to their direct delivery to the site of action in late endosomal and finally lysosomal compartments (Achord et al., 1978, Dahms, 1996).

This secretion-recapture mechanism represents the basis of cross-correction therapy, which can be utilised by therapeutic strategies for lysosomal storage disorders caused by lysosomal enzyme deficiency. While certain non-enzyme soluble lysosomal proteins are sorted and trafficked via the mannose-6-phosphate receptor system (Hahn et al., 1998, Leimig et al., 2002), all membrane-bound and transmembrane lysosomal proteins, such as NPC1, are not (Sands and Davidson, 2006). This lack of cross-correction is thought to represent a major challenge for the development of effective gene therapy in these diseases, as correction of a cell would depend on direct transduction and gene expression. Ultimately, in the absence of cross-correction, amelioration of pathology is thought to require gene delivery to large numbers of cells.

Following the identification of lysosomal storage disorders as ideal candidates for the development of gene therapy, a vast number of preclinical studies utilising different approaches have been carried out in a range lysosomal storage disorder animal models. The therapeutic effects demonstrated in a number of these studies have resulted in a series of both completed and currently ongoing clinical trials within the field of gene therapy treatment for lysosomal storage disorders (**Table 4**). Initial preclinical studies in mouse models utilised the *ex vivo* gene therapy approach,

with retroviral and lentiviral vectors for lysosomal storage disorder treatment via gene therapy. The potential benefit of *ex vivo* gene therapy for these disorders is demonstrated by the fact that transplantation of haematopoietic stem cells from compatible donors has been carried out in patients with certain lysosomal storage disorders for over 20 years (Lund, 2013). In addition to therapeutic enzyme delivery in the viscera, these haematopoietic stem cells can also differentiate into cells that can cross the blood-brain barrier for therapeutic protein delivery to the central nervous system (CNS). Along with avoiding the challenge of finding a compatible donor, there are two other main advantages to the use of modified autologous cells rather than donor cells. Firstly, the significant reduction in the risk of graft-versus-host disease and secondly, enhanced therapeutic potential as viral gene delivery can result in supraphysiological levels of therapeutic lysosomal enzyme expression (Biffi, 2016). Preclinical studies in a variety of models have shown promising results in the clearance of storage material from both haematopoietic and non-haematopoietic cells, which translated to amelioration of neurological and visceral disease manifestations (Liang et al., 2007, van Til et al., 2010, Visigalli et al., 2010, Harrison et al., 2013, Wakabayashi et al., 2015). These studies also demonstrated that therapeutic efficacy correlated with enzyme expression levels and genetically engineered cells expressed higher therapeutic protein levels compared to standard donor cells, which was identified as a crucial factor in the prevention of neurological deficits.

Several early clinical trials utilised retroviral vector transduced autologous cells to treat Type I Gaucher disease (ClinicalTrials.gov Identifier: NCT00001234 and NCT00004294), Fabry disease (ClinicalTrials.gov Identifier: NCT00001234) and MPSII (ClinicalTrials.gov Identifier: NCT00004454) (Dunbar et al., 1998, Alexander et al., 2007, Byrne et al., 2012). While the relative safety of the procedure was confirmed with no severe adverse affects, low levels of therapeutic protein expression resulted in no improvement to disease pathology or progression. Following promising early studies in the mouse model for metachromatic leukodystrophy using novel lentiviral vectors (Biffi et al., 2004), a phase I/II clinical trial was carried out in three presymptomatic patients, where the lentiviral vector was used to deliver a functional copy of the *ARSA* gene (Biffi et al., 2013). The treated haematopoietic stem cells successfully engrafted within the patients, resulting in

stable ARSA protein expression at supraphysiological levels in haematopoietic lineages and in the cerebrospinal fluid. Assessment 24 months post-treatment in these patients suggested that the onset of disease had not progressed and further long-term evaluation will determine the complete clinical potential of this treatment. Combined with no adverse effects related to vector use, no significant immune response was observed against the transgene and therapeutic protein. This trial demonstrated the first successful use of *ex vivo* gene therapy for the treatment of a lysosomal storage disorder.

Taking the promise of this trial into account, there are still significant challenges for the treatment of lysosomal storage disorders by *ex vivo* gene therapy. The patients treated in the trial were diagnosed with the late infantile form of metachromatic leukodystrophy and treated before the development of disease manifestations. Previous experience with cell transplantation (Rovelli, 2008) indicates that this form of treatment in patients with more aggressive forms of lysosomal storage disorders or patients with prior disease progression may not be as effective, as therapeutic protein levels in visceral and central nervous system tissues can take months to increase following treatment. Toxicity or immune response to high levels of the therapeutic protein systemically must also be taken into account (Gentner et al., 2010), as supraphysiological levels of the therapeutic protein are needed for the amelioration of both visceral and especially neurological pathology. As therapeutic efficacy is linked to enzymes levels, lysosomal storage disorders with severer neurological disease may require high levels of transgene expression, although there have been attempts at restricting therapeutic protein expression to specific tissues (Sergijenko et al., 2013). For optimal engraftment of haematopoietic stem cells, preconditioning of the host also has to be carried out to a certain degree. Finally, as with enzyme replacement therapy, only diseases due to a deficiency in a soluble lysosomal enzyme that can take advantage of cross-correction will be viable targets for *ex vivo* gene therapy. Disorders caused by the loss of other lysosomal protein functions, such as NPC1 for Niemann-Pick Type C, will require *in vivo* administration.

Disease	Vector	Gene	Delivery	Phase	Clinical Trial
Metachromatic leukodystrophy	Lentivirus	<i>ARSA</i>	HSCT	I/II	NCT01560182
Fabry	Retrovirus	<i>GLA</i>	HSCT	I	NCT00001234
MPSII	Retrovirus	<i>L2SN</i>	HSCT	I/II	NCT00004454
Gaucher Type I	Retrovirus	<i>GBA</i>	PBSC	I	NCT00004294
MPS IIIa	AAV9	<i>SGSH</i>	IV	I/II	NCT02716246
MPS IIIa	AAVrh10	<i>SGSH, SUMF1</i>	IC	I/II	NCT01474343 NCT02053064
MPSIIIb	AAV5	<i>NAGLU</i>	IC	I/II	ISRCTN19853672
Metachromatic leukodystrophy	AAVrh10	<i>ARSA</i>	IC	I/II	NCT01801709
Neuronal Ceroid Lipofuscinosis	AAV2	<i>CLN2</i>	IC	I	NCT00151216
Neuronal Ceroid Lipofuscinosis	AAVrh10	<i>CLN2</i>	IC	I/II	NCT01414985 NCT01161576
Neuronal Ceroid Lipofuscinosis	AAV9	<i>CLN6</i>	IT	I/II	NCT02725580
Pompe	AAV9	<i>GAA</i>	IM	I	NCT02240407
Pompe	AAV1	<i>GAA</i>	IM	I/II	NCT00976352

**Table 4: Completed and ongoing clinical trials using gene therapy for the treatment of lysosomal storage disorders.**

Data collected from the U.S. National Institutes of Health clinical trial database (<https://clinicaltrials.gov/> on 20-12-2016). HSCT, *ex vivo* transduction and haematopoietic stem cell transplant; PBSC, *ex vivo* transduction and peripheral blood stem cell transplantation; IV, intravenous; IC, intracerebral; IT, intrathecal; IM, intramuscular.

*In vivo* gene therapy refers to the direct injection of a gene delivery vector to a certain tissue or circulatory system and has been successfully applied in a series of lysosomal storage disorder animal models and is also currently being translated into clinical trials (**Table 4**). Early studies demonstrated the potential of this approach with the delivery of lentiviral or rAAV vectors targeted towards the liver, either via intravenous or direct tissues administration. Therapeutic efficacy was due to the liver acting as a source of the therapeutic protein, which resulted in significant therapeutic protein expression throughout other peripheral organs via cross-correction (Gao et al., 2000, Mango et al., 2004, Liu et al., 2005b, Ma et al., 2007). A comparison study in a mouse model of MPSVI revealed this gene therapy approach to be as effective as enzyme replacement therapy, with the added benefit of only a single administration (Ferla et al., 2014). However, pathology in MPSVI is limited to the viscera, unlike the majority of lysosomal storage disorders that are also characterised by progressive neurological disease. The major disadvantage to liver directed gene therapy, as with enzyme replacement therapy, is the limited movement of therapeutic protein across the blood-brain barrier to allow delivery to the CNS. While there have been efforts to enhance the transit of therapeutic protein across the blood-brain barrier, such as fusion with trans-blood-brain barrier active motifs (Boado et al., 2013), liver directed gene therapy approach may not be sufficient for the amelioration of the severe neurological pathology exhibited by most lysosomal storage disorders.

### 1.7.1 Gene delivery to the CNS

The crossing of therapeutic protein across the blood-brain barrier following either enzyme replacement therapy, *ex vivo* or liver targeted gene *in vivo* gene therapy is inefficient. As a result, there are many neurovisceral lysosomal storage disorders with no or limited treatment options and the main obstacle in treating this class of disorders is overcoming the blood-brain barrier (BBB) to deliver therapeutic protein to cells in the central nervous system. Although there are exceptions, the majority of viral vectors have also been shown to be ineffective at crossing the mature BBB following intravenous administration, which has resulted in the development of a series of different approaches for effective gene delivery to the CNS.

The most obvious approach at bypassing the BBB and treating neurological pathology by gene therapy is the direct administration of recombinant viral vectors into CNS compartments, which can be accomplished by injection into the brain parenchyma or into the cerebrospinal fluid. Although direct administration of viral vectors via intracranial injections into the parenchyma of the brain is an intrusive and complex procedure, its use has been investigated in the context of treating lysosomal storage disorders, which has also progressed into several clinical trials (**Table 4**). Early studies utilised lentiviral, rAAV2 and rAAV5 vectors, due to their known neurotropic tropism, with injections targeting specific brain regions, such as the hippocampus, putamen and striatum. The rationale behind this approach was cross-correction of both nearby and distal cells from secretion of the therapeutic lysosomal enzyme from locally transduced cells. Certain AAV serotypes have also been demonstrated to undergo axonal transport allowing even broader distribution (Salegio et al., 2013). Although successful transduction of both neuronal and glial cells was observed, the spread from the site of injection was limited with rAAV2, rAAV5 and to an even lesser extent with lentiviral vectors (Consiglio et al., 2001, Brooks et al., 2002, Cressant et al., 2004, Sevin et al., 2006). Cells at the site of injection demonstrated some form of correction, however the lack of spread resulted in a therapeutic gradient (Cachon-Gonzalez et al., 2006). The identification and characterisation of other AAV serotypes has led to significant improvements in viral vector spread following intracranial injection. AAV9 and AAVrh10 based vectors in particular have shown promise, due to not only improved spread, but also their highly efficient axonal transport (Cearley and Wolfe, 2007, Piguet et al., 2012). Administration into areas with divergent connections, including the thalamus, cerebellar nuclei and ventral tegmental area have also reportedly shown enhancement of vector spread (Dodge et al., 2005, Cearley and Wolfe, 2007, Salegio et al., 2010, Bu et al., 2012). Despite these improvements, multiple bilateral intraparenchymal injection sites have been necessary to show therapeutic efficacy in lysosomal storage disease animal models (Cheng, 2014). These lessons have been carried through to clinical trials (**Table 4**), such as where patients treated for MPSIIIa with an AAVrh10 vector received 12 simultaneous intracranial injections into the white matter of the basal ganglia (Tardieu et al., 2014). This trial demonstrated significantly improved safety profile compared to previous trials for neuronal ceroid

lipofuscinosis (*CLN2*) (Worgall et al., 2008), with no adverse outcomes, however the numbers were too small to show significant therapeutic benefit. The question remains whether this approach will be or can be adapted to be sufficient for treating the neurological manifestations of lysosomal storage disorders. The practicality of additional injection sites if necessary must also be taken into account, as each further site adds potential risk to the procedure (Souweidane et al., 2010).

A less invasive and less spatially restricted approach for CNS delivery is the infusion of vector into the cerebrospinal fluid, either via intracerebroventricular (ICV) or intrathecal (IT) injection. Transduction of cells within the ventricular system, including ependymal cells, would result in the constant secretion of therapeutic protein throughout the cerebrospinal fluid (CSF) and neighbouring tissue, allowing widespread cross-correction potential similar to direct ERT delivery to the CSF (Kakkis et al., 2004, Chang et al., 2008, Dodge et al., 2009). The eventual drainage of the CSF into the venous system may also promote further systemic distribution (Haurigot et al., 2013). However, exclusive transduction of cells in the ventricular system would not be effective for non-soluble lysosomal proteins, such as NPC1 in Niemann-Pick Type C. The use of rAAV vectors that have demonstrated improved distribution following intraparenchymal injections, such as AAV9, results in the escape of vector out of the CSF into nearby tissue for even broader correction potential. Intracerebroventricular administration into neonatal mice has been reported to result in extensive widespread gene delivery in both neuronal and glial cell populations (Kim et al., 2014, McLean et al., 2014). Studies in adult and larger animal models have also demonstrated promising results of widespread gene delivery in multiple brain regions, following ICV rAAV9 vector administration (Samaranch et al., 2012, Haurigot et al., 2013, Meyer et al., 2015). ICV rAAV vector administration has also been evaluated in lysosomal storage disease animal models, demonstrated by rAAV1, rAAV2 and rAAV4 induced reduction in storage material throughout the brain of MPSVII mice (Elliger et al., 1999, Passini et al., 2003, Liu et al., 2005a), and amelioration of MPSIIIA neurovisceral pathology in both a murine (Ribera et al., 2015) and canine model (Haurigot et al., 2013), following ICV rAAV9 administration.

Direct delivery to the CSF can also be achieved by intrathecal administration into the intervertebral cistern of the spinal cord or the subarachnoid space in the cisterna magna. The rationale behind these approaches is identical to ICV administration, however the clinical procedures are less invasive. Intrathecal administration of rAAV has been reported to result in widespread and efficient transduction of motor neurons and dorsal root ganglia in the spinal cord, in both smaller and larger animal models (Bevan et al., 2011, Snyder et al., 2011, Dayton et al., 2012, Federici et al., 2012, Gray et al., 2013, Hordeaux et al., 2015). Promisingly, transduction of both neurons and glial cell populations could also be observed throughout the brain, with the brainstem demonstrating the highest transduction efficiency. In the context of lysosomal storage disorders, preclinical studies in mouse models of MPSI and MPSII administered intrathecally with rAAV2 and rAAV9 vectors respectively, resulted in regional reduction of storage material and brain pathology (Watson et al., 2006, Hinderer et al., 2016). Widespread CNS correction was also reported in a larger feline model of MPSI following intrathecal administration of rAAV9 (Hinderer et al., 2014), further supporting translation into the clinic.

Finally, an alternative and non-invasive strategy in delivering a viral vector to the CNS is the intravenous administration of vectors that have been demonstrated to cross the BBB. Studies have identified AAV serotypes AAV9 and AAVrh10 as the currently most effective serotypes at crossing the BBB, with widespread neuronal transduction in the CNS following intravenous administration in neonatal mice (Foust et al., 2009, Zhang et al., 2011). Subsequent studies demonstrated the successful transduction of neurons and astrocytes in both adult mice and non-human primates injected systemically with AAV9, however the efficiency was significantly reduced compared to neonatal animals (Duque et al., 2009, Gray et al., 2011b, Samaranch et al., 2012). Intravenous administration of rAAV9 has also been evaluated in lysosomal storage disorder models, with MPSIIIA and MPSIIIB treated adult mice and neonatally treated MPSI dogs demonstrating correction of neurological disease (Fu et al., 2011, Ruzo et al., 2012, Hinderer et al., 2015). While these studies have demonstrated therapeutic efficacy, it remains to be seen how effective this approach will be in upcoming clinical trials (**Table 4**). As the level of therapeutic protein has been shown to be crucial for CNS treatment efficacy, high systemic doses may be required to achieve the necessary influx of vector into the

CNS. This factor will be especially crucial for the treatment of lysosomal storage disorders that can't take advantage of cross-correction, such as Niemann-Pick Type C. The need for higher systemic vector doses subsequently increases the cost of trials and therapy, with the added the potential for immune response challenges, due to high levels of both vector and encoded protein in the viscera. Recent advances in the targeted evolution of AAV capsid variants has resulted in the development of a series of next generation rAAV vectors that show increased tissue specificity and transduction efficiency, which may reduce required doses (Lisowski et al., 2015). One variant in particular, AAV-PHP.B, demonstrated a 40-fold increase in CNS transduction efficiency compared to AAV9 when administered intravenously into adult mice (Deverman et al., 2016). While extremely promising, the tropism and efficiency of these novel rAAV vector variants in larger non-human primate models and ultimately patients remains to be evaluated.

## **1.8 Gene therapy for Niemann-Pick Type C disease**

Following these promising results of viral vector mediated gene therapy in preclinical studies for several lysosomal storage disorders and their current translation into clinical trials, the potential use of gene therapy is expanding to other and more challenging disorders. The therapeutic application of gene therapy to Niemann-Pick Type C1 has generally been considered to be especially challenging, as the NPC1 protein is a large non-secreted transmembrane protein that can't take advantage of mannose-6-phosphate receptor based secretion and recapturing (Vanier, 2010). In the absence of cross-correction, the amelioration of pathology in individual cells can only be achieved through direct viral vector transduction. Any gene therapy approach is therefore expected to require both efficient and extensive transduction of diseased tissue to demonstrate therapeutic potential.

Although NP-C is characterised by neurovisceral pathology, extremely severe and fatal visceral pathology is generally only observed in a minority of patients, such as neonatal cases with acute liver failure. Otherwise visceral pathology is mainly

limited to hepatosplenomegaly and is completely absent in 15% of patients at the time of diagnosis (Vanier, 2010). Apart from severe neonatal or adult-onset cases, all NP-C patients will ultimately develop a progressive and fatal neurological disease (Vanier, 2013). Taking these factors into consideration, the first prioritisation of gene therapy for NP-C should therefore be the focus on amelioration of the neurological pathology. Limiting the majority of the viral vector dose to the CNS will also have the additional benefit reducing potential immune response in the relatively immune privileged brain (Sack and Herzog, 2009, Muldoon et al., 2013), compared to the extremely high systemic doses that may be required for sufficient vector to cross the blood-brain barrier.

Several complementary studies have suggested that neurodegeneration in NP-C is cell-autonomous, with the isolated loss of NPC1 in neurons responsible for neurodegeneration and progressive neurological disease manifestations (Lopez and Scott, 2013). An early chimeric mouse study revealed that *Npc1*<sup>-/-</sup> Purkinje cell loss was not affected by *Npc1*<sup>+/+</sup> glial cells, whereas *Npc1*<sup>+/+</sup> Purkinje cells survived and were not affected by surrounding *Npc1*<sup>-/-</sup> glial cells (Ko et al., 2005). These findings were mirrored by studies in other conditional knockout animal models, where the loss of NPC1 function in neurons only was sufficient in recapitulating neurodegeneration and neurological disease progression (Elrick et al., 2010, Yu et al., 2011). Finally, in a Tet-inducible *Npc1*<sup>-/-</sup> mouse model, NPC1 activity in neurons resulted in the correction of neurodegeneration, whereas disease progression was not significantly affected by astrocytic NPC1 activity (Lopez et al., 2011). Interestingly, the selective reconstitution of NPC1 in Purkinje neurons only resulted in a delay of neurological disease onset, with the rescue of other neuronal populations in other brain regions such as the thalamus crucial for further reducing disease progression rate and improving survival (Lopez et al., 2011). In combination, these studies demonstrate the priority of strong and widespread neuronal transduction, if a gene therapy approach for Niemann-Pick Type C is to be successful in treating the neurological manifestations of the disease.

An additional challenge in the development of gene therapy for NP-C1 is linked to the relatively large size of the human *NPC1* complementary DNA (cDNA), which will have to be integrated into a functional and efficient viral vector. As previously

discussed, while rAAV are currently considered the optimal approach for gene delivery to the CNS (**Section 1.5.3**), their limited packaging capacity potentially affects the viability of their use for effective *NPC1* delivery. Other viral vectors reviewed in previous sections, such as adenoviral vectors (**Section 1.5.1**) or lentiviral vectors (**Section 1.5.2**) have sufficient packing capacity, however their transduction spread and efficiency throughout the CNS may not be sufficient for NP-C.

## 1.9 Aims: Rationale and Significance

Although preclinical evaluation in the NP-C mouse model has identified several treatment options that can slow disease progression, there is currently no major disease modifying or curative treatment available for Niemann-Pick Type C. Advances in the field of gene therapy and viral vector technology have recently led to a surge of promising preclinical studies in a range of lysosomal storage disorder animal models, with clinical translation now moving forward in the form of a series of clinical trials (**Table 4**).

The overall aim of this project is the development and evaluation of gene therapy in the *Npc1*<sup>-/-</sup> mouse model, in the context of a potential future therapy for Niemann-Pick Type C1. As discussed in the previous section (**Section 1.8**), this gene delivery approach will aim to primarily focus on treating the neurological pathology of NP-C, via widespread and efficient neuronal transduction. The gene delivery vector will therefore be administered directly to the CSF via intracerebroventricular administration for optimal spread throughout the brain. For this proof of concept study, administration will be carried out in neonatal mice to achieve the best possible spread of gene delivery vector.

The chosen gene delivery vector will have to incorporate the relatively large human *NPC1* cDNA. Homology is relatively conserved between the human and murine NPC1 protein and cDNA, at 86% and 84% respectively (**Supplementary Figure S1** and **Supplementary Figure S2**). Therefore the human version of *NPC1*

(Supplementary Figure S3) will be used throughout the study to aid potential downstream clinical translation. Due to the large size of the *NPCI* cDNA, the optimal vector for incorporating, delivering and expressing the transgene throughout the brain will have to be evaluated. This vector will then be used in a series of studies in wild-type mice, investigating tropism, transgene expression and potential vector related toxicity.

The evaluated vector will subsequently be used in an initial preclinical study in the *Npc1*<sup>-/-</sup> mouse model, with the aim of primarily analysing safety but also potential therapeutic efficacy in the form of survival, weight and various parameters of motor function throughout their lifespan. Additionally, gene therapy treated *Npc1*<sup>-/-</sup> mice brains will be examined for amelioration of neurodegeneration, inflammation and lipid storage.

Finally, gene therapy will be compared in certain parameters with other small molecule drugs shown to have efficacy in the *Npc1*<sup>-/-</sup> mouse model, including the European Medicines Agency approved miglustat and HP- $\beta$ -CD that is currently in clinical trials, to put into context the therapeutic potential that gene therapy may have in the current NP-C arena.

## 2 Materials and Methods

### 2.1 AAV vector construct design

During the design of the *hNPC1* construct to be used for rAAV vector production certain factors were taken into consideration to strike a balance between maximising AAV-*hNPC1* production efficiency and AAV-*hNPC1* expression efficacy. The combination of large *hNPC1* transgene size and limited rAAV packaging capacity resulted in a series of major changes to the template rAAV, which are presented in detail in **Chapter 3**. The template construct containing the human synapsin I promoter expression cassette flanked by AAV2 ITRs was kindly provided by Dr. J. Tordo (Department of Infectious Diseases, King's College London, UK). Through subsequent rounds of cloning described in Sections **3.4-3.5** enhanced green fluorescent protein (*eGFP*), Woodchuck hepatitis virus posttranscriptional regulatory element (*WPRE*) and human growth hormone polyadenylation signal (*hGHpA*) sequences were removed and replaced with Kozak, *hNPC1* and Simian virus 40 polyadenylation signal (*SV40pA*) sequences to produce the final *pAAV.hSynI.hNPC1.SV40pA* construct used for AAV2/9-hSynI-hNPC1-SV40pA (AAV9-hNPC1) vector production and subsequent *in vitro* and *in vivo* testing. Sources and details for the other plasmids used in this study can be found in **Table 5**.

## 2.2 Cloning

### 2.2.1 Bacterial transformation

Plasmid DNA was transformed into competent *Escherichia coli* bacteria for subsequent amplification and cloning. To reduce the risk of recombination events resulting from the highly repetitive inverted terminal repeats regions, recombinase negative (*recB* and *recJ* deficient) SURE competent cells (Agilent Technologies, Santa Clara, USA) were used for the cloning of rAAV constructs. Per transformation reaction, 50µl of bacterial suspension was thawed on ice and the sample DNA was subsequently added to the suspension and incubated on ice for 30 minutes. Samples were then heat-shock treated for 45 seconds at 42°C and incubated on ice again for 2 minutes. The transformation mix was transferred into 150µl of S.O.C. medium (ThermoFisher Scientific, Paisley, UK) and incubated for 1 hour at 37°C and shaking at 225rpm. This culture was spread on to lysogeny broth (LB) agar (ThermoFisher) plates containing either ampicillin (100µg/ml, Sigma-Aldrich, Dorset, UK) or kanamycin (50µg/ml, Sigma-Aldrich) and incubated overnight at 37°C to select for positive colonies. The DNA from resulting colonies was analysed by restriction enzyme digest, polymerase chain reaction (PCR) or Sanger sequencing to confirm successful and correct plasmid transformation for downstream applications.

### 2.2.2 Plasmid amplification and purification

Positive colonies were inoculated in 5ml of LB broth (Sigma-Aldrich) with the relevant antibiotic and grown overnight at 37°C with shaking at 225rpm. The culture was then centrifuged at 6,000 x g (Eppendorf 5415D, Stevenage, UK) for 10 minutes and the resulting bacterial pellet was used for plasmid DNA purification with a 'QIAprep Spin Miniprep Kit' (QIAGEN, Hilden, Germany), as per manufacturers protocol. For larger scale plasmid amplification and purification 500µl of overnight culture was added to 500ml of LB broth with selective antibiotic and grown overnight at 37°C with shaking at 225rpm. Plasmid DNA was purified from this culture using 'Plasmid Maxi Kit' (QIAGEN) following the manufacturer's

instructions. The resulting DNA pellet was resuspended in dH<sub>2</sub>O and the final DNA concentration and purity was determined by spectrophotometry through measurements of absorbance at 260nm and 280nm (NanoDrop 1000, Thermo Scientific).

Plasmid Name	Relevant Characteristics	Source
<i>pCMV6.hNPC1.Neo</i>	CMV promoter driving human <i>NPC1</i> cDNA	Platt FM, Department of Pharmacology, Oxford, UK
<i>pSUB201-Caggs-GFP</i>	Contains <i>eGFP</i> and <i>SV40pA</i> sequences	Tordo J., Department of Infectious Diseases, King's College London, UK
<i>pAAV.hSynI.flox.eGFP.WPRE.hGHpA</i>	AAV2 ITRs flanking cassette containing human synapsin I promoter, <i>eGFP</i> transgene and WPRE element.	Tordo J., Department of Infectious Diseases, King's College London, UK
<i>pAAV.hSynI.hNPC1.hGHpA</i>	AAV2 ITR construct with hSynI driving <i>hNPC1</i> cDNA and human growth hormone pA sequence	This Study
<i>pAAV.hSynI.hNPC1.SV40pA</i>	AAV2 ITR construct with hSynI driving <i>hNPC1</i> cDNA and the late SV40 pA sequence	This Study
<i>pAAV.hSynI.eGFP.SV40pA</i>	<i>hNPC1</i> replaced by <i>eGFP</i> reporter gene.	This Study
<i>pU57.NPC1O</i>	Codon optimised <i>NPC1</i> sequence	Genscript, China
<i>pHGTI</i>	Adenovirus helper plasmid	(Streck et al., 2006)
<i>pDG9</i>	AAV9 <i>cap</i> and AAV2 <i>rep</i> genes	Tordo J., Department of Infectious Diseases, King's College London, UK
<i>pCCL.SIN.cPPT.CMV.V.eGFP.WPRE</i>	Lentiviral construct with CMV promoter driving <i>eGFP</i> reporter	Howe S., Institute for Child Health, London, UK
<i>pMDG2</i>	Vesicular stomatitis virus envelope expression plasmid	Plasmid Factory, Bielefeld, Germany
<i>pCMVdR.8.74</i>	Encapsidation plasmid lacking Vif-, Vpr-, Vpu-, and Nef-accessory HIV-1 proteins	Plasmid Factory, Bielefeld, Germany

**Table 5: Plasmids used in this study**

### 2.2.3 Polymerase Chain Reaction

All polymerase chain reactions were carried out with high fidelity proof reading *Pfu* DNA polymerase (Promega, Madison, USA). Desired sequences were amplified from 50-75ng of plasmid template DNA using primer pairs (Sigma-Aldrich) flanking these regions at the 5' and 3' ends, introducing additional restriction enzyme sites if necessary, and a mix of equimolar deoxynucleotide triphosphates (dNTPs, VWR, Leicestershire, UK). The sets of primers used for the amplification of each sequence are listed in **Table 6**. PCR products were subsequently analysed by DNA electrophoresis to confirm correct size or purified using 'QIAquick PCR Purification Kit' (QIAGEN), following manufacturers protocol, for further downstream cloning.

#### Example of PCR reaction mix (30µl reaction volume):

template DNA	50-75ng
dNTPs	200µM
Forward Primer (5' > 3')	1µM
Reverse Primer (3' > 5')	1µM
10X <i>Pfu</i> Buffer	3µl
<i>Pfu</i> DNA polymerase	0.125u (unit)
dH <sub>2</sub> O to final volume	30µl

#### Example of standard cycle conditions (35 cycles of denaturation, annealing and extension):

Initial denaturation	95°C	5 minutes
<b>Denaturation</b>	<b>95°C</b>	<b>1 minutes</b>
<b>Annealing</b>	<b>T<sub>m</sub></b> (melting temperature adapted for each primer set)	<b>30 seconds</b>
<b>Extension</b>	<b>72°C</b>	<b>2 minutes/kb</b>
Final Extension	72°C	4 minutes/kb

PCR Product	Forward Primer	Reverse Primer	Template Source
<i>hNPC1</i> cDNA	<i>hNPC1.KpnI.Fw</i> 5'AATGGTACCGCCACCA TGACCGCTCG 3'	<i>hNPC1.BglII.Rv</i> 5'CAATAGATCTCTAGAA ATTTAGAAGCCGTTTCG 3'	<i>pCMV6neo.hNPC1</i>
<i>SV40pA</i>	<i>SV40.BglII.Fw</i> 5'CAATAGATCTCAGACA TGATAAGATACA 3'	<i>SV40.PmlI.Rv</i> 5'CAATCACGTGTAAAAA ACCTCCCACA 3'	<i>pSUB201-Caggs-</i> <i>GFP</i> Gift from J.Tordo
<i>eGFP</i> cDNA	<i>eGFP.KpnI.Fw</i> 5'ATAGGTACCGCCACCA TGGTGAGCAAGGCGA3'	<i>eGFP.KpnI.Rv</i> 5'CAATAGATCTCTACTT GTACAGCTCGTCCA 3'	<i>pSUB201-Caggs-</i> <i>GFP</i> Gift from J.Tordo

**Table 6: List of oligonucleotides used in this study**

### 2.2.4 Restriction enzyme digest

Plasmid DNA and PCR amplicons were digested with restriction enzymes sourced from New England Biolabs Inc. (Ipswich, USA), where 1µg of DNA was digested for a minimum of 1 hour at 37°C unless stated otherwise. Resulting DNA fragments were separated by size on an agarose gel via electrophoresis.

#### Example of restriction enzyme reaction (25µl reaction volume):

DNA	1µg
10X Restriction Buffer	2.5µl
Enzyme	0.5µl (1u)
dH <sub>2</sub> O to final volume of	25µl

### 2.2.5 DNA electrophoresis

DNA fragments were separated on a 0.8-2% (w/v) agarose gel (Invitrogen), depending on fragment size, using 1X Tris-acetate-ethylenediaminetetraacetic acid (TAE) buffer. Safeview (Applied Biological Materials, Richmond, Canada) was added to the agarose at a dilution of 1:10,000 for DNA visualisation. Samples were loaded onto the gel using 1X Orange G gel-loading buffer (Sigma-Aldrich) with

either 1kb Plus (ThermoFisher Scientific) or HyperLadder 1kb (Bioline, London, UK) molecular weight markers to determine DNA fragment size. Gels were run at 100V (PowerPac Basic, Biorad, California, USA) for 30-90 minutes, depending on fragment size, and visualised under a ultraviolet (UV) transilluminator (Ingenius, Syngene, Cambridge, UK).

#### **1X TAE:**

Tris (pH 7.6)	40mM
Ethylenediaminetetraacetic acid (EDTA)	1mM
Acetic acid	20mM

### **2.2.6 DNA extraction**

Desired DNA fragments were isolated from agarose gel under low level UV light and subsequently extracted and purified using a 'QIAquick Gel Extract Kit' (QIAGEN) following manufacturer's protocol. DNA was eluted in a final volume of 30µl of dH<sub>2</sub>O and resulting DNA concentration and purity was determined by spectrophotometry through measurement of absorbance at 260nm and 280nm.

### **2.2.7 Ligation**

Purified DNA fragments were ligated overnight at 4°C using bacteriophage T4 DNA ligase (Promega), following manufacturer's protocol with insert to vector ratios of 1:1 or 3:1.

#### **Example of ligation reaction (10µl reaction volume):**

vector	100ng
insert	1:1 or 3:1 (ratio of insert to vector)
10X T4 DNA Ligase Buffer	1µl
T4 DNA Ligase	1u (unit)
dH <sub>2</sub> O to final volume of	10µl

### 2.2.8 DNA sequencing

Plasmid DNA and sequencing primers were sent externally to SourceBioscience for Sanger sequencing ([www.lifesciences.sourcebioscience.com](http://www.lifesciences.sourcebioscience.com), Nottingham, UK). Resulting DNA electropherograms were visualised and analysed using MacVector v15.0.

## 2.3 Tissue Culture

### 2.3.1 Culture of cell lines

The human embryonic kidney (HEK) 293T cell line, a variant of the HEK-293 cell line expressing the late SV40 large T antigen to enhance protein and viral production (DuBridg e et al., 1987), and neuroblastoma cell line SH-SY5Y were used in this study. Cell lines were grown in standard growth medium of Dulbecco's modified Eagle's medium (DMEM; Gibco, ThermoFisher Scientific) with: high glucose (4.5 mg/ml), GlutaMAX (0.8 mg/ml), pyruvate (0.1 mg/ml) and supplemented with 10% heat-inactivated foetal bovine serum (FBS; Sigma-Aldrich), penicillin (100 units/ml) and streptomycin (100 µg/ml). All cells were grown on poly-D-lysine coated 6-well plates, T75 and T175 flasks and 100mm dishes to maintain adherence (Nunc, ThermoFisher Scientific). Cells were incubated at 37°C in 5% CO<sub>2</sub> for an average of 48-72 hours between passaging.

### 2.3.2 Cell culture passaging

After 48-72 hours cells were passaged at 80-90% confluency. Cells were washed with Dulbecco's Phosphate-Buffered Saline (DPBS, Gibco) and detached with a trypsin and EDTA (Gibco) mix. The culture containing the detached cells was spun at 200 x g for 5 minutes and the resulting pellet was gently resuspended in fresh

growth media. The culture was regularly split at a 1:5 ratio into a new flask or dish. To avoid genetic drift, cells beyond passage 20 were discarded and freshly thawed passage 3 cells were allowed to recover until passage 5, before being utilised.

### **2.3.3 Transfection**

Cells were seeded in a 6 well plate (Nunc) at a ratio of 200,000 cells/well with standard growth media and incubated for 24 hours. Plasmid DNA was mixed with the transfection agent linear polyethylenimine MAX (PEI MAX Mw ~40000, Polysciences Inc., Warrington, USA) at a ratio of 1:3 in reduced serum media Opti-MEM (Gibco). Transfection mix was incubated at room temperature for 15 minutes to allow DNA-PEI complex formation and was subsequently added to the cells in the standard growth media. After 24 hours the media was replaced with fresh standard growth media and incubated for a further 24 - 48 hours at which point cells were either imaged or collected for downstream protein analysis.

### **2.3.4 *In vitro* protein expression analysis**

To confirm successful overexpression of the transgene from the construct following transfection *in vitro*, Western blotting against the expressed transgene protein was carried out. 48 - 72 hours post-transfection cells were collected for protein extraction. 100µl of cold radioimmunoprecipitation assay buffer (RIPA) lysis buffer (ThermoFisher Scientific) with 1X protease inhibitor cocktail (ThermoFisher Scientific) was added per well and incubated on ice for 5 minutes, swirling the plate every minute. Cells were then scraped and collected at the bottom of the well and the lysate was transferred to 1.5ml microcentrifuge tubes. Resulting lysates were incubated on ice for 30 minutes, after which debris was pelleted by centrifugation at 14,000 x g, 4°C for 20 minutes. Lysate was carefully extracted and overall protein concentration was determined by Pierce BCA Protein Assay (LifeTechnologies, ThermoFisher Scientific). Sample protein concentrations were normalised to 1µg/µl to standardise loading volumes. 1X LDS Sample buffer (LifeTechnologies) and 1X Sample Reducing agent (LifeTechnologies) were added to the samples, which were

then incubated at 37°C for 30 minutes to denature proteins, while simultaneously avoiding clumping of transmembrane proteins. 20 - 40µg of protein was subsequently loaded per well on a NuPAGE Bis-Tris 4 - 12% polyacrylamide gel, with 10µl of molecular weight marker RPN800E (Amersham, GE Healthcare, Buckinghamshire, UK) to confirm molecular weight of visualised bands. Proteins were separated via sodium dodecyl sulphate (SDS) PAGE electrophoresis with 1X MES running buffer (LifeTechnologies) run at 120V for 2 hours.

Proteins were transferred on to methanol activated polyvinyl difluoride membrane (Millipore, Watford, UK) via semi-dry transfer. Filter paper and activated membrane were soaked in transfer buffer and placed in the semi-dry transfer unit (Biorad Transblot SD, Biorad), before carefully placing the gel on top. Additional filter paper was used to cover the gel before closing the unit, which clamped the filter, membrane and gel together. Semi-dry transferring was run at 400mA for 1 hour, after which the membrane, now containing the transferred proteins, was briefly washed in phosphate-buffered saline (PBS) before blocking endogenous protein binding by incubating in 1X tris-buffered saline (TBS) with 3% Tween20 and 5% bovine serum albumin (BSA) for 1 hour at 4°C. Membranes were subsequently incubated overnight at 4°C with primary antibodies for NPC1 (1:10,000, ab134113, Abcam, Cambridge, UK) and β-Tubulin (1:2,000, ab6161, Abcam) in 1X TBS with 3% Tween20 and 3% BSA overnight at 4°C. After three 5 minute washes in 1X TBS with 3% Tween20, horseradish peroxidase conjugated secondary antibodies goat anti-rabbit IgG (1:2,000, ab6721, Abcam) and goat anti-rat IgG (1:10,000, ab97057, Abcam) were added to 1X TBS with 3% Tween20 and 3% BSA and incubated with the membrane for 2 hours at room temperature. Membranes were washed a final three times and developed using the enhanced chemiluminescence system SuperSignal West Pico kit (LifeTechnologies), as per manufacturers protocol. Chemiluminescence was imaged using a GeneGnome imager (Syngene).

**1X TBS (1000ml):**

Tris	6.04g
NaCl	8.5g
1M HCl	3.2ml
dH <sub>2</sub> O to final volume of	1000ml

**Transfer Buffer (1000ml):**

methanol (100%)	200ml
Tris	3g
glycine	14.2g
dH <sub>2</sub> O to final volume of	1000ml

## 2.4 Virus Production

### 2.4.1 Lentiviral vector preparation

A 2<sup>nd</sup> generation lentiviral vector packaging system was used to produce the VSV-G.CCL.SIN.cPPT.CMV.eGFP.WPRE lentiviral vector. 100mm dishes (Nunc) were seeded with  $1 \times 10^7$  HEK-293T cells per dish and grown to 70-80% confluence. Cells were then triple transfected with 40 $\mu$ g of *pCCL.SIN.cPPT.CMV.eGFP.WPRE* lentiviral vector construct, 10 $\mu$ g of vesicular stomatitis virus envelope glycoprotein (VSV-G) encoding envelope plasmid *pMDG2* and 30 $\mu$ g of packaging plasmid *pCMVdR8.74* per dish. Plasmids and transfection agent PEI (branched Mw ~25,000, Sigma-Aldrich) at a final concentration of 1mM were added to 10ml of serum free Opti-Modified Eagle's medium (Opti-MEM, Gibco), mixed and incubated at room temperature for 20 minutes to allow for PEI-DNA complex formation. HEK-293T cells were washed with Opti-MEM, before adding 10ml of the transfection mix per dish and incubated at 37°C, 5% CO<sub>2</sub> for 4 hours, after which the mix was replaced with fresh standard growth media. Supernatant was subsequently collected 48 and 72

hours post-transfection, centrifuged at 3,000 x g for 10 minutes and filtered through a 0.22µm filter (Millipore) to remove cell debris. Virus was pelleted by centrifugation overnight (16 - 18 hours) at 3,500 x g, 4°C, with the resulting pellet being resuspended in Opti-MEM and stored at -80°C.

### **2.4.2 Lentiviral vector titration**

Lentiviral titer was obtained by quantification of the viral envelope protein p24. The ZeptoMetrix p24 antigen enzyme-linked immunosorbent assay was used as per manufacturers protocol (ZeptoMetrix, Buffalo, USA), where quantity of sample viral envelope protein p24 is determined by comparison to a standard curve, created by standards of known p24 concentration. The resulting titre for the VSV-G.CCL.SIN.cPPT.CMV.eGFP.WPRE vector used in this study was  $9.2 \times 10^8$  vp/ml.

### **2.4.3 AAV vector preparation**

To produce recombinant AAV2/9 vectors, HEK-293T cells were transiently triple transfected with the ITR-containing plasmid carrying the transgene cassette, a helper plasmid expressing both AAV2 Rep and AAV9 Cap and a third construct containing the adenovirus helper functions. The combined transfection and resulting viral protein expression resulted in rAAV2/9 vector particle production (**Figure 7**).

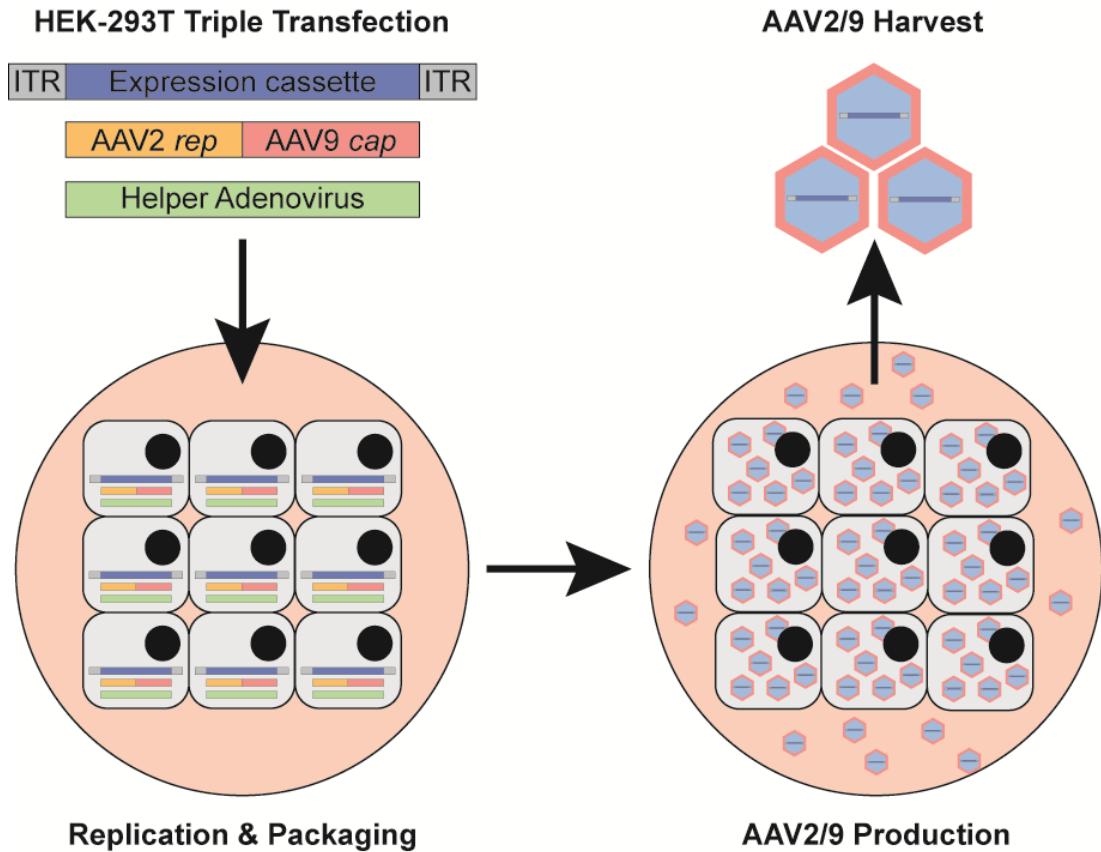


**Figure 7: Representative diagram of triple transfection in HEK293T cells, resulting in AAV2/9 vector production.**

$5 \times 10^8$  HEK-293T cells were added to a total volume of 1L of standard growth media, seeded in a 10 layered CellSTACK (Corning, 6360 cm<sup>2</sup>, ThermoFisher Scientific) and incubated at 37°C in 5% CO<sub>2</sub> for 16 to 30 hours. 160µg of AAV transgene plasmid, 160µg of capsid plasmid AAV2/9 (*pDG9*) and 480µg of adenovirus helper plasmid (*pHGT1*) were added to serum free DMEM, to which 2.8ml of 3.5mg/ml PEI MAX was added. The transfection mixture was subsequently mixed and incubated at room temperature to allow DNA-PEI complex formation, after which 1L of fresh standard growth media was added. CellSTACK media was replaced with completed transfection media and incubated for 72 hours at 37°C in 5% CO<sub>2</sub>.

After 72 hours, the resulting AAV particles were collected and purified from both cells and supernatant. The supernatant was removed from the CellSTACK and centrifuged at 1,800 x g for 10 minutes to collect dislodged cells. Simultaneously cells remaining in the CellSTACK were washed with sterile PBS, detached via

trypsinisation and pelleted by centrifugation at 1,800 x *g* for 10 minutes. The resulting cell pellets were resuspended in 20ml of AAV lysis buffer and lysed by 3 freeze-thaw cycles (-80°C to 37°C) with regular 5 minute vortexing at each interval. Viral particles were precipitated from the collected supernatant by adding 31.3g of ammonium sulphate (Sigma-Aldrich) per 100ml of supernatant, which was shaken vigorously until dissolved and subsequently incubated on ice for 30 minutes. The mixture was centrifuged at 8,300 x *g* and the resulting pellet was resuspended in 20ml of AAV lysis buffer. Cell and supernatant lysates then underwent benzonase treatment to degrade cellular DNA and RNA by adding MgCl<sub>2</sub> to a final concentration of 1mM and 5000 units of benzonase (Sigma-Aldrich) and were incubated at 37°C for 1 hour. The lysates were then cleared by centrifugation at 4,200 x *g* for 30 minutes, combined and purified by iodixanol density gradient centrifugation.

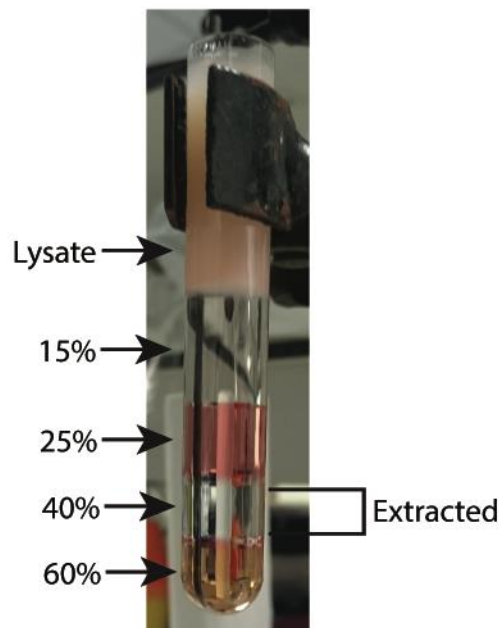


**Figure 8: Image of completed iodixanol gradient in ultracentrifuge tube prior to centrifugation.**

Extracted indicates fraction containing packaged AAV particles post-centrifugation, which were extracted for downstream concentration.

The gradient was carefully created in ultracentrifuge tubes (Beckman Instruments, High Wycombe, UK) by overlaying the supernatant to slowly pipetted Optiprep

iodixanol (Sigma-Aldrich) solutions of increasing steps (15%, 25%, 40% and 60%). Completed tubes were centrifuged (Sorvall Discovery 90SE, ThermoFisher Scientific) for 3 hours at 200,000 x g using a TH641 (ThermoFisher Scientific) rotor. As a result the viral particles concentrated to the 40% band, which was extracted with a 19G11/2 needle attached to a 3ml syringe (**Figure 8**). The extracted sample was diluted in sterile PBS to a total volume of 50ml, 0.22µm filter sterilised and concentrated. The viral particles were concentrated in a Vivaspin20 with a 100,000 Mw cut-off centrifugal concentrator (Sartorius Stedim Biotech, Epsom, UK) with repeated spins at 3,000 x g until a final volume of 500 - 1000µl was achieved. Concentrated virus was finally titered and stored at -80°C for further use.

**1X AAV lysis buffer:**

NaCl	150mM
Tris pH 8.5	50mM

**2.4.4 AAV vector titration**

A combination of two methods was used to determine AAV titer, quantifying either viral capsid protein or number of viral genomes in a sample. In the first method AAV viral capsid proteins were separated by SDS page gel electrophoresis and the VP3 protein was quantified using a standard curve created by known quantities of bovine serum albumin (BSA, Sigma-Aldrich) standards (Kohlbrenner et al., 2012). AAV samples were diluted in 6X AAV SDS loading buffer and heated at 95°C for 5 minutes to breakdown the capsid and denature proteins. BSA standards (250ng, 500ng, 750ng and 1000ng) and AAV samples were run on a NuPAGE Bis-Tris 4 - 12% polyacrylamide gel (LifeTechnologies) at 120V for 2 hours. The gel was fixed in gel fix solution for 30 minutes, before staining for 3 hours at room temperature with 'SYPRO Ruby' (LifeTechnologies) for protein visualisation. Band visualisation and quantification was performed using a UV transilluminator (Ingenius, Syngene). VP3 band volume was analysed using the BSA standard curve, resulting in titration of viral protein per ml.

**6X AAV SDS loading buffer (10ml):**

SDS	0.8g
Tris pH 6.8	5ml
glycerol	5ml
bromophenol blue	4mg
$\beta$ -mercaptoethanol	5%

**Gel fix solution (500ml):**

Methanol	250ml
Glacial acetic acid	35ml
dH <sub>2</sub> O	215ml

Concentrated vector genome content was determined using alkaline agarose gel electrophoresis (Fagone et al., 2012). AAV sample dilutions were mixed with 8.5 $\mu$ l of 4X alkaline sample buffer, which were then loaded on a 0.8% agarose gel made with alkaline running buffer. The gel was run with 1X alkaline running buffer overnight at 20V and 4°C. Gels were washed in 0.1M Tris (pH 8.0) for 1 hour, stained post-electrophoresis for 2 hours with 4X GelRed stain (Biotium, Fremont, USA) and subsequently visualised on a UV transilluminator (Ingenius, Syngene). Band quantification was carried out and compared against a HyperLadder 1kb (Bioline Reagents, London, UK) standard curve.

**50X Alkaline running buffer (500ml):**

NaOH	2.5M
EDTA pH 8.0	50mM
dH <sub>2</sub> O to a final volume of	500ml

**4X alkaline sample loading buffer (1ml):**

glycerol	200 $\mu$ l
50X alkaline running buffer	80 $\mu$ l
SDS (20% w/v)	60 $\mu$ l
xylene cyanol	10mg
dH <sub>2</sub> O to a final volume of	1ml

## 2.5 *In vivo* experiments

### 2.5.1 Animals

Wild-type CD-1 mice were used for preliminary vector testing and expression analysis in collaboration with Dr. S. Waddington (Institute for Women's Health, University College London, UK). Wild-type and *Npc1*<sup>-/-</sup> BALB/c mice (Pentchev et al., 1984) were used for AAV9-hNPC1 vector efficacy studies in collaboration with A. Colaco, D. Smith and Prof. FM. Platt (Department of Pharmacology, University of Oxford, UK). Any mice that lost 1g of body weight within a 24-hour period were considered to have reached their humane end-point and were sacrificed. All animal studies were approved by the UK Home Office for the conduct of regulated procedures under license (Animal Scientific Procedures Act, 1986) and according to ARRIVE guidelines and recommendations.

### 2.5.2 Vector administration

All vector administrations were carried out on P0/1 neonatal pups as previously described (Kim et al., 2014). Vectors were administered via bilateral intracerebroventricular (ICV) injection, targeting the anterior horn of the lateral ventricle (**Figure 9**). Prior to procedure, pups were incubated on ice for 1 minute to anaesthetise and were placed on a cold flat surface during injection. Injection sites were identified at 2/5 of the distance directly from the lambda suture to the eye and a loaded 33-gauge needle (Hamilton, Reno, USA) with syringe was inserted perpendicular to the surface of the skull at a depth of 3mm from the tip of the needle. A maximum of 5µl was then slowly injected, after which the needle was carefully withdrawn and the procedure was repeated on the contralateral ventricle. Injected neonates were subsequently warmed and returned to the dam. For preliminary vector testing injected and uninjected control CD-1 mice underwent terminal exsanguination at 1-month (P30) post-injection. *Npc1*<sup>-/-</sup> and AAV9-hNPC1 treated *Npc1*<sup>-/-</sup> BALB/c mice were also sacrificed via terminal exsanguination at their respective humane end-point.

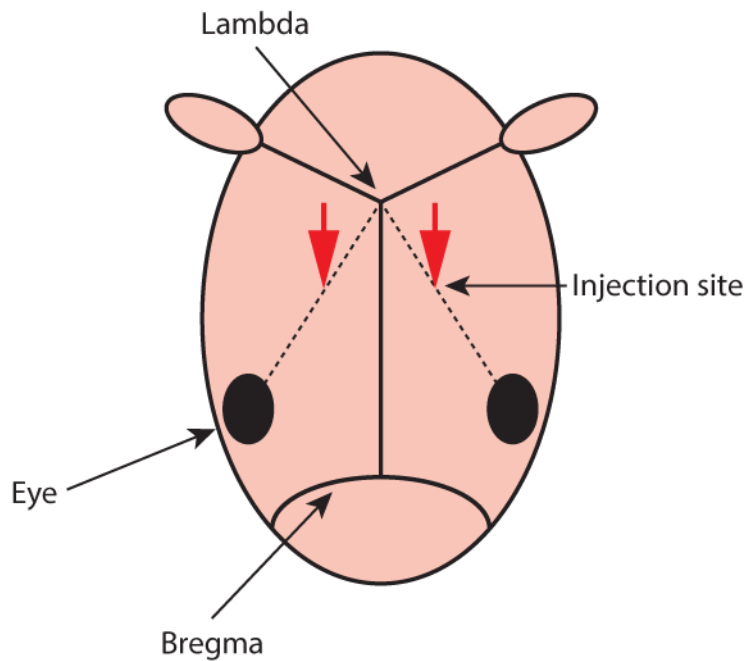


**Figure 9: Illustration of injection sites (red arrows) used for P0/1 neonatal bilateral ICV administration.**

### 2.5.3 Drug administration

Small molecule drugs hydroxypropyl- $\beta$ -cyclodextrin (HP- $\beta$ -CD, Sigma-Aldrich) and miglustat shown to have therapeutic efficacy in the *Npc1*<sup>-/-</sup> model were analysed to compare AAV9-hNPC1 therapeutic efficacy. Upon weaning at 3 weeks of age, cohorts of *Npc1*<sup>-/-</sup> mice began receiving either treatments. HP- $\beta$ -CD was administered by weekly intraperitoneal injection at a dose of 4,000mg/kg. Miglustat was supplemented as a dry admixture to powdered RM1 mouse chow at a dose of 1,200mg/kg/day (Actelion Pharmaceuticals Ltd., Basel, Switzerland) as previously described (Williams et al., 2014). Treatment continued until the treated *Npc1*<sup>-/-</sup> mice reached their humane end-points.

### 2.5.4 Behavioural analysis – Rearing

From 5 weeks of age, weekly rearing measurements were carried out on control wild-type mice, untreated *Npc1*<sup>-/-</sup> and treated *Npc1*<sup>-/-</sup> cohorts in an open field setting. Mice were individually placed in an open and empty cage and rears were counted

manually during a 5-minute period. A rear was recorded when a mouse reared on its hind legs using the side of the cage as support.

### **2.5.5 Behavioural analysis – Tremor**

Tremor analysis was carried out on control, untreated and treated cohorts weekly, starting at 5 weeks of age using a commercial tremor monitor (San Diego Instruments, San Diego, USA) as previously described (Smith et al., 2009). Individual mice were placed inside the apparatus on an anti-vibration table and monitored for 256 seconds, after 30 seconds of acclimatisation time. The output (amplitude/time) was analysed using LabView software, to give a measurement of power at each monitored frequency (0-64Hz). *Npc1*<sup>-/-</sup> mice demonstrate an age-dependent increase in 32-55hz high frequency tremor (Lloyd-Evans et al., 2008) and data within this range was analysed in detail in this study.

### **2.5.6 Behavioural analysis – Gait**

Gait monitoring was performed by using the automated gait analysis CatWalk system (Noldus, Wageningen, Netherlands). From 5 weeks of age, mice were monitored weekly by being individually placed at one end of the CatWalk and were filmed freely walking across a filmed section with a backlit stage. A minimum of five successful runs were recorded per session, where a run across the stage was deemed successful if standard run criteria were met, including: speed, duration of run, direction and minimum number of steps. Paw prints during successful runs were checked, assigned and analysed using the CatWalk XT software v10.6 (Noldus) to produce footprint, stride and overall run measurements.

### **2.5.7 Tissue harvest**

Mice to be sacrificed underwent terminal exsanguination by transcardial perfusion with sterile PBS under isoflurane-induced anaesthesia. A lateral incision through the

skin and abdominal wall was made below the rib cage to expose the pleural cavity. The sternum was lifted to reveal the diaphragm, which was cut to access the heart, where a small incision to the right atrium was made. 10 - 20ml of PBS was then slowly injected into the left ventricle with a 24 gauge needle, where liver and organ blanching indicated successful perfusion. Brains and visceral organs were subsequently extracted and either fixed in PBS with 4% paraformaldehyde for immunohistochemistry or snap frozen on dry ice and stored at -80°C for protein and glycosphingolipids analysis.

## **2.6 Expression Analysis**

### **2.6.1 Double gelatine coating of slides**

To increase tissue adhesion and allow downstream washes, all microscope slides (Superfrost, VWR) were double coated with a fine layer of gelatine. 2.5g of gelatine powder (VWR) and 0.25g of chromium (III) potassium sulphate 12-hydrate (VWR) were added to 500ml of dH<sub>2</sub>O, which was subsequently warmed to 45°C with constant stirring. While maintaining the mix at 45°C, slides were briefly immersed in slide racks and then left to dry overnight at 56°C. The process was repeated a second time to produce double coated microscope slides, which were used for histology, immunohistochemistry and immunofluorescent studies.

### **2.6.2 Immunohistochemistry**

After 48 hours of fixation in PBS with 4% (w/v) paraformaldehyde, tissues were transferred into 30% sucrose (Sigma-Aldrich) in PBS for cryoprotection. Brains were subsequently cryosectioned in the coronal or sagittal plane at -20°C using a Leica CM3050 cryostat microtome to a 40µm thickness. Resulting sections were stored at 4°C in TBSAF in a 96-well (Nunc) consecutive format by rows, from dorsal to ventral. 3,3'-diaminobenzidine (DAB, Sigma-Aldrich) mediated

immunohistochemistry (IHC) was used for transgene expression and pathological marker analyses. Representative sections were chosen by selecting brain sections in the 96-well plates in 6 column intervals (e.g. columns 2, 8, 14, etc.) and were washed in 1X TBS. Endogenous peroxidase activity was depleted by incubating sections with 1% hydrogen peroxide (H<sub>2</sub>O<sub>2</sub>, Sigma-Aldrich) in 1X TBS for 30 minutes, followed by three 5 minute washes in 1X TBS. Non-specific protein binding was blocked via incubation in 15% normal serum (Sigma-Aldrich) in TBS-T for 30 minutes. Sections were incubated overnight at 4°C in 10% normal serum in TBS-T with primary antibodies (**Table 7**). Following washes in 1X TBS, sections were incubated in 10% normal serum in TBS-T with corresponding biotinylated secondary antibodies (**Table 7**) at room temperature for 2 hours. Following washes, sections were incubated with Vectastain avidin-biotin solution (ABC, Vector Laboratories, Peterborough, UK), where reagents A and B were diluted 1:1,000 in 1X TBS, mixed and incubated for 2 hours at room temperature. Staining was visualised with 0.05% DAB (Sigma-Aldrich) and 0.003% H<sub>2</sub>O<sub>2</sub> in 1X TBS in limited light conditions.

The completed staining reaction was stopped via the addition of ice cold 1X TBS, after which the sections were washed three times for 5 minutes in 1X TBS, mounted on to double gelatine-coated slides and air-dried overnight. To further dehydrate and clean sections, dried slides were dipped in 100% ethanol (EtOH) for 30 seconds and transferred into Histo-Clear (National Diagnostics, Hesse, UK) for 30 minutes. Mounting agent DPX (VWR) was used to coverslip (VWR) the slides, which were then left to dry for 3 days. Sections were analysed by light microscopy on a Nikon Eclipse E600 light microscope and representative images were captured using a Nikon DS-Fi1 camera (Nikon, New York, USA).

Primary antibody	Host	Source	Dilution
Anti - eGFP	Rabbit	Abcam (ab290)	1:10,000
Anti - NPC1	Rabbit	Abcam (ab134113)	1:500
Anti - GFAP	Mouse	Millipore (MAB3402)	1:2,000
Anti - CD68	Rat	AbD Serotech (MCA1957)	1:100
Anti - Calbindin	Rabbit	Swant (CB38)	1:10,000
Anti - LAMP1	Rabbit	Abcam (ab24170)	1:2,000

Secondary antibody	Host	Source	Dilution
Biotinylated Anti - Rabbit IgG	Goat	Vector Lab Inc. (BA-1000)	1:1,000
Biotinylated Anti - Rat IgG	Goat	Vector Lab Inc. (BA-9400)	1:1,000
Biotinylated Anti - Mouse IgG	Goat	Vector Lab Inc. (BA-9200)	1:1,000

**Table 7: List of antibodies used for IHC in this study**

**1X TBS (1000ml):**

Tris	6.04g
NaCl	8.5g
1M HCl	3.2ml
dH <sub>2</sub> O to final volume of	1000ml

**1X TBS-T (1000ml):**

1X TBS	997ml
TRITON X-100	3ml

**1X TBSAF (1000ml):**

1X TBS	545ml
sodium azide 10 % (w/v)	5ml
ethylene glycol	300ml
sucrose	150g

### 2.6.3 Quantitative analysis of immunohistochemical staining

Levels of glial fibrillary acidic protein (GFAP), cluster of differentiation 68 (CD68), lysosomal-associated membrane protein 1 (LAMP1) and calbindin immunohistochemical staining were measured by quantitative thresholding image analysis, as previously described (Rahim et al., 2012). For each region of interest 10 non-overlapping images were captured using a live video camera (Nikon, DS-Fil) mounted onto a Nikon Eclipse E600 light microscope at x40 magnification with constant light intensity. Images were analysed using Image-Pro Premier (Media Cybernetics, Cambridge, UK), where immunoreactivity was measured using a constant darkness threshold that is applied to all images within that set of antigen staining. Data is presented as the mean percentage area of immunoreactivity per unit area  $\pm$  standard deviation (S.D.) for each region.

### 2.6.4 Immunofluorescence and scanning confocal microscopy

Immunofluorescence (IF) was used for the analysis of cell tropism and subcellular localisation of NPC1 following AAV9-hNPC1 administration. 40 $\mu$ m brain cryosections were initially stained as described for IHC (**Section 2.6.2**), however different primary antibody concentrations were used (**Table 8**). Secondary antibodies with Alexa Fluor conjugates were used to differentiate between co-stained proteins. Following incubation with the secondary antibodies, sections were washed three times for 5 minutes with 1X TBS and subsequently counterstained with 4',6-diamidino-2-phenylindole (DAPI, Sigma-Aldrich) for nuclear visualisation. A 1mg/ml stock solution of DAPI in dH<sub>2</sub>O was further diluted 1:1,000 with 1X TBS and applied to the sections in limited light conditions for 5 minutes. After, sections were washed three times for 5 minutes in 1X TBS and mounted on to double gelatine-coated slides. Mounted sections were briefly dried, then coverslipped with Fluoromount G (SouthernBiotech, Birmingham, USA) and visualised with a Zeiss LSM 710 laser scanning confocal microscope (Carl Zeiss AG, Cambridge, UK).

Primary Antibody	Host	Source	Dilution
Anti - NPC1	Rabbit	Abcam (ab134113)	1:100
Anti - NeuN	Mouse	Millipore (MAB377)	1:500
Anti - CD68	Rat	AbD Serotech (MCA1957)	1:100
Anti - GFAP	Mouse	Millipore (MAB2402)	1:2,000
Anti - LAMP1	Rat	Abcam (ab25245)	1:500

Secondary Antibody	Host	Source	Dilution
Alexa488 conjugated Anti - Rabbit IgG	Goat	LifeTechnolgies (A-11008)	1:200
Alexa568 conjugated Anti - Mouse IgG	Goat	LifeTechnolgies (A-11004)	1:200
Alexa568 conjugated Anti - Rat IgG	Goat	LifeTechnolgies (A-11077)	1:200

**Table 8: List of antibodies used for IF in this study**

### 2.6.5 Brain section histology

Nissl staining was carried out for the visualisation of general brain and neuronal cytoarchitecture (Scott and Willett, 1966). Every sixth 40µm section from a cryosectioned brain was mounted on double gelatine-coated slides and left to dry overnight, before staining with cresyl violet. Sections were incubated in filtered 0.05% cresyl fast violet with 0.05% acetic acid (VWR) in distilled water for 30 minutes at 60°C, followed by brief rinses in ascending series of graded alcohol from 50% to 100%. Slides were subsequently incubated in Histo-Clear for 30 minutes and coverslipped with DPX for imaging and stereology.

Filipin staining was carried out on mounted 40µm brain cryosections to analyse unesterified cholesterol accumulation observed in *Npc1*<sup>-/-</sup> mice (Kruth et al., 1986). Filipin (Sigma-Aldrich) was diluted in PBS to a working concentration of 100µg/ml and applied to brain sections for 1 hour at room temperature in limited light conditions. Sections were then washed at room temperature with PBS three times for

5 minutes. Staining was visualised with a Zeiss LSM 710 laser scanning confocal microscope (Carl Zeiss AG) under DAPI settings.

### 2.6.6 Stereology

Neuronal counts, cortical thickness measurements and regional volume estimates were carried out on 40 $\mu$ m Nissl stained brain sections using StereoInvestigator software (MBF Bioscience, Vermont, USA) on a Nikon Optiphot light microscope (Nikon) attached to a Q-Imaging Model 01-MBF-2000R-CLR-12 camera (MBF Bioscience).

Regional volumes for the ventral posterior medial and lateral nuclei (VPM/VPL) of the thalamus and the substantia nigra pars reticulata (SNR) were obtained via Cavalieri estimator probe (Kielar et al., 2007) using a 10x objective, where a 50 $\mu$ m<sup>2</sup> sampling grid was superimposed on every sixth section over each region of interest and number of points within the area were counted.

Cortical thickness in the somatosensory barrelfield cortex (S1BF) region was obtained by calculating the mean of 10 perpendicular line measurements from the corpus callosum white matter to the pial surface on every sixth section within the region of interest (Kielar et al., 2007).

Neuronal cell number within the S1BF, VPM/VPL and SNR regions was estimated using the optical fractionator probe (West et al., 1991). Using a 100x objective, only Nissl stained cells with a neuronal morphology and clearly identifiable nucleus were counted (**Figure 10**). A border was traced around the region of interest, a grid was then superimposed and neurones were counted within a series of 50 $\mu$ m x 50 $\mu$ m dissector frames, which were automatically arranged according to the sampling grid size. Every sixth section containing the region of interest was analysed and grid sizes were used as followed: S1BF, 225 $\mu$ m x 225  $\mu$ m; VPM/VPL, 175 $\mu$ m x 175 $\mu$ m; SNR 150 $\mu$ m x 150 $\mu$ m. A coefficient of error (CE) between 0.05 and 0.1 was obtained for all counts indicating sufficient sampling efficiency (Gundersen et al., 1999).

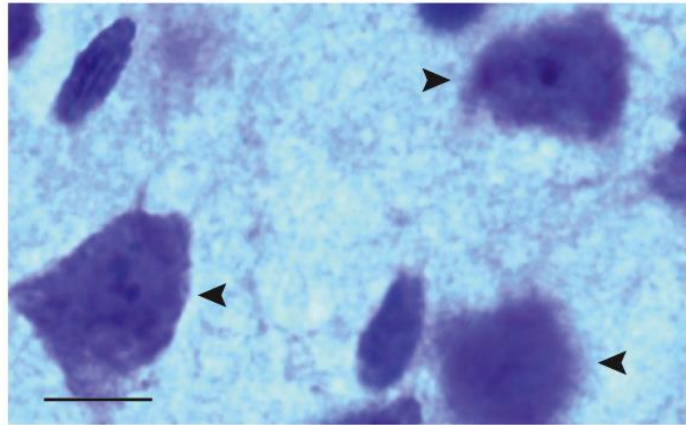


**Figure 10: Example of cells identified as neurons for neuronal quantification**

Representative image within the S1BF region of the cortex from a Nissl stained brain section from a wild-type mouse. Arrows signal cells identified and counted as neurons. Scale bar: 20 $\mu$ m.

### 2.6.7 Western blotting of tissue protein extract

Tissues were homogenized using an Ultra-Turrax TP (IKA Labortechnik, Wasserburg, Germany) on ice in 300 $\mu$ l of RIPA lysis buffer (ThermoFisher Scientific) per 100mg of tissue with 1X protease inhibitor cocktail (ThermoFisher Scientific). Lysates were subsequently treated as previously described in **Section 2.3.4**.

## 2.7 Biochemical glycosphingolipid analysis

Glycosphingolipids (GSL) were analysed in collaboration with M. Huebecker as described by Neville and co-workers (2004). Lipids from tissue homogenates were extracted with chloroform:methanol (1:2, v/v) overnight at 4°C. GSLs were further purified using solid phase C18 columns (Kinesis, St Neots, UK). After elution, the GSL fractions were dried down under a stream of nitrogen and treated with ceramide glycanase (prepared *in house* from the medicinal leech *Hirudo medicinalis/verbena*) to obtain oligosaccharides from GSLs. Liberated glycans were then fluorescently-labelled with anthranillic acid (2-AA). Excess 2AA-label was removed using DPA-6S SPE columns (Supelco, PA, USA). Purified 2AA-labelled oligosaccharides were

separated and quantified by normal phase high-performance liquid chromatography (NP-HPLC) as previously described by Neville et al. (2004). The NP-HPLC system consisted of a Waters Alliance 2695 separations module and an in-line Waters 2475 multi  $\lambda$  fluorescence detector set at Ex  $\lambda$  360nm and Em  $\lambda$  425nm. The solid phase used was a 4.6 x 250mm TSK gel-Amide 80 column (Anachem, Luton, UK). A standard 2AA-labelled glucose homopolymer ladder (Ludger, Oxfordshire, UK) was included to determine the glucose units (GU) of the HPLC peaks. Individual GSL species were identified by their GU values and quantified by comparison of integrated peak areas with a known amount of 2AA-labelled BioQuant chitotriose standard (Ludger). Results were normalised to protein content.

## 2.8 Statistical Analysis

All statistical analyses were carried out with GraphPad Prism software (Version 6.0e). Two-sample comparisons were performed using Student's *t* test and multiple comparisons were analysed by two-way analysis of variance (ANOVA) followed by Tukey's honest significant difference (HSD) test. All graphs are plotted as the mean  $\pm$  the standard deviation (S.D.) unless stated otherwise and statistical significance was assumed for  $p < 0.05$ . ns - non significant, \*  $p < 0.05$ , \*\*  $p < 0.01$ , \*\*\*  $p < 0.001$ , \*\*\*\*  $p < 0.0001$ .

# 3 Development of a functional and efficient hNPC1 viral vector

## 3.1 Introduction

As detailed in the previous chapters, although recombinant AAV (rAAV) vectors are currently the standard vector of choice for efficient and widespread delivery to the CNS, the integration of the relatively large hNPC1 cDNA of 3.8kb in to a size limited rAAV construct of 4.7kb would be challenging. Initial rAAV-hNPC1 construct variations conceived at the start of this study utilising standard rAAV templates would have resulted in a final oversized construct of ~5kb and over. While relatively larger genes have previously been integrated into functional rAAV vectors, which result in an oversized rAAV genome, the packaging efficiency and resulting viral production and transduction efficiency were significantly reduced (Dong et al., 1996, Lai et al., 2010, Wu et al., 2010, Choi et al., 2014). Lower viral titers and potential truncation of oversized viral genomes would result in reduced numbers of cells being successfully transduced with the complete construct. Major adjustments to a standard rAAV construct would therefore have to be made in order to reduce vector genome size, thereby maximising packaging and production efficiency, while also attempting to maintain high levels of transgene expression. Due to the previously described lack of cross-correction potential of the NPC1 protein (**Section 1.8**), the transduction of the highest number of cells possible will be crucial for maximum therapeutic efficacy. While other viral and non-viral vectors with larger packaging capacity can be utilised, their transduction spread and efficiency within the brain may not be sufficient for NP-C. Taking these points into consideration, the delivery of hNPC1 would have to balance a variety of factors including transduction

spread, expression levels and production efficiency in the context of realistic clinical potential.

### 3.2 Chapter Aims

This chapter aims to start with the presentation of the results of a gene delivery vector study, which was carried out to determine the optimal vector to be used for widespread delivery of hNPC1 throughout the brain, after ICV administration. This is followed by the development and synthesis of a rAAV construct capable of efficiently expressing the complete human NPC1 protein to supraphysiological levels. The results of *in vitro* testing of the hNPC1 plasmid construct and *eGFP* reporter equivalent are subsequently presented to justify the continuation of these variants for AAV9-hNPC1 vector production, used in initial *in vivo* testing. Vector production analysis is followed by results of transgene expression, vector tropism and toxicity studies *in vivo*, where wild-type mice were administered neonatally with the produced vector. In combination, the results presented in this chapter validate the use of the produced AAV9-hNPC1 vector for subsequent preclinical studies in the *Npc1*<sup>-/-</sup> mouse model.

### 3.3 Vector Study

Although AAV is currently the vector of choice for gene delivery to the brain, one of its major limitations is the restricted packaging size that it has. This can be problematic for larger genes such as NPC1. Other commonly used vectors do not have such a restricted packaging capacity. Therefore, before committing to a potentially more complex AAV-based approach, a side-by-side evaluation of different vectors was conducted. All vectors were designed to express an *eGFP* reporter gene, under the control of the strong and constitutively active cytomegalovirus promoter (Damdindorj et al., 2014), to allow a direct comparison of

vector spread and *eGFP* expression (Rahim et al., 2012). Administration of individual vectors was carried via intracerebroventricular injection to the neonatal mouse brain at the highest possible dose for each respective vector, to compare the efficiency of transduction. As AAV9 vectors have previously shown to result in extensive transgene expression throughout the brain following ICV injection (McLean et al., 2014), an AAV2/9.CMV.eGFP.WPRE vector was sourced from the Penn Vector Core facility (University of Pennsylvania, Philadelphia, PA, US) at a titre of  $6 \times 10^{13}$  vg/ml and a total dose of  $6 \times 10^{11}$  vg was administered. Due to the previously mentioned issue of immunogenicity associated with human adenoviral serotypes (Jooss and Chirmule, 2003, Bessis et al., 2004), the canine adenovirus serotype 2 (CAV-2), shown to have a low rate of pre-existing neutralising antibodies in mice and humans compared to hAd5 vectors (Kremer et al., 2000) was evaluated. CAV-2 was kindly provided by Dr. E. Kremer (Institut de Génétique Moléculaire de Montpellier, France) at a titre of  $1 \times 10^{12}$  vp/ml and a total dose of  $1 \times 10^{10}$  vp was administered. The lentiviral LV.VSV-G.CCL.SIN.cPPT.CMV.eGFP.WPRE vector used in this study was produced in collaboration with Dr. S. Howe (UCL Institute of Child Health, London, UK) to a titer of  $9.2 \times 10^8$  vp/ml and a total dose of  $9.2 \times 10^6$  vp was administered. Finally a non-viral vector was also evaluated, although as previously stated (**Section 1.6**) these vectors have shown poor and short-term transfection efficiency (Kenny et al., 2013). A novel non-viral vector cationic complex containing a CMV.eGFP construct was kindly provided by Prof. S. Hart (Institute of Child Health, London, UK) and a total of  $10\mu\text{l}$  of nanocomplex formulation was administered.

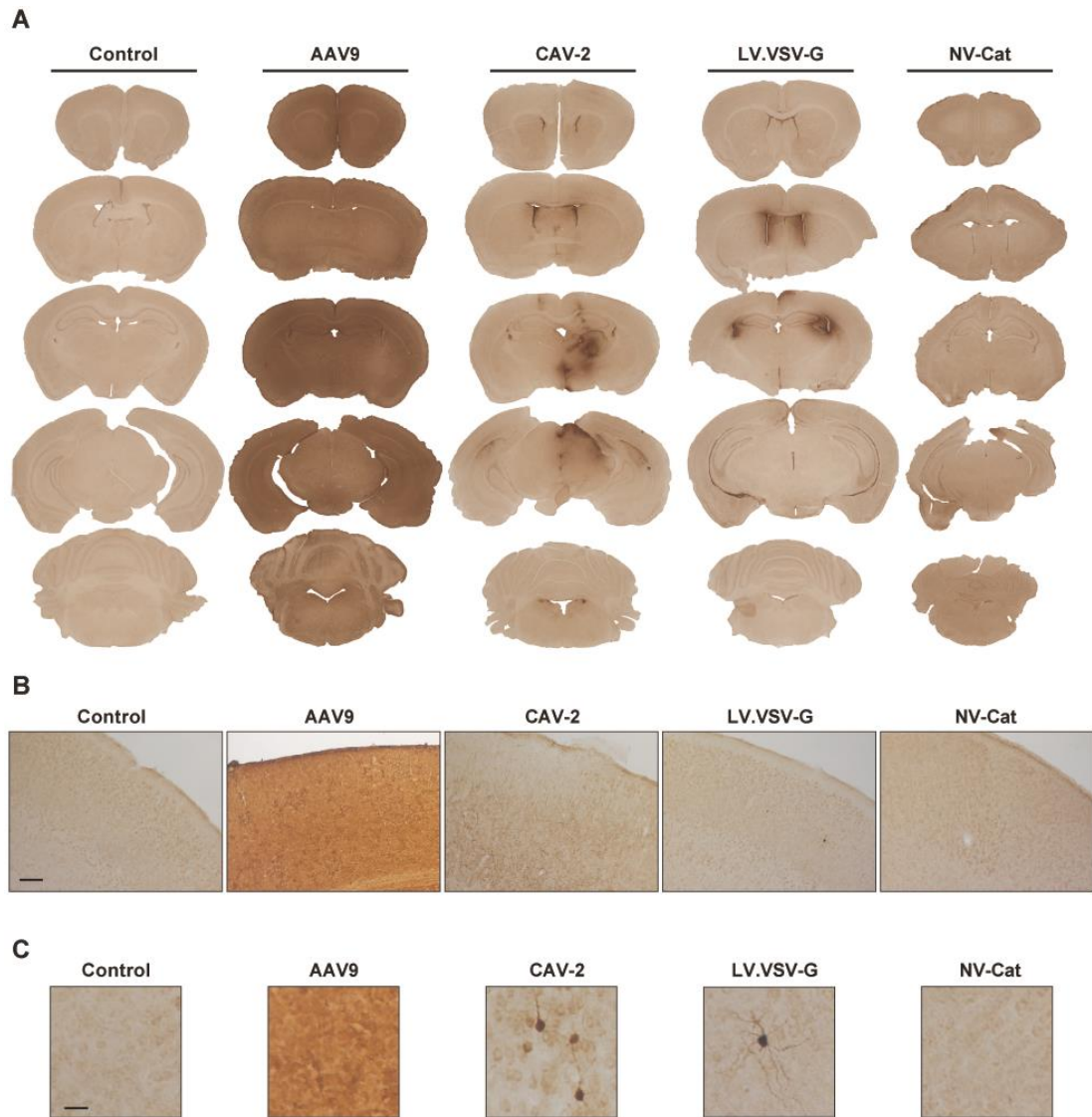


**Figure 11: Vector study comparing eGFP expression in mouse brains following P0 bilateral intracerebroventricular administration of gene delivery vectors.**

Vectors expressing *eGFP* driven by the CMV promoter were administered at their highest possible dose into P0 wild-type mice via bilateral ICV injection ( $n = 3$  for each group). Brains were harvested 14 (non-viral) or 30 (viral) days post-injection, sectioned and analysed by anti-eGFP IHC. Gene delivery vectors and doses: AAV2/9.CMV.eGFP.WPRE (AAV9,  $6 \times 10^{11}$  vg), canine adenoviral vector CAV-2.CMV.eGFP (CAV-2,  $1 \times 10^{10}$  vp), lentiviral vector LV.VSV-G.CCL.SIN.cPPT.CMV.eGFP.WPRE (LV.VSV-G,  $9.2 \times 10^6$  vp) and  $10\mu\text{l}$  of non-viral cationic complex containing CMV.eGFP (NV-Cat).

- (A) Images of whole brain representative sections presented rostral to caudal, exhibiting eGFP expression.
- (B) Representative images from the S1BF region of the cerebral cortex. Scale bar:  $100\mu\text{m}$ .
- (C) Higher magnification images from the S1BF region of the cerebral cortex. Scale bar:  $20\mu\text{m}$ .

P0/1 CD-1 wild-type pups were administered with the individual vectors via bilateral ICV injection. Viral vector injected and non-injected control mice were sacrificed 30 days post-injection to analyse sustained transgene expression into adulthood. However, mice injected with the non-viral vector were sacrificed at 14 days post-injection, due to the previously observed transient expression resulting from these complexes (Kenny et al., 2013).

Immunohistochemistry with anti-eGFP antibody was carried out on whole-brain sections and representative images were captured by light microscope (**Figure 11A**). No significant background staining was present in the brains of uninjected P30 control mice, however widespread rostrocaudal eGFP expression was observed throughout the entire brain of age-matched mice injected with AAV2/9.CMV.eGFP.WPRE. eGFP expression was extensive enough in brains injected with AAV2/9.CMV.eGFP.WPRE, that identification of clear cellular morphology was challenging at higher magnifications (**Figure 11B-C**). Age-matched brains injected with other viral vectors showed both extremely limited efficiency of transduction and distribution through the brain, when compared to the AAV2/9 vector. No eGFP positive cells could be identified in mice injected with the non-viral cationic complex at 14 days post-injection, indicating short transient expression or limited transfection efficiency. However, as anticipated following ICV administration directly in to the cerebral spinal fluid, eGFP positive ependymal cells lining the luminal surface of the ventricle walls could be observed following CAV-2 administration. Positive eGFP staining was also observed around the site of injection and at higher magnifications these cells appeared to show a neuronal morphology. However, in remaining areas of the brain the spread of transduction was either severely limited or absent.

A similar transduction profile was also observed in brains injected with VSV-G.CCL.SIN.cPPT.CMV.eGFP.WPRE, as ependymal cells throughout the ventricles in the brain exhibited positive eGFP staining and the distribution of transduced cells in the brain was anatomically limited. At higher magnification individual eGFP positive cells with neuronal and glial morphology could be observed. Interestingly, extensive levels of eGFP expression were observed in the olfactory bulbs of P30 mice injected neonatally with VSV-G.CCL.SIN.cPPT.CMV.eGFP.WPRE, compared

to the relatively limited transduction in all other brain areas (**Figure 12A**). In combination with high levels of ependymal cell transduction around the lateral ventricle, it was hypothesised that the lentiviral vector had transduced cells in the rostral migratory stream. The rostral migratory stream is a migratory route of neural progenitors known as neuroblasts, from the subventricular zone surrounding the lateral ventricle towards and into the olfactory bulb (Pencea et al., 2001). These migrating neuroblasts subsequently mature into neurons and in certain situations can migrate to sites of damage, where they may play a role in regeneration (Capilla-Gonzalez et al., 2015). To analyse the potential transduction of the rostral migratory stream, sagittal sections from the brains of P30 mice injected neonatally with VSV-G.CCL.SIN.cPPT.CMV.eGFP.WPRE underwent immunohistochemistry against eGFP (**Figure 12B**). Imaged under light microscopy, a distinct line of eGFP positive cells could be observed originating from subventricular zone of the lateral ventricle and extending into the olfactory bulb (**Figure 12C**). Additionally, in collaboration with Prof. T. McKay and Ms. L. Fitzpatrick (St. George's University of London), immunofluorescent co-staining of eGFP and Nestin, an intermediate filament protein expressed in neuronal precursor cells (Wang et al., 2011), was carried out (**Figure 12D**). Confocal microscopy imaging revealed that the previously observed stream of eGFP positive cells also exhibited positive Nestin expression, confirming neuroblast transduction within the rostral migratory stream.

Although this observation may or may not be of direct interest or benefit for the treatment of NP-C, the subventricular zone is one of only two areas of active and proliferating stem cell niches in the central nervous system (Gage, 2000) and the ability to target and transduce these neural progenitors with a viral vector may in the future be of novel therapeutic benefit.

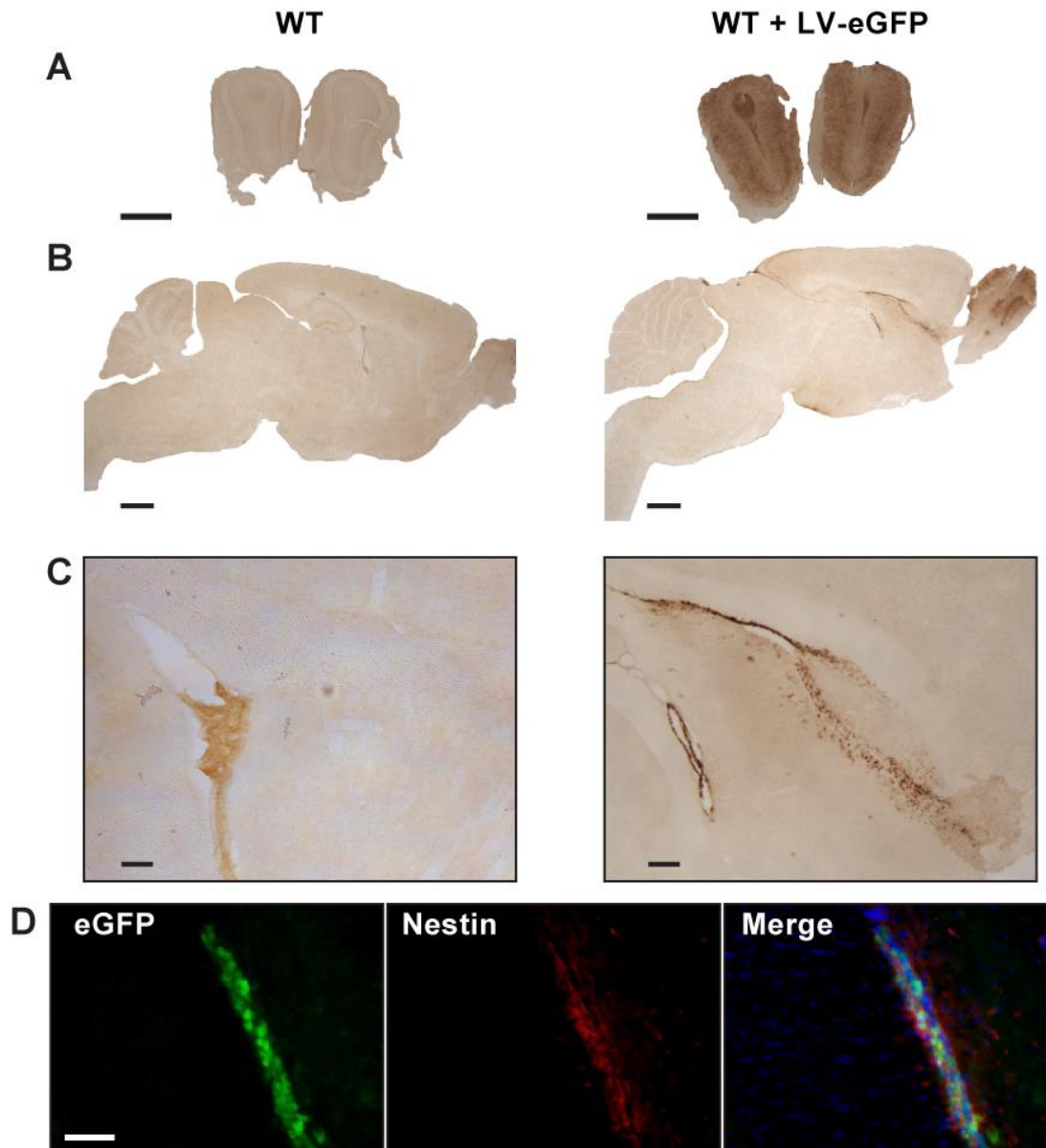


**Figure 12: Lentiviral vector transduction of neuroblasts in the rostral migratory stream.**

- (A) Representative coronal sections of olfactory bulbs from a P30 mouse brain administered P0 with VSV-G.CCL.SIN.cPPT.CMV.eGFP.WPRE (WT + LV-eGFP) and age-matched uninjected control (WT). Scale bar: 250 $\mu$ m.
- (B) Representative sagittal sections of a P30 mouse brain administered at P0 with VSV-G.CCL.SIN.cPPT.CMV.eGFP.WPRE and age-matched uninjected control. Scale bar: 1000 $\mu$ m.
- (C) Magnification of the lateral ventricle subventricular zone exhibited in (B). Scale bar: 50 $\mu$ m.
- (D) Co-localisation of eGFP positive cells from the RMS with neural progenitor cell marker Nestin. Scale bar: 50 $\mu$ m. [Performed in collaboration with Prof. T. McKay and Ms L. Fitzpatrick at St. George's University of London.]

The transgene expression levels and spread of transduction resulting from neonatal ICV AAV2/9 administration compared to the other delivery vectors was clearly superior. As previously stated (**Section 1.8**) widespread and efficient transduction of as many cells possible will be crucial for maximal therapeutic efficacy for Niemann-Pick Type C. While adenoviral and lentiviral vectors may have potential for treatments able to take advantage of cross-correction to amplify therapeutic efficacy, the lack of transduction efficiency would most likely be too limited for therapeutic hNPC1 delivery. As a result of the vector study, despite the obstacles of rAAV packaging capacity and potential downstream production challenges, an AAV2/9 vector based approach was chosen as the delivery mechanism for hNPC1 gene delivery.

### 3.4 Incorporating hNPC1 into an rAAV construct

Following the highly efficient transduction of neural cells throughout the brain demonstrated by the AAV2/9 vector in the vector study, a strategy to incorporate the relatively large human NPC1 cDNA into a functional and clinically relevant rAAV construct was devised, as appropriate for use in a preclinical study. Furthermore, the constructs and vectors used and tested in the murine *Npc1*<sup>-/-</sup> model throughout this study therefore express the clinically relevant human NPC1 cDNA and human NPC1 protein, as opposed to the murine variants. Human and murine NPC1 cDNA and protein sequences share an 84% and 86% homology respectively (**Supplementary Figure S1** and **Supplementary Figure S2**), so the functionality of human NPC1 was expected to be conserved in the murine model. Due to the susceptibility of neuronal loss in NP-C disease, the transduction of the maximum number of neurons possible was prioritised. Additionally, a previous study demonstrated in a chimeric mouse model of NP-C, that neuronal loss is primarily a cell-autonomous defect (Ko et al., 2005). *Npc1*<sup>-/-</sup> Purkinje cells were not rescued by surrounding *Npc1*<sup>+/+</sup> glial cells, however *Npc1*<sup>+/+</sup> Purkinje cells were not lost when surrounded by *Npc1*<sup>-/-</sup> glial cells. Consequently the decision to prioritise maximal AAV-mediated NPC1 production in neurons led to the decision of choosing the strong human neuronal promoter

synapsin I (*SynI*) to drive hNPC1 expression. A rAAV construct containing the *hSynI.flox.eGFP.WPRE.hGHpA* expression cassette flanked by AAV2 ITRs was kindly provided by Dr. J. Tordo (Department of Infectious Diseases, King's College London, UK). To accommodate the large NPC1 gene, the first consideration was the removal from the template construct of as much DNA as possible, deemed non-essential for basic transgene expression. These non-essential sequences included the original eGFP transgene, flanking *loxP* sites and the woodchuck hepatitis virus post-transcriptional regulatory element (WPRE) sequence. The WPRE sequence is frequently added to viral expression cassettes to enhance transgene expression (Zufferey et al., 1999), though the extent of enhancement can vary with different promoters and cell types (Klein et al., 2006). However, due to the WPRE sequence length of 609bp and limited rAAV packaging capacity, it was chosen not to be included in the hNPC1 construct.

Removal of these sequences and incorporation of the hNPC1 gene was carried out by restriction enzyme digest and subsequent ligation. The template plasmid *pAAV.hSynI.flox.eGFP.WPRE.hGHpA* was digested with restriction enzymes *KpnI* and *BglII*, which cut directly downstream of the *SynI* promoter and directly upstream at the start of the *hGHpA* sequence (**Figure 13A**). The products of this digest underwent agarose gel electrophoresis, where the predicted 3.9kb segment consisting of the remaining construct and plasmid backbone was observed (**Figure 13D**). The human NPC1 cDNA was amplified via PCR from the *pCMV6neo.hNPC1* template plasmid kindly provided by Prof. FM Platt (Department of Pharmacology, University of Oxford, Oxford, UK). Primers were additionally designed to incorporate the translation enhancing Kozak consensus sequence (Kozak, 2005) and the *KpnI* and *BglII* restriction enzyme sites directly at the 5' and 3' end of the hNPC1 cDNA respectively (**Figure 13B**). The resulting PCR product was subsequently digested with *KpnI* and *BglII* restriction enzymes to produce sticky ends compatible to the previously digested backbone and underwent agarose gel electrophoresis, where the predicted 3.8kb hNPC1 cDNA segment was observed (**Figure 13D**). The 3.9kb rAAV backbone and 3.8kb hNPC1 insert were then extracted from the gel, purified and ligated at a molar ratio of 1:3 backbone to insert respectively, to produce *pAAV.hSynI.hNPC1.hGHpA* (**Figure 13C**). Incorporation of the insert was initially confirmed by *KpnI* restriction enzyme digest and agarose gel electrophoresis, which

revealed the predicted clear single band of *pAAV.hSynI.hNPC1.hGHpA* at ~7.8kb (**Figure 13E**). 5' ITR to 3' ITR automated Sanger sequencing (Source Biosciences) was additionally carried out to confirm complete and un-mutated hNPC1 incorporation and correct integration at the desired ligation sites (**Figure 13F-G**). The completed *pAAV.hSynI.hNPC1.hGHpA* construct had an oversized 5' ITR to 3' ITR viral genome of 5,154bp. To further reduce the rAAV-hNPC1 construct size, the human growth hormone polyadenylation signal sequence, at 496bp in length, was identified as the next modification target.

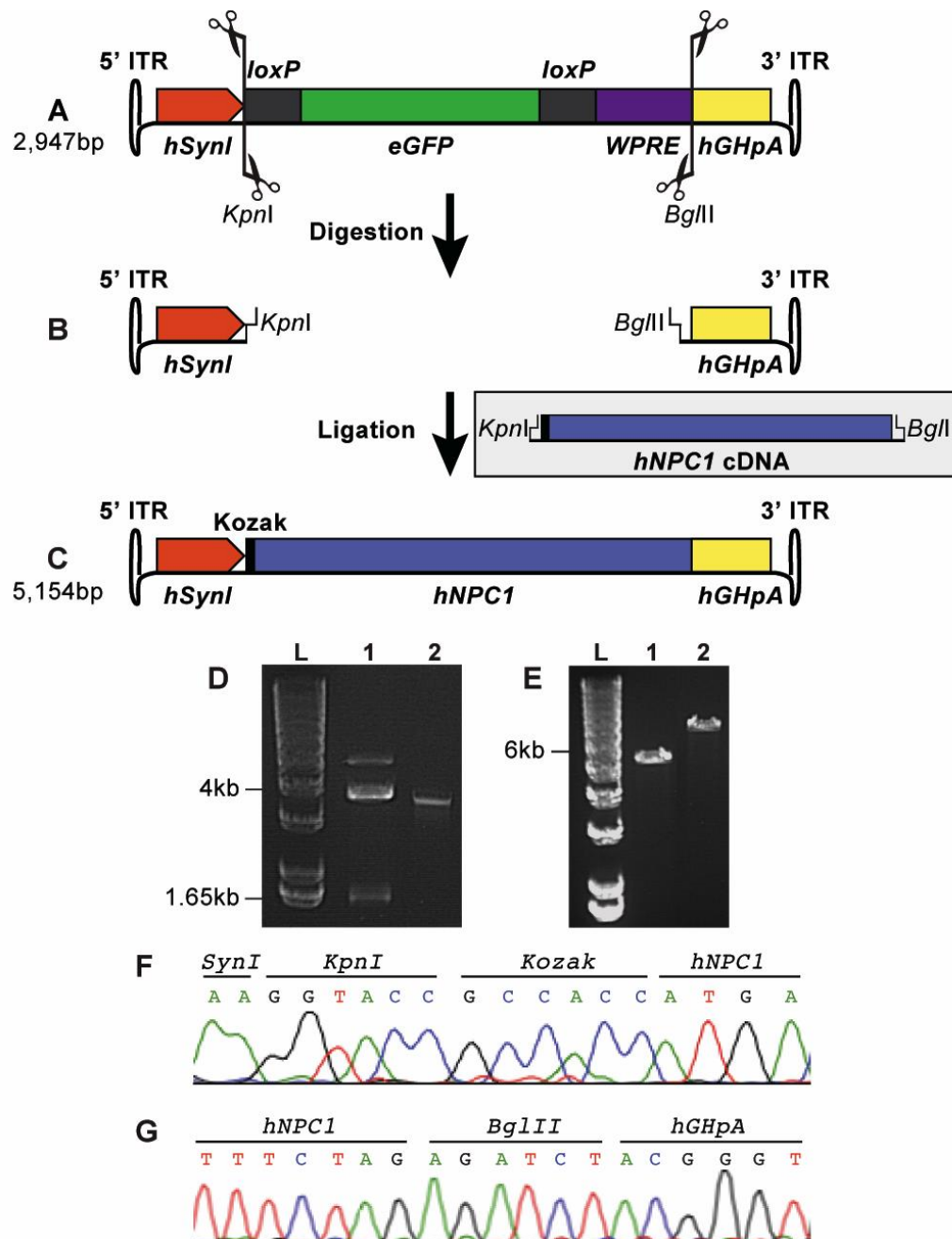


**Figure 13: Summary of hNPC1 cDNA integration into a rAAV construct to produce pAAV.hSynI.hNPC1.hGHpA.**

- (A) Illustration of pAAV.hSynI.flox.eGFP.WPRE.hGHpA template construct.
- (B) Illustration of pAAV.hSynI.flox.eGFP.WPRE.hGHpA template following *KpnI* and *BglII* restriction enzyme digest.
- (C) Illustration of resulting pAAV.hSynI.hNPC1.hGHpA construct.
- (D) Image of *KpnI* and *BglII* double digest of 1 – pAAV.hSynI.flox.eGFP.WPRE.hGHpA template, 2 – hNPC1 cDNA PCR product. L – Ladder.
- (E) Image of *KpnI* confirmation digest of 1 – pAAV.hSynI.flox.eGFP.WPRE.hGHpA template, 2 – pAAV.hSynI.hNPC1.hGHpA construct. L – Ladder.
- (F) Section of Sanger sequencing electropherogram verifying 5' ligation site.
- (G) Section of Sanger sequencing electropherogram verifying 3' ligation site.

### 3.5 Introduction of SV40pA signal sequence

Significant reductions in efficient viral genome packaging and subsequent viral vector production efficiency have been observed in rAAV vectors with genomes exceeding 4.9-5kb. In an attempt to further reduce problems with downstream vector packaging and production efficiency, the 496bp human growth hormone polyadenylation signal sequence was replaced with the commonly used 193bp SV40 late polyadenylation signal sequence (Fitzgerald and Shenk, 1981). This change shortened the viral genome to 4,858bp, under the 4.9kb threshold (**Figure 14**).

The hGHpA signal sequence was removed from the *pAAV.hSynI.hNPC1.hGHpA* construct via restriction enzyme digest with *Bgl*III and *Pml*I restriction enzymes, cutting directly downstream of the *hNPC1* cDNA stop codon and upstream of the 3'ITR respectively (**Figure 14A**). Digest products were analysed by agarose gel electrophoresis, where the predicted 7.2kb band, consisting of the remaining construct and plasmid backbone, was observed (**Figure 14D**). The *SV40pA* signal sequence was amplified from the *pSUB201-Caggs-GFP* template plasmid via PCR, utilising primers designed to incorporate *Bgl*III and *Pml*I restriction enzyme sites directly at the 5' and 3' ends of the SV40pA signal sequence respectively (**Figure 14B**). The products of this PCR reaction were digested with restriction enzymes *Bgl*III and *Pml*I, to produce the sticky ends necessary for ligation with the digested backbone and were analysed by agarose gel electrophoresis, where the predicted 200bp band was observed (**Figure 14D**). The required 7.2kb backbone band and 0.2kb SV40pA band were subsequently extracted, purified and ligated to produce *pAAV.hSynI.hNPC1.SV40pA* (**Figure 14C**). The produced construct was verified by ITR to ITR automated Sanger sequencing (**Figure 14E-F**), confirming a final vector genome size of 4,858bp.

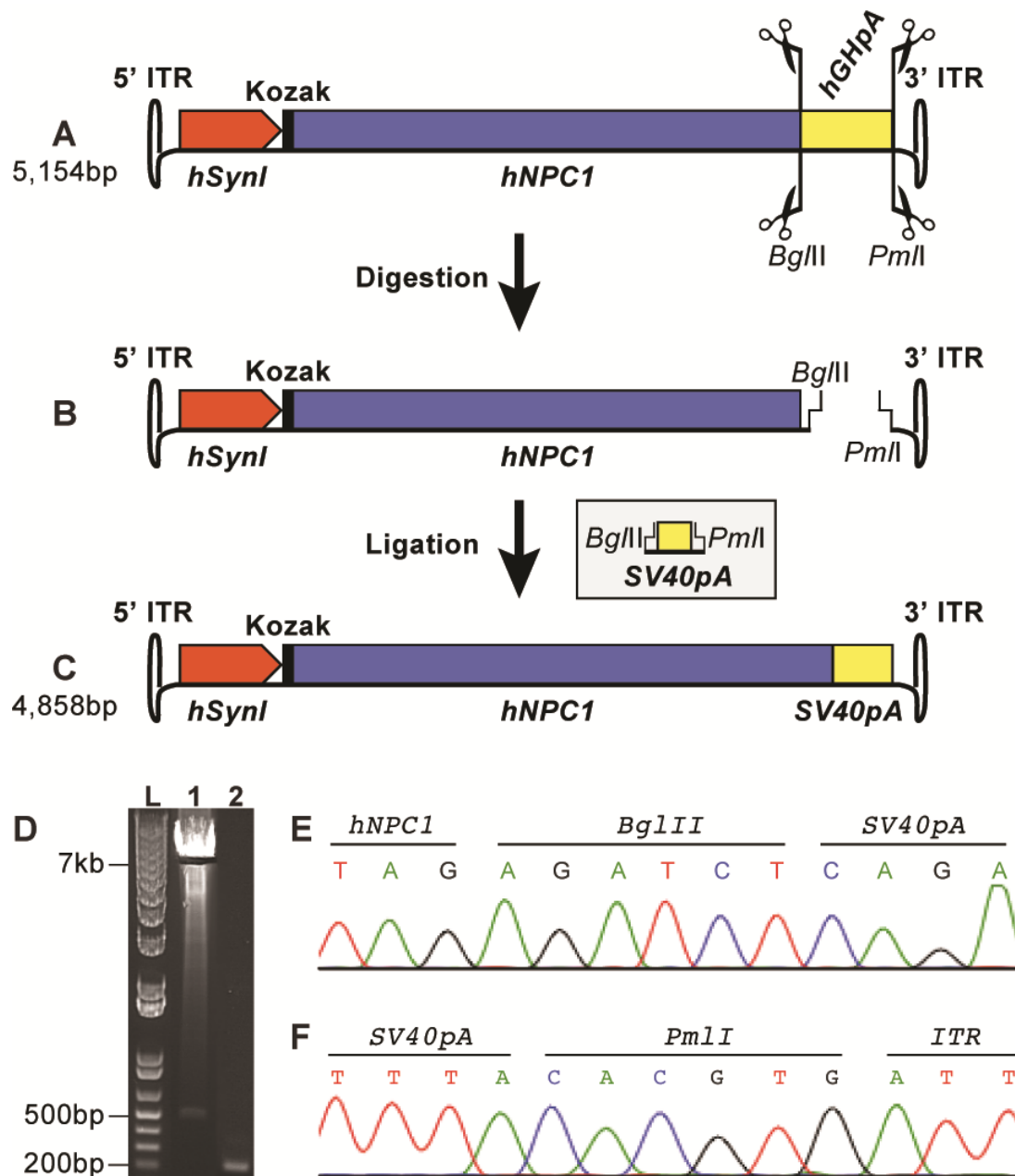


**Figure 14: Summary of SV40pA signal sequence integration to produce pAAV.hSynI.hNPC1.SV40pA.**

(A) Illustration of pAAV.hSynI.hNPC1.hGHpA template construct.

(B) Illustration of pAAV.hSynI.hNPC1.hGHpA template following BglII and PmlI restriction enzyme digest.

(C) Illustration of resulting pAAV.hSynI.hNPC1.SV40pA construct.

(D) Image of BglII and PmlI double digest of 1 – pAAV.hSynI.hNPC1.hGHpA template with extracted band, 2 – SV40pA PCR product. L – Ladder.

(E) Section of Sanger sequencing electropherogram verifying 5' ligation site.

(F) Section of Sanger sequencing electropherogram verifying 3' ligation site.

The *pAAV.hSynI.hNPC1.SV40pA* construct remains over the standard AAV wild-type genome size of 4.7kb, however under the 4.9kb threshold at which vector production and transduction efficiency have been observed to be significantly affected (Wu et al., 2010, Choi et al., 2014). Alterations or minimising of either the promoter or polyadenylation signal sequences to reduce construct size further would have required changes to the wild-type sequences, which may potentially have impacted transgene expression. As a result, the *pAAV.hSynI.hNPC1.SV40pA* viral vector construct was used for basic *in vitro* and *in vivo* testing before being used for a preclinical study in the *Npc1*<sup>-/-</sup> mouse model.

### 3.6 Synthesis of eGFP reporter construct

Following discussion with collaborators and others researchers working in the NP-C field, we were advised that the commercial antibodies available against the NPC1 protein were not highly efficient. Therefore, to facilitate initial *in vitro* and *in vivo* analysis of the novel *pAAV.hSynI.hNPC1.SV40pA* viral vector, a clone replacing the *hNPC1* cDNA with an *eGFP* reporter gene was created (**Figure 15**). The *hNPC1* cDNA was extracted via the previously utilised *KpnI* and *BglIII* restriction enzymes from the *pAAV.hSynI.hNPC1.SV40pA* plasmid (**Figure 15A**). PCR was used to amplify the *eGFP* reporter gene from the *pSUB201-Caggs-GFP* template plasmid, utilising primers introducing a Kozak consensus sequence and the *KpnI* and *BglIII* restriction enzyme sites at the 5' and 3' ends of the *eGFP* gene respectively (**Figure 15B**). The PCR product was also digested with *KpnI* and *BglIII* restriction enzymes and was analysed by agarose gel electrophoresis together with the backbone digest products. The predicted 3.6kb backbone band and 0.7kb *eGFP* insert band were extracted from the gel, purified and underwent ligation to produce the *pAAV.hSynI.eGFP.SV40pA* (**Figure 15C**). Confirmation of complete *eGFP* integration was carried out by automated Sanger sequencing (**Figure 15D-E**). Produced viral vector plasmids *pAAV.hSynI.eGFP.SV40pA* and *pAAV.hSynI.hNPC1.SV40pA* subsequently underwent *in vitro* testing, to confirm vector functionality.

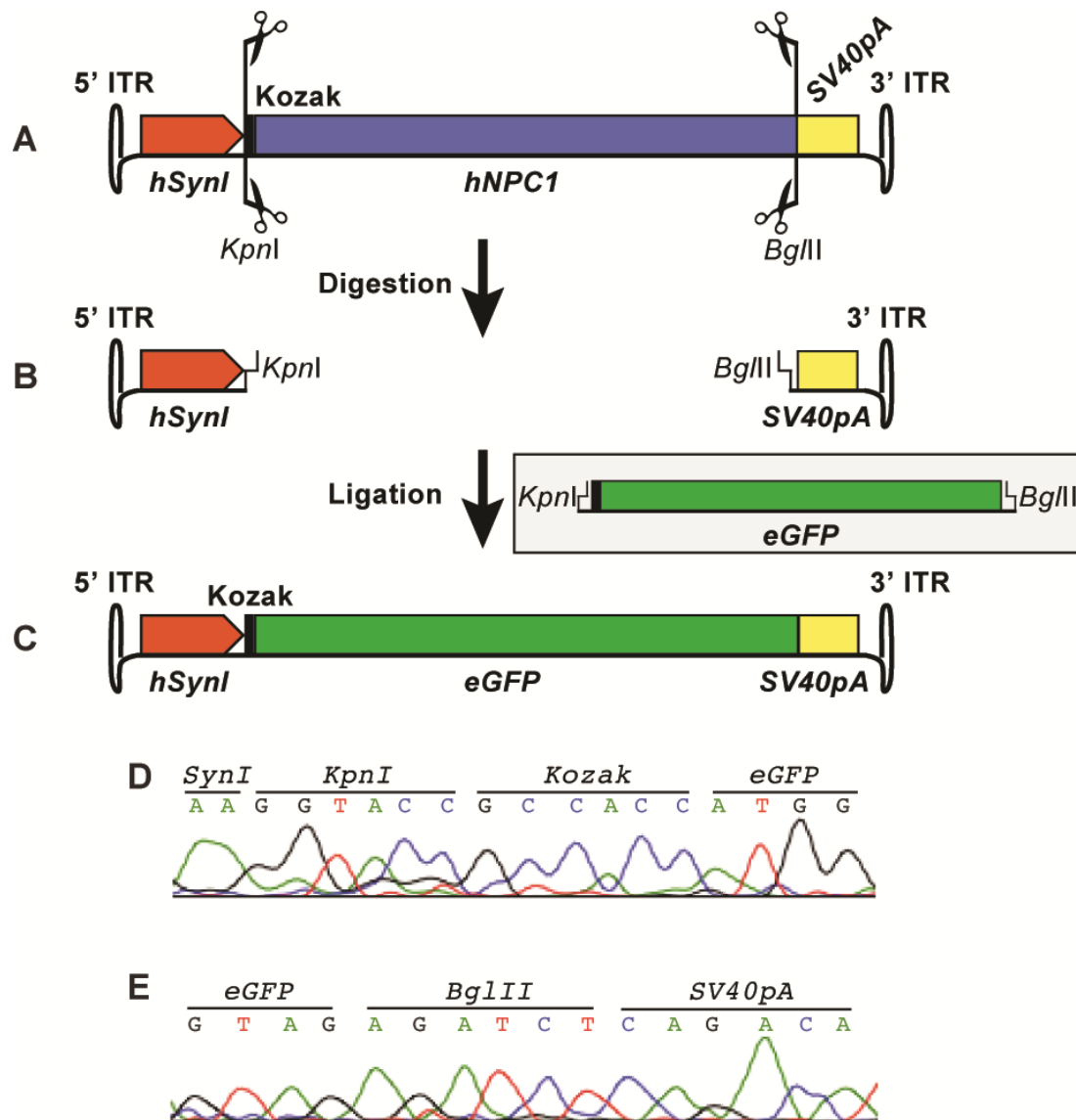


**Figure 15: Summary of *hNPC1* replacement with *eGFP* reporter gene to produce *pAAV.hSynI.eGFP.SV40pA*.**

- (A) Illustration of *pAAV.hSynI.hNPC1.SV40pA* template construct.  
 (B) Illustration of *pAAV.hSynI.hNPC1.SV40pA* template following *KpnI* and *BglII* restriction enzyme digest.  
 (C) Illustration of resulting *pAAV.hSynI.eGFP.SV40pA* construct.  
 (D) Section of Sanger sequencing electropherogram verifying 5' ligation site.  
 (E) Section of Sanger sequencing electropherogram verifying 3' ligation site.

### 3.7 *In vitro* testing confirms functional hNPC1 and eGFP constructs

To verify if the *pAAV.hSynI.eGFP.SV40pA* and *pAAV.hSynI.hNPC1.SV40pA* plasmids were capable of expressing their transgenes and respectively encoded proteins, a series of transfections in wild-type HEK-293T cells was carried out (**Figure 16**). The amount of NPC1 protein 72 hours post-transfection was analysed by Western blot in cells transfected with *pAAV.hSynI.hNPC1.SV40pA* plasmid. NPC1 levels were compared to cells transfected with the original hNPC1 expression plasmid *pCMV6.hNPC1.Neo* as a positive control and endogenous levels of NPC1 in the untransfected control cells (**Figure 16**).

Staining with an anti-NPC1 antibody revealed that a single band at the predicted size of 170kDa was present in all groups, representing the NPC1 protein (**Figure 16A**). A statistically significant overexpression of NPC1 was observed in samples transfected with both expression plasmids compared to endogenous control levels, indicating successful expression of the hNPC1 transgene (**Figure 16B**). The eGFP reporter construct *pAAV.hSynI.eGFP.SV40pA* was also transfected into human neuroblastoma SH-SY5Y cells to confirm functional transgene expression (**Figure 16C**). 48 hours post-transfection cells were imaged using fluorescent microscopy, where no background eGFP expression was observed in untransfected control cells. Cells transfected with the construct exhibited positive whole cell eGFP fluorescence, indicating functional transgene and downstream protein expression.

As a result of *in vitro* confirmation of the *pAAV.hSynI.eGFP.SV40pA* and *pAAV.hSynI.hNPC1.SV40pA* transgene expression capability, both constructs were used to produce AAV2/9 viral vectors for subsequent *in vivo* testing.

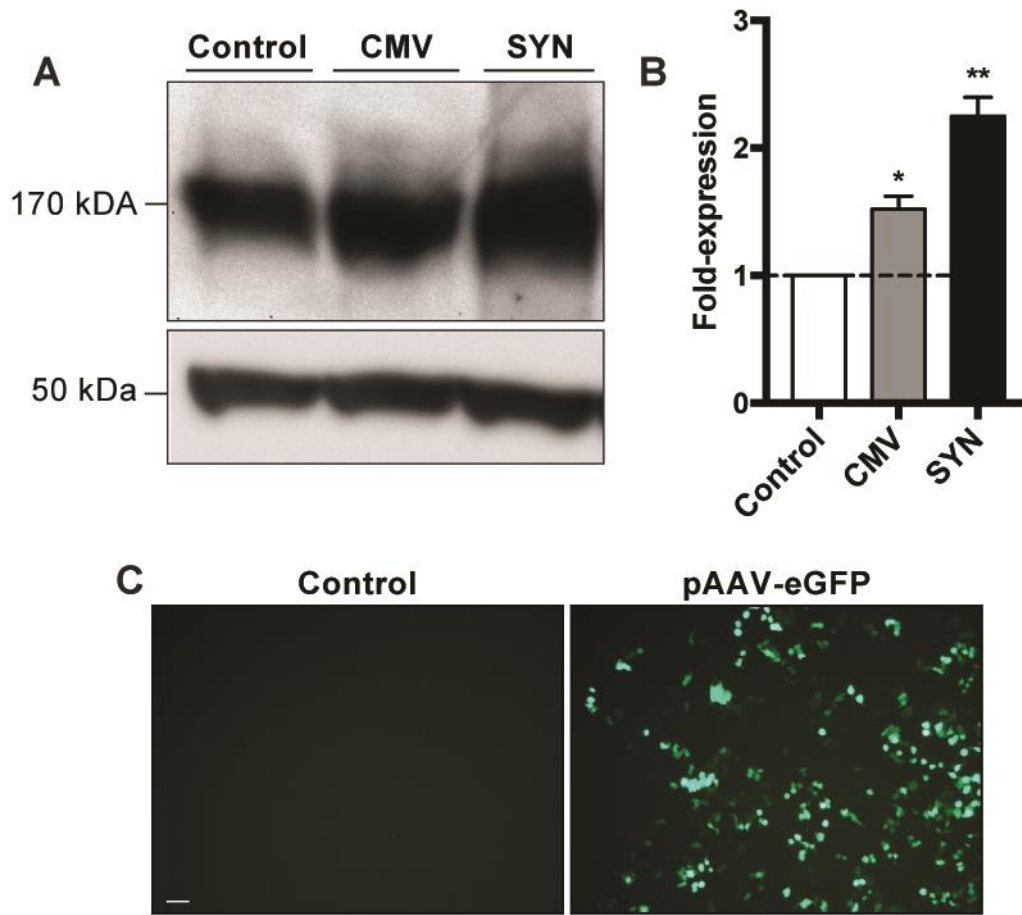


**Figure 16: *In vitro* hNPC1 and eGFP expression.**

- (A) Western blot analysis of NPC1 levels in HEK-293T cells following transfection with positive control *pCMV6.hNPC1.Neo* (CMV) and *pAAV.hSyn1.hNPC1.SV40pA* (SYN) compared to endogenous NPC1 in untransfected negative control (Control). 170kDa band represents NPC1 protein. 50kDa band represents the  $\beta$ -tubulin loading control.
- (B) Densitometric quantification of NPC1 bands normalised against loading control and expressed as fold change of endogenous control NPC1 levels. Data represented as mean  $\pm$  S.D., compared by One-way ANOVA. \*  $p < 0.05$ ; \*\*  $p < 0.01$ ;  $n = 2$  blots with 3 samples per group.
- (C) Fluorescent microscopy images of untransfected control SH-SY5Y cells and cells transfected with *pAAV.hSyn1.eGFP.SV40pA* construct ( $n = 3$  per group) resulting in eGFP expression. Scale bar: 40 $\mu$ m.

### 3.8 No elevation in NPC1 following codon optimisation of hNPC1 cDNA

With the aim of increasing NPC1 protein expression efficiency of the newly produced rAAV construct, codon optimisation of the human *NPC1* cDNA was carried out. The final NPC1 amino acid sequence was not modified, however specific changes to the cDNA sequence and resulting codon distribution were made with the aim of improving the rate and stability of translation (Plotkin and Kudla, 2011). In total 30% of the wild-type hNPC1 nucleotide sequence was changed however the resulting NPC1 amino acid sequence remained conserved. Design and synthesis of the optimised NPC1 sequence (*NPC1O*) was outsourced to Genscript (China), with a Kozak sequence and *KpnI* restriction enzyme site incorporated directly at the 5' end of *NPC1O* and a *BglII* restriction enzyme site directly after the stop codon. The synthesised *NPC1O* sequence was extracted from the *pU57.NPC1O* template via *KpnI* and *BglII* restriction enzyme digest. The wild-type *NPC1* cDNA was simultaneously removed from the *pAAV.hSynI.hNPC1.SV40pA* with identical restriction enzymes. Digest products were then separated by agarose gel electrophoresis, where the desired bands were extracted purified and ligated to produce the *pAAV.hSynI.hNPC1O.SV40pA* construct (**Figure 17A**).

A series of transfections in HEK-293T cells with the original hNPC1 construct *pAAV.hSynI.hNPC1.SV40pA* and codon optimised *NPC1O* construct *pAAV.hSynI.hNPC1O.SV40pA* were carried out, to compare resulting NPC1 expression by Western blot (**Figure 17B**). Wild-type non-transfected control samples showed low-level endogenous hNPC1. As previously presented in **Section 3.7**, cells transfected with the *pAAV.hSynI.hNPC1.SV40pA* construct exhibited significantly higher expression of NPC1, compared to endogenous levels (**Figure 17C**). Transfection of the codon optimised *pAAV.hSynI.hNPC1O.SV40pA* construct also resulted in significantly higher NPC1 expression, compared to untransduced control cells. However, no significant difference in NPC1 amount was observed in cells transfected with the two constructs, indicating that this specific codon optimised variant did not further enhance NPC1 expression. As a result of these findings, the original *pAAV.hSynI.hNPC1.SV40pA* construct was chosen for vector production, as

the function of the NPC1 protein produced by wild-type cDNA expression did not have to be tested and confirmed.

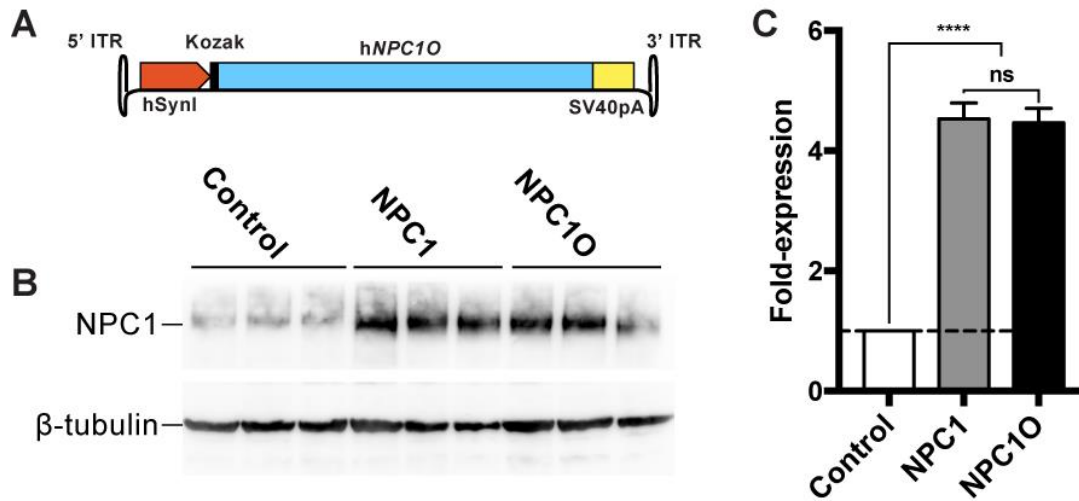


**Figure 17: *In vitro* testing of codon optimised hNPC1O cDNA in HEK-293T cells.**

- (A) Illustration of codon optimised *pAAV.hSynI.hNPC1O.SV40pA* construct.
- (B) Western blot analysis of NPC1 levels in HEK-293T cells following transfection with wild-type *NPC1* cDNA construct *pAAV.hSynI.hNPC1.SV40pA* (NPC1) and codon optimised construct *pAAV.hSynI.hNPC1O.SV40pA* (NPC1O), compared to endogenous NPC1 in untransfected negative control (Control).  $\beta$ -tubulin staining used for loading control.
- (C) Densitometric quantification of NPC1 bands normalised against loading control and expressed as fold change of endogenous NPC1 levels.  $n = 2$  blots with 3 samples per group. Data represented as mean  $\pm$  S.D., compared by One-way ANOVA. ns - non significant, \*\*\*\*  $p < 0.001$

### 3.9 Successful production of oversized AAV2/9-hNPC1 viral vector

The aim of the initial round of AAV9-hNPC1 viral vector production was to identify whether fully packaged and functional viral particles could be produced from the oversized *pAAV.hSynI.hNPC1.SV40pA* construct, at a titer viable for further preclinical studies. AAV2/9-SynI-hNPC1-SV40pA (AAV9-hNPC1) was produced in HEK-293T cells that were harvested and lysed 72 hours post-transfection. Viral particles were then purified by iodixanol gradient ultracentrifugation, where viral particles accumulate and are extracted from a band of known iodixanol density.

Iodixanol gradient ultracentrifugation also results in the beneficial sorting of lighter empty capsids from packaged capsids (Lock et al., 2010), thereby increasing dose efficiency by reducing the administration of non-functional empty capsids. Concentrated viral titer was determined by viral genome and viral particle quantification analysis, where viral capsid protein ratios and complete packaging of the oversized viral genome were simultaneously analysed (**Figure 18**).

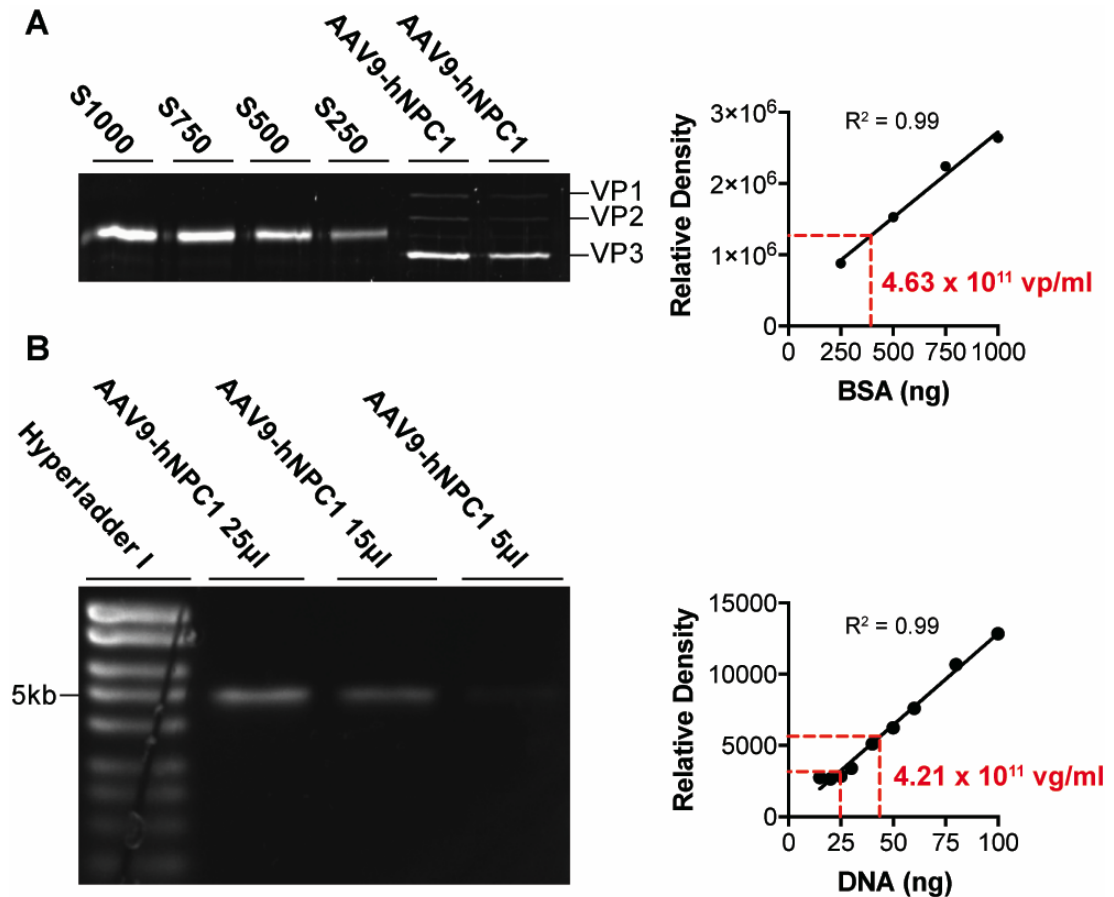


**Figure 18: AAV2/9-SynI-hNPC1-SV40pA titration and vector genome analysis.**

- (A) Viral capsid protein VP3 quantification via SDS-PAGE gel electrophoresis. Titer of concentrated sample was subsequently quantified by densitometric comparison with known BSA quantity standards (S1000 – 1000ng, S750 – 750ng, S500 – 500ng, S250 – 250ng). Resulting viral particle titer of  $4.63 \times 10^{11}$  vp/ml.
- (B) Vector genome quantification against Hyperladder I standard by alkaline gel electrophoresis. Single viral vector genome band at 5kb. Resulting viral genome titer of  $4.21 \times 10^{11}$  vg/ml.

The amount of viral capsid protein VP3 in samples of concentrated AAV9-hNPC1 was quantified against a set of known quantity bovine serum albumin standards, via SDS PAGE gel electrophoresis and subsequent band visualisation by SYPRO Ruby

staining (**Figure 18A**). The resulting titer from the first round of AAV9-hNPC1 production was significantly lower than the standard expected titer of at least  $1 \times 10^{13}$  vp/ml, at  $4.63 \times 10^{11}$  viral particles per ml. Bands representing the remaining larger and less abundant VP1 and VP2 capsid proteins were also observed. Alkaline gel electrophoresis of viral DNA followed by GelRed band visualisation was carried out to quantify the amount of viral genome in a concentrated sample against the Hyperladder I standard (**Figure 18B**). Using this method, the resulting titer of AAV9-hNPC1 was  $4.21 \times 10^{11}$  viral genome copies per ml, comparable to the  $4.63 \times 10^{11}$  vp/ml measured by viral capsid quantification. As anticipated, reductions in final viral titer may have been related to the oversized viral genome of *pAAV.hSynI.hNPC1.SV40pA*. However, crucially the analysis of the AAV9-hNPC1 viral genome confirmed complete packaging of the oversized viral genome, without any indications of major truncation variants, as indicated by a clean single band at 4.9kb.

Although the final titer of AAV9-hNPC1 was 22-fold lower than the titer expected during a standard AAV preparation, the production of viral particles containing the fully packaged *AAV.hSynI.hNPC1.SV40pA* genome was successful. Further optimisation of vector production protocol can be carried out, in attempt to boost viral titer. However as a starting point, this vector was used to carry out initial *in vivo* studies, to confirm functionality of the vector following administration.

### 3.10 AAV2/9-eGFP viral vector production

The eGFP reporter variant of AAV9-eGFP was produced in an identical fashion, using the *pAAV.hSynI.eGFP.SV40pA* construct. Quantification of the viral capsid VP3 in a sample of concentrated AAV9-eGFP, resulted in a viral titer of  $4.8 \times 10^{13}$  vp/ml (**Figure 19**). As transgene and resulting viral genome size was the only differentiating factor between both constructs and the production process, the over 100-fold titer difference in concentrated viral particle yield supported the previously suggested affect of oversized viral genome on vector production efficiency. The

produced AAV9-eGFP vector was subsequently used for *in vivo* dose testing, compared with the AAV9-hNPC1 vector.

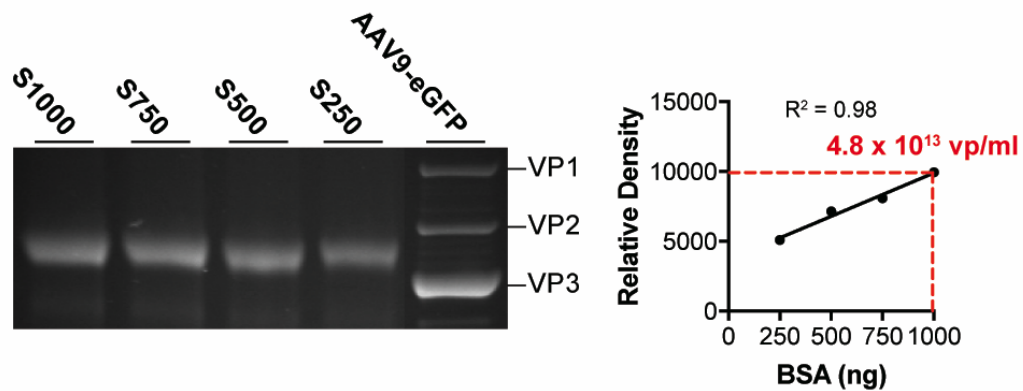


**Figure 19: AAV2/9-SynI-eGFP-SV40pA titration**

AAV titration by quantification of viral capsid protein VP3 via SDS-PAGE gel electrophoresis. Subsequent densitometric comparison with known BSA quantity standards (S1000 – 1000ng, S750 – 750ng, S500 – 500ng, S250 – 250ng) resulted in a viral particle titer of  $4.8 \times 10^{13}$  vp/ml.

### 3.11 Overexpression of NPC1 following low dose AAV9-hNPC1 administration

To confirm the production of a functional AAV9-hNPC1 vector, a low dose of  $4 \times 10^9$  viral particles of AAV9-hNPC1 was administered via bilateral intracerebroventricular injection to P0/1 wild-type mice. At P30, injected mice ( $n = 3$ ) and uninjected age-matched wild-type control mice ( $n = 3$ ) were sacrificed and the brains were harvested and processed for anti-NPC1 immunohistochemistry (**Figure 20**). Analysis of stained brain sections via light microscopy revealed minimal and diffuse positive staining of endogenous NPC1 in the brains of uninjected control brains (**Figure 20A-B**). However, in comparison, the AAV9-hNPC1 administered brains exhibited strong staining in brain regions including the cerebral cortex, thalamus, substantia nigra, cerebellum and brain stem. As expected with low dose vector administration, transduction was not ubiquitous, yet distinct populations of cells showed clear NPC1 expression. Analysis at higher magnification revealed that NPC1 staining was limited to within the soma, specifically in the cytoplasm, of

transduced cells and was punctate in distribution, suggesting localisation to within late endosomes/lysosomes (**Figure 20B**). The robust nature of NPC1 staining also suggested the presence of supraphysiological levels of NPC1 (Millard et al., 2000) in cells following AAV9-hNPC1 administration, compared to the minimal staining of endogenous NPC1 observed in uninjected control mice. Cells exhibiting positive NPC1 staining appeared neuronal in morphology, within all examined brain regions. The brains of mice administered with AAV9-hNPC1 and age-matched uninjected controls were also homogenised and examined for NPC1 levels via Western blot (**Figure 20C**). Wild-type control mice exhibited low level staining of endogenous NPC1, however brains administered with AAV9-hNPC1 again demonstrated supraphysiological levels of NPC1. Critically AAV mediated expression of the NPC1 protein was of the expected ~170kDa size with a clear single band visible, suggesting NPC1 truncation had not occurred despite the oversized viral genome.

These initial results confirmed that the produced AAV9-hNPC1 vector was functional *in vivo* and despite low dose administration, AAV9-hNPC1 was capable of NPC1 delivery and NPC1 expression in regions throughout the brain to supraphysiological levels. Following the observation of inefficient staining of endogenous murine NPC1, additional *in vivo* testing with the eGFP reporter equivalent AAV9-eGFP was also carried out. The aim of AAV9-eGFP administration analysis was to evaluate whether low-level NPC1 expression was being accurately identified with the utilised NPC1 antibodies and additionally gauge transgene expression following higher dose administration.

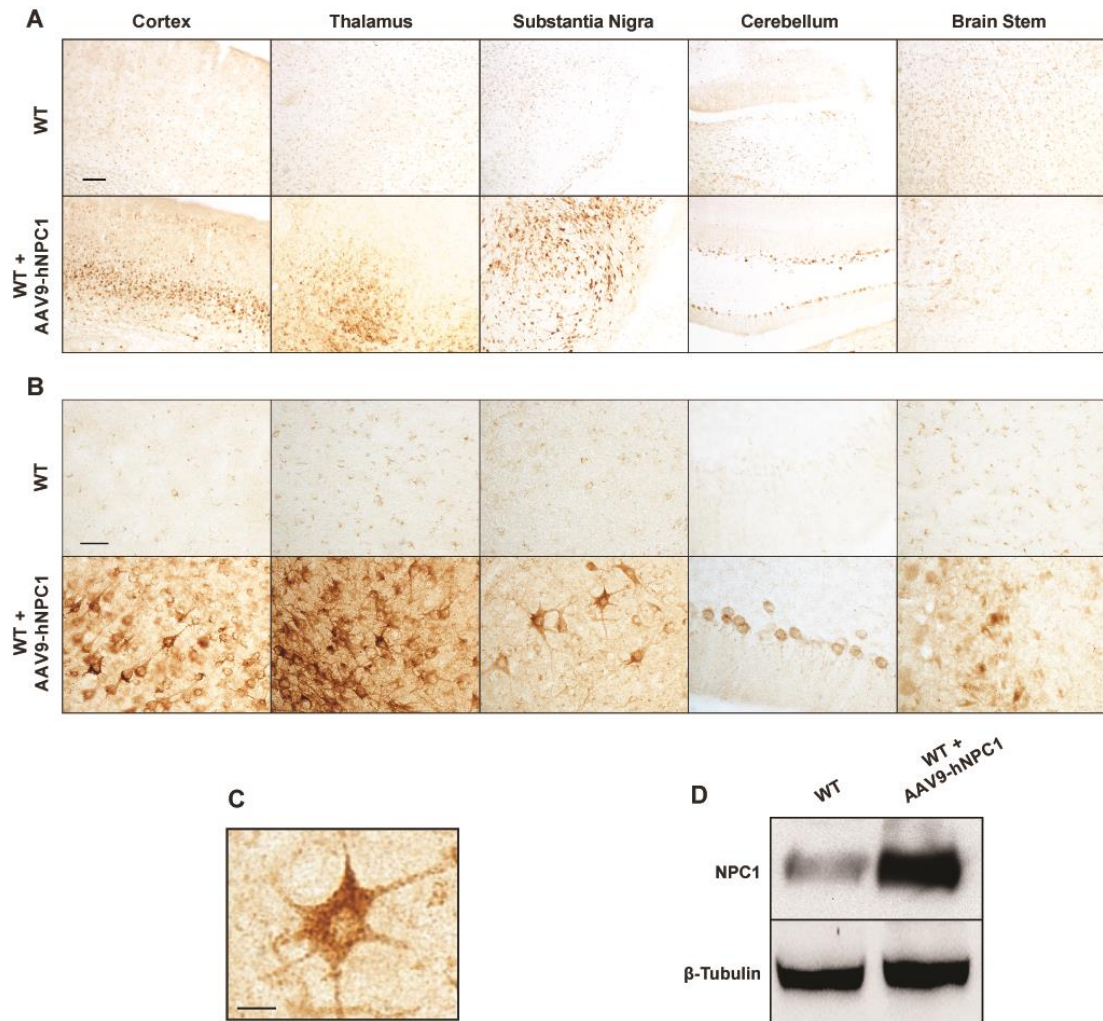


**Figure 20: hNPC1 expression to supraphysiological levels in various brain regions following low dose AAV9-hNPC1 administration to neonatal wild-type mice.**

(A) hNPC1 expression detected by IHC within the brains of P30 wild-type mice, injected neonatally via ICV administration with a low dose of  $4 \times 10^9$  GC of AAV-hNPC1. Selected regions reflect areas significantly affected by NP-C pathology. Scale bar:  $100\mu\text{m}$ .

(B) Higher magnification images from selected regions. Scale bar:  $60\mu\text{m}$ .

(C) High magnification image of cell demonstrating punctate staining of overexpressed NPC1. Scale bar:  $10\mu\text{m}$

(D) Western blot analysis of NPC1 levels in full brain lysates of wild-type uninjected and AAV9-hNPC1 administered wild-type mice. 170kDa band represents NPC1 protein. 50kDa band represents the  $\beta$ -tubulin loading control.

### 3.12 Dose dependent increase of eGFP expression following AAV9-eGFP administration

To compare the transduction profile of low dose AAV9-hNPC1 administration, a titre-matched low dose of  $4 \times 10^9$  viral particles of AAV9-eGFP was administered via bilateral intracerebroventricular injection to P0/1 wild-type mice. An additional group of pups were injected with a higher dose of  $5 \times 10^{11}$  viral particles, to evaluate the spread of expression achievable at the currently highest possible doses for neonatal administration. Uninjected littermates were used as age-matched controls. After 30 days, low dose administered ( $n = 3$ ), high dose administered ( $n = 3$ ) and uninjected age matched wild-type control mice ( $n = 3$ ) were sacrificed, brains were harvested and processed for anti-eGFP immunohistochemistry (**Figure 21**). Stained brain sections were analysed and imaged via light microscopy, which revealed extensive and widespread eGFP expression in identical areas of the brain, as previously observed following titer-matched AAV9-hNPC1 administration, for both low and high dose AAV9-eGFP administration (**Figure 21A-B**). Minimal background staining was observed in uninjected control sections. Brains administered with low dose AAV9-eGFP exhibited increased levels of eGFP positive staining, relative to the NPC1 positive staining observed following identical low dose AAV9-hNPC1 administration. The cortex and substantia nigra in particular showed more ubiquitous positive staining, following low dose AAV9-eGFP administration. This may be explained by higher efficiency of the anti-eGFP antibody, allowing the positive staining of lower eGFP levels. However the fact that eGFP expresses not just in the soma, but also throughout all cellular processes must be taken in to account. This was confirmed at higher magnification (**Figure 21B**), where clear axonal staining was observed in the cortex and cerebellum.

As expected, brains administered with a higher dose of  $5 \times 10^{11}$  vp AAV9-eGFP exhibited increased levels of eGFP expression throughout the observed areas, compared to low dose administration. Again, eGFP expression in the cortex, thalamus and substantia nigra was extremely high. eGFP staining in these areas was so extensive that at higher magnification individual cells bodies and cell morphology could not be identified (**Figure 21B**). Additionally, a further increase in individual

eGFP positive cells was observed in the cerebellum and brain stem. As a result of the saturation of positive staining observed following AAV9-eGFP administration, brains administered with low dose AAV9-NPC1 were used for vector tropism analysis.

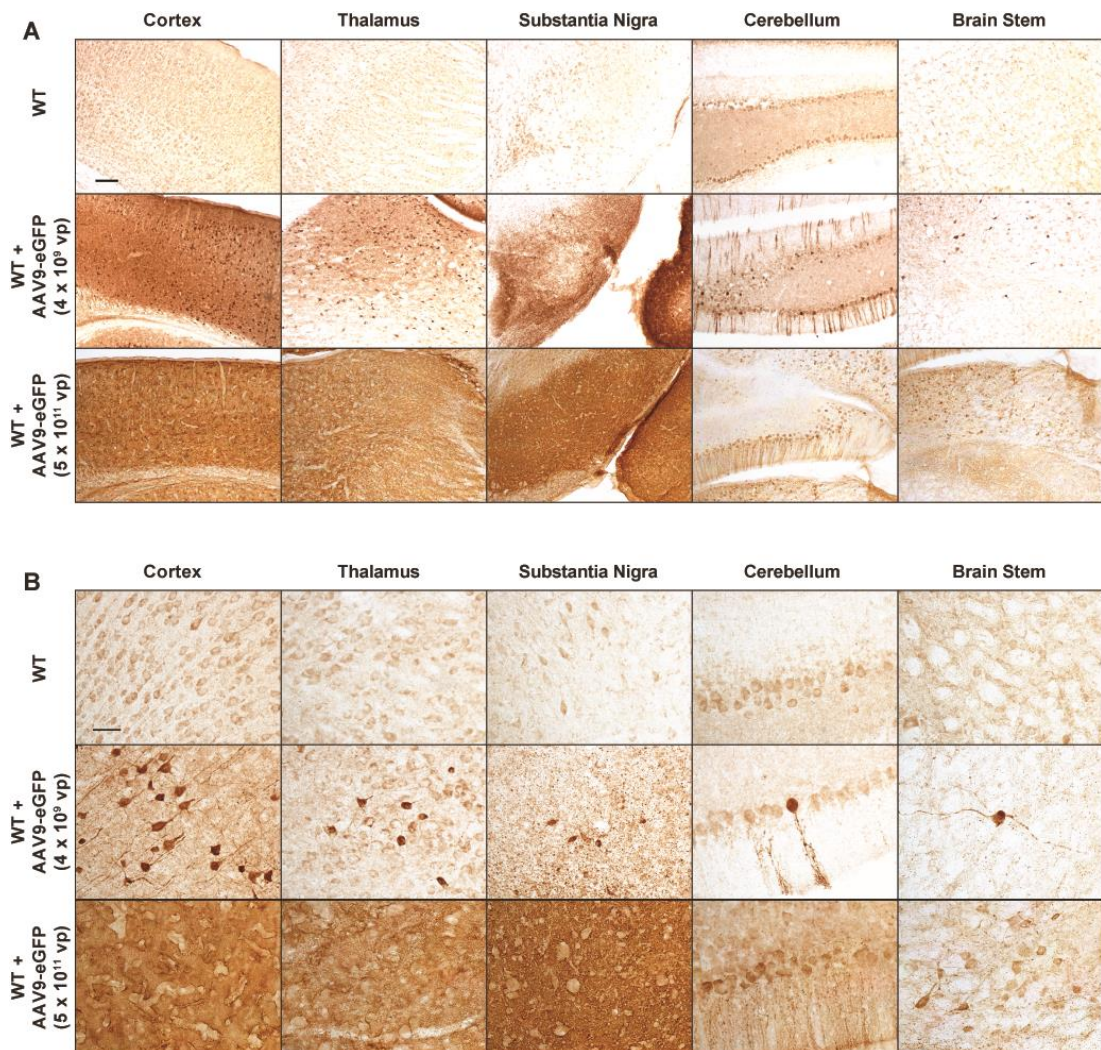


**Figure 21: Widespread eGFP expression following low and high dose AAV9-eGFP administration to neonatal wild-type mice.**

- (A) eGFP expression detected by IHC within the brains of P30 wild-type mice, injected neonatally via ICV administration with a low dose of  $4 \times 10^9$  vp or a high dose of  $5 \times 10^{11}$  vp. Selected regions reflect areas significantly affected by NP-C pathology. Scale bar: 100 $\mu$ m.
- (B) Higher magnification images from selected regions. Scale bar: 60 $\mu$ m.

### 3.13 Neuronal tropism of AAV9-hNPC1 vector

To investigate the tropism and confirm previous observations of neuronal cell transduction with the AAV9-hNPC1 vector, a series of immunofluorescence studies utilising cell lineage specific markers was carried out. Brain sections from P30 mice administered as neonates with low dose AAV9-hNPC1 and age-matched uninjected control mice were labelled with the nucleic acid marker DAPI and antibodies against the neuron-specific marker NeuN and NPC1 (**Figure 22**). Sections were examined by scanning confocal microscopy, which revealed minimal staining of endogenous murine NPC1 in uninjected control mice. However, brain sections from injected mice revealed supraphysiological levels of NPC1 within the cytoplasm of transduced cells, as shown in representative images taken from the S1BF region of the cerebral cortex. As previously observed, the staining appeared punctate and limited to the soma, suggesting late endosomal/lysosomal localisation of the overexpressed NPC1 protein. NPC1 positive cells were crucially also found to be expressing neuron-specific NeuN on the nuclear membrane, confirming successful neuronal transduction and NPC1 expression following AAV9-hNPC1 administration.

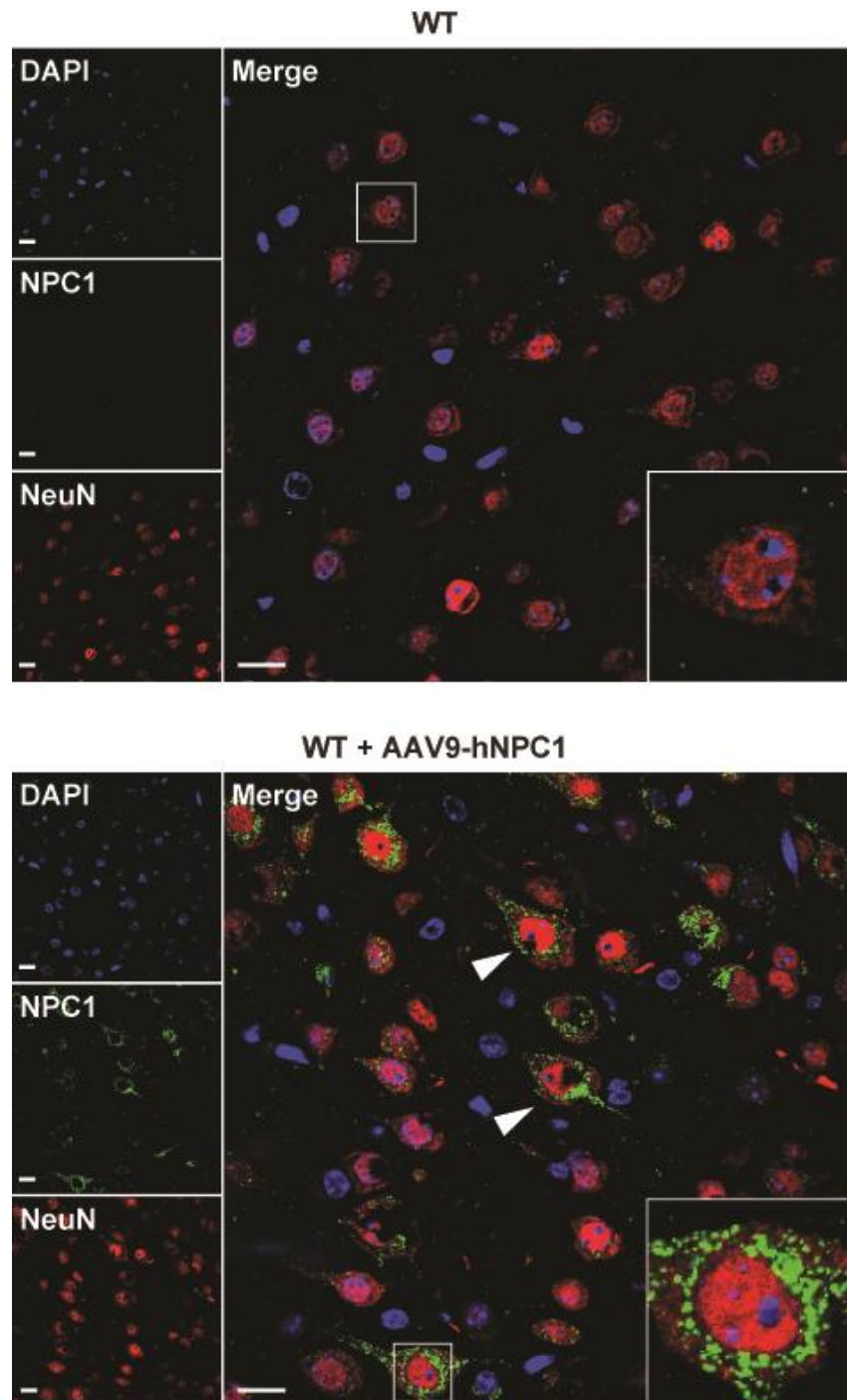


**Figure 22: Neuronal overexpression of hNPC1 protein following AAV9-hNPC1 administration.**

Representative confocal images showing immunofluorescence staining of the cortical S1BF region from P30 wild-type mice following neonatal AAV9-hNPC1 administration ( $n = 3$ ). AAV9-hNPC1 induced overexpression of hNPC1 (green) in cells positive for neuronal marker NeuN (red), confirming neuronal vector tropism. Nuclei were counterstained with DAPI (blue). Arrows signal neurones with clear perinuclear staining of hNPC1, indicating hNPC1 localisation within late endosomal/lysosomal vesicles. Scale bar: 20 $\mu$ m.

Expression of hNPC1 following AAV9-hNPC1 administration was expected to be limited to neurons, due to the use of the strong neuronal promoter *hSynI*. However, to conclusively evaluate potential NPC1 expression in glial cells, immunofluorescent labelling with the fibrillary astrocyte marker GFAP and pan-macrophage marker CD68 was carried out in combination with NPC1 staining (**Figure 23**). Analysis by confocal microscopy again revealed strong hNPC1 expression in the S1BF region, following AAV9-hNPC1 administration. However, no NPC1 positive cells were also found to be labelled with GFAP, confirming the lack of astrocyte tropism of the AAV9-hNPC1 vector (**Figure 23A**). Similarly, labelling of microglia with CD68 could not detect overexpression of NPC1 in CD68 positive cells (**Figure 23B**). CD68 positive cells were few in number and displayed a resting morphology in both uninjected controls and AAV9-hNPC1 administered mice. The absence of hNPC1 overexpression in astrocytes and microglia confirmed the expected strong neuronal tropism of the AAV9-hNPC1 vector. Although ubiquitous expression of NPC1 in other non-neuronal cell populations within the CNS may be beneficial and explored in the future, the initial aim of strong neuronal transduction had been achieved.

It was crucial to investigate whether the exogenously expressed hNPC1 protein was undergoing correct intracellular trafficking to within late endosomal/lysosomal compartments. Immunofluorescence studies were conducted using antibodies against the lysosomal specific protein LAMP1, which resides within the membrane of late endosomes/lysosomes (Howe et al., 1988, Viitala et al., 1988), and antibodies against the NPC1 protein. Confocal imaging revealed co-localisation of LAMP1 and NPC1 within late endosomal/lysosomal vesicles in neurons within brains administered with AAV9-hNPC1 (**Figure 24**). LAMP1 staining in administered brain sections appeared similar to the staining observed in uninjected wild-type control sections. Although trafficking of AAV9-hNPC1 induced NPC1 specifically to the lysosomal membrane could not be confirmed at this resolution using conventional scanning confocal microscopy, the localisation to within late endosomes/lysosomes was successfully demonstrated.

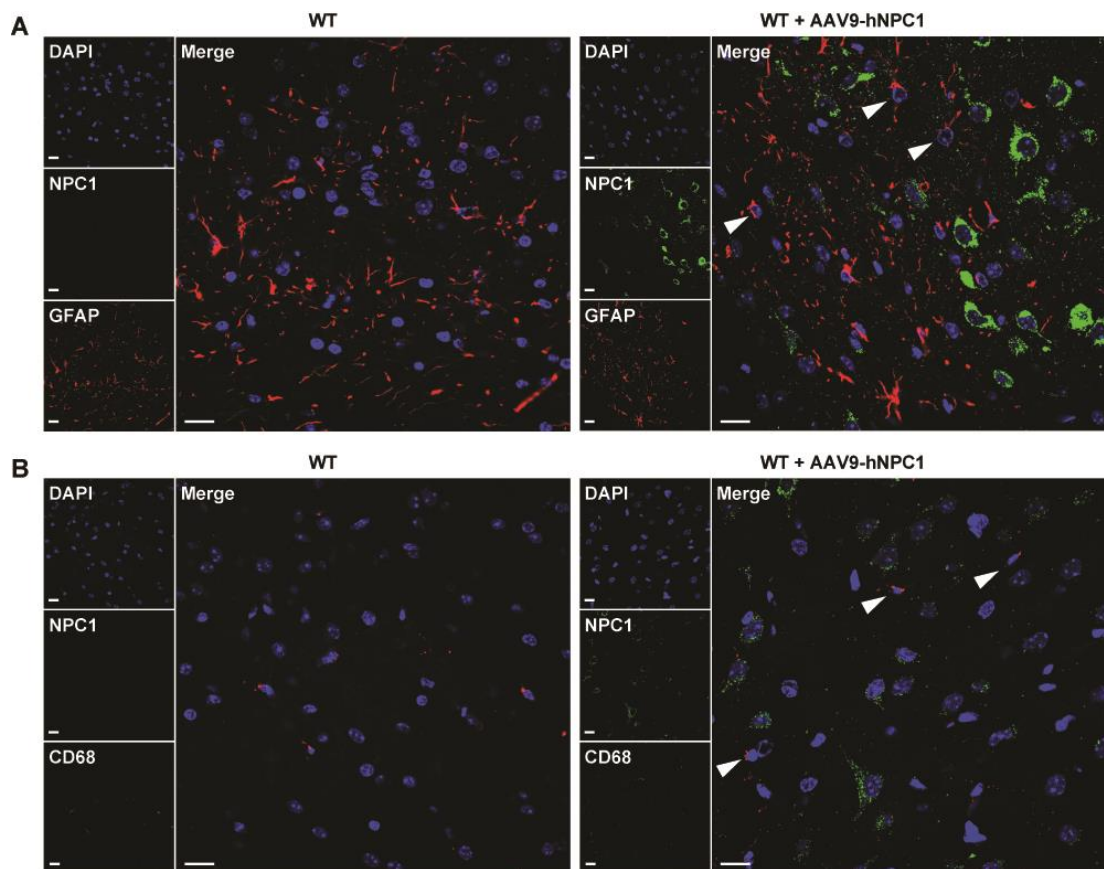


**Figure 23: Glial cells do not exhibit overexpression of hNPC1 protein following AAV9-hNPC1 administration.**

Representative confocal images showing immunofluorescent staining of the cortical S1BF region from P30 wild-type mice following neonatal AAV9-hNPC1 administration (n = 3).

- (A) Astrocytes identified via anti-GFAP (red) staining demonstrated lack of AAV9-hNPC1 induced overexpression of hNPC1 (green). Nuclei were counterstained with DAPI (blue). Arrows signal astrocytes exhibiting endogenous levels of murine NPC1. Scale bar: 20 $\mu$ m.
- (B) Resting microglia demonstrated by positive CD68 staining (red) did not exhibit hNPC1 overexpression following AAV9-hNPC1 administration. Nuclei were counterstained with DAPI (blue). Arrows indicate resting microglia. Scale bar: 20 $\mu$ m.

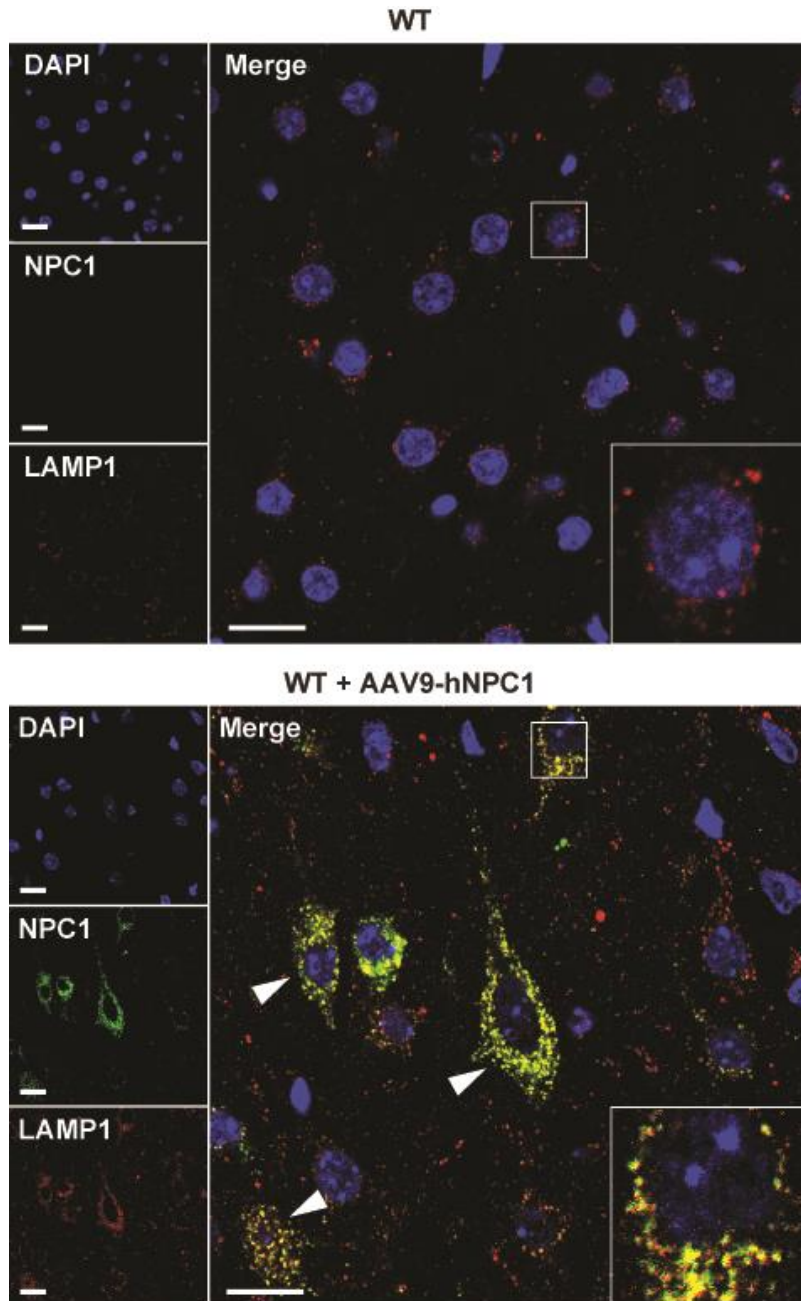


**Figure 24: Lysosomal localisation of hNPC1 protein following AAV9-hNPC1 administration.**

Representative confocal images showing immunofluorescent staining of the cortical S1BF region from P30 wild-type mice following neonatal AAV9-hNPC1 administration ( $n = 3$ ). Confirmation of hNPC1 (green) localisation to late endosomal/lysosomal vesicles, via co-localisation with lysosomal-associated membrane protein 1 (LAMP1, red), compared to uninjected wild-type control. Nuclei were counterstained with DAPI (blue). Arrows indicate cells with clear hNPC1 overexpression co-localising with LAMP1. Scale bar: 20 $\mu$ m.

### 3.14 No toxicity associated to supraphysiological levels of NPC1 following AAV9-hNPC1 administration

Brain sections of mice administered with low dose AAV9-hNPC1 were evaluated for potential cytotoxicity or inflammatory response, resulting from the administration of AAV9-hNPC1 or downstream NPC1 overexpression to supraphysiological levels. This was carried out by immunohistochemical analysis of sections stained with antibodies against the astrocytic marker glial fibrillary acid protein (GFAP) and the microglial marker CD68, to screen for astrogliosis and a microglia-mediated inflammatory response respectively (**Figure 25**). No change in resting astrocyte and microglial cell morphology, or increase in staining intensity was observed when compared to brain sections from uninjected control mice in any of the brain regions examined, such as within the cerebral cortex (**Figure 25A**). Brain sections from a mouse model of the neuronopathic Gaucher disease (Enquist et al., 2007), known to display an acute inflammatory response, was used as a positive control (*Gba1*<sup>-/-</sup>) for both markers.

Thresholding analysis was carried out on a series of representative images from 3 of the most well transduced regions of the brain, to quantify GFAP and CD68 positive staining (**Figure 25B-C**). Sections from low dose AAV9-hNPC1 administered wild-type mice (n = 3), age-matched uninjected wild-type control mice (n = 3) and positive control *Gba1*<sup>-/-</sup> mice (n = 3) were analysed. No statistically significant difference was measured between AAV9-hNPC1 administered mice and uninjected control mice for both GFAP (**Figure 25B**) and CD68 (**Figure 25C**) positive staining in all brain regions. As expected, the positive control sections from *Gba1*<sup>-/-</sup> mice showed a statistically significant increase in both GFAP and CD68 staining, when compared to brain sections from AAV9-hNPC1 administered and uninjected wild-type mice ( $p < 0.0001$ ). These results confirm that neither the administration of AAV9-hNPC1, or subsequent overexpression of hNPC1 to supraphysiological levels does not trigger an astrocyte- or microglia-mediated immune response. In conclusion the produced AAV9-hNPC1 viral vector was suitable for the use in preclinical therapeutic efficacy studies in the *Npc1*<sup>-/-</sup> mouse model.

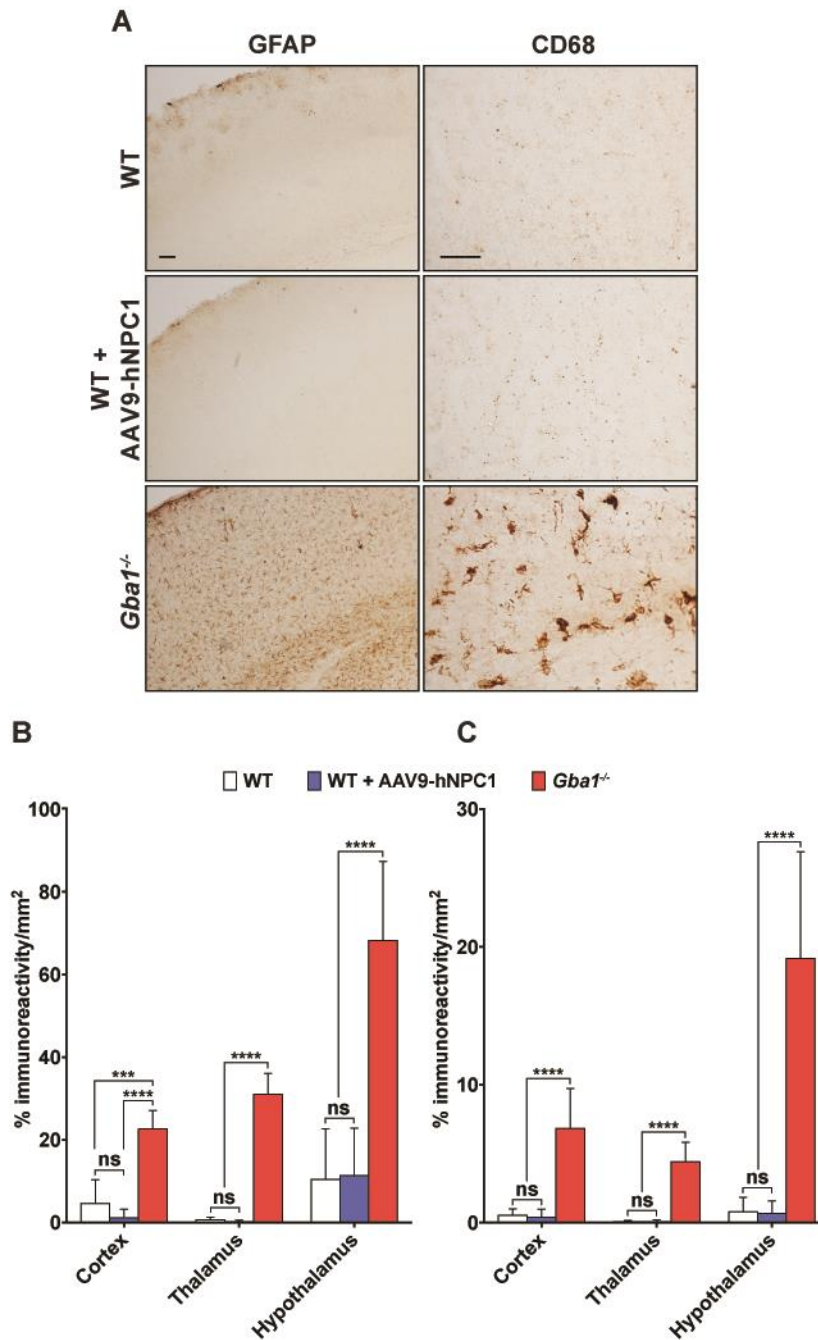


**Figure 25: No astrocyte- or microglia-mediated immune response, as a result of hNPC1 overexpression in wild-type mice.**

Analysis of brain sections subjected to anti-CD68 and -GFAP immunohistochemistry and resulting quantification of P30 wild-type mice administered neonatally with AAV9-hNPC1 (n=3), age-matched uninjected control mice (n=3) and positive control *Gba1*<sup>-/-</sup> mice (n=3).

(A) Representative images from the somatosensory barrelfield cortex region of CD68 and GFAP stained brain sections. Scale bars: 50µm.

(B/C) Quantification of positive anti-GFAP (B) and anti-CD68 (C) immunoreactivity from regions with high levels of AAV9-hNPC1 induced hNPC1 overexpression. Data presented as mean ± S.D., compared by two-way ANOVA and Tukey's HSD test. ns, non significant, \*\*\*  $p < 0.001$ , \*\*\*\*  $p < 0.0001$ .

### 3.15 Summary

The results presented in this chapter aim to demonstrate why a recombinant adeno-associated viral vector gene delivery system was chosen for the development of NP-C gene therapy. rAAV vectors are currently considered the ideal method for widespread and efficient transduction of the CNS, as reflected by their frequent use in clinical trials for other lysosomal and neurodegenerative disorders, such as mucopolysaccharidosis type IIIA (Tardieu et al., 2014). The initial vector study carried out in this project further emphasised this point, where an AAV2/9 vector resulted in transgene expression throughout the brain following neonatal ICV administration, compared to the limited spread around the site of injected observed with lentiviral and adenoviral vectors. However, as a result of rAAV vector's restricted packaging capacity, the integration of the relatively large hNPC1 cDNA into a functional and efficient construct was challenging. Several cloning steps were carried out to remove or replace essential transgene expression enhancer elements with shorter variants, to produce the final *pAAV.hSynI.hNPC1.SV40pA* construct. Although still oversized, this construct was shown to express hNPC1 *in vitro* and was used to successfully produce fully packaged AAV9-hNPC1 viral vector particles, albeit at a lower than expected titer.

Preliminary *in vivo* testing demonstrated that low dose neonatal ICV administration of AAV9-hNPC1 resulted in NPC1 overexpression in wild-type mice to supraphysiological levels within brain regions associated with severe NP-C neurodegeneration. The vector exhibited a strong neuronal tropism and overexpressed hNPC1 successfully localised to within late endosomal/lysosomal compartments. Additionally, comparison studies with an eGFP variant showed the potential further spread and expression levels that could be achieved with a higher dose administration. Crucially, the administration of AAV9-hNPC1 and resulting overexpression of hNPC1 in murine brains to supraphysiological levels was proven to not cause toxicity, or an astrocyte- or microglia-mediated immune response. It was therefore decided to undertake a preclinical study with low dose AAV9-hNPC1 in the *Npc1*<sup>-/-</sup> mouse model, while simultaneously optimising vector production to increase viral titer to allow further studies with higher dose administration.

# 4 Preclinical low dose AAV9-hNPC1 study in the *Npc1*<sup>-/-</sup> mouse model

## 4.1 Introduction

To evaluate the potential therapeutic efficacy of the AAV9-hNPC1 vector produced in the previous chapter, a preclinical study of neonatal low dose gene therapy was carried out in the *Npc1*<sup>-/-</sup> mouse model. As previously described, the *Npc1*<sup>-/-</sup> mouse model accurately mimics the behavioural, neuropathological and biochemical defects seen in human patients, including weight loss, tremor and ataxic gait symptoms. To gauge potential therapeutic efficacy of the tested therapy, a range of behavioural and locomotor studies were carried out on the animal cohorts, including monitoring of: survival, weight, rearing in an open field environment, tremor and gait. As the human and murine sequences of *NPC1* cDNA and encoded NPC1 protein share a respective homology of 84% and 86% (**Supplementary Figure S1** and **Supplementary Figure S2**), it was hypothesised that hNPC1 would retain its functionality in the *Npc1*<sup>-/-</sup> mouse model. All *in vivo* studies were carried out in collaboration with D. Smith, L. Morris, A. Colaço and F. Platt (Department of Pharmacology, University of Oxford). The same low titer preparation of AAV9-hNPC1 vector produced in the previous chapter was given via ICV administration into P0 *Npc1*<sup>-/-</sup> pups, at a total dose of  $4.6 \times 10^9$  GC. Mice deemed to have reached their humane endpoint, by losing 1g during a 24-hour period, were sacrificed for detailed neuropathology examination outlined in **Chapter 5**.

## 4.2 Chapter aims

The aim of this chapter is to present the results of the first preclinical study with neonatal low dose AAV9-hNPC1 via ICV administration in the *Npc1*<sup>-/-</sup> mouse model. This chapter will focus on the therapeutic efficacy of low dose AAV9-hNPC1 on survival, weight, behaviour, locomotor, neurodegenerative and coordination deficiencies associated with the *Npc1*<sup>-/-</sup> mouse model. Additionally for several of these parameters the therapeutic efficacy of low dose gene therapy is also compared to miglustat, the only currently licensed treatment for NP-C in Europe (Santos-Lozano et al., 2015) and HP- $\beta$ -CD, a promising therapy currently being evaluated in clinical trials (Liu et al., 2009). Summary of the animal cohorts and doses for this study can be found in **Table 9**. The aim of this comparison is to evaluate where this initial study of low dose gene therapy lies on the current NP-C treatment spectrum.

Cohort	N (Male/Female)	Dose	Administration
Wild-type	6 (3/3)	-	-
<i>Npc1</i> <sup>-/-</sup>	8 (4/4)	-	-
<i>Npc1</i> <sup>-/-</sup> + AAV9-hNPC1	8 (4/4)	Single dose of 4.6 x 10 <sup>9</sup> GC at P0/1	ICV
<i>Npc1</i> <sup>-/-</sup> + miglustat	8 (4/4)	1,200mg/kg/day from P21	Oral
<i>Npc1</i> <sup>-/-</sup> + HP- $\beta$ -CD	11 (6/5)	4,000mg/kg/week from P21	IP

**Table 9: Animal cohorts of preclinical low dose AAV9-hNPC1 study.**

### 4.3 Extension of lifespan in *Npc1*<sup>-/-</sup> mice following low dose AAV9-hNPC1 treatment

Wild-type, untreated *Npc1*<sup>-/-</sup>, gene therapy treated *Npc1*<sup>-/-</sup>, miglustat treated *Npc1*<sup>-/-</sup> and HP- $\beta$ -CD treated *Npc1*<sup>-/-</sup> mice were monitored daily and any mice deemed to have reached their humane endpoint of 1g weight loss in a 24-hour period were sacrificed (**Figure 26**). Consistent with previous studies, untreated *Npc1*<sup>-/-</sup> mice had an average lifespan of 75 days, with 7 out of 8 mice sacrificed between 70-80 days. *Npc1*<sup>-/-</sup> mice treated daily from P21 with the glucosylceramide synthase inhibitor miglustat had an average lifespan of 108 days and consistent with previous reports lived significantly longer than untreated *Npc1*<sup>-/-</sup> mice ( $p < 0.0001$ ). *Npc1*<sup>-/-</sup> mice treated with a single administration of low dose AAV9-hNPC1 had an average lifespan of 116.5 days and also lived significantly longer than untreated *Npc1*<sup>-/-</sup> mice ( $p < 0.0001$ ). There was no significant difference between the average survival of *Npc1*<sup>-/-</sup> mice following treatment with miglustat or low dose gene therapy ( $p = 0.09$ ). *Npc1*<sup>-/-</sup> mice treated weekly with HP- $\beta$ -CD had an average lifespan of 168 days with a significant increase in survival compared to untreated *Npc1*<sup>-/-</sup> ( $p < 0.0001$ ), miglustat treated *Npc1*<sup>-/-</sup> mice ( $p < 0.0001$ ) and AAV9-hNPC1 treated *Npc1*<sup>-/-</sup> mice ( $p < 0.0001$ ). Considerable variance was observed in the lifespan of these HP- $\beta$ -CD treated *Npc1*<sup>-/-</sup> mice, with a range of 135 to 210 days.

These initial results demonstrate that even low dose treatment of *Npc1*<sup>-/-</sup> mice with AAV9-hNPC1 results in a 55.3% increase in the lifespan of *Npc1*<sup>-/-</sup> mice. This duration of survival is comparable to *Npc1*<sup>-/-</sup> mice treated with the only current NP-C approved drug in Europe, miglustat. However, continual treatment with HP- $\beta$ -CD resulted in a 124% increase in lifespan of *Npc1*<sup>-/-</sup> mice, significantly higher than a single low dose AAV9-hNPC1.

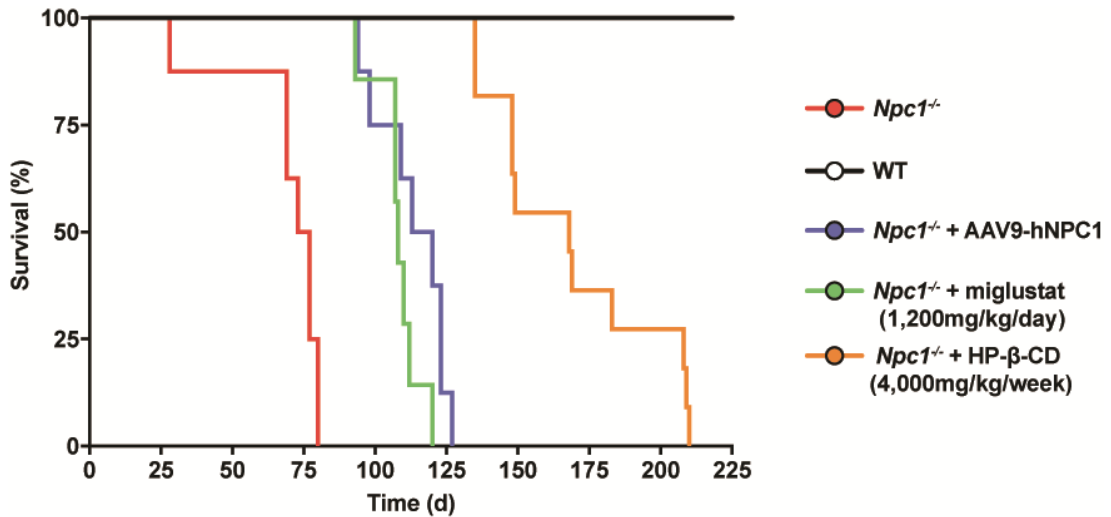


**Figure 26: Efficacy of low dose gene therapy and competing therapies on the lifespan of *Npc1*<sup>-/-</sup> mice.**

Kaplan-Meier survival curve of wild-type (n=6), untreated *Npc1*<sup>-/-</sup> mice (n=8, 75 days), *Npc1*<sup>-/-</sup> mice with daily oral administration of 1,200mg/kg of miglustat (n=8, 108 days), *Npc1*<sup>-/-</sup> mice treated with weekly intraperitoneal administration of 4,000mg/kg of HP-β-CD (n=11, 168 days) and *Npc1*<sup>-/-</sup> mice treated neonatally with a single ICV administration of  $4 \times 10^9$  GC of AAV9-hNPC1 (n=8, 116.5 days). Logrank test (Mantel-Cox) comparing survival curves results in significant increases in the life span of the treated *Npc1*<sup>-/-</sup> mice compared to untreated *Npc1*<sup>-/-</sup> ( $p < 0.0001$ ).

#### 4.4 Improved weight gain in *Npc1*<sup>-/-</sup> mice treated with low dose AAV9-hNPC1

The weight of untreated and treated mice was tracked until 19 weeks of age, or until their humane endpoint had been reached (**Figure 27**). Untreated *Npc1*<sup>-/-</sup> mice demonstrated initial weight gain until 5 weeks of age, at which point their weights plateaued (**Figure 27A**). From 7 weeks of age, the time point at which NP-C symptoms become apparent in this model, a constant reduction in weight was observed until their humane endpoint had been reached. In agreement with previous reports, a significant reduction in body weight gain was observed in *Npc1*<sup>-/-</sup> mice treated with miglustat, which is known to cause osmotic diarrhoea and suppress appetite (Priestman et al., 2008). This significant loss of weight gain was present throughout the duration of their lifespan, compared to both untreated *Npc1*<sup>-/-</sup> mice and all other treatment cohorts, and as a result mice had a consistently lower average weight of approximately  $8g \pm 1.2g$ . HP-β-CD treated *Npc1*<sup>-/-</sup> mice exhibited weight

gain comparable to untreated *Npc1*<sup>-/-</sup> mice until 7 weeks of age, after which their weight was maintained and ultimately started to decline at week 13. However, compared to age-matched wild-type controls, significant differences in the weight of HP- $\beta$ -CD treated *Npc1*<sup>-/-</sup> mice were observed at all monitored time points. In comparison, no significant difference in weight was observed in AAV9-hNPC1 treated *Npc1*<sup>-/-</sup> mice compared to wild-type weights up until 12 weeks of age. The weight of gene therapy treated *Npc1*<sup>-/-</sup> mice subsequently decreased to within the HP- $\beta$ -CD treated weight range, with a comparable slow decline in weight until their humane endpoint had been reached.

When the weights of the monitored cohorts were separated by gender, considerable differences between male (**Figure 27B**) and female (**Figure 27C**) cohorts was observed (Voikar et al., 2002). The weight gap between untreated *Npc1*<sup>-/-</sup> and age-matched wild-type mice was reduced in male mice compared to female mice, with no significant difference between wild-type and untreated *Npc1*<sup>-/-</sup> male mice until 7 weeks of age. In comparison, there was a significant difference in weight between untreated *Npc1*<sup>-/-</sup> and wild-type female mice throughout their life span. The difference between the weights of wild-type and *Npc1*<sup>-/-</sup> female mice treated with HP- $\beta$ -CD and low dose AAV9-hNPC1 was also significantly reduced. As a result, no statistical difference was observed between wild-type and gene therapy treated *Npc1*<sup>-/-</sup> female mice until 14 weeks of age.

Low dose gene therapy treatment of *Npc1*<sup>-/-</sup> mice resulted in significantly improved initial weight gain and continued steady weight maintenance until approximately 15 weeks of age, after which a steady weight decline was observed. While no significant difference in lifespan was observed between miglustat and AAV9-hNPC1 therapy, a substantial difference in weight between the two treatments was seen. Combined with the severe gastrointestinal side effects associated with the use of miglustat in patients, these results demonstrate a clear benefit of gene therapy treatment, even at this very low dose.

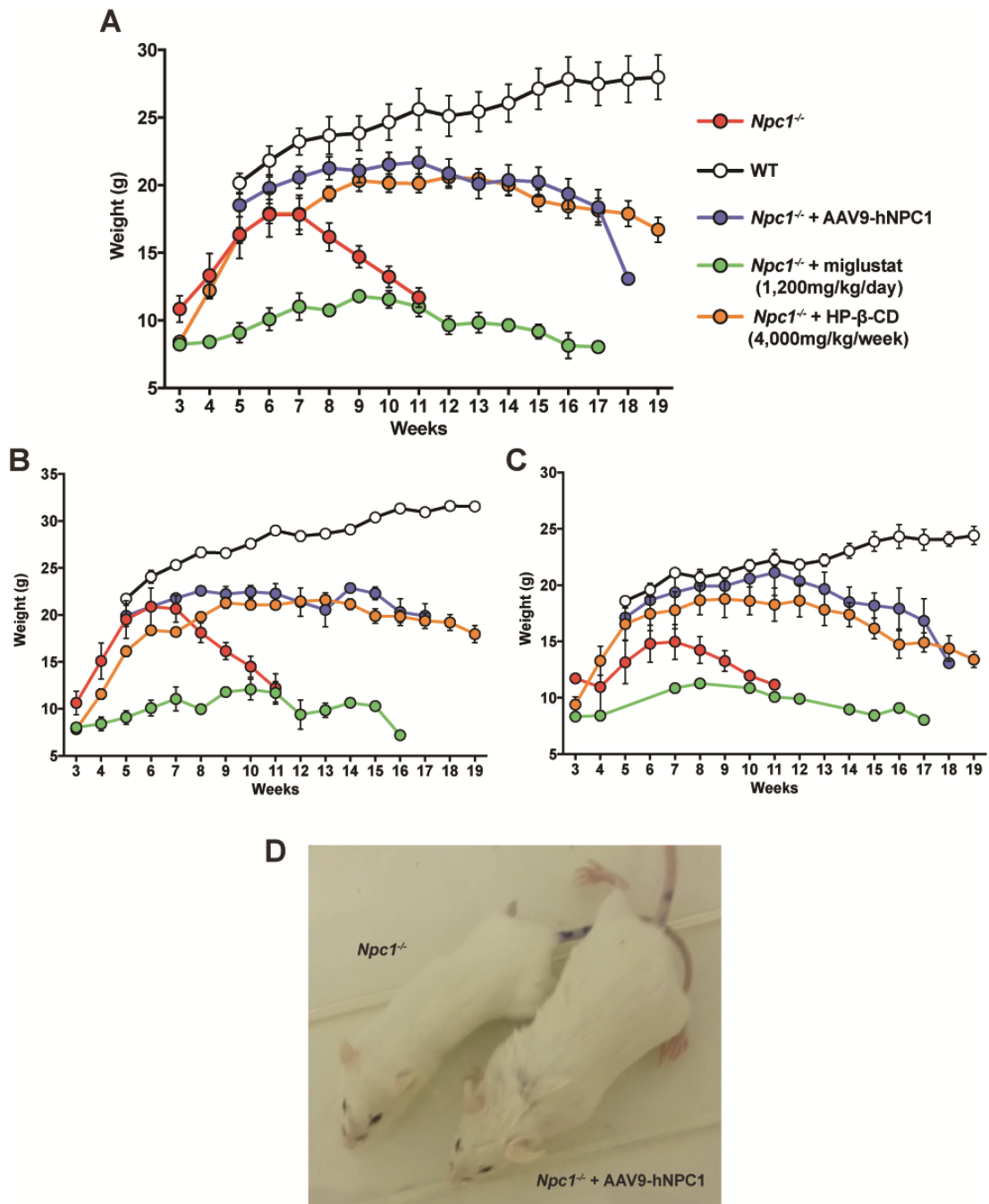


**Figure 27: Improvement in weight loss in *Npc1*<sup>-/-</sup> mice following low dose AAV9-hNPC1 treatment.**

Weekly weight monitoring of wild-type (n=6), untreated *Npc1*<sup>-/-</sup> mice (n=8), *Npc1*<sup>-/-</sup> mice with daily oral administration of 1,200mg/kg of miglustat (n=8), *Npc1*<sup>-/-</sup> mice treated with weekly intraperitoneal administration of 4,000mg/kg of HP-β-CD (n=11) and *Npc1*<sup>-/-</sup> mice treated neonatally with a single ICV administration of 4 x 10<sup>9</sup> GC of AAV9-hNPC1 (n=8). Male to female ratio of 1:1 in each monitored cohort. Data represented as weekly weight mean ± SEM.

(A) Male and female combined weekly weight data.

(B) Male weekly weight data.

(C) Female weekly weight data.

(D) Visual comparison of 10-week old untreated *Npc1*<sup>-/-</sup> mouse (left) and age-matched AAV9-hNPC1 treated *Npc1*<sup>-/-</sup> mouse (right).

## 4.5 Normalisation of neurological, locomotor and coordination symptoms in *Npc1*<sup>-/-</sup> mice following low dose AAV9-hNPC1 treatment

To evaluate the therapeutic efficacy of low dose AAV9-hNPC1 treatment on basic locomotor and coordinative function, a series of repeated performance tests were carried out. One of the studies conducted was an open field test, where mice were placed in an open field environment and monitored for their ability to conduct rearing events, which requires a combination of coordination, hind-limb strength and natural exploratory behaviour. Up to 7 weeks of age, no statistically significant difference was observed in the number of average rearing events between wild-type, untreated *Npc1*<sup>-/-</sup> and AAV9-hNPC1 treated *Npc1*<sup>-/-</sup> mice (**Figure 28**). However, by 8 weeks of age the untreated *Npc1*<sup>-/-</sup> mice showed a significant decrease in the number of average rearing events when compared to age-matched wild-type control mice ( $p = 0.004$ ) and AAV9-hNPC1 treated *Npc1*<sup>-/-</sup> mice ( $p = 0.002$ ). There was no significant difference between wild-type and *Npc1*<sup>-/-</sup> mice treated with AAV9-hNPC1. This was also seen at 9 weeks of age, at which point the untreated *Npc1*<sup>-/-</sup> mice had reached their humane endpoint and were sacrificed. The complete normalisation in the number of rearing events was consistent throughout the lifespan of the *Npc1*<sup>-/-</sup> mice treated with AAV9-hNPC1, with no significant difference measured when compared to the age-matched control wild-type mice.

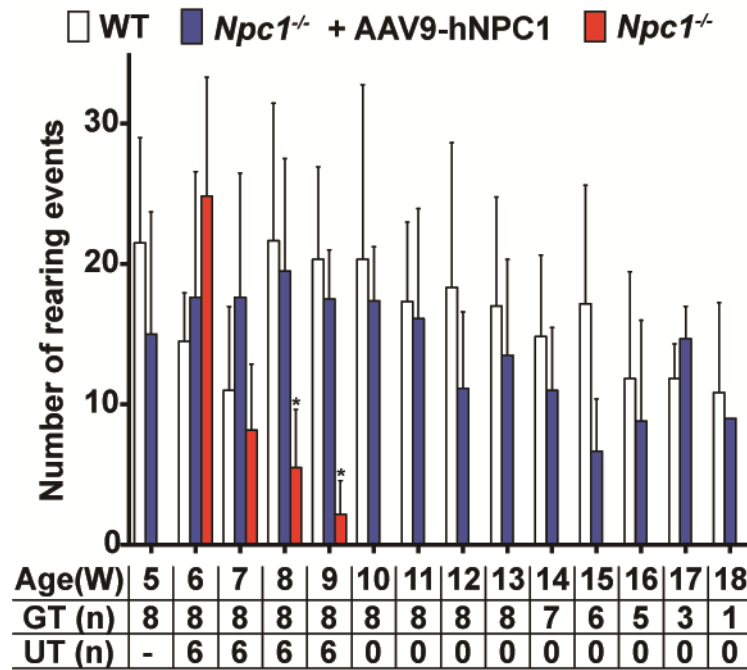


**Figure 28: Permanent normalisation of rearing count in *Npc1*<sup>-/-</sup> mice following low dose AAV9-hNPC1 treatment.**

Sustained normalisation of locomotor and co-ordination symptoms of AAV9-hNPC1 treated *Npc1*<sup>-/-</sup> mice in an open field setting, where number of rearing events were monitored during a 5-minute period. Data represented as mean  $\pm$  S.D., compared by two-way ANOVA followed by Tukey's HSD test. \*  $p < 0.05$ . W, weeks of age; GT, gene therapy treated *Npc1*<sup>-/-</sup>; UT, untreated *Npc1*<sup>-/-</sup>; n, sample size.

*Npc1*<sup>-/-</sup> mice exhibit a noticeable tremor from 7 to 8 weeks of age (Lloyd-Evans et al., 2008, Smith et al., 2009), a trait often exhibited by NP-C patients. The efficacy of low dose gene therapy treatment on the tremor of *Npc1*<sup>-/-</sup> mice was evaluated against competing therapies using an automated tremor sensor, where mice were placed and monitored for a 256 second period. The resulting amplitude of tremors from frequencies 1 - 64hz were recorded in wild-type, untreated *Npc1*<sup>-/-</sup> and *Npc1*<sup>-/-</sup> mice treated with AAV9-hNPC1, miglustat or HP- $\beta$ -CD (**Figure 29**). As measurements at frequencies below 30hz are affected by general mouse behaviour and grooming, only high frequency tremor data from 32 to 55hz was analysed. The mice cohorts were recorded at 9 (**Figure 29A**) and 16 weeks of age (**Figure 29B**), at which time points untreated *Npc1*<sup>-/-</sup> mice and low dose AAV9-hNPC1 treated *Npc1*<sup>-/-</sup> mice were reaching the end-stage of their average lifespan respectively. At 9 weeks, end-stage untreated *Npc1*<sup>-/-</sup> mice demonstrated the characteristic high frequency tremor compared to age-matched wild-type mice. However, *Npc1*<sup>-/-</sup> mice treated with miglustat, HP- $\beta$ -CD or AAV9-hNPC1 all demonstrated no high frequency tremor,

comparable to age-matched wild-type mice. Comparison of high frequency mean amplitudes confirmed no significant difference of the treated cohorts with wild-type mice (**Figure 29C**). All *Npc1*<sup>-/-</sup> mice that received treatment had significantly lower mean amplitudes of tremor compared to untreated *Npc1*<sup>-/-</sup> mice ( $p < 0.0001$ ). This normalisation in tremor was sustained at 16 weeks of age in *Npc1*<sup>-/-</sup> treated mice cohorts, with no significant difference to age-matched wild-type mice.

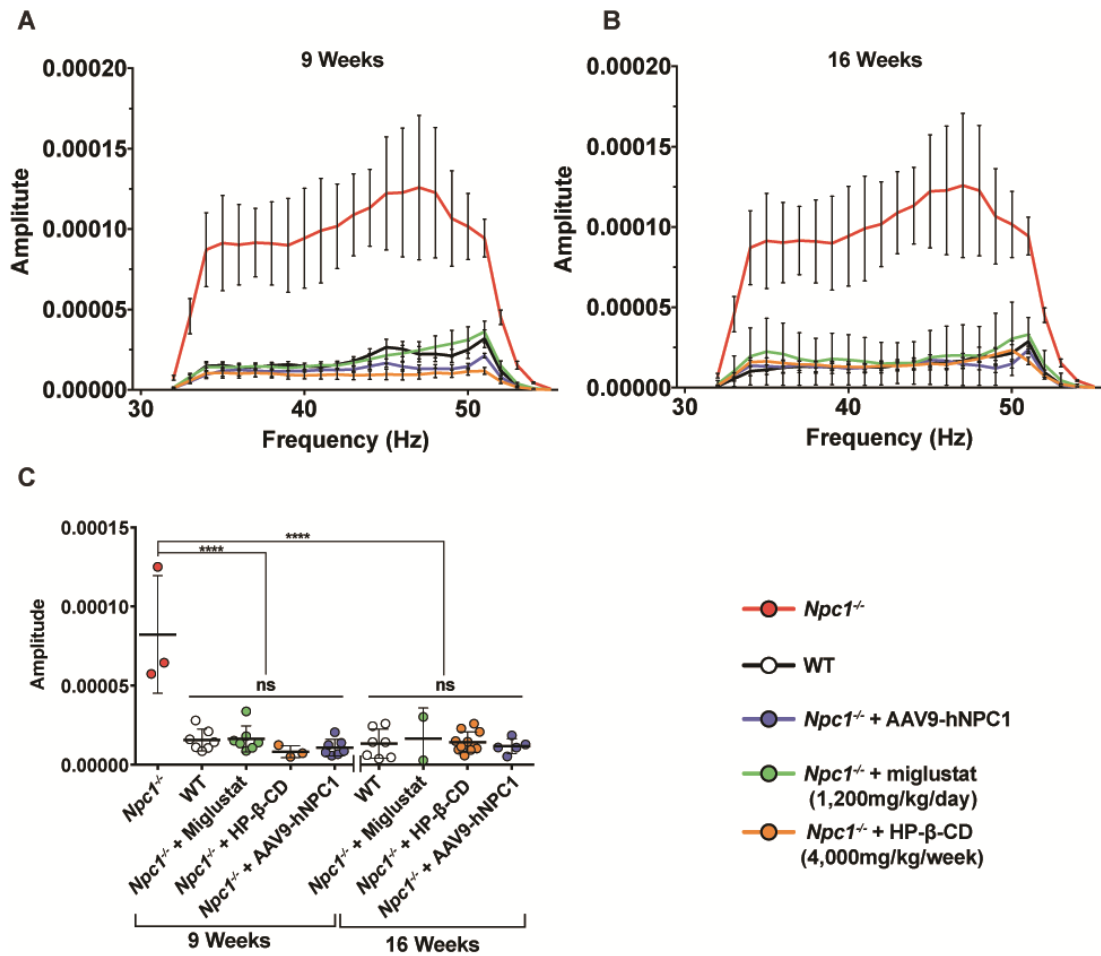


**Figure 29: Permanent normalisation of high frequency tremor in *Npc1*<sup>-/-</sup> mice following low dose AAV9-hNPC1 treatment.**

High frequency tremor analysis comparing untreated *Npc1*<sup>-/-</sup>, AAV9-hNPC1 treated *Npc1*<sup>-/-</sup> and wild-type mice. Measurements were taken at 9 and 16 weeks of age: wild-type (week 9 and 16, n = 7), untreated *Npc1*<sup>-/-</sup> (week 9, n = 3), *Npc1*<sup>-/-</sup> with 1,200mg/kg miglustat via oral administration (week 9, n = 7; week 16, n = 2); *Npc1*<sup>-/-</sup> with 4,000mg/kg HP-β-CD via intraperitoneal administration (week 9, n = 3; week 16, n = 11) and AAV9-hNPC1 treated *Npc1*<sup>-/-</sup> mice (week 9, n = 7; week 16, n = 5).

- (A) High frequency tremor data recorded at 9 weeks of age. Data represented as mean ± SEM.
- (B) High frequency tremor data recorded at 16 weeks of age, compared to untreated *Npc1*<sup>-/-</sup> data from 9 weeks of age. Data represented as mean ± SEM.
- (C) Comparison of averaged high frequency amplitudes. Data represented as mean ± S.D., compared by two-way ANOVA followed by Tukey's HSD test, \*\*\*\*  $p < 0.0001$ .

Ataxia is a prevalent neurological symptom presented in NP-C patients and is recapitulated in *Npc1*<sup>-/-</sup> mice, which develop abnormal gait from 7 weeks of age (Maue et al., 2012). Automated gait analysis (Noldus CatWalk XT) was used qualitatively and quantitatively to assess gait in wild-type control mice, untreated *Npc1*<sup>-/-</sup> mice and AAV9-hNPC1 treated mice (**Figure 30**). In wild-type control mice hind paw prints were in close proximity to the front paw prints, with a typical alternate step sequence of right front, left hind, left front and right hind (**Figure 30A**). 9-week old untreated end-stage *Npc1*<sup>-/-</sup> mice demonstrated clear irregular gait compared to age-matched wild-type and older end-stage *Npc1*<sup>-/-</sup> mice treated with low dose AAV9-hNPC1. No obvious differences were observed between 9-week old wild-type mice and 16-week old AAV9-hNPC1 treated *Npc1*<sup>-/-</sup> mice. To quantify this, the data from the CatWalk was analysed using the CatWalk XT 10.6 software.

The quantified data from the three mice cohorts was subsequently compared at 9 and 16 weeks of age (**Figure 30B**). At 9 weeks of age, significant AAV9-hNPC1 induced improvements were observed in treated *Npc1*<sup>-/-</sup> mice, compared to age-matched untreated *Npc1*<sup>-/-</sup> mice in a range of analysed parameters, including: stride length (distance between two consecutive paw placements of the same paw;  $p < 0.0001$ ), swing speed (time between two consecutive paw placements;  $p = 0.02$ ), regularity index (degree of interlimb coordination;  $p < 0.0001$ ), step sequence (duration of time with a normal alternative step sequence;  $p < 0.0001$ ), body speed ( $p < 0.0001$ ), support single (duration of glass plate contact with single paw;  $p < 0.0001$ ), support lateral (duration of glass plate contact with two side paws;  $p < 0.0001$ ) and support girdle (duration of glass plate contact with two front or hind paws;  $p < 0.001$ ). In 6 out of 8 of these parameters no statistically significant difference was observed between the low dose AAV9-hNPC1 treated *Npc1*<sup>-/-</sup> mice and age-matched wild-type mice. At 16 weeks of age normalisation of the gene therapy treated *Npc1*<sup>-/-</sup> mice to wild-type levels was maintained in 5 out of the 8 monitored parameters. When compared to 9-week old end-stage untreated *Npc1*<sup>-/-</sup> data, 16-week old AAV9-hNPC1 treated *Npc1*<sup>-/-</sup> mice demonstrated significant improvements in all parameters.

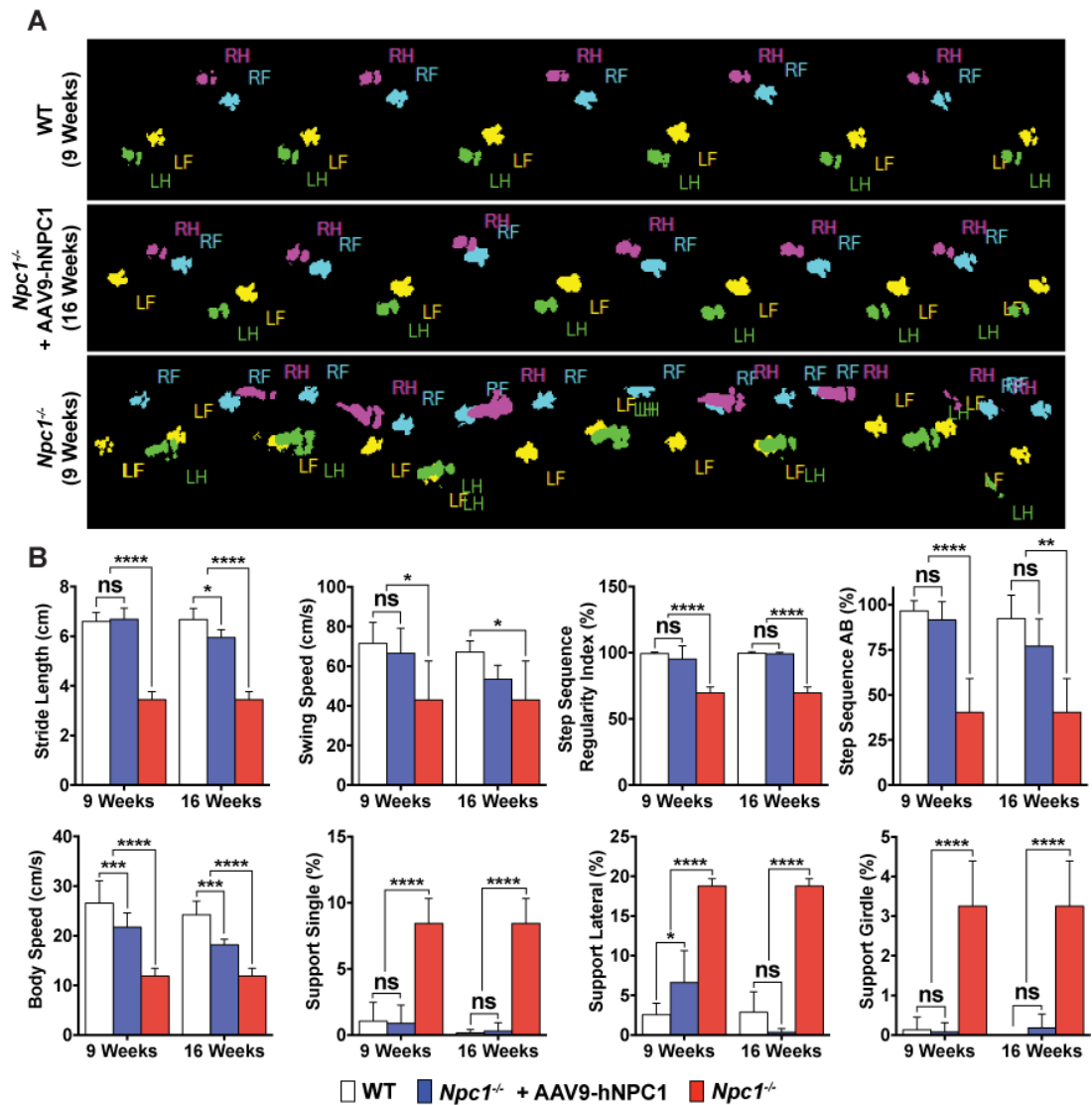


**Figure 30: Permanent normalisation or significant improvement in the gait of *Npc1*<sup>-/-</sup> mice following low dose AAV9-hNPC1 administration.**

- (A) Graphical representation of paw prints captured during an average run using the Noldus CatWalk automated gait analyser. Runs represent 9-week old wild-type, 9-week old end-stage *Npc1*<sup>-/-</sup> and 16-week old AAV9-hNPC1 treated *Npc1*<sup>-/-</sup> mice. Individual paws are identified via unique colours, with a normal alternating step sequence of: right front (RF, blue), left hind (LH, green), left front (LF, yellow) and right hind (RH, purple).
- (B) Automated gait analysis (Noldus CatWalk XT 10.6) quantification of 5 valid run average from wild-type (n=6), untreated *Npc1*<sup>-/-</sup> (n=3) and AAV9-hNPC1 treated *Npc1*<sup>-/-</sup> mice (week 9, n = 8; week 16 n = 4). Wild-type and AAV-hNPC1 treated *Npc1*<sup>-/-</sup> mice measurements were taken at 9 and 16 weeks of age and compared to 9-week old end-stage *Npc1*<sup>-/-</sup> data. Data represented as mean  $\pm$  S.D., compared by two ANOVA followed by Tukey's HSD test. ns - non significant, \* p < 0.05, \*\* p < 0.01, \*\*\* p < 0.001, \*\*\*\* p < 0.0001.

## 4.6 Summary

The results in this chapter demonstrate that a single low dose of AAV9-hNPC1 administered via intracerebroventricular injection into neonatal *Npc1*<sup>-/-</sup> mice resulted in a significant increase in lifespan and weight gain, and either permanent normalisation or significant improvement of locomotor and coordination systems. This initial preclinical study with low dose gene therapy treatment resulted in a 55% increase in the lifespan of *Npc1*<sup>-/-</sup> mice, which is equivalent to the survival extension exhibit by miglustat, currently the only European Medicines Agency approved treatment for Niemann-Pick Type C. However low dose administration of AAV9-hNPC1 also resulted in significant improvements to the weights of *Npc1*<sup>-/-</sup> mice, compared to the extreme lack of weight gain observed in *Npc1*<sup>-/-</sup> mice treated with miglustat. The reduced weight of these mice is reflected by miglustat's appetite suppressing effect (Priestman et al., 2008) and disturbances to the gastrointestinal tract that correlate with the gastrointestinal side effects seen in 80% of treated patients, which can in severe cases lead to miglustat discontinuation (Belmatoug et al., 2011). The improvements observed to *Npc1*<sup>-/-</sup> body weight following low dose gene therapy treatment were comparable to HP-β-CD treatment, however weekly administration of HP-β-CD did result in a significant increase in lifespan, compared to low dose ICV AAV9-hNPC1 treatment. *Npc1*<sup>-/-</sup> mice developed neurological symptoms from 7 weeks of age, reflective of symptoms present in Niemann-Pick Type C patients. Low dose gene therapy treated mice presented normalisation of these symptoms to wild-type levels, as demonstrated by rearing, tremor and gait studies. Even at the point where the gene therapy treated *Npc1*<sup>-/-</sup> mice had reached their humane-endpoint, due to 1g of weight loss during a 24-hour period, the normalisation or improvement of these parameters was maintained. The combination of these results indicates improvements to both life expectancy and the quality of life of *Npc1*<sup>-/-</sup> mice in this initial study, following single low dose AAV9-hNPC1 treatment.

# 5 Analysis of neurodegeneration and neuropathology following low dose AAV9-hNPC1 treatment

## 5.1 Introduction

The data presented in the previous chapter summarised the therapeutic efficacy of low dose AAV9-hNPC1 treatment on lifespan, neurological symptoms and quality of life of *Npc1*<sup>-/-</sup> mice. Although there were significant improvements and in some cases even normalisation of certain disease manifestations, treated *Npc1*<sup>-/-</sup> mice still exhibited disease progression. As a result, the efficacy of this treatment on the underlying neurodegeneration and neuropathology needed to be evaluated. Previous examination of transgene expression following low dose AAV9-hNPC1 (**Section 3.11**) and AAV9-eGFP (**Section 3.12**) administration resulted in transduction throughout crucial areas of the brain in terms of NP-C pathology, however large populations of neurons remained untransduced. Additionally, due to the rationale of using a strong neuronal promoter, glial cells would have remained untransduced (**Section 3.13**). Taking these two factors into account, neurodegeneration and neuroinflammation would continue to a certain extent, in these low dose gene therapy treated *Npc1*<sup>-/-</sup> mice.

## 5.2 Chapter Aims

The aim of this chapter is to further evaluate treatment efficacy by presenting the results of a series of neuropathology studies, which were carried out on the brains of

*Npc1*<sup>-/-</sup> mice treated with low dose AAV9-hNPC1. Due to the limited amount of vector and time available for this initial low dose study, all *Npc1*<sup>-/-</sup> mice administered with AAV9-hNPC1 were aged out until their respective humane end-points, to allow higher power statistical analysis of survival, weight and motor-function. As a result, the brains of these end-stage P120 AAV9-hNPC1 treated *Npc1*<sup>-/-</sup> mice were compared with the significantly younger end-stage P65 untreated *Npc1*<sup>-/-</sup> mice. While the addition of age-matched treated mice for comparison would be desirable and may show higher therapeutic efficacy at that time point, the following results demonstrate that even at their humane end-point the gene therapy treated *Npc1*<sup>-/-</sup> mice exhibited significant neurological improvements. The extent of neuronal loss, atrophy, astrogliosis, microglial activation and lysosomal staining are analysed and quantified throughout regions of the brain previously shown to be severely affected in the *Npc1*<sup>-/-</sup> brain (Pressey et al., 2012). The effect of low dose gene therapy treatment on biochemistry, specifically cholesterol and glycosphingolipid accumulation in the brain is also addressed. While this study has focused on the neurological implications of Niemann-Pick Type C disease, the visceral pathology remains important. To assess disease progression in the viscera, where hNPC1 expression following low dose AAV9-hNPC1 treatment via ICV injection is expected to be extremely limited, concentrations of glycosphingolipids in the liver are compared in treated, untreated and wild-type mice.

### **5.3 Low dose AAV9-hNPC1 treatment ameliorates neurodegeneration in *Npc1*<sup>-/-</sup> mice**

To examine the ability of low dose gene therapy to prevent neurodegeneration in the *Npc1*<sup>-/-</sup> mice, brains from end-stage untreated *Npc1*<sup>-/-</sup> mice (P65), age-matched wild-type control mice (P65) and end-stage *Npc1*<sup>-/-</sup> mice treated with AAV9-hNPC1 (P120) were harvested, fixed and sectioned. Nissl staining is widely used to study the cytoarchitectonics of the brain, as well as the morphology and pathology of neurons. The dye ‘cresyl violet’ binds to DNA and RNA, each highly concentrated in the nuclei and ribosomes of the rough endoplasmic reticulum respectively (Scott and

Willett, 1966). Although nucleic acids in all cells are stained, the relatively high concentration of ribosomes and rough endoplasmic reticulum in the cytoplasm of neurons (Knowles et al., 1996) allows the differentiation between neural and glial cell populations (**Figure 10**).

In the first, instance Nissl staining of the sections allowed for an assessment of brain architecture and revealed improvement in the 120-day old end-stage *Npc1*<sup>-/-</sup> mice that had received low dose gene therapy, when compared to the untreated *Npc1*<sup>-/-</sup> mice that died significantly earlier at 65 days (**Figure 31A**). This was most obvious in the cerebral cortex, thalamus and substantia nigra, which showed significant pathology in the end-stage untreated *Npc1*<sup>-/-</sup> brain. The end-stage untreated *Npc1*<sup>-/-</sup> mice showed significant deterioration in brain tissue and cytoarchitecture at 65 days of age with loss of cellular density and degeneration. However in comparison, *Npc1*<sup>-/-</sup> gene therapy treated mice at 120 days of age demonstrated a significant improvement in both preservation of brain tissue and cytoarchitecture, comparable to the brain sections from wild-type mice.

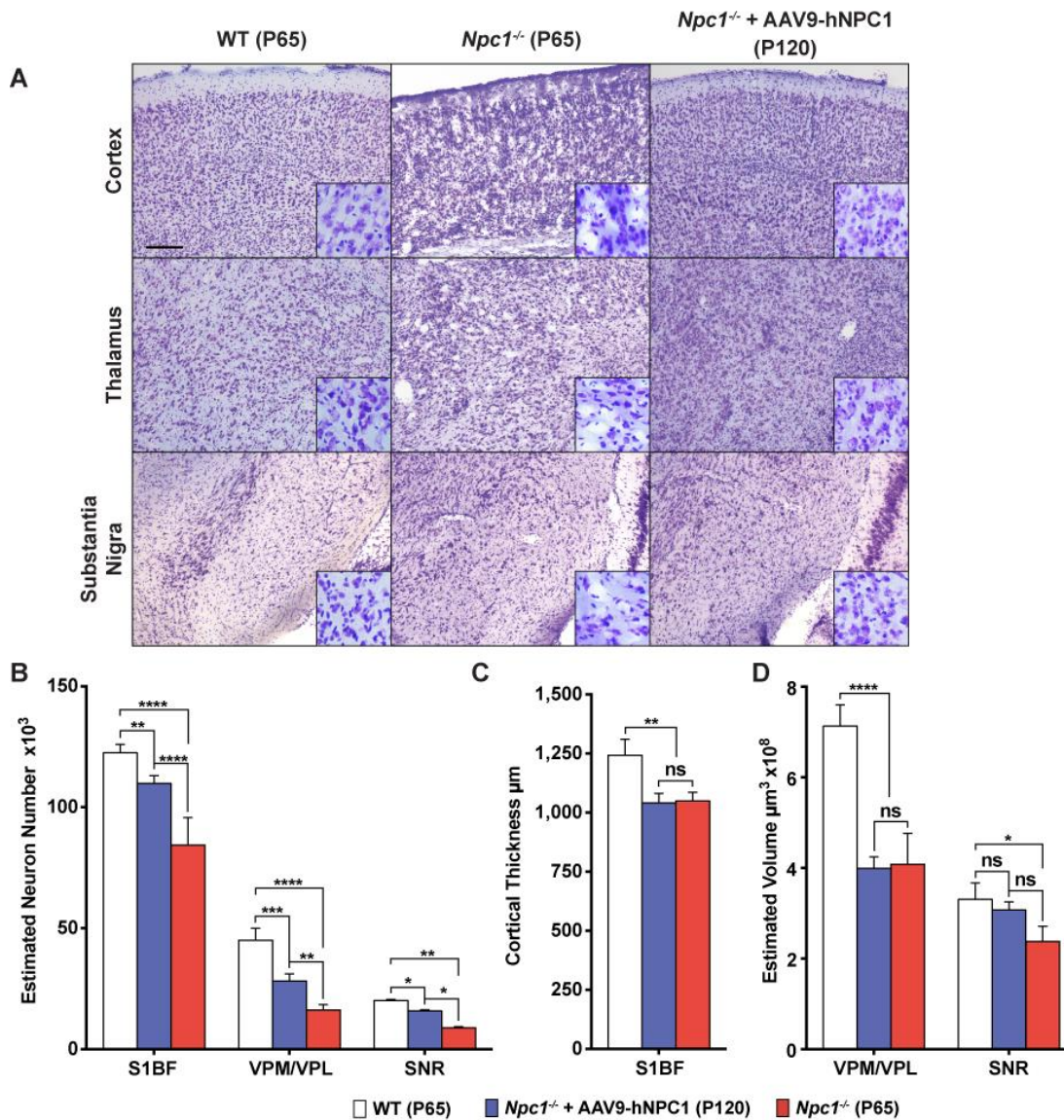


**Figure 31: Amelioration of neurodegeneration in AAV9-hNPC1 treated *Npc1*<sup>-/-</sup> mice.**

End-stage AAV9-hNPC1 treated *Npc1*<sup>-/-</sup> mice (P120, n = 3) were compared to end-stage untreated *Npc1*<sup>-/-</sup> mice (P65, n = 3) and wild-type mice (P65, n = 3). Data represented as mean ± S.D., compared by two-way ANOVA followed by Tukey's HSD test. ns – non significant; \*  $p < 0.05$ ; \*\*  $p < 0.01$ ; \*\*\*  $p < 0.001$ ; \*\*\*\*  $p < 0.0001$ .

- (A) Representative images of NP-C disease characterised brain regions from Nissl stained sections, illustrating deterioration of brain architecture in end-stage untreated *Npc1*<sup>-/-</sup> mice compared to end-stage AAV9-hNPC1 treated *Npc1*<sup>-/-</sup> and wild-type (WT) control mice. Scale bar: 100μm.
- (B) Optical fractionator estimates of neuron number from the somatosensory barrelfield cortex (S1BF), ventral posterior medial and lateral nuclei (VPM/VPL) and the substantia nigra pars reticulata (SNR) demonstrating amelioration of neuronal loss in end-stage AAV9-hNPC1 treated *Npc1*<sup>-/-</sup> mice compared to end-stage untreated *Npc1*<sup>-/-</sup> mice.
- (C) Cortical atrophy in end-stage untreated *Npc1*<sup>-/-</sup> and end-stage AAV9-hNPC1 treated *Npc1*<sup>-/-</sup> mice, measured via cortical thickness of the S1BF region.
- (D) Cavalieri estimates of VPM/VPL and SNR regional volumes.

To quantify the effect of low dose AAV9-hNPC1 treatment on neuronal loss in *Npc1*<sup>-/-</sup> mice, stereological counts of neurons from Nissl stained sections were carried out (**Figure 31B**). Brain regions analysed included the somatosensory barrelfield cortex (S1BF) region of the cortex, the ventral posterolateral and ventral posteromedial nuclei (VPM/VPL) regions of the thalamus and the substantia nigra pars reticulata. In all three regions, untreated end-stage *Npc1*<sup>-/-</sup> mice exhibited a significant decrease in the estimated number of neurones, compared to age-matched wild-type mice at approximately 65 days of age. However in comparison, there was a significant increase in the number of neurons in all quantified regions in end-stage AAV9-hNPC1 treated *Npc1*<sup>-/-</sup> mice at approximately 120 days of age. These improvements translated to a mean average increase of 30% in the S1BF, 73% in the thalamus and 79% in the substantia nigra, when compared to the untreated *Npc1*<sup>-/-</sup> mice that died at approximately 65 days of age. Although treated *Npc1*<sup>-/-</sup> mice showed amelioration in neurodegeneration, the neuronal counts were not completely normalised and remained significantly lower than the counts from wild-type control mice in all three regions examined. These results were not unexpected, as studies in previous chapters showed low dose administration did not result in complete transduction of cell populations in these regions.

This was further reflected by the significant increase of brain region atrophy, observed in end-stage AAV9-hNPC1 treated *Npc1*<sup>-/-</sup> mice, despite amelioration of neurodegeneration. Measurements of cortical thickness in the S1BF region of the cortex revealed that end-stage *Npc1*<sup>-/-</sup> mice (P120) treated with AAV9-hNPC1 had significantly reduced cortical thickness, when compared to control wild-type mice (P65) (**Figure 31C**). Furthermore, there was no significant difference when compared to end-stage untreated *Npc1*<sup>-/-</sup> mice (P65). Using the Cavalieri stereological probe for regional volume measurements, end stage AAV9-hNPC1 treated *Npc1*<sup>-/-</sup> showed significant atrophy of the VPL/VPM region, when compared to wild-type control mice (**Figure 31D**). Again, no significant difference was observed when compared to end-stage untreated *Npc1*<sup>-/-</sup> mice. Volumetric measurements in the substantia nigra revealed sustained tissue volume in the *Npc1*<sup>-/-</sup> mice treated with AAV9-hNPC1, with no significant difference to control wild-type mice. End-stage untreated *Npc1*<sup>-/-</sup> mice had significant atrophy in this area compared to age-matched control wild-type mice.

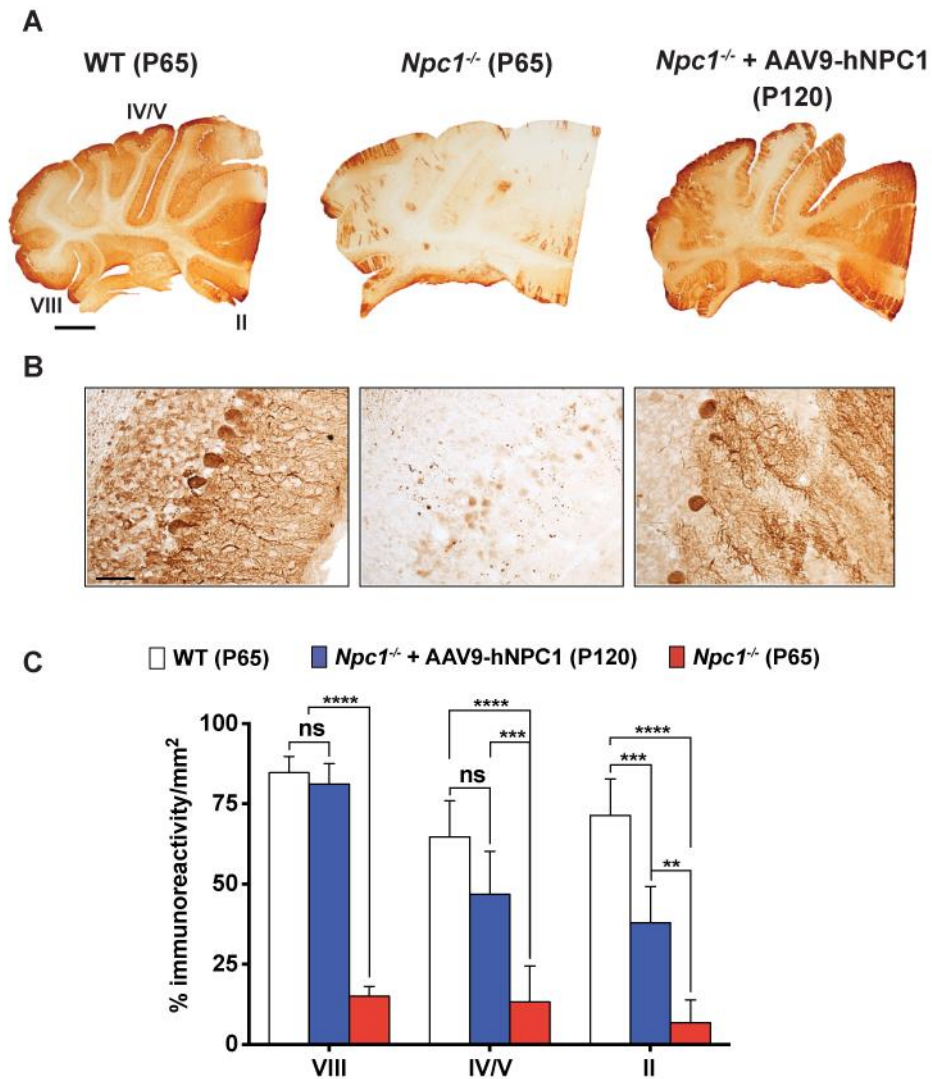


**Figure 32: Amelioration of Purkinje cells loss in the cerebellum of *Npc1*<sup>-/-</sup> mice following low dose AAV9-hNPC1 treatment.**

Cerebellar sections immunostained for Purkinje cell marker calbindin from wild-type (P65, n = 3), untreated end-stage *Npc1*<sup>-/-</sup> (P65, n = 3) and AAV9-hNPC1 treated end-stage *Npc1*<sup>-/-</sup> mice (P120, n = 3). Data represented as mean  $\pm$  S.D., compared by two-way ANOVA followed by Tukey's HSD test. ns - non significant; \*\*  $p < 0.01$ ; \*\*\*  $p < 0.001$ ; \*\*\*\*  $p < 0.0001$ .

- (A) Representative images of whole cerebellar sections stained for Purkinje cell marker calbindin. Scale bar: 1000 $\mu$ m.
- (B) Representative images from the II cerebellar lobule of sections stained for Purkinje cell marker calbindin. Scale bar: 40 $\mu$ m.
- (C) Quantification of immunoreactivity for calbindin positive staining revealing normalisation or amelioration of Purkinje cell loss within the VIII, IV/V and II cerebellar lobules of end-stage *Npc1*<sup>-/-</sup> mice treated with AAV9-hNPC1 compared to end-stage untreated *Npc1*<sup>-/-</sup> mice.

The loss of Purkinje cells in the cerebellum is a hallmark characteristic of neurodegeneration in patients with Niemann-Pick Type C (Vanier, 2010) and is also

observed from 7 weeks of age in *Npc1*<sup>-/-</sup> mice (Sarna et al., 2003). However, the analysis of Purkinje cells via Nissl staining is challenging, due to their relatively low levels of staining compared to the compact and numerous granule cells (Whitney et al., 2008). Evaluation of Purkinje cell loss was therefore carried out via immunostaining using the Purkinje cell-specific marker calbindin-D28k (Bastianelli, 2003). A light microscopy examination of brain sections from 9-week old end-stage untreated *Npc1*<sup>-/-</sup> mice showed a substantial loss of positive calbindin staining in the cerebellum, representing Purkinje cell degeneration, compared to age-matched control wild-type mice (**Figure 32A-B**). However, calbindin positive Purkinje cells were clearly visible in higher numbers in cerebellar sections from 17-week old *Npc1*<sup>-/-</sup> mice treated with low dose AAV9-hNPC1, when compared to 9-week-old untreated *Npc1*<sup>-/-</sup> mice.

To quantify this observation, image thresholding analysis was conducted in discrete regions of the cerebellar sections from wild-type, untreated *Npc1*<sup>-/-</sup> and gene therapy treated *Npc1*<sup>-/-</sup> mice (**Figure 32C**). Measurements of percentage immunoreactivity per unit area within the VIII, IV/V and II cerebellar lobules showed a significant loss of calbindin positive Purkinje cells in sections from 9-week old end-stage untreated *Npc1*<sup>-/-</sup> mice, compared to age-matched control wild-type mice ( $p < 0.0001$ ). However, measurements taken from the VIII ( $p < 0.0001$ ), II ( $p = 0.0011$ ) and IV/V ( $p = 0.0005$ ) regions of 17-week old end-stage AAV9-hNPC1 treated *Npc1*<sup>-/-</sup> mice showed a significantly higher rate of calbindin positive Purkinje cell staining, when compared to 9-week old end-stage untreated *Npc1*<sup>-/-</sup> mice. Furthermore, there was no significant difference in measurements taken in the VIII and IV/V lobules between control wild-type and end-stage treated *Npc1*<sup>-/-</sup> mice, suggesting extensive survival of Purkinje cells in response to low dose gene therapy.

The combination of stereological and immunohistochemical analysis of brain sections from the low dose AAV9-hNPC1 treated *Npc1*<sup>-/-</sup> mice revealed significant amelioration of neurodegeneration or complete neuroprotection in brain regions most severely affected by NP-C, even when the treated mice had reached their humane endpoint. Importantly, while neuron numbers were not rescued to wild-type levels in certain brain regions, these improvements can be correlated to the normalisation of neurological symptoms presented in the previous chapter.

## 5.4 Limited amelioration of inflammatory response in *Npc1*<sup>-/-</sup> mice following low dose AAV9-hNPC1 administration

We next investigated whether low dose AAV-mediated gene therapy could ameliorate the microglia-mediated inflammatory response and astrogliosis previously observed in the *Npc1*<sup>-/-</sup> mouse model (Pressey et al., 2012). Immunohistochemistry with antibodies against CD68 (**Figure 33**) to label microglia and GFAP (**Figure 34**) to label fibrillary astrocytes were used to assess levels of neuroinflammation in wild-type (P65, n = 3), untreated end-stage *Npc1*<sup>-/-</sup> (P65, n = 3) and AAV9-hNPC1 treated end-stage *Npc1*<sup>-/-</sup> mice (P120, n = 3). Analysis of brain sections from these groups revealed extensive microglial activation in untreated end-stage *Npc1*<sup>-/-</sup> mice, which exhibited widespread CD68 positive staining of activated and engorged microglia throughout all regions of the brain examined, compared to low level resting microglial staining in age-matched wild-type mice (**Figure 33A**). 120-day old AAV9-hNPC1 treated *Npc1*<sup>-/-</sup> mice displayed microglial activation comparable to 65-day old end-stage untreated *Npc1*<sup>-/-</sup> mice. However, quantification of CD68 positive immunoreactivity in brain regions known to be acutely affected in the *Npc1*<sup>-/-</sup> mouse revealed significantly reduced levels of immunoreactivity in the substantia nigra (SNR,  $p = 0.0005$ ) and II lobule of the cerebellum ( $p = 0.003$ ), following low dose AAV9-hNPC1 treatment (**Figure 33B**). Other analysed areas exhibited no significant differences in levels of microglial activation in the older end-stage AAV-hNPC1 treated *Npc1*<sup>-/-</sup> mice (P120) compared to the younger end-stage untreated *Npc1*<sup>-/-</sup> mice (P65), with the exception of the brain stem (Gi) and cortex (S1BF) where an increase in CD68 positive staining was measured.

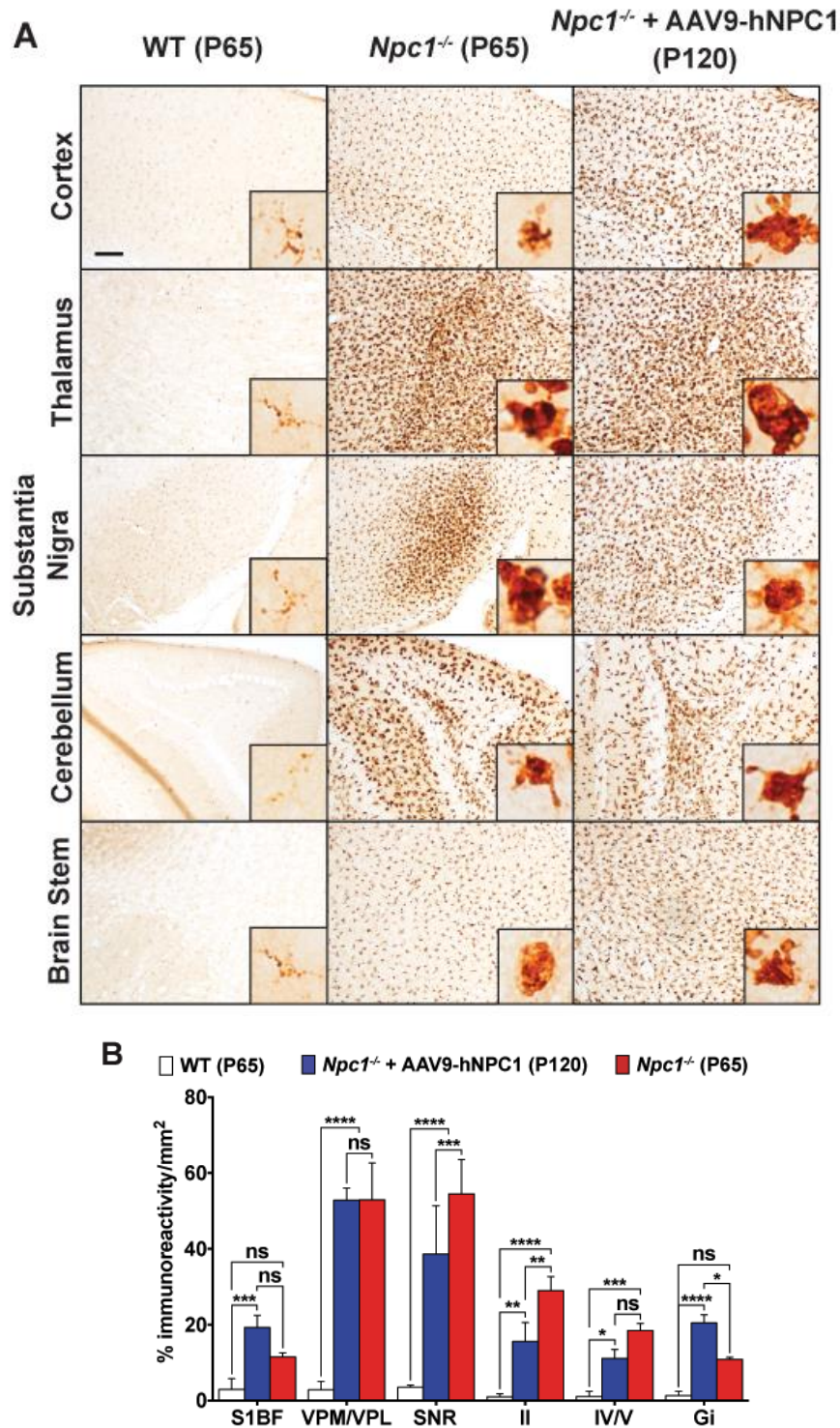


**Figure 33: Limited amelioration of microglial activation in end-stage *Npc1*<sup>-/-</sup> mice following low dose AAV9-hNPC1 treatment.**

Quantification of microglial marker CD68 in end-stage AAV9-hNPC1 treated *Npc1*<sup>-/-</sup> mice (P120, n = 3) compared to end-stage untreated *Npc1*<sup>-/-</sup> (P65, n = 3) and wild-type control mice (P65, n = 3).

(A) Representative images from NP-C disease characterised brain regions of wild-type, untreated *Npc1*<sup>-/-</sup> and AAV9-hNPC1 treated *Npc1*<sup>-/-</sup> sections, stained for microglial marker CD68. Scale bars: 100µm. Insets show positively stained individual cells at higher magnification.

- (B) Quantification of microglial activation via immunoreactivity quantification of CD68 positive staining. Data represented as mean  $\pm$  S.D., compared by two-way ANOVA followed by Tukey's HSD test. ns – non significant, \*  $p < 0.05$ ; \*\*  $p < 0.01$ ; \*\*\*  $p < 0.001$ ; \*\*\*\*  $p < 0.0001$ . S1BF – somatosensory barrelfield cortex; VPM/VPL – ventral posterior medial and lateral nuclei of the thalamus; SNR – substantia nigra pars reticulata; II – II lobule of the cerebellum; IV/V – IV/V lobules of the cerebellum; Gi – gigantocellular reticular nucleus.

The efficacy of low dose AAV9-hNPC1 on the extent of astrogliosis in *Npc1*<sup>-/-</sup> mice was evaluated via immunostaining of the glial fibrillary acid protein. Analysis of brain sections from 9-week old end-stage untreated *Npc1*<sup>-/-</sup> mice stained for GFAP revealed widespread astrogliosis throughout all examined areas (**Figure 34A**). 17-week old end-stage AAV9-hNPC1 treated *Npc1*<sup>-/-</sup> mice exhibited a similar GFAP staining profile, apart from the cerebellum where astrogliosis appeared to be reduced compared to untreated *Npc1*<sup>-/-</sup> mice. Quantification of GFAP positive immunoreactivity supported this finding, with significantly lower levels of GFAP positive staining reported in the II ( $p = 0.0007$ ) and IV/V lobules ( $p < 0.0001$ ) of the cerebellum (**Figure 34B**). No differences were observed within the thalamus (VPM/VPL) and substantia nigra (SNR), however the somatosensory cortex (S1BF,  $p = 0.002$ ) and brain stem (Gi,  $p = 0.01$ ) exhibited higher levels of GFAP positive staining compared to 9-week old untreated *Npc1*<sup>-/-</sup> mice.

The significant reduction in both CD68 and GFAP positive staining within areas of the cerebellum from end-stage AAV9-hNPC1 treated *Npc1*<sup>-/-</sup> mice support the previously suggested survival of Purkinje cells and normalisation of neurological symptoms, as a result of low dose AAV9-hNPC1 treatment. In other brain regions of gene therapy treated *Npc1*<sup>-/-</sup> mice, microglial activation and astrogliosis were either identical or higher, compared to untreated *Npc1*<sup>-/-</sup> mice. However as previously mentioned, the gene therapy treated *Npc1*<sup>-/-</sup> mice were analysed and compared at a significantly older time point and were also at their humane endpoint.

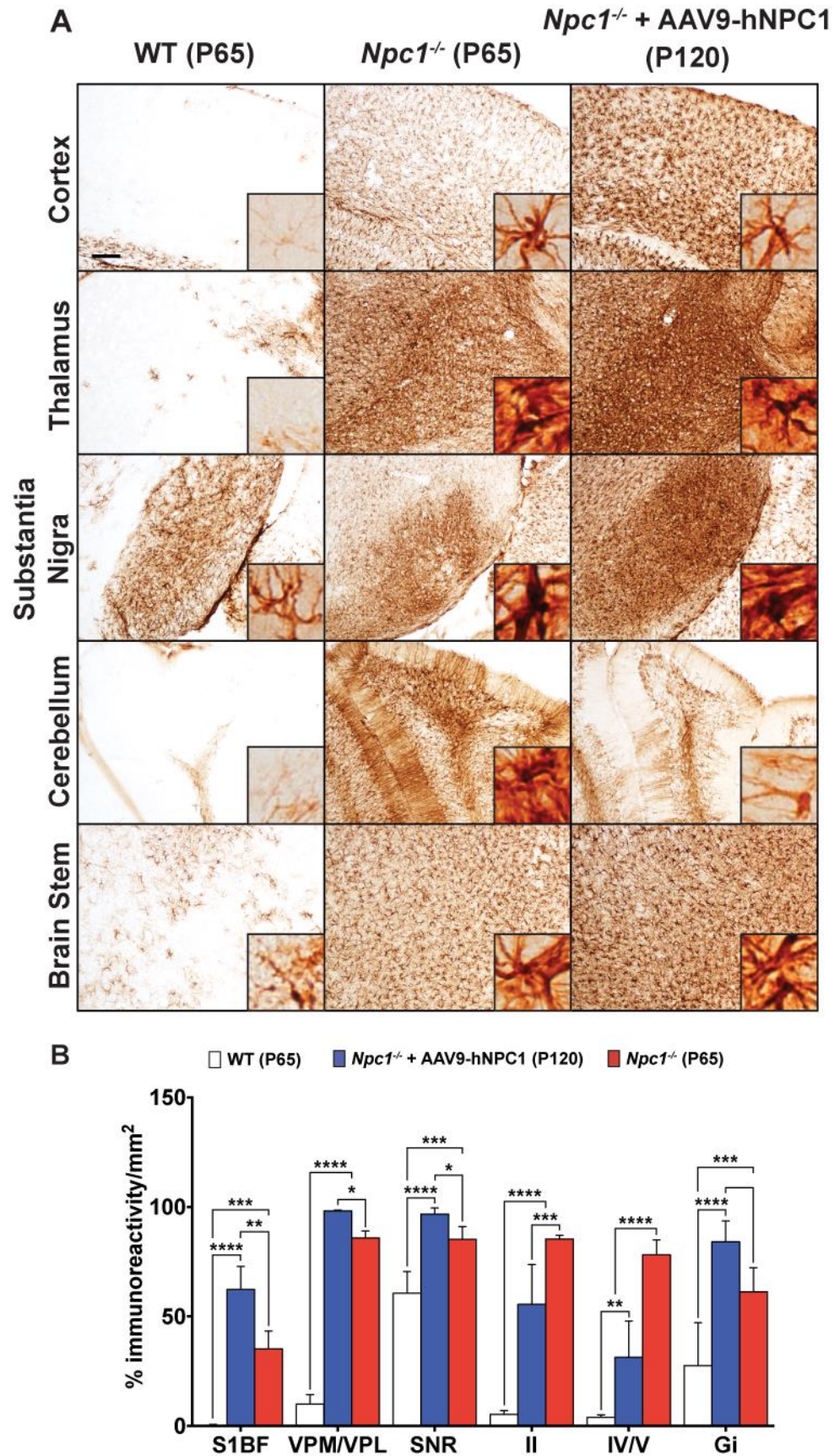


Figure 34: Limited amelioration of astrogliosis in end-stage *Npc1*<sup>-/-</sup> treated with low dose AAV9-hNPC1.

Quantification of astroglial marker GFAP in end-stage AAV9-hNPC1 treated *Npc1*<sup>-/-</sup> mice (P120, n = 3) compared to end-stage untreated *Npc1*<sup>-/-</sup> (P65, n = 3) and wild-type control mice (P65, n = 3).

- (A) Representative images from NP-C disease characterised brain regions of wild-type, untreated *Npc1*<sup>-/-</sup> and AAV9-hNPC1 treated *Npc1*<sup>-/-</sup> sections, stained for astroglial marker GFAP. Scale bars: 100µm. Insets show positively stained individual cells at higher magnification.
- (B) Quantification of astrogliosis via immunoreactivity quantification of GFAP positive staining. Data represented as mean ± S.D., compared by two-way ANOVA followed by Tukey's HSD test. ns – non significant, \*  $p < 0.05$ ; \*\*  $p < 0.01$ ; \*\*\*  $p < 0.001$ ; \*\*\*\*  $p < 0.0001$ . S1BF – somatosensory barrelfield cortex; VPM/VPL – ventral posterior medial and lateral nuclei of the thalamus; SNR – substantia nigra pars reticulata; II – II lobule of the cerebellum; IV/V – IV/V lobules of the cerebellum; Gi – gigantocellular reticular nucleus.

## 5.5 Gene therapy ameliorates increase of lysosomal staining in *Npc1*<sup>-/-</sup> mice

To test the corrective effect of gene therapy on the late endosomal/lysosomal compartment, immunohistochemistry using an antibody against the lysosomal-associated membrane glycoprotein 1 (LAMP1) was carried out (**Figure 35**). LAMP1 was used as a marker for the expanded lysosomal compartment resulting from lipid storage, previously observed in *Npc1*<sup>-/-</sup> mice (Demais et al., 2016). Sections from 9-week old end-stage untreated *Npc1*<sup>-/-</sup> brains (n = 3) were compared to age-matched wild-type (n = 3) and 17-week old end-stage AAV9-hNPC1 treated *Npc1*<sup>-/-</sup> brains (n = 3). A distinctive low level punctate staining was observed in wild-type mice, compared to untreated *Npc1*<sup>-/-</sup> mice, where cells displayed a significantly increased LAMP1 positive staining (**Figure 35A**). Cells with a LAMP1 staining profile similar to untreated *Npc1*<sup>-/-</sup> mice were also observed in 17-week old end-stage AAV9-hNPC1 treated *Npc1*<sup>-/-</sup> mice. However, quantification of LAMP1 immunoreactivity showed a significant reduction of average LAMP1 positive staining, to within wild-type levels in the somatosensory cortex (S1BF,  $p < 0.0001$ ) and II lobule of the cerebellum (II,  $p = 0.05$ ) in low dose gene therapy treated *Npc1*<sup>-/-</sup> mice (**Figure 35B**). Other highly affected disease brain regions of the longer surviving gene therapy treated *Npc1*<sup>-/-</sup> mice exhibited average LAMP1 reactivity comparable to 9-week old end-stage untreated *Npc1*<sup>-/-</sup> mice.

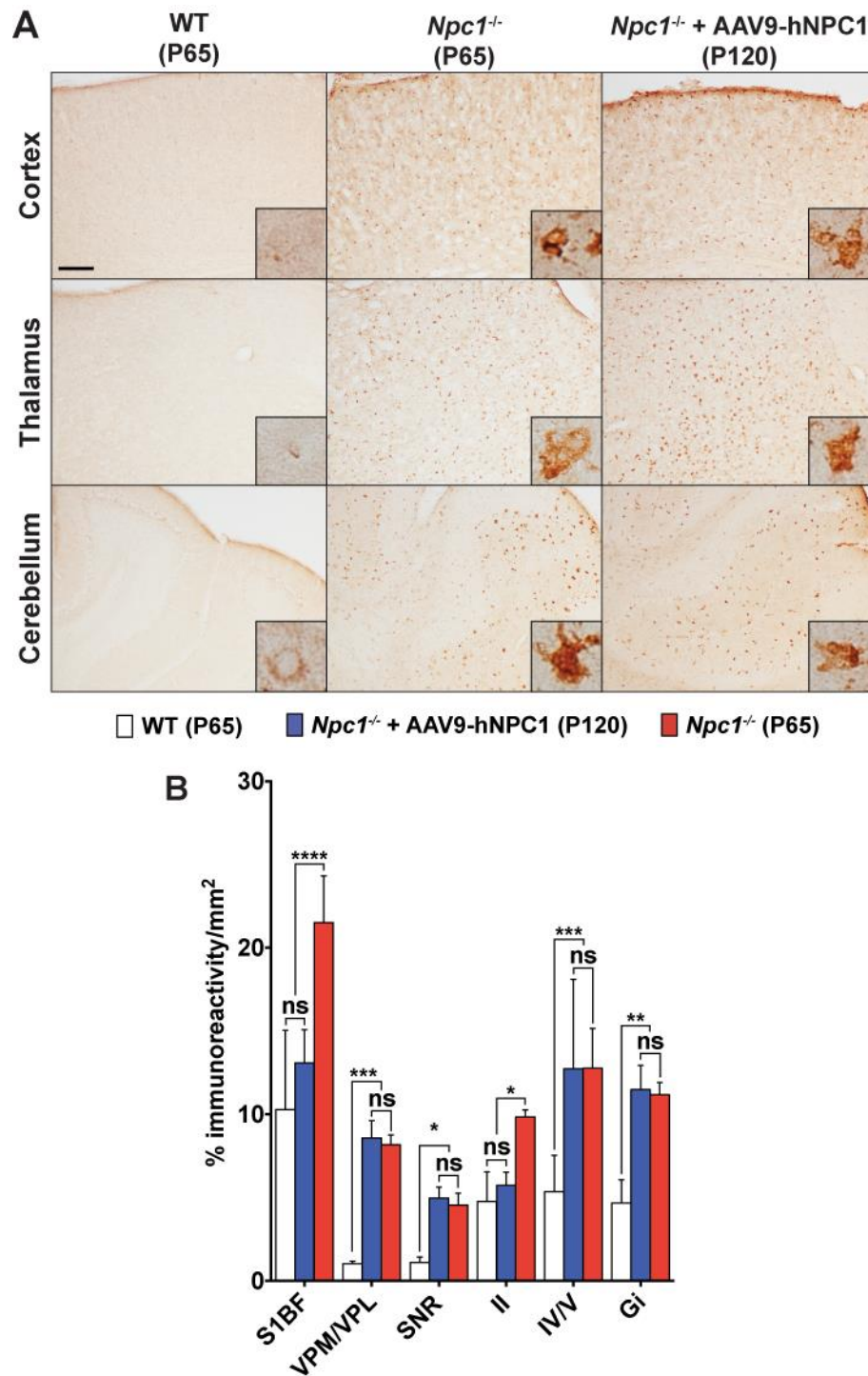


**Figure 35: Regional reduction of increased LAMP1 staining in end-stage *Npc1*<sup>-/-</sup> mice following low dose AAV9-hNPC1 treatment.**

Quantification of LAMP1 lysosomal marker in end-stage AAV9-hNPC1 treated mice (P120, n=3) compared to end-stage untreated *Npc1*<sup>-/-</sup> (P65, n=3) and WT mice (P65, n=3). Data represented as mean  $\pm$  S.D., compared by two-way ANOVA followed by Tukey's HSD test. ns, non significant; \*  $p < 0.05$ ; \*\*  $p < 0.01$ ; \*\*\*  $p < 0.001$ ; \*\*\*\*  $p < 0.0001$ .

(A) Representative images from brain areas severely affected by NP-C neuropathology of brain sections stained for lysosomal marker LAMP1. Scale

bars: 100µm. Insets show positively stained individual cells at higher magnification.

- (B) Quantification of LAMP1 positive immunoreactivity in LAMP1 stained brain sections. Data represented as mean ± S.D., compared by two-way ANOVA followed by Tukey's HSD test. ns – non significant, \*  $p < 0.05$ ; \*\*  $p < 0.01$ ; \*\*\*  $p < 0.001$ ; \*\*\*\*  $p < 0.0001$ . S1BF – somatosensory barrelfield cortex; VPM/VPL – ventral posterior medial and lateral nuclei of the thalamus; SNR – substantia nigra pars reticulata; II – II lobule of the cerebellum; IV/V – IV/V lobules of the cerebellum; Gi – gigantocellular reticular nucleus.

## 5.6 Low dose gene therapy results in redistribution of lipids in *Npc1*<sup>-/-</sup> mice

The *Npc1*<sup>-/-</sup> mouse model recapitulates many of the prominent features of human Niemann-Pick Type C disease, including progressive neurodegeneration, neuroinflammation and resulting neurological symptoms. *Npc1*<sup>-/-</sup> mice also exhibit the severe accumulation of a range of lipids within late endosomal/lysosomal compartments (Walkley and Suzuki, 2004), as observed in NP-C patients (Vanier, 1983, Vanier, 1999). One of these lipid species is the abnormal accumulation of unesterified cholesterol within late endosomal/lysosomal compartments. The filipin test remains a standard tool for NP-C disease diagnosis in patients (Vanier et al., 2016), where the fluorescent filipin stain is used to localise and quantitate unesterified cholesterol (Kruth et al., 1986).

To evaluate the effect of low dose gene therapy on unesterified cholesterol distribution and accumulation, filipin staining was performed on 120-day old end-stage AAV9-hNPC1 treated *Npc1*<sup>-/-</sup> brain sections, which were subsequently compared to 65-day old end-stage untreated *Npc1*<sup>-/-</sup> and wild-type brain sections (**Figure 36**). As expected, untreated *Npc1*<sup>-/-</sup> mice exhibited high levels of filipin staining, with widespread accumulation clearly visible in individual cells within the cortex and thalamus, with many exhibiting clear neuronal morphology (white arrows). Positive filipin staining in age-matched wild-type control mice was either weak or absent. End-stage AAV9-hNPC1 treated *Npc1*<sup>-/-</sup> mice exhibited positive filipin staining within the cortex and thalamus, however compared to end-stage untreated *Npc1*<sup>-/-</sup> mice the staining was less extensive and appeared more diffuse. In

the thalamus in particular, the number of clear filipin positive cells was decreased in *Npc1*<sup>-/-</sup> mice treated with AAV9-hNPC1, compared to untreated *Npc1*<sup>-/-</sup> mice. A decrease in well-defined filipin positive cells was also observed, potentially indicating a deceleration or alteration in the distribution of lipid accumulation in neuronal cell populations.

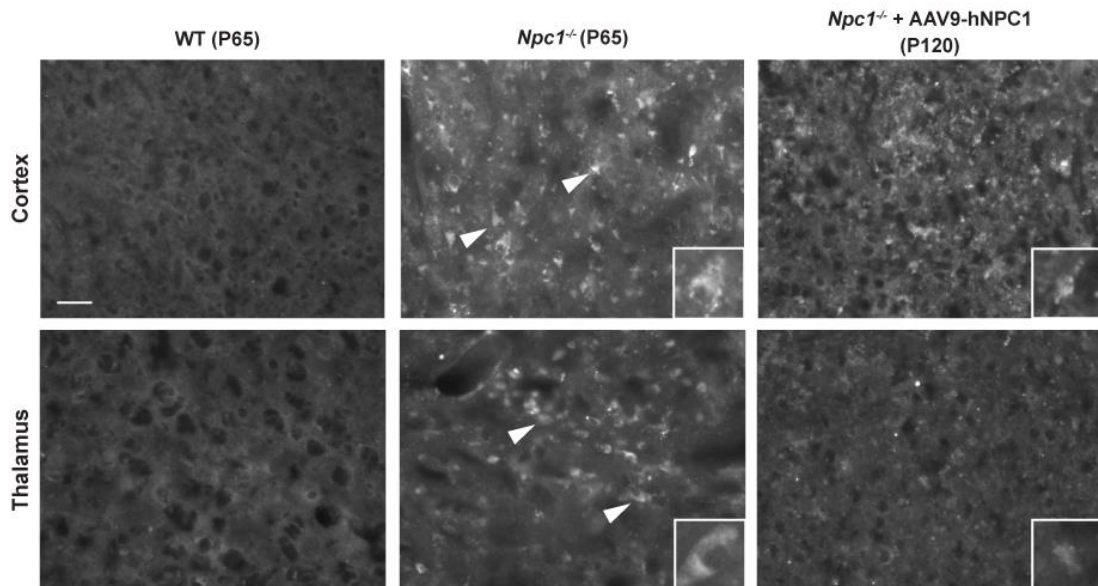


**Figure 36: Redistribution of positive unesterified cholesterol filipin staining in the cortex and thalamus of *Npc1*<sup>-/-</sup> mice following low dose AAV9-hNPC1 treatment.**

Representative images demonstrating the redistribution of unesterified cholesterol accumulation, via filipin staining, in the somatosensory barrelfield cortex and ventral posterior medial and lateral nuclei of the thalamus of AAV9-hNPC1 treated *Npc1*<sup>-/-</sup> mice (P120), compared to untreated end-stage *Npc1*<sup>-/-</sup> (P65) and wild-type mice (P65). Arrows and inset images indicate filipin staining in cells with a neuronal morphology. Scale bar: 100 $\mu$ m.

The extent of individual lipid species accumulation differs in individual organs of *Npc1*<sup>-/-</sup> mice and NP-C patients (Fan et al., 2013). Although unesterified cholesterol accumulation is observed in the brain, the predominant species to accumulate are sphingolipids, including sphingosine and gangliosides, such as GM2 and GM3. In comparison the liver predominantly accumulates cholesterol, GM2 and to a lesser extent GM3 gangliosides. To evaluate the effect of low dose gene therapy on the accumulation of glycosphingolipids (GSL) in *Npc1*<sup>-/-</sup> mice, glycosphingolipids quantification was performed on whole brain and liver tissue lysates in collaboration with M. Huebecker (Department of Pharmacology, University of Oxford) (**Figure 37**). GSL concentrations in the brains from end-stage AAV9-hNPC1 treated *Npc1*<sup>-/-</sup>

mice (P120, n = 8) were compared to end-stage untreated *Npc1*<sup>-/-</sup> (P65, n = 3) and wild-type control mice (P65, n = 6) (**Figure 37A**). Untreated *Npc1*<sup>-/-</sup> mice brains exhibited significantly higher concentrations of total glycosphingolipids tested, compared to normal wild-type levels ( $p < 0.0001$ , 2 - fold increase in mean average). Consistent with previous reports GM2 and GM3 gangliosides concentrations were observed at high levels in untreated *Npc1*<sup>-/-</sup> brains (Fan et al., 2013). Other notable increases in GSL species included the glycolipid lactosylceramide and gangliosides GA2, GA1 and GM1a. Brains from the significantly older end-stage *Npc1*<sup>-/-</sup> mice treated with low dose AAV9-hNPC1 (P120) demonstrated comparable levels of total GSL concentration as the younger end-stage untreated *Npc1*<sup>-/-</sup> brains (P65). However, a significant decrease in GM2 ( $p = 0.0001$ ), a key ganglioside accumulated in the brain in NP-C disease, was observed in end-stage gene therapy treated mice (Gondre-Lewis et al., 2003).

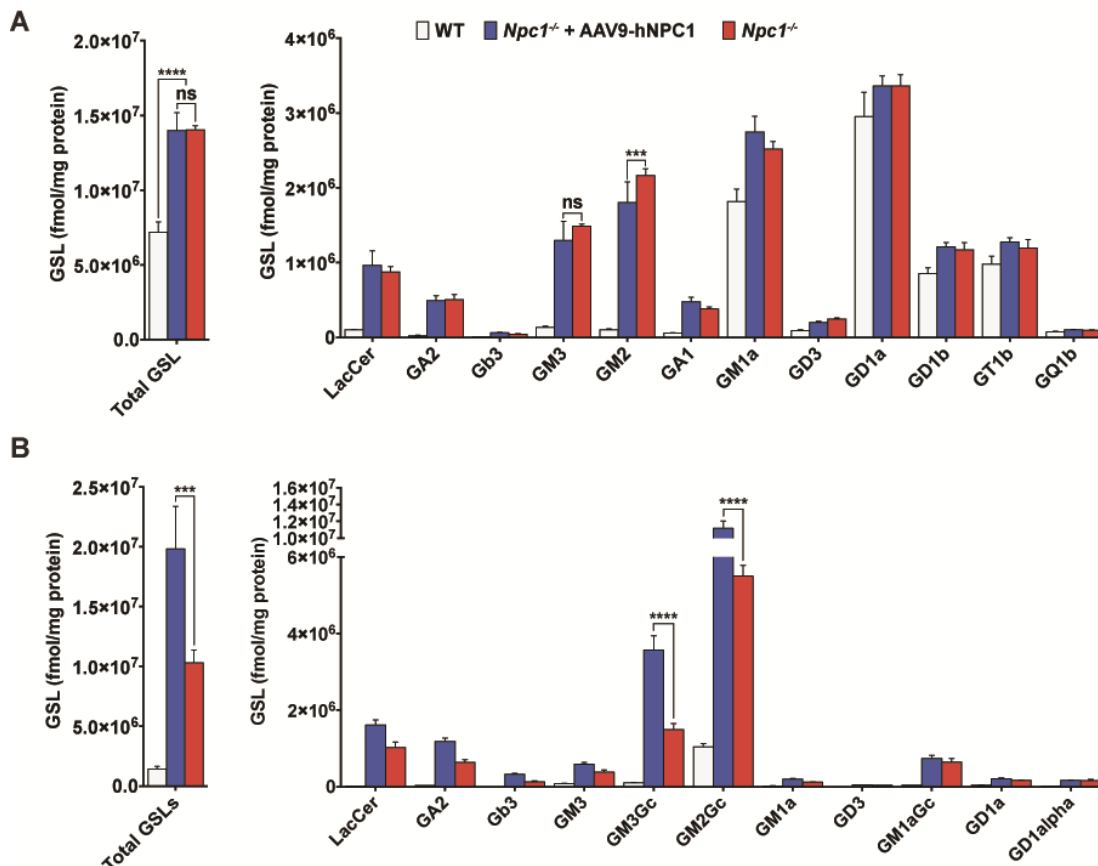


**Figure 37: Glycosphingolipid quantification of brain and liver tissue lysates from *Npc1*<sup>-/-</sup> mice following low dose AAV9-hNPC1 treatment.**

Quantification of total and individual GSL species extracted from brains (A) and livers (B) of wild-type (P65, n = 6), end-stage untreated *Npc1*<sup>-/-</sup> (P65, n = 3) and end-stage AAV9-hNPC1 treated *Npc1*<sup>-/-</sup> mice (P120, n = 8). Data represented as mean ±

S.D., compared by two-way ANOVA followed by Tukey's HSD test. ns - non significant; \*\*\*  $p < 0.001$ ; \*\*\*\*  $p < 0.0001$ . GSL – glycosphingolipid; LacCer – lactosylceramide; GA2 – gangliotriglycosylceramide; Gb3 – globotriaosylceramide; GM3 – II<sup>3</sup>-a-N-acetylneuraminyllactosylceramide; GM2 - II<sup>3</sup>a-N-acetylneuraminylgangliotriglycosylceramide; GA1 – gangliotetraglycosylceramide; GM1a - II<sup>3</sup>a-N-acetylneuraminylgangliotetraglycosylceramide; GD3 - II<sup>3</sup>-a-N-acetylneuraminyla-2,8-N-acetylneuraminyllactosylceramide; GD1a - II<sup>3</sup>, IV<sup>3</sup>-a,a-Di-N-acetylneuraminylgangliotetraglycosylceramide; GD1b - II<sup>3</sup>-a-N-acetylneuraminyla-2,8-N-acetylneuraminylgangliotetraglycosylceramide; GT1b - II<sup>3</sup>-a-N-acetylneuraminyla-2,8-N-acetylneuraminyl-IV<sup>3</sup>-a-N-acetylneuraminylgangliotetraglycosylceramide; GQ1b - II<sup>3</sup>-a-N-acetylneuraminyla-2,8-N-acetylneuraminyl-IV<sup>3</sup>-a-N-acetylneuraminyla-2,8-N-acetylneuraminylgangliotetraglycosylceramide; GM3Gc - II<sup>3</sup>-a-N-glycolylneuraminyllactosylceramide; GM2Gc - II<sup>3</sup>-a-N-glycolylneuraminylgangliotriglycosylceramide; GM1aGc - II<sup>3</sup>-a-N-glycolylneuraminylgangliotetraglycosylceramide; GD1alpha - II<sup>3</sup>,IV<sup>3</sup>-a,a-Di-N-acetylneuraminylgangliotetraglycosylceramide.

Although this study and low dose administration was targeted to the brain, it was important to also analyse potential ongoing visceral pathology. As a result, liver glycosphingolipid concentrations from the different animal cohorts were measured (**Figure 37B**). 9-week old end-stage untreated *Npc1*<sup>-/-</sup> mice again exhibited significantly increased total GSL levels, compared to age-matched wild-type control mice ( $p < 0.0001$ ). Similarly, gene therapy treated *Npc1*<sup>-/-</sup> also exhibited significantly higher levels of total liver GSL compared to wild-type control ( $p < 0.0001$ ). However, unlike in the brain, total liver GSL levels were significantly higher in these end-stage gene therapy treated mice, with a 1.9 - fold increase compared to the younger end-stage untreated *Npc1*<sup>-/-</sup> mice ( $p = 0.0002$ ). Analysis of individual GSL species revealed an increase in all individual GSL levels, however the accumulation of GM2Gc and GM3Gc gangliosides in particular were higher in the *Npc1*<sup>-/-</sup> mice with ICV AAV9-hNPC1 treatment. These liver GSL results suggest that untreated organs continue to accumulate lipids, past the levels observed in untreated *Npc1*<sup>-/-</sup> mice, for a significantly longer period of time, due to the extension in lifespan that brain-directed gene therapy offers. In comparison the GSL levels in the brains of end-stage ICV treated *Npc1*<sup>-/-</sup> mice were similar to end-stage untreated *Npc1*<sup>-/-</sup> despite their significantly longer lifespan.

## 5.7 Summary

This chapter details the results of a series of neuropathology and biochemical studies evaluating the effect of low dose AAV9-hNPC1 gene therapy on *Npc1*<sup>-/-</sup> mice. Significant reductions in the amount of neuronal loss were observed throughout all analysed areas of the brain, including complete neuroprotection of the Purkinje cells in certain areas of the cerebellum to normal levels. While the number of neurons were not completely normalised in all areas (**Section 5.3**), this partial amelioration did lead to the normalisation or improvement of neurological symptoms and quality of *Npc1*<sup>-/-</sup> mice life (**Chapter 4**). Despite the amelioration of neuronal loss in all areas of the brain, the atrophy of these regions remained untreated in gene therapy treated *Npc1*<sup>-/-</sup> mice. Analysis of neuroinflammatory and lysosomal markers also revealed regional amelioration of microglial activation, astrogliosis and quantity of lysosomal staining, particularly in the cerebellum of *Npc1*<sup>-/-</sup> mice treated with low dose AAV9-hNPC1. In the remaining areas no difference was observed between treated and untreated *Npc1*<sup>-/-</sup> mice. The results of biochemical analysis of unesterified cholesterol and glycosphingolipid accumulation followed a similar trend of partial amelioration. Although positive unesterified cholesterol accumulation was observed in the brains of gene therapy treated *Npc1*<sup>-/-</sup> mice, the staining appeared more diffuse and cells with clear neuronal morphology were limited or absent. The effect of low dose AAV9-hNPC1 treatment on brain lipid accumulation was further demonstrated by GSL quantification, where a significant reduction in ganglioside GM2 was observed in the brain of gene therapy treated *Npc1*<sup>-/-</sup> mice. Total brain GSL levels of the older P120 AAV9-hNPC1 treated *Npc1*<sup>-/-</sup> mice were also comparable to the levels observed in the P65 untreated *Npc1*<sup>-/-</sup> mice, despite the large increase in lifespan, suggesting a deceleration of GSL accumulation. In comparison the liver of gene therapy treated *Npc1*<sup>-/-</sup> mice, which should remain untransduced following low dose ICV AAV9-hNPC1 administration, exhibited a 1.9 - fold increase in total GSL levels relative to untreated *Npc1*<sup>-/-</sup> mice. The addition of age-matched comparison of AAV9-hNPC1 treated and untreated *Npc1*<sup>-/-</sup>, may further clarify the effect of low dose ICV gene therapy and will be carried out in the future.

The next step in this study was to conduct a second preclinical study in the *Npc1*<sup>-/-</sup> mouse model, where an increase in AAV9-hNPC1 dose was evaluated for increased therapeutic efficacy.

# 6 Ongoing high dose AAV9-hNPC1 study

## 6.1 High dose AAV9-hNPC1 survival study

The preclinical low dose study covered in the previous two chapters, confirmed the safety and demonstrated promising therapeutic efficacy of neonatal ICV AAV9-hNPC1 administration in the *Npc1*<sup>-/-</sup> mouse model. Very low dose treatment resulted in a 55% increase in the lifespan of treated *Npc1*<sup>-/-</sup> mice, with the correction of multiple locomotor function indices, however only partial amelioration of neurodegeneration, neuroinflammation and lipid storage was observed. The partial transduction of brain areas resulting from low dose AAV9-hNPC1 administration was hypothesised as being the primary possible cause for incomplete neuronal rescue and continued activation of neuroinflammatory cells. The dose evaluation study carried out previously with low dose AAV9-eGFP ( $4.6 \times 10^9$  vp) clearly demonstrated transduction of cell populations in brain regions critical to NP-C pathology, however transduction was not ubiquitous (**Figure 21**). In comparison, high dose AAV9-eGFP ( $5 \times 10^{11}$  vp) administration resulted in a visible increase in the spread of transduction throughout the same regions, albeit ubiquitous neuronal transduction was still not observed. To follow on from the initial preclinical low dose study presented in the previous chapters, a second study was carried out in the *Npc1*<sup>-/-</sup> mouse model, where the dose was increased by 54-fold, from  $4.6 \times 10^9$  GC to  $2.5 \times 10^{11}$  GC. High titer AAV9-hNPC1 was sourced from Vector BioLabs (Malvern, Pennsylvania) at a titer of  $2.5 \times 10^{13}$  GC/ml. This increased dose reflects those used in other preclinical gene therapy studies utilising ICV administration, such as the injection of AAV2/1 into neonatal GM1-gangliosidosis mice (Broekman et al., 2007). The primary aim of this high dose proof of concept study was to evaluate any toxicity and the potential enhancing therapeutic effect in *Npc1*<sup>-/-</sup> mice, compared to

low dose AAV9-hNPC1, miglustat and HP- $\beta$ -CD treatment. In total, 7 *Npc1*<sup>-/-</sup> mice were treated P0/1 with  $2.5 \times 10^{11}$  GC of AAV9-hNPC1 via bilateral ICV administration, which were subsequently monitored and compared to the animal cohorts from the low dose study (**Table 10**). Identical to the previous preclinical study, any mouse exhibiting a 1g-weight loss within a 24-hour period was deemed to have reached their humane endpoint and was sacrificed.

Cohort	N (Male/Female)	Dose	Administration
<i>Npc1</i> <sup>-/-</sup> + HD AAV9-hNPC1	7 (3/4)	Single dose of $2.5 \times 10^{11}$ GC at P0/1	ICV
Wild-type + HD AAV9-hNPC1	3 (1/2)	Single dose of $2.5 \times 10^{11}$ GC at P0/1	ICV
Wild-type	6 (3/3)	-	-
<i>Npc1</i> <sup>-/-</sup>	8 (4/4)	-	-
<i>Npc1</i> <sup>-/-</sup> + LD AAV9-hNPC1	8 (4/4)	Single dose of $4.6 \times 10^9$ GC at P0/1	ICV
<i>Npc1</i> <sup>-/-</sup> + miglustat	8 (4/4)	1,200mg/kg/day from P21	Oral
<i>Npc1</i> <sup>-/-</sup> + HP- $\beta$ -CD	11 (6/5)	4,000mg/kg/week from P21	IP

**Table 10: List of animal cohorts compared throughout this study.**

High dose (HD) AAV9-hNPC1 treated *Npc1*<sup>-/-</sup> mice compared to cohorts from low dose preclinical study (**Table 9**), including untreated, low dose (LD) AAV9-hNPC1, miglustat and HP- $\beta$ -CD treated *Npc1*<sup>-/-</sup> mice and wild-type mice.

## 6.2 No toxicity associated with high dose AAV9-hNPC1 administration

Although no vector related toxicity was observed following low dose administration, potential toxicity associated with a further increase in both vector dose and downstream hNPC1 overexpression was evaluated. Wild-type mice administered P0/1 ICV with  $2.5 \times 10^{11}$  GC of AAV9-hNPC1 (n=3) were sacrificed at 30 days of age for evaluation of neuroinflammatory markers, with comparison of age-matched negative control uninjected wild-type mice (n=3) and P11 positive control *Gba1*<sup>-/-</sup> mice, which have previously been shown to demonstrate an acute form

of neuroinflammation (Enquist et al., 2007). Following the observations of particularly extensive eGFP expression in the cortex of AAV9-eGFP injected wild-type mice (**Figure 21**), the toxicity analysis was focused on the S1BF region of the somatosensory cortex. Evaluation of brain sections was carried out by immunohistochemical analysis with antibodies against the astrocytic marker glial fibrillary acid protein (GFAP) and the microglial marker CD68, to screen for astrogliosis and microglial activation respectively (**Figure 38**).

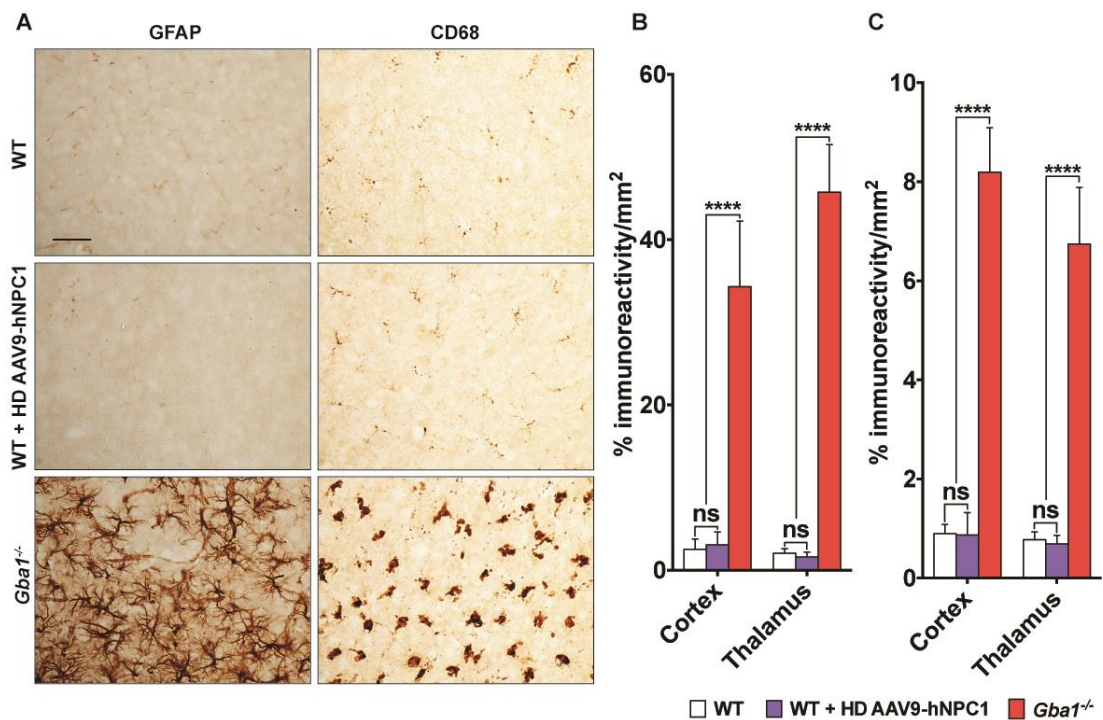


**Figure 38: No neurological toxicity resulting from high dose AAV9-hNPC1 administration**

Analysis of brain sections subjected to anti-CD68 and anti-GFAP immunohistochemistry and resulting quantification of P30 wild-type mice administered neonatally with  $2.5 \times 10^{11}$  GC of AAV9-hNPC1 (n=3), age-matched uninjected control mice (n=3) and positive control *Gba1*<sup>-/-</sup> mice (n=3).

(A) Representative images from the somatosensory barrelfield cortex region of CD68 and GFAP stained sections. Scale bars: 50 $\mu$ m.

(B/C) Quantification of positive anti-GFAP (B) and anti-CD68 (C) immunoreactivity from regions with high levels of AAV9-hNPC1 induced hNPC1 overexpression. Data presented as mean  $\pm$  S.D., compared by two-way ANOVA and Tukey's HSD test. ns, non significant, \*\*\*\*  $p < 0.0001$ .

As with low dose AAV9-hNPC1 administration, no change in resting astrocyte and microglial cell morphology was observed in brains administered with high dose AAV9-hNPC1 compared to brain sections from uninjected control mice, while severe astrogliosis and microglial activation was observed in *Gba1*<sup>-/-</sup> brain sections

(**Figure 38A**). Thresholding analysis of GFAP (**Figure 38B**) and CD68 (**Figure 38C**) immunoreactivity in the cortical S1BF region demonstrated no statistical significance between uninjected control mice and high dose AAV9-hNPC1 administered mice. In comparison to these groups, a significant increase in both GFAP ( $p < 0.0001$ ) and CD68 ( $p < 0.0001$ ) staining was measured in *Gba1*<sup>-/-</sup> brain sections. These results further confirmed that no neurotoxicity resulted from extensive and widespread overexpression of NPC1 to supraphysiological levels in the brain of AAV9-hNPC1 administered mice.

### 6.3 Enhanced survival and weight of *Npc1*<sup>-/-</sup> mice following high dose AAV9-hNPC1 treatment

*Npc1*<sup>-/-</sup> mice administered ICV with a single dose of  $2.5 \times 10^{11}$  GC AAV9-hNPC1 (n=7) exhibited no obvious indications of severe adverse affects in the weeks following vector administration procedure. At the time of thesis submission, 3 of the 7 *Npc1*<sup>-/-</sup> mice treated with high dose AAV9-hNPC1 were sacrificed as they had reached their humane endpoint, with an average survival of 151 days. However at the point of thesis submission, the remaining 4 *Npc1*<sup>-/-</sup> mice treated with high dose AAV9-hNPC1 demonstrated continued survival. Assuming a minimal average survival of 151 days, treatment of *Npc1*<sup>-/-</sup> mice with high dose AAV9-hNPC1 resulted in a significant extension in lifespan compared to untreated *Npc1*<sup>-/-</sup> mice ( $p < 0.0001$ ), miglustat treated *Npc1*<sup>-/-</sup> mice ( $p < 0.0001$ ) and low dose AAV9-hNPC1 treated *Npc1*<sup>-/-</sup> mice ( $p = 0.0001$ ) (**Figure 39**). Although this survival study remains ongoing, assuming an average survival of 151 days, there is no significant difference between AAV9-hNPC1 and systemic HP- $\beta$ -CD treatment. Future completion of this survival study will reveal if ICV treatment with high dose AAV9-hNPC1 further improve or surpass the 168-day average survival age of *Npc1*<sup>-/-</sup> treated with HP- $\beta$ -CD. Although this survival study is still currently ongoing, the results at this stage have demonstrated that enhanced survival correlated with increased AAV9-hNPC1 dose.

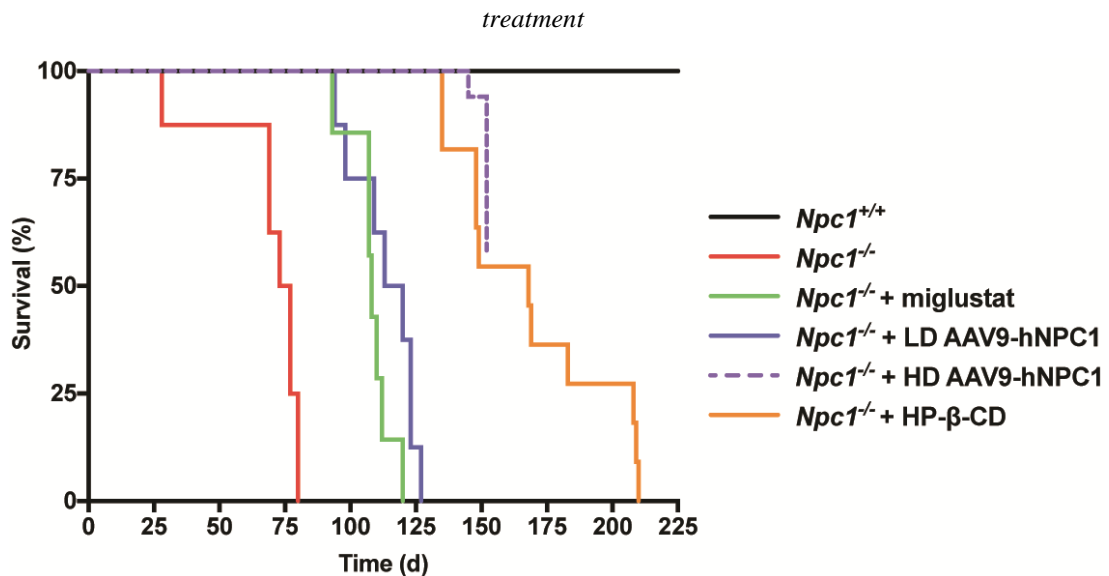


**Figure 39: High dose AAV9-hNPC1 treatment further enhances survival of *Npc1*<sup>-/-</sup> mice.**

Kaplan-Meier survival curve depicts continued survival of 4 out of 7 *Npc1*<sup>-/-</sup> mice treated with a single ICV administration of  $2.5 \times 10^{11}$  GC of AAV9-hNPC1 (n=7) at approximately 151 days of age ( $\pm 21$  days, HD AAV9-hNPC1). Data is compared to cohorts from the previous low dose study: wild-type (n=6), untreated *Npc1*<sup>-/-</sup> mice (n=8, 75 days), *Npc1*<sup>-/-</sup> mice with daily oral administration of 1,200mg/kg of miglustat (n=8, 108 days), *Npc1*<sup>-/-</sup> mice treated with weekly intraperitoneal administration of 4,000mg/kg of HP-β-CD (n=11, 168 days) and *Npc1*<sup>-/-</sup> mice treated neonatally with a single ICV administration of low  $4 \times 10^9$  GC of AAV9-hNPC1 (n=8, 116.5 days, LD AAV9-hNPC1).

The weight of high dose AAV9-hNPC1 treated *Npc1*<sup>-/-</sup> mice was monitored weekly and compared to the weight data from the low dose study animal cohorts (**Figure 40**). *Npc1*<sup>-/-</sup> mice treated with a single high dose AAV9-hNPC1 demonstrated sustained weights throughout their lives compared to untreated *Npc1*<sup>-/-</sup> mice, where dramatic weight loss was observed after 7 weeks of age. Weight of high dose AAV9-hNPC1 treated *Npc1*<sup>-/-</sup> mice was maintained at level comparable to both low dose AAV9-hNPC1 and HP-β-CD treated *Npc1*<sup>-/-</sup> mice until 17 weeks of age. After 17 weeks of age, the weight of high dose treated *Npc1*<sup>-/-</sup> mice remained stable with no significant weight loss observed, compared to the decline of low dose AAV9-hNPC1 and HP-β-CD treated *Npc1*<sup>-/-</sup> mice. However the weights were not normalised, as the high dose AAV9-hNPC1 treated *Npc1*<sup>-/-</sup> mice exhibited significantly lower weight compared to wild-type mice throughout their lifespan.

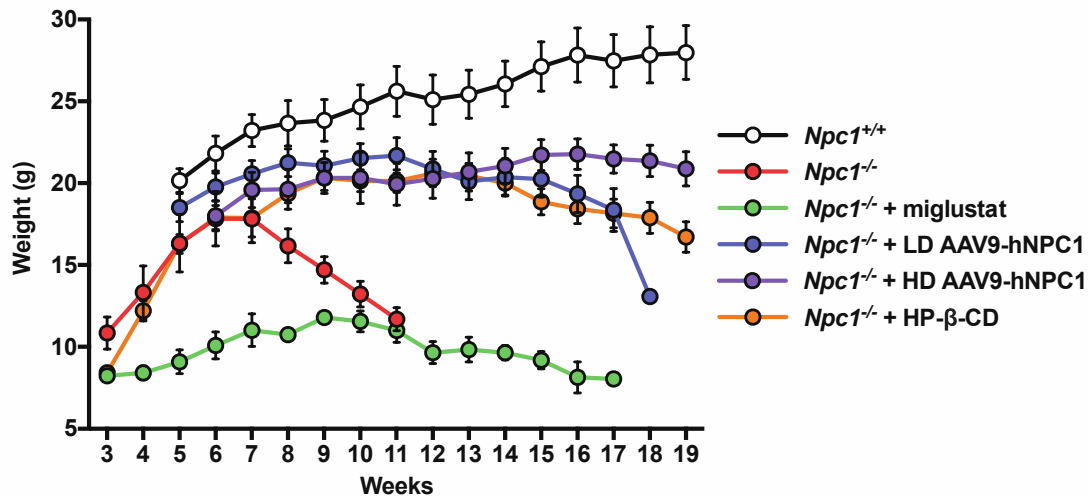


**Figure 40: Sustained weight improvement in *Npc1*<sup>-/-</sup> mice following high dose AAV9-hNPC1 treatment.**

Weekly weight monitoring of *Npc1*<sup>-/-</sup> mice treated neonatally with a single ICV administration of high dose of AAV9-hNPC1 (HD AAV9-hNPC1, 2.5 x 10<sup>11</sup> GC, n=7) until 19 weeks of age. Compared to weight data from low dose study including, wild-type (n=6), untreated *Npc1*<sup>-/-</sup> mice (n=8), *Npc1*<sup>-/-</sup> mice with daily oral administration of 1,200mg/kg of miglustat (n=8), *Npc1*<sup>-/-</sup> mice treated with weekly intraperitoneal administration of 4,000mg/kg of HP-β-CD (n=11), *Npc1*<sup>-/-</sup> mice treated neonatally with a single ICV administration of low dose (LD, 4 x 10<sup>9</sup> GC) of AAV9-hNPC1 (n=8). Data represented as weekly weight mean ± SEM.

## 6.4 Early indications of locomotor normalisation following administration of high dose AAV9-hNPC1

At the time of thesis submission this high dose survival study remained ongoing, with 4 out of 7 AAV9-hNPC1 treated *Npc1*<sup>-/-</sup> mice still alive with an average lifespan of 151 days (±21 days). Therefore, the data available for detailed analysis and presentation in this section was limited to the monitoring of rearing activity to assess improvements in locomotor function.

## AAV9-hNPC1

□ WT   ■ *Npc1*<sup>-/-</sup> + LD AAV9-hNPC1   ■ *Npc1*<sup>-/-</sup> + HD AAV9-hNPC1   ■ *Npc1*<sup>-/-</sup>

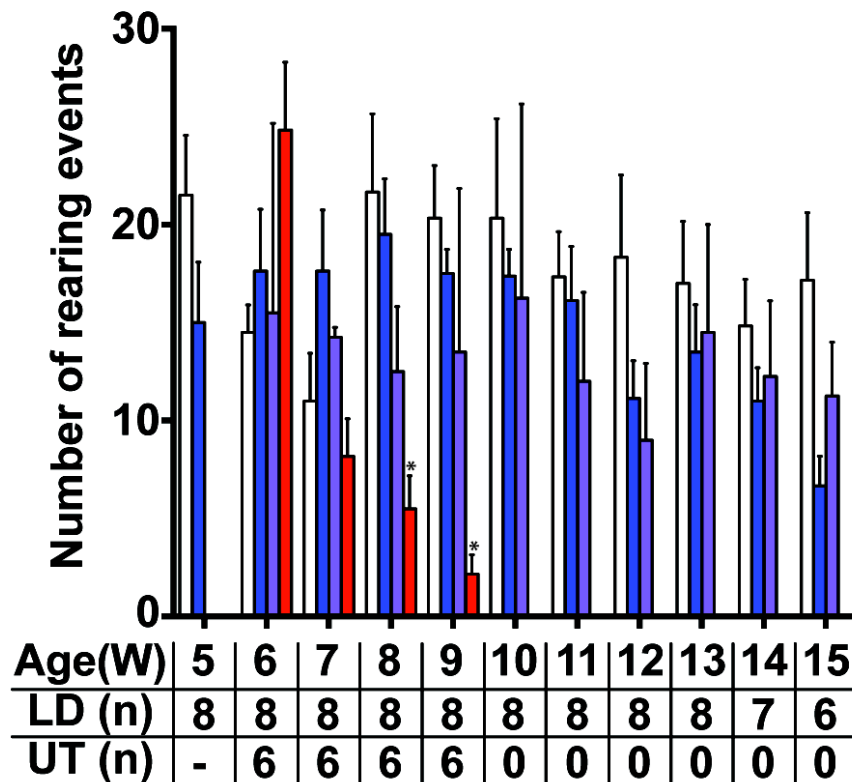


**Figure 41: Correction of rearing activity in high and low dose AAV9-hNPC1 treated *Npc1*<sup>-/-</sup> mice.**

Sustained normalisation of locomotor and co-ordination symptoms of high dose AAV9-hNPC1 treated *Npc1*<sup>-/-</sup> mice (n=6) in an open field setting, where number of rearing events were monitored during a 5-minute period. As study remained ongoing, data presented until 15 weeks of age and compared with low dose study. Data represented as mean  $\pm$  S.D., compared by two-way ANOVA followed by Tukey's HSD test. \*  $p < 0.05$ . W, weeks of age; LD, low dose gene therapy treated *Npc1*<sup>-/-</sup>; UT, untreated *Npc1*<sup>-/-</sup>; n, sample size.

The treatment of *Npc1*<sup>-/-</sup> mice with low dose AAV9-hNPC1 resulted in the permanent correction of key locomotor function readouts associated with NP-C disease progression (**Chapter 4**). These parameters were also monitored weekly in the *Npc1*<sup>-/-</sup> mice treated with high dose AAV9-hNPC1, to confirm whether sustained correction was being achieved. The number of rearing events from *Npc1*<sup>-/-</sup> mice treated with high dose AAV9-hNPC1 was analysed in an open field environment and was subsequently compared to rearing data from the low dose study cohorts (**Figure 41**). The act of rearing demonstrates a combination of coordination, hind-limb strength and natural exploratory behaviour, with a significant reduction in the number of rearing events correlating to disease progression in *Npc1*<sup>-/-</sup> mice (**Figure**

28). *Npc1*<sup>-/-</sup> mice treated with high dose AAV9-hNPC1 exhibited significantly higher numbers of rearing events, compared to untreated *Npc1*<sup>-/-</sup> mice after 7 weeks of age. Comparable to low dose treatment, high dose AAV9-hNPC1 treatment of *Npc1*<sup>-/-</sup> mice demonstrated correction of rearing activity, with no significant differences compared to age-matched wild-type mice in the data available at the point of thesis submission. Continued monitoring of this cohort will reveal if high dose treatment results in the permanent correction of rearing deficiencies to wild-type parameters, past the survival point achieved with low dose AAV9-hNPC1 treatment.

## 6.5 Completion of high dose ICV AAV9-hNPC1 study

At the point of thesis submission, only 3 of the 7 *Npc1*<sup>-/-</sup> mice in the cohort treated P0/1 with a high dose of  $2.5 \times 10^{11}$  GC of AAV9-hNPC1 (n=7) had reached their humane endpoints. As the primary focus of this high dose study was survival analysis, no treated mice were prematurely sacrificed for analysis, as this would have reduced the statistical power of this survival study. Although the data presented throughout this section was therefore limited, high dose AAV9-hNPC1 treatment was demonstrated to result in a further significant enhancement of lifespan compared to untreated, miglustat and low dose AAV9-hNPC1 treated *Npc1*<sup>-/-</sup> mice. There was also no significant difference between high dose gene therapy and HP- $\beta$ -CD treatment in terms of survival in *Npc1*<sup>-/-</sup> mice. Early weight and rearing data, also indicated either equivalent or further improvement compared to low dose AAV9-hNPC1 treated *Npc1*<sup>-/-</sup> mice data. The 4 remaining treated *Npc1*<sup>-/-</sup> mice in this survival study will be continued to be monitored until their humane endpoints are reached, at which point detailed analysis of various locomotor parameters throughout their lifespan will be added to survival and weight data. As with the low dose study, the brains will be analysed for amelioration of neurodegeneration and neuroinflammation and storage material accumulation via lysosomal marker and glycosphingolipid analysis.

The results of analyses from this proof of concept survival studies will be critical in evaluating whether this neurological focused approach of targeting extensive neuronal rescue is sufficient for long-term therapeutic benefit of *Npc1*<sup>-/-</sup> mice. Although this increase in AAV9-hNPC1 dose has already exhibited an enhancement to the lifespan and weight of *Npc1*<sup>-/-</sup> mice, the resulting final average survival and affect on neuroinflammation and neurovisceral lipid storage will indicate if the broadened transduction of other non-neuronal cells in the brain or vital visceral tissues needs to be investigated.

Comparison of data sets from both the low and high dose administration studies in *Npc1*<sup>-/-</sup> mice will also allow the evaluation of dose response in terms of neurological disease amelioration. As the ultimate aim of this work is clinical translation, the identification of this dose to therapeutic benefit correlation may also be beneficial in assessing potential doses required in larger animal models or human patients.

# 7 Discussion

## 7.1 Overview

Loss of function mutations to the *NPC1* gene give rise to the rare lysosomal storage disorder Niemann-Pick Type C disease. This is characterised by severe neurodegeneration that results in progressive neurological disease manifestations and ultimately premature death. NP-C disease models and patients exhibit an accumulation of a range of lipid species, and while NPC1 dysfunction has been linked to various potential cell pathology pathways, the exact mechanism of how NPC1 dysfunction results in cellular pathology still remains unclear. There is currently no curative treatment for NP-C disease, although several small molecule treatments have demonstrated therapeutic efficacy by slowing disease progression (**Section 1.3.7**). However, these potential treatment options are associated with notable disadvantages, such as adverse side effects or the need for repeated invasive administration for the duration of the patient's life.

Following recent clinical successes in the field of gene therapy (Maguire et al., 2008, Stroes et al., 2008, Nathwani et al., 2011) and promising preclinical results for lysosomal storage disorders (**Section 1.7**), the potential use of viral vector mediated gene therapy has expanded to diseases previously considered as more challenging targets. Disorders caused by loss of function mutations to non-soluble lysosomal membrane-bound proteins, including NP-C disease, have been classified as challenging gene therapy targets due to the absence of cross-correction potential. Cell rescue is therefore dependent on successful gene delivery and downstream NPC1 expression in individual cells. However, advances in viral vector gene delivery systems have led to the identification and production of a variety of viral vectors, such as rAAV9 vectors, which are capable of efficient and extensive transduction *in vivo*.

To this end, this project has investigated the use of a viral gene delivery system for the treatment of Niemann-Pick Type C disease. The primary aim of this study was the development of a viral vector expressing the human *NPCI* cDNA and the subsequent preclinical evaluation of this vector in a mouse model of NP-C disease. Results and information gained from these proof of concept studies, would allow further optimisation and testing of this approach thereby aiding the ultimate long-term goal of clinical translation.

The work and results presented in this study have outlined the successful development of a functional AAV vector system that is capable of efficient *NPCI* cDNA delivery and downstream expression. A series of preclinical survival studies in a mouse model of NP-C have demonstrated increased survival and significant therapeutic efficacy utilising this gene delivery system, in a disease that has until recently thought to be an unsuitable target for effective gene therapy. This work therefore provides important findings and implications for the future development of gene therapy for not only Niemann-Pick Type C disease, but also other challenging lysosomal storage disorders involving membrane-bound proteins and monogenic neurological disorders.

Each chapter of this thesis has presented a summary discussion to provide insight into the scientific rationale and approach for subsequent chapters and experiments. This final chapter will further supplement these discussions by evaluating the overall presented findings and the wider context and implications of this work. The aims outlined in the Introduction chapter (**Section 1.9**) will be addressed along with the limitations of the methods and approaches used throughout this study. Finally, important future experiments and general future work will also be discussed.

## 7.2 AAV construct for optimised expression of larger transgenes

The initial challenge addressed in this study was the issue of balancing sufficient viral vector packaging capacity with transduction efficiency. While AAV based viral vectors are currently regarded as the optimal approach for gene delivery to the brain, the incorporation of larger transgenes into functional rAAV vectors remains a major obstacle. At 3.8kb the human *NPCI* cDNA pushes the upper limit of efficient AAV construct packaging, with oversized genomes resulting in a significant reduction of downstream transgene expression (Dong et al., 1996, Lai et al., 2010, Wu et al., 2010, Choi et al., 2014). This limitation has also been a common problem in the development of efficient rAAV vectors for other more common genetic diseases, such as haemophilia A, cystic fibrosis and Duchenne muscular dystrophy. A series of different strategies to increase AAV packaging capacity beyond 4.7kb without creating an oversized genome have been established, including transgene overlapping, trans-splicing or a hybrid combination of both techniques, whereby dual rAAV vectors are administered simultaneously and the constructs recombine in the cell post-transduction (Trapani et al., 2014, Chamberlain et al., 2016, Hirsch et al., 2016). However, the resulting transgene expression efficiency of these strategies can vary greatly and the complex constructs can require significant optimisation.

Before committing to a potentially complex AAV-based approach, a gene delivery vector comparison study was carried out at the beginning of this project. This comparison was used to evaluate whether alternative gene delivery systems without the packaging capacity constraints of AAV vectors could be of potential use for efficient transduction throughout the brain (**Section 3.3**). Following ICV administration, lentiviral and canine adenoviral based vectors demonstrated limited localised transduction of neural cells, with transgene expression predominantly around the site of injection and in the ependymal cells lining the luminal surface of the ventricle walls. This limited transduction profile may have been sufficient for lysosomal storage disorders involving soluble acid hydrolases that can take advantage of cross-correction, with transduced ependymal cells excreting therapeutic protein into the CSF for widespread distribution. This has been demonstrated by the

neurological correction of MPS VII mice following intracranial canine adenovirus administration (Ariza et al., 2014). However, we expected that effective NP-C gene therapy would require the transduction of significantly higher numbers of neural cells in several brain areas, due to the lack of potential cross-correction. Similar to other studies (Kim et al., 2014, McLean et al., 2014), the extensive transgene expression throughout all monitored brain regions following neonatal ICV administration with an AAV9 vector (**Section 3.3**) led to the decision to utilise an AAV9 vector for *NPC1* delivery, despite potential downstream complications associated with an oversized vector genome.

Although the *NPC1* cDNA was considered relatively large for incorporation into a standard rAAV construct, the decision was made to utilise a basic AAV gene delivery system as opposed to exploring more complex approaches. Initial rAAV-hNPC1 constructs based on commonly utilised rAAV template vectors conceived at the start of this study resulted in a final oversized construct of 5.0kb and over. Previous studies analysing the effect of oversized rAAV vector genomes on packaging efficiency and downstream transgene expression have identified a critical packaging capacity threshold at approximately 5.0kb, after which transgene expression is significantly reduced (Wu et al., 2010, Choi et al., 2014). This project therefore focused on the modification and optimisation of a standard rAAV template construct to reduce the completed *NPC1* construct size under this threshold, as opposed to a likely less efficient and more complex dual vector approach.

Modification of the template rAAV construct for large transgene expression was carried out by the removal of all sequences and spacers that were not essential for transgene expression. As a result of these changes, the final rAAV-hNPC1 construct remained oversized by 200bp at 4.9kb, however it was under the critical 5.0kb threshold. *In vitro* testing of the construct plasmid confirmed the significant overexpression of the complete NPC1 protein compared to endogenous NPC1 levels (**Section 3.7**). The completed construct was subsequently used to successfully produce AAV9-hNPC1 viral vectors, which were analysed for vector genome integrity and quantification (**Figure 18**). Despite the oversized nature of the final AAV9-hNPC1 vector, complete packaging of the viral genome was observed, which crucially indicated the absence of genome truncation variants that would have

significantly lowered functional *NPC1* expression levels. The titer of this first batch of vector was significantly lower than the average viral titer obtained during a standard rAAV vector preparation, however this was partially expected due to the oversized nature of the rAAV-hNPC1 construct. At  $4.6 \times 10^{11}$  GC, this 22-fold reduction in titer compared to standard preparations was sub-optimal, however this initial preparation was utilised to confirm successful transduction and NPC1 overexpression, following P0 ICV administration *in vivo* (**Section 3.11**). As expected transduction was far from ubiquitous, however despite this low dose significant viral spread was still achieved, as cell populations demonstrated overexpression of NPC1 throughout all observed brain regions, including sites relatively distant from the site of injection such as the cerebellum and brain stem. Importantly, the production of the full length NPC1 protein was also confirmed, which further supports that despite the marginally oversized vector genome, no truncated variants of either the genome or downstream NPC1 protein were being produced. It is important to note that the method of rAAV vector purification utilised in this study may have potentially enhanced dose efficiency, as iodixanol centrifugation results in the separation of empty viral capsids from packaged viral capsids (Lock et al., 2010), thereby increasing the number of active viral particles available for transgene cassette expression in a given dose.

In combination, these results demonstrate that although the final minimal rAAV construct may still not be suitable for the incorporation and expression of extremely large transgenes, such as the dystrophin gene for Duchene muscular dystrophy, this construct can be effectively utilised for efficient gene delivery to the brain, with expression of transgenes potentially up to 4kb. Further modifications may allow the expression of even larger transgenes, such as through the use of minimal promoters (Ostedgaard et al., 2005), extreme minimal polyadenylation signal sequences (McFarland et al., 2006) or the use of AAV pseudotypes demonstrated to have enhanced packaging capacity, such as AAV2/5 (Allocca et al., 2008, Wu et al., 2010). The observed reduction in viral titer in the first batch represented an additional challenge, however optimisation and up-scaling of the vector preparation protocol can be carried out to improve production efficiency and the AAV9-hNPC1 can be produced to a more standard titer of  $>1 \times 10^{13}$  GC.

## 7.3 Suitability of AAV9-hNPC1 for NP-C disease

At the start of this project we hypothesised that in addition to achieving efficient expression of NPC1 in as many cells as possible, several other important criteria would have to be met for a *NPC1* gene delivery vector to achieve significant therapeutic efficacy in both NP-C animal models and future NP-C patients (**Section 1.8**). While NP-C is a neurovisceral disease, in the majority of patients the visceral pathology is limited to non-fatal and often temporary hepatosplenomegaly, with only rare and extreme cases leading to fatal liver failure (Vanier, 2010). However, in comparison almost all NP-C patients will ultimately develop a progressive and fatal neurological disease. As a result, the treatment of the neurological aspects of NP-C was prioritised in this study. The efficient transduction of as many cells throughout the CNS was therefore targeted, leading to the ultimate use of an ICV AAV9 vector delivery system, as detailed in the previous section.

In a series of complementary studies, neurodegeneration has been shown to occur in a cell autonomous fashion in NP-C disease, with loss of NPC1 function in neurons thought to be primarily responsible for the progressive neurodegeneration and neurological disease manifestations (Lopez and Scott, 2013). The delivery and robust expression of *NPC1* in large populations of neurons was therefore identified as crucial for achieving significant therapeutic efficacy in the neurological aspects of NP-C disease. This was achieved through the choice of the well characterised, neuronal-selective and constitutively active human synapsin I promoter for NPC1 expression, with even low dose AAV9-hNPC1 administration resulting in NPC1 overexpression throughout brain regions critical to NP-C neuropathology (**Section 3.11**). At approximately 480bp, the human synapsin I promoter also had the additional benefit of a relatively small size, compared to other promoters commonly used for neuronal expression, such as the chicken-beta actin promoter at 1.6-1.8kb (Shevtsova et al., 2005, Gray et al., 2011a), thereby further increasing vital packaging space. While the human synapsin I promoter is ideal for significant and long-term transgene expression in neurons, no activity has been observed in other cells of the CNS (DeGennaro et al., 1983). This exclusively neuronal expression was confirmed in this study via a series of AAV9-hNPC1 vector tropism experiments,

with significant NPC1 overexpression exhibited in transduced neuronal cells, however no NPC1 overexpression was observed in either astrocytes or microglia (**Section 3.13**). It is important to note that a previous study has demonstrated that the loss of NPC1 function solely in astrocytes does not result in neuronal toxicity or is sufficient in causing neurodegeneration and neurological disease recapitulation (Yu et al., 2011). Similarly, disease progression was not significantly altered by expression of functional NPC1 within astrocytes in otherwise NPC1-deficient mice (Lopez et al., 2011). In comparison, the conditional loss of neuronal NPC1 function was sufficient in recapitulating neurological disease (Elrick et al., 2010, Yu et al., 2011) and neuron specific NPC1 expression within NPC1-deficient mice resulted in the prevention of neurological disease progression (Lopez et al., 2011). Microglial activation also appears to be secondary to neuronal loss, as an *Npc1* chimeric mouse model demonstrated that microglial activation was only observed within the proximity of dead or dying NPC1-deficient neurons, whereas nearby wild-type neurons remained unaffected (Ko et al., 2005). So while a rAAV vector that can achieve ubiquitous expression of NPC1 in all neural cell types may be ideal, in the first instance in this proof of concept study we have targeted the neurons. As a result of the strong and efficient activity of the human synapsin I promoter in neurons, P0 ICV administration of AAV9-hNPC1 in wild-type mice resulted in the overexpression of the NPC1 protein to supraphysiological levels (**Section 3.11**). As intercellular secretion and uptake of the overexpressed NPC1 protein is not possible, there is likely little benefit in the overexpression of NPC1 above wild-type levels, as targeted by gene therapy approaches for disorders with soluble lysosomal proteins. Importantly, a series of neuropathology studies demonstrated that AAV9-hNPC1 vector administration and the resulting downstream human NPC1 overexpression did not result in any indications of toxicity throughout the brain, in the form of either astrogliosis or a microglial-mediated inflammatory responses (**Section 3.14**). These findings are supported by an early study using prion-promoter-driven *Npc1* cDNA expression to rescue neurodegeneration in a different NP-C mouse model, with no long-term toxicity associated with over 10-fold levels of endogenous *Npc1* expression (Loftus et al., 2002). While a complete GLP-compliant toxicological survey will be required to confirm the safety of this treatment in a clinical context, these are important early considerations from a preclinical safety and toxicology point of view.

Timing and route of administration were also carefully considered to achieve optimal spread and delivery throughout as much of the brain as possible. Intravenous administration for CNS delivery has become a realistic target, as certain rAAV serotypes have been demonstrated to cross the blood-brain barrier extremely well in neonatal mice (Foust et al., 2009, Zhang et al., 2011). However, in older adult mice the efficiency of rAAV movement across the blood-brain barrier reduces significantly (Duque et al., 2009, Gray et al., 2011b), resulting in an ultimate reduction of neurological therapeutic efficacy. As the approach taken in this study was to maximise CNS transduction, we concluded that direct administration into the CNS, while more invasive, would greatly improve vector bioavailability in the brain. A less invasive intrathecal route of administration into the CSF was also considered, however as only a single round of administration will be possible, the benefit of potentially increased efficiency resulting from ICV administration directly into lateral ventricle may outweigh the disadvantage of it being a more invasive procedure. Neonatal administration was chosen as the time point for vector administration in this proof of concept project, in an attempt to maximise the transduction efficiency and viral spread of the AAV9-hNPC1 vector. As a result, evaluation of the therapeutic efficacy of AAV9-hNPC1 was carried in optimal conditions.

The initial *in vivo* test of AAV9-hNPC1 in wild-type mice supported these decisions, as even at a significantly lower dose, efficient neuronal NPC1 expression in a large number of cells within brain areas particularly affected by NP-C induced neuropathology, including the cortex, thalamus and cerebellum, was being achieved (**Figure 20**). High magnification imaging of these transduced cells also revealed a distinct punctate distribution of the overexpressed NPC1 protein, which was confirmed as successful localisation of the NPC1 protein to within LAMP1 positive structures, including late endosomes and lysosomes, via scanning confocal microscopy of immunofluorescence staining (**Figure 24**). It was important to show that hNPC1 protein was able to traffic correctly to endosomal and lysosomal compartments given that the human *NPC1* and murine *Npc1* cDNA and protein sequence are not completely conserved. As these sequences share a relatively high homology, at 84% and 86% respectively, we decided to utilise the human *NPC1*

cDNA for evaluation in an NP-C mouse model to facilitate potential future clinical translation. While incorporation of the murine *Npc1* variant may have been more effective in mouse models, many of the preclinical experiments carried out in this project would have had to have been repeated with the human variant.

In combination, these points and considerations support why the AAV9-hNPC1 vector designed and produced in this project was not only a suitable candidate for the preclinical evaluation in a *Npc1*<sup>-/-</sup> mouse model, but also in a configuration that could be realistically translated for future clinical use.

## 7.4 Therapeutic efficacy of AAV9-hNPC1

A series of preclinical studies have been carried out in the *Npc1*<sup>-/-</sup> mouse model in this study, with low and high dose AAV9-hNPC1 treatment evaluated for their therapeutic efficacy on survival, weight and amelioration of neurological NP-C disease manifestations. The reasons to initially carry out a low dose study followed by a subsequent high dose study were threefold. (1) In the initial wild-type *in vivo* vector testing, the levels of NPC1 overexpression observed in widespread cell populations appeared promising, with AAV9-hNPC1 induced expression in all brain regions severely affected by NP-C associated neurodegeneration, despite the very low dose; (2) given that the exact function of the NPC1 protein remains currently unclear we wanted to be cautious with the dose in the first round of preclinical testing; (3) taking the limited timeframe into consideration, rather than solely focusing on vector production optimisation, we reasoned that valuable preclinical results could be gained from the readily available low titre AAV9-hNPC1 batch, with a subsequent high dose study when higher titer vector was available. In the first round of preclinical testing, AAV9-hNPC1 was therefore administered at a relatively low dose of  $4 \times 10^9$  GC ( $4 \times 10^{12}$  GC/kg), compared to other studies using rAAV vectors in neonates via the same route of injection, where up to approximately  $3 \times 10^{14}$  GC/kg has been utilised (Broekman et al., 2007).

Encouragingly, low dose AAV9-hNPC1 ICV treatment of *Npc1*<sup>-/-</sup> mice resulted in an average 55% increase in lifespan and significant weight improvements, compared to untreated *Npc1*<sup>-/-</sup> mice (**Chapter 4**). The improvements to lifespan and weight were accompanied with permanent normalisation or improvement in various indices of neurological disease manifestations, including rearing, tremor and gait. These promising results confirm that even at a very low dose, the AAV9-hNPC1 vector designed in this project was capable of significant and long-term therapeutic efficacy in a disease that was until recently considered a difficult target for effective gene therapy treatment. Further analysis of brain sections from these end-stage low dose AAV9-hNPC1 treated *Npc1*<sup>-/-</sup> mice (**Chapter 5**) revealed significant or permanent neuronal rescue in all quantified brain regions, including the cortex, thalamus, substantia nigra and complete normalisation to wild-type levels in several regions of the cerebellum. The partial preservation of neurons had been expected, as previous low dose AAV9-hNPC1 vector evaluation in wild-type mice demonstrated that transduction of neurons was not ubiquitous. This therefore implies that at least in this animal model of NP-C, universal or extensive neuronal rescue through AAV9-hNPC1 transduction may not be necessary to achieve significant therapeutic benefits. These clear therapeutic effects on critical clinical endpoints in this model are encouraging since motor co-ordination and ataxia are hallmark symptoms in NP-C patients. However, despite AAV9-hNPC1 treatment and significant neuronal rescue, the regional atrophy and inflammatory responses observed in the brains of untreated *Npc1*<sup>-/-</sup> mice remained present in these low dose *Npc1*<sup>-/-</sup> treated mice. The reason for these findings is unclear, although several theories are proposed: (1) following non-ubiquitous transduction, the untransduced cells underwent continued neurodegeneration resulting in neuroinflammation, which may also account for the regional atrophy; (2) alternatively, as NPC1 expression was restricted to neurons, other neural cells may have continued to accumulate storage material leading ultimately to cellular pathology and an inflammatory response. However, it is important to note that significant amelioration of neuroinflammation was observed in several brain regions, indicating that gene therapy was having an affect on the extent of neuroinflammation within treated brains. This was particularly apparent in the cerebellum, as significant neuronal rescue within the simple and paramedian lobules of the cerebellum correlated with a reduction in both astroglial and microglial induced neuroinflammation. Additionally, as this was a survival study, the brain

sections of the low dose gene therapy treated *Npc1*<sup>-/-</sup> mice were analysed at their end-stage, at a significantly older time point. This may have allowed longer pathology progression in cells and areas left untransduced following low dose AAV9-hNPC1 administration. Comparison of younger gene therapy treated *Npc1*<sup>-/-</sup> mice with age-matched untreated *Npc1*<sup>-/-</sup> mice may in future clarify the efficacy of AAV9-hNPC1 treatment on glial cell activation, however due to time constraints this was not investigated during the course of this project.

As NP-C disease is a lysosomal storage disorder, the effect of gene therapy treatment on the accumulation of various lipid species has also been investigated in this project (**Section 5.6**). Analysis of cholesterol accumulation in the brain revealed that significant amounts of unesterified cholesterol were present within cells, above the levels observed in wild-type brains. However, there was a clear difference in the profile of positively stained filipin cells between low dose AAV9-hNPC1 treated and untreated *Npc1*<sup>-/-</sup> mice. The positive and clear staining of cells exhibiting neuronal morphology observed in the untreated *Npc1*<sup>-/-</sup> mice could not be detected in the gene therapy treated *Npc1*<sup>-/-</sup> mice, which were characterised by a more diffuse staining profile. The number of filipin positive cells also appeared to be reduced as a result of low dose gene therapy treatment, which was particularly evident within the thalamus. A possible explanation for this change in filipin staining may be a redistribution of unesterified cholesterol accumulation within the brains of gene therapy treated *Npc1*<sup>-/-</sup> mice. Due to the exclusive expression of NPC1 protein in neurons, lipid accumulation may have been ameliorated in rescued neurons, however other untransduced neural cells such as astrocytes and microglia will continuously accumulate lipids. This theory is supported by the reduction of filipin positive cells with neuronal morphology in gene therapy treated *Npc1*<sup>-/-</sup> mice, indicating amelioration of neuronal cholesterol accumulation. Additionally, the diffuse filipin staining observed in low dose AAV9-hNPC1 treated *Npc1*<sup>-/-</sup> brains may represent glial cells and their processes, however further evaluation of the filipin stain in combination with neural cell markers will be necessary to support this hypothesis.

Quantification of glycosphingolipids within the brain revealed no significant difference between the high total GSL concentrations observed in untreated and older low dose gene therapy treated *Npc1*<sup>-/-</sup> mice. However, compared to untreated

*Npc1*<sup>-/-</sup> mice, low dose AAV9-hNPC1 administration resulted in the significant reduction of GM2, one of the key glycosphingolipids species known to accumulate within the brain of *Npc1*<sup>-/-</sup> mice and NP-C patients (Fan et al., 2013) and its accumulation has been linked to neuronal degeneration and dysfunction in both NP-C and other storage disorders (Siegel and Walkley, 1994, Walkley, 1995). Taking the significantly longer lifespan of AAV9-hNPC1 administered *Npc1*<sup>-/-</sup> mice into account, we hypothesised that if lipid accumulation was left unaffected by gene therapy, the GSL concentrations in the brain of these significantly older mice would have accumulated beyond the levels demonstrated by the younger untreated *Npc1*<sup>-/-</sup> mice. However, as the total brain GSL concentrations in brains of low dose gene therapy treated *Npc1*<sup>-/-</sup> mice were comparable to untreated *Npc1*<sup>-/-</sup> mice, there may have been a deceleration of GSL accumulation. This theory was supported by the observation of highly elevated GSL levels within the livers of ICV AAV9-hNPC1 treated *Npc1*<sup>-/-</sup> mice, which were significantly higher than liver GSL levels in untreated *Npc1*<sup>-/-</sup> mice. This would be expected from a gene therapy approach targeted to the brain and not the viscera. Combined with the longer lifespan, the visceral tissue may have continuously accumulated lipids beyond the average levels observed in untreated younger *Npc1*<sup>-/-</sup> mice. A future comparison of age-match gene therapy treated and untreated *Npc1*<sup>-/-</sup> mice may answer these points more definitively, where comparable GSL levels in the liver and a reduction in brain GSL accumulation would confirm a deceleration of CNS GSL accumulation. This highly significant build-up of glycosphingolipids species within the liver confirmed that the focus of neuronal rescue combined with low dose ICV administration had not addressed the visceral pathology of NP-C.

Although visceral symptoms are common in NP-C patients, severe and fatal visceral pathology has been limited to a minority of patients, with neurological disease manifestations thought to ultimately be responsible for severe disease progression and death. However, following the observation of extreme GSL levels in the liver of low dose AAV9-hNPC1 treated *Npc1*<sup>-/-</sup> mice, the importance and potential impact of visceral pathology and visceral lipid accumulation in this model has to be taken into consideration. While the *Npc1*<sup>-/-</sup> mouse model utilised in this study does not replicate the fact that missense mutations are found in the majority of patients (Carstea et al., 1997, Bauer et al., 2002, Park et al., 2003), it does generally recapitulate the

behavioural, neuropathological and biochemical defects seen in human patients. Although similar lipid storage profiles have been observed in the viscera of *Npc1*<sup>-/-</sup> mice, compared to human patients, the accumulation in the liver of *Npc1*<sup>-/-</sup> mice is more severe than in the spleen, which is the opposite to human disease (Vanier, 2015). This inherent enhanced lipid accumulation in the liver of *Npc1*<sup>-/-</sup> mice may have been further amplified in ICV AAV9-hNPC1 administered *Npc1*<sup>-/-</sup> mice, where the viscera was left untreated and pathology was allowed to continuously progress during the longer lifespan, as supported by the finding of extreme liver GSL concentrations in treated *Npc1*<sup>-/-</sup> mice. As a result of this high lipid accumulation rate in the liver, pathology associated with the liver or other visceral tissues may have become more critical over time in the older gene therapy treated *Npc1*<sup>-/-</sup> mice. Additionally, severe visceral storage may also be capable of affecting CNS pathology via the movement of toxic, water-soluble metabolites across the blood-brain barrier, subsequently contributing to neurodegeneration and inflammation (Jones and Weissenborn, 1997). While a significant extension in *Npc1*<sup>-/-</sup> mouse lifespan has been achieved by the neurologically focused AAV9-hNPC1 treatment, the reason for these mice reaching their humane endpoint via significant weight loss remains unclear. At their humane endpoints, AAV9-hNPC1 treated *Npc1*<sup>-/-</sup> mice did not exhibit the standard *Npc1*<sup>-/-</sup> phenotype, as all indices of neurological disease were either normalised or significantly improved. We initially hypothesised that while extremely promising, the modest number of neurons transduced following low dose AAV9-hNPC1 treatment may have been sufficient in rescuing the neurological phenotype, with continued degeneration of large populations of untransduced neurons ultimately contributing to disease progression and weight loss. As a result of the 54-fold increase in viral particles administered, high dose AAV9-hNPC1 administration is expected to result in significantly higher numbers of transduced neurons and subsequent therapeutic efficacy. However, while a significant improvement over low dose treatment has been observed in the lifespan and weight of gene therapy treated *Npc1*<sup>-/-</sup> mice, 3 of the 7 high dose AAV9-hNPC1 treated *Npc1*<sup>-/-</sup> mice were ultimately sacrificed due to significant weight loss. Future analysis of these brains will reveal the extent of neuronal rescue, however similar to low dose treatment, at their humane endpoint these high dose treated *Npc1*<sup>-/-</sup> mice did not exhibit the classical *Npc1*<sup>-/-</sup> neurological phenotype. Although the ratio of transduced neurons following high dose administration may still not be sufficient, these findings

indicate that there may be additional factors, such as visceral pathology, contributing towards the ultimate death of high dose AAV9-hNPC1 treated *Npc1*<sup>-/-</sup> mice. As with low dose treatment, the ICV administration of high dose AAV9-hNPC1 into the CSF should result in basal visceral transduction, resulting in continued visceral lipid accumulation. However, if this were to be the primary cause of deterioration in gene therapy treated cohorts, the average survival should not be affected by the increase in AAV9-hNPC1 dose within the CNS, as visceral tissues should remain unaffected at both doses. It is important to note that in the high dose study, the 54-fold increase in vector administration may cause additional leakage of the vector into the blood stream, such as through the eventual drainage of CSF into the venous system (Haurigot et al., 2013). Additionally, although the human synapsin I promoter is exclusively neuronal in the CNS, synapsin I protein expression has been observed in visceral tissue (Bustos et al., 2001). Synapsin I promoter activity has recently been demonstrated within the livers of mice following intravenous administration of an AAV9-synapsin vector (Jackson et al., 2016). An increase in ICV AAV9-hNPC1 dose may therefore result in NPC1 production and subsequent clearance of lipids within transduced liver cells. This factor may contribute to the extended survival observed following high dose AAV9-hNPC1 treatment compared to low dose, however future tissue transduction evaluation and further visceral analysis will be needed to confirm potential liver transduction.

The conclusion of the high-dose gene therapy survival study, subsequent tissue analysis and comparison with the data from the low dose cohort will give a clearer indication of the complete neurological and visceral therapeutic efficacy of neonatal ICV AAV9-hNPC1 treatment of *Npc1*<sup>-/-</sup> mice. However, the experiments presented in this project demonstrate critical proof of concept results, where administration of AAV9-hNPC1 to *Npc1*<sup>-/-</sup> mice resulted in a significant therapeutic benefit. This includes either normalisation or significant improvements in a number of key readouts including lifespan, quality of life and indices of behaviour, neuropathology and biochemistry, as determined in a well-characterised mouse model of NP-C.

## 7.5 Limitations

This project focused on the development of a functional AAV9-hNPC1 gene delivery vector, optimised for efficient transgene expression in neurons and was used in a series of preclinical survival studies. While significant improvements in lifespan, weight, locomotor function and neurodegeneration were observed, there are important limitations regarding the approach and utilised methods that need to be highlighted.

Firstly, the clinical translation of results from P0/1 neonatal administration approach for the evaluation of *NPC1* gene delivery vector must be considered, as neonatal pre-symptomatic administration will not reflect the likely standard scenario of clinical application. Although there are exceptions, as in certain rare cases NP-C can be diagnosed either *in utero* or post-natally through the presence of severe hepatosplenomegaly or ascites (Spiegel et al., 2009), though in the majority of circumstances patients are diagnosed after the onset of symptoms. Fast and efficient diagnosis remains a key issue for NP-C patients, however recent advances in the identification of NP-C biomarkers and their screening may significantly improve this diagnostic delay (Welford et al., 2014, Giese et al., 2015, Reunert et al., 2016). These advances in diagnostics may also enable the development of comprehensive neonatal screening, which would allow initiation of therapy, such as gene therapy, in neonates. Alternatively, this neonatal gene therapy approach may be viable in cases where the diagnosis of an NP-C patient leads to the subsequent diagnosis of a pre- or very early- symptomatic sibling.

As the major aim of this project was demonstrating proof of concept of therapeutic efficacy resulting from ICV AAV9-hNPC1 treatment, vector administration was carried out as early as possible to achieve optimal transduction spread. Previous studies have demonstrated that ICV administration of rAAV9 into neonatal mice resulted in extensive and widespread transgene expression throughout the entire CNS (Kim et al., 2014, McLean et al., 2014). However, as the brain is not fully developed at this early stage of administration, the transduction profiles observed in this study may differ when translated to an adult brain. A number of studies have investigated

the transduction efficiency of ICV rAAV9 vector administration in adult rodents and larger animal models, where widespread transgene expression throughout the brain could still be observed (Samaranch et al., 2012, Haurigot et al., 2013, Donsante et al., 2016).

Another important point to address is the translatability of results from the relatively small brain size of a mouse or more specifically neonatal mouse, compared to the much larger human brain. A common criticism with the small size of the neonatal mouse brain is that the general plasticity of the brain at that time point allows the administration of relatively high rAAV doses in relation to overall brain size. While correct, it is also important to note that total CSF volume increases with larger brain size, from 0.035ml in mice to approximately 140ml in humans, allowing the relative dose to be scaled up with delivery of significantly larger volumes over longer time periods possible within the CSF of larger brains (Gray et al., 2013). For example, in this study neonatal mice were administered with a low dose of  $4.6 \times 10^9$  GC and high dose  $2.5 \times 10^{11}$  GC, compared to the significantly higher dose of  $5.5 \times 10^{12}$  vector genomes of AAV vector administered ICV in adult non-human primates (Gray et al., 2013), representing a 1,100-fold and 22-fold increase respectively. It will be important to re-evaluate ICV administration of AAV9-hNPC1 in the slightly larger and fully developed adult *Npc1*<sup>-/-</sup> mouse brain, to compare with the proof of concept efficacy results produced following the neonatal ICV administration in *Npc1*<sup>-/-</sup> mice. Ideally this vector could also be tested in a larger model of NP-C disease, such as the well-characterised feline NP-C model. However, the information gained in terms of additional clinical translational value of AAV9 efficacy between a murine and feline NP-C model compared to human NP-C patients may be limited, mainly as a result of the unpredictable nature rAAV transduction profiles between species. As with all gene therapy studies, it is currently impossible to predict how efficient and widespread rAAV9 transduction will be in the large brains of human patients when administered into the CSF. However, the use of rAAV9 vectors has already translated through to the clinical trials using this approach for spinal muscular atrophy type 1 (ClinicalTrials.gov Identifier: NCT02725580) and CLN6 Batten disease (ClinicalTrials.gov Identifier: NCT02725580).

One of the major limitations of the preclinical studies carried out in the *Npc1*<sup>-/-</sup> mouse model during this project was the lack of data for age-matched gene therapy treated AAV9-hNPC1 *Npc1*<sup>-/-</sup> mice, to allow clear comparisons with 9-week old end-stage untreated *Npc1*<sup>-/-</sup> mice. Design, modification and production of the AAV9-hNPC1 construct and vector required significant amounts of time, leading to a limited timeframe for preclinical vector evaluation. As the primary aim of this study was to establish proof of concept results that ICV administration of AAV9-hNPC1 in neonatal *Npc1*<sup>-/-</sup> mice could demonstrate significant therapeutic benefit and extension of lifespan, we decided to conduct a survival study, where all animals were kept until their respective humane endpoints. The main reason for prioritising the ageing out of all mice cohorts was to allow higher power statistical analysis of survival, weight and motor-function, rather than reducing potential significance by sacrificing a minimum of 3 treated *Npc1*<sup>-/-</sup> mice at 9 weeks of age for neuropathology and biochemistry analysis. As a result these analyses were carried out on end-stage AAV9-hNPC1 treated *Npc1*<sup>-/-</sup> mice, which are compared with significantly younger untreated *Npc1*<sup>-/-</sup> mice. The future addition of age-matched AAV9-hNPC1 treated *Npc1*<sup>-/-</sup> samples may clarify some of the points raised in this chapter, such as the possible deceleration of brain lipid accumulation, or may even demonstrate greater significant therapeutic effects at that time point. On the other hand, the analysis of end-stage *Npc1*<sup>-/-</sup> tissue allowed the recognition of significant, long-term neuronal rescue in all analysed brain regions, accompanied with regional reductions in neuropathological and lysosomal markers.

Finally, as this project aimed for a neurologically focused gene therapy approach for NP-C disease, the majority of analysis was naturally targeted towards the CNS and neurological disease manifestations associated with neurodegeneration. However as previously discussed in this chapter, ongoing visceral pathology may play a role if left untreated by the AAV9-hNPC1 vector evaluated in this study. In future, more in depth analysis of visceral tissue pathology following ICV AAV9-hNPC1 treatment, with a particular focus on the liver, may clarify the extent of the affect of progressive visceral pathology on gene therapy treated *Npc1*<sup>-/-</sup> mice and also potentially further demonstrate the importance of visceral pathology in NP-C disease.

## 7.6 AAV9-hNPC1 and competing NP-C therapies

To place the therapeutic efficacy of this gene therapy study in the context of other competing therapies in the NP-C arena, AAV9-hNPC1 treatment has been directly compared to miglustat and HP- $\beta$ -CD treatment in *Npc1*<sup>-/-</sup> mice in terms of survival, weight and tremor analysis. ICV administration of AAV9-hNPC1 in neonatal *Npc1*<sup>-/-</sup> mice resulted in a significant extension of lifespan at both low and high doses. Low dose treatment extended the survival of *Npc1*<sup>-/-</sup> mice (116.5 days  $\pm$  12.22) to that exhibited by miglustat treated mice (108  $\pm$  8.071), which represents the only currently licenced drug for NP-C disease within the EU. Interestingly, gene therapy did not exhibit the adverse side effects seen in the miglustat treated mice. This was most evident through the inability of miglustat treated mice to gain weight, due to the known appetite suppressive properties associated with this drug (Priestman et al., 2008). Furthermore, miglustat also inhibits gastrointestinal disaccharidases leading to the disruption of gastrointestinal function, which is present in 80% of patients receiving miglustat within the first 6 months of treatment and 60% of patients long-term (Remenova et al., 2015), and is the most common cause of discontinuation of use (Belmatoug et al., 2011, Lyseng-Williamson, 2014). Both treatment options resulted in the normalisation of NP-C induced tremor in *Npc1*<sup>-/-</sup> mice throughout their lifespan. These results demonstrate that even at a low dose, ICV treatment of *Npc1*<sup>-/-</sup> mice with AAV9-hNPC1 is comparable to the therapeutic efficacy of miglustat, without the associated adverse effects.

Although the high dose survival study remained ongoing at the time of thesis submission, a further extension in lifespan from low dose gene therapy treatment (116.5 days  $\pm$  12.22) was recorded in *Npc1*<sup>-/-</sup> mice treated with a 54-fold higher dose of AAV9-hNPC1 (151 days  $\pm$  21). Assuming 151 days as the minimal survival, the extended survival exhibited by *Npc1*<sup>-/-</sup> mice following high dose AAV9-hNPC1 treatment was comparable to the survival achieved by systemic HP- $\beta$ -CD treatment (168  $\pm$  29.31), with no significant difference between the two options. Future completion of the high dose survival study will clarify if high dose AAV9-hNPC1 further improves on the 151-day lifespan or potentially surpasses the 168-day average survival age demonstrated in *Npc1*<sup>-/-</sup> treated with viscerally with HP- $\beta$ -CD.

These treatments also exhibited comparable improvements in the weights of *Npc1*<sup>-/-</sup> mice until 17 weeks of age, after which continued stabilisation in the weight of high dose gene therapy treated *Npc1*<sup>-/-</sup> mice was contrasted by the decline in weight of HP- $\beta$ -CD treated *Npc1*<sup>-/-</sup> mice. As with low dose AAV9-hNPC1 and miglustat treatment, HP- $\beta$ -CD treated *Npc1*<sup>-/-</sup> mice demonstrated the normalisation of tremor at both 9 and 16 weeks of age, indicating therapeutic efficacy on the neurological disease manifestations of NP-C. As HP- $\beta$ -CD has been shown to inefficiently cross the blood-brain barrier (Pontikis et al., 2013), high dose systemic administration of HP- $\beta$ -CD is required to have a significant neurological effect (Vite et al., 2015). However, pulmonary toxicity has been observed in *Npc1*<sup>-/-</sup> cats treated intravenously with high doses of HP- $\beta$ -CD (Vite et al., 2015). Alternatively, HP- $\beta$ -CD can be injected directly into the CSF allowing the safer administration of lower doses to achieve similar neurological improvements. However, this approach requires administration of HP- $\beta$ -CD every two weeks via invasive intrathecal administration, which is currently being evaluated in an ongoing clinical trial in NP-C patients (Phase II/III ClinicalTrials.gov Identifier: NCT02534844). There are also concerns relating to ototoxicity and subsequent hearing loss that have been observed in mice (Crumling et al., 2012) and cats (Ward et al., 2010) following HP- $\beta$ -CD treatment. Therefore, while HP- $\beta$ -CD is promising, there are concerns around the viability of long-term administration and potential toxicity that a gene therapy approach could avoid, as the ICV single injection of high dose AAV9-hNPC1 resulted in a comparable extension of lifespan.

The results of this project are encouraging, as we have demonstrated significant therapeutic efficacy of ICV AAV9-hNPC1 administration in a disease, which has until recently been considered as a relatively challenging target, due to the lack of cross-correction potential and large transgene size. The rise in gene therapy preclinical and clinical successes combined with the progression of viral vector technology has led to the expansion of viable gene therapy targets, with increased attention given to these more challenging disorders. Along with this project, two recently published studies have investigated the potential use of AAV9 vectors for the treatment of NP-C disease, both supporting our findings of significant neuropathological improvements in *Npc1*<sup>-/-</sup> mice following gene therapy treatment. However, there are significant differences in terms of construct variations, route of

administration and general approach between the different studies. One of the recent studies demonstrated that high dose intravenous administration of AAV9 vectors carrying the hNPC1 cDNA to neonatal (P1-3,  $1 \times 10^{11}$  GC) and pre-symptomatic weanling mice (P20-25,  $1 \times 10^{12}$  GC) significantly extended the lifespan, with reduced neuropathology and liver cholesterol accumulation in the *Npc1*<sup>-/-</sup> mouse at 9 weeks of age (Chandler et al., 2016). The approach of intravenous administration allows the transduction of visceral tissues in combination with neural transduction, as rAAV9 vectors are capable of crossing the blood-brain barrier, however efficiency is significantly reduced from neonatal to adult period (Duque et al., 2009, Foust et al., 2009, Gray et al., 2011b). The authors additionally compared the use of the neuron-specific promoter CamKII with a more ubiquitous shortened EF1a promoter in terms of survival and weight, following gene therapy treatment. High dose injection of the neuron specific AAV9 vector resulted in a mean survival of 97 days ( $\pm 18.5$ ) following neonatal intravenous administration and 103 days ( $\pm 29.7$ ) when injected into weanling *Npc1*<sup>-/-</sup> mice. Although the humane endpoints between studies will vary, as this work has been carried out in the same NP-C animal model used in this study using a comparable technique, these results can tentatively be compared with the results from this study (**Figure 42**). These survival results are comparable to the survival of miglustat treated *Npc1*<sup>-/-</sup> mice and are significantly lower than *Npc1*<sup>-/-</sup> mice treated ICV with both high and low dose AAV9-hNPC1 vector. Treatment with the CamKII vector resulted in the correction of cholesterol accumulation in transduced neurons and the significant increase of Purkinje neurons within several lobules of the cerebellum compared to untreated treated *Npc1*<sup>-/-</sup> mice, however in contrast to this study this analysis was only carried out at 9 weeks of age. In combination with a lack of behavioural analysis, it is difficult to assess the long-term efficacy of this approach on the disease progression of *Npc1*<sup>-/-</sup> mice. Interestingly, the intravenous administration of an AAV9 vector with the human NPC1 cDNA controlled by a ubiquitous shortened EF1a promoter resulted in a significant improvement in survival of *Npc1*<sup>-/-</sup> mice (166 days  $\pm 89.2$ ) relative to the neuron specific promoter. These results are comparable to the survival observed in *Npc1*<sup>-/-</sup> mice treated systemically with HP- $\beta$ -CD and high dose AAV9-hNPC1, with no significant difference between all groups. As subsequent neuropathology analysis was limited to the observation of reduced filipin staining within the pons and liver of 9-week old treated brains, the full impact of this treatment on both neurological and

visceral pathology remains unclear. Additionally, the transduction profile of the shortened EF1a AAV9 vector within the brains or visceral tissue was not addressed, allowing minimal comparison. Given the dominance of neurodegeneration in fatal NP-C symptoms and the need for high levels of transduction, we have prioritised the brain for maximum treatment using an ICV administration directly into the CSF. We have subsequently demonstrated that administration of AAV9-hNPC1 into neonatal *Npc1*<sup>-/-</sup> mice resulted in the significant long-term protection of neurons within brain areas most severely affected by NP-C neurodegeneration, such as the cortex, thalamus, substantia nigra and cerebellum, however this has been at the expense of the viscera. The efficiency of transduction within the brain of intravenously administered weanling mice would be expected to be significantly reduced compared to direct ICV administrations into the CSF of neonatal mice, however both approaches have demonstrated comparable levels of survival. This observation may indicate that additional transduction of non-neuronal cells, such as glial cells in the brain or hepatocytes in the viscera may benefit towards the long-term survival of *Npc1*<sup>-/-</sup> mice.

A

Cohort	Dose / Timing	Administration	Average survival (days)	Standard deviation	N	Source
untreated	-	-	69	17	8	This Study
miglustat	1,200mg/kg/day	Oral	108	8	8	This Study
HP- $\beta$ -CD	4,000mg/kg/week from P21	IP	168	29	11	This Study
LD AAV9-SYN-hNPC1	Single dose of 4.6 x 10 <sup>9</sup> GC at P0/1	ICV	116.5	12.2	8	This Study
HD AAV9-SYN-hNPC1	Single dose of 2.5 x 10 <sup>11</sup> GC at P0/1	ICV	152	3	7	This Study
AAV9-CaMKII-hNPC1	Single dose of 1 x 10 <sup>11</sup> GC at P1-3	IV	97	18.5	6	(Chandler et al., 2016)
AAV9-CaMKII-hNPC1	Single dose of 1 x 10 <sup>12</sup> GC at P20-25	IV	103	29.7	9	(Chandler et al., 2016)
AAV9-EFS-hNPC1	Single dose of 1.3 x 10 <sup>12</sup> GC at P20-25	IV	166	89.2	7	(Chandler et al., 2016)
AAV9-CMV-mNpc1	Single dose of 2.5 x 10 <sup>11</sup> GC at P4	ICA	94	4	16	(Xie et al., 2017)

B

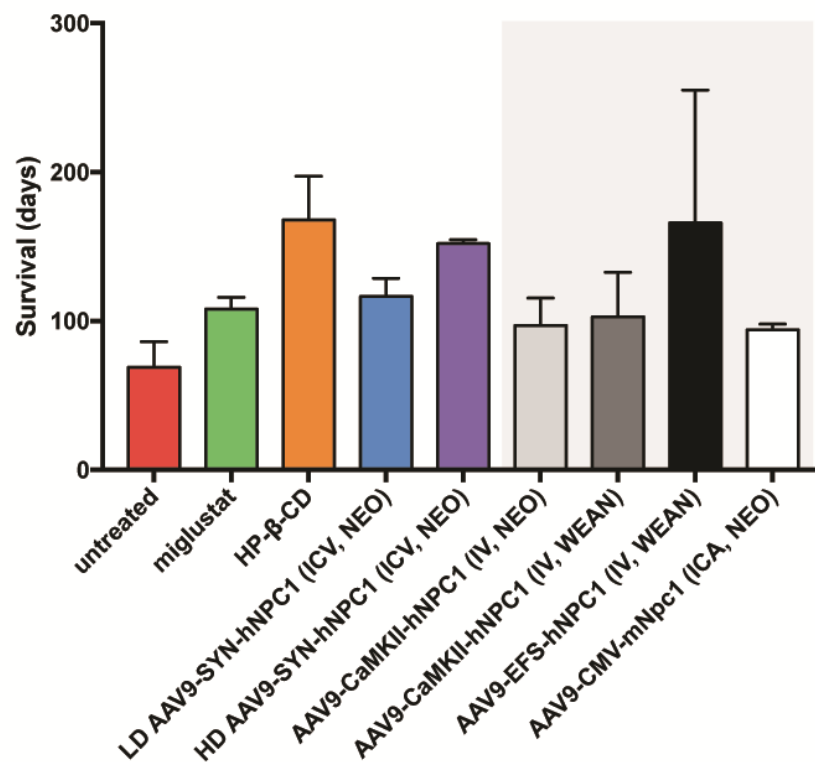


**Figure 42: Summary of average survival data of *Npc1*<sup>-/-</sup> mice in recent NP-C gene therapy studies.**

IP, intraperitoneal; IV, intravenous; ICV, intracerebroventricular; ICA, intracardiac; LD, low dose; HD, high dose; NEO, neonatal; WEAN, weanling. Data represented as mean  $\pm$  S.D.

Another recent study demonstrated that high dose ( $2.5 \times 10^{11}$  vector genomes) intracardiac administration of AAV9 vectors carrying a modified murine *Npc1* cDNA variant under the control of the viral CMV promoter into *Npc1*<sup>-/-</sup> mice resulted in increased survival, delayed Purkinje cell loss and improved locomotor activity (Xie et al., 2017). The moderate improvement in lifespan achieved with this approach (94 days  $\pm$  4) is significantly less than that from low dose ICV AAV9-hNPC1 treatment in this study (**Figure 42**). Similar to Chandler et al. (2016), neuropathology and locomotor function were only analysed at 9 weeks of age and not conducted on end-stage *Npc1*<sup>-/-</sup> mice. The end-stage phenotype or humane endpoint is not described, however the authors hypothesise that the limited improvement following intracranial AAV9 delivery may possibly be attributed to insufficient neuronal transduction within the brain of treated *Npc1*<sup>-/-</sup> mice. Alternatively, *Npc1* expression may have been affected by silencing of the transcriptional activity of the CMV promoter through methylation, which has previously been described following *in vivo* gene delivery with a viral vector (Brooks et al., 2004). Taken together, these studies demonstrate that lysosomal storage disorders, such as Niemann-Pick Type C that can't take advantage of cross-correction may not be as refractory to gene therapy as previously thought. Direct injection into the CNS may represent the optimal route of administration for the treatment of the neuropathology and associated disease manifestations, however a certain level of visceral expression in combination with efficient CNS transduction may be required for long-term survival. ICV administration also allows more efficient transduction of the CNS using lower doses, thereby increasing safety, which from a clinical, economic and vector manufacturing point of view, the scale-up to human parameters would be practically and financially more feasible. An interesting compromise between the two approaches could be a low dose dual ICV and intravenous administration as previously demonstrated in a mouse model of multiple sulfatase deficiency, where dual administration of an AAV9 vector enhanced systemic therapy compared to single administration routes alone (Spampanato et al., 2011).

## 7.7 Future Work

Several recommendations for future work have already been suggested throughout this chapter, however certain key experiments to further improve and clarify some of the results and observations presented in this thesis are addressed here.

In the short-term, conclusion of the high dose AAV9-hNPC1 study in *Npc1*<sup>-/-</sup> mice remains the top priority, as complete survival and weight data will allow a more effective comparison with low dose AAV9-hNPC1 treatment and other recently published gene therapy approaches for NP-C disease. Detailed neuropathology analysis of end-stage high dose treated *Npc1*<sup>-/-</sup> brains will confirm if further improvements in the number of permanently rescued neurons has been achieved and whether this translates to reduced neuroinflammation. Similarly, analysis of visceral tissue in comparison with tissue from end-stage untreated *Npc1*<sup>-/-</sup> mice will be crucial in clarifying the extent of continued and long-term visceral disease progression. The additional analysis of tissue samples from 9 week-old gene therapy treated *Npc1*<sup>-/-</sup> mice to allow age-matched comparison with untreated *Npc1*<sup>-/-</sup> mice would also be of great benefit. Age-matched comparison data in combination with the end-stage data presented in this project would reveal if the extent to which neurological and visceral NP-C disease progresses, following brain directed gene therapy.

While the approach utilised during this project was focused on the treatment of the neurological aspects of NP-C disease, our findings in combination with the results published in other NP-C gene therapy studies indicate that while neuronal transduction is crucial in the amelioration of major disease manifestations, this transduction may be needed in combination with *NPC1* expression in certain visceral tissues to achieve long-term survival. Additional effort should therefore be invested into the analysis of visceral diseases progression and whether this plays a crucial role in disease progression, which is amplified in these significantly older gene therapy treated *Npc1*<sup>-/-</sup> mice, ultimately leading to their deterioration. Although the visceral pathology is non-fatal in the majority of NP-C patients, the potential impact of continued and long-term visceral lipid accumulation may become amplified over time. As previously discussed, a valuable future study may therefore be the

evaluation of combination approaches, where the CNS focused ICV AAV9-hNPC1 administration is combined with a systemic directed therapy. This could either be achieved through combinational therapy with small molecule drugs such as miglustat and HP- $\beta$ -CD, where lower systemic doses could be administered, leading to the potential reduction in the impact of the adverse side effects associated with the two drugs. Alternatively, this could also be accomplished through a dual AAV approach, with simultaneous ICV and intravenous AAV9-hNPC1 administration. While, the synapsin I promoter has been demonstrated to express within the liver (Jackson et al., 2016), the activity of this promoter in other visceral tissues will need to be assessed. Otherwise a series of more ubiquitous promoters could be evaluated for enhanced systemic transgene expression.

The translation of these studies and results from neonatal to adult administration will be crucial, as pre-symptomatic neonatal administration will only be viable in rare cases. Ideally preclinical studies would be carried out with adult ICV AAV9-hNPC1 administration in two stages. First, administration into pre-symptomatic adult *Npc1*<sup>-/-</sup> mice between 4 and 5 weeks of age as a further proof of concept experiment, followed by a second study where symptomatic *Npc1*<sup>-/-</sup> mice are administered ICV with AAV9-hNPC1 between 6 and 7 weeks of age, which represents the most likely clinical use scenario.

Finally, while the improvements in neuropathology and neurological disease manifestations presented here are encouraging, there is certainly further scope for significant optimisation and improvement of the vector for enhanced CNS transduction efficiency. Due to the lack of any potential for cross-correction in this disease, transduction efficiency will be of paramount importance for ultimate therapeutic efficacy in both NP-C animal models and human patients. The creation of novel AAV capsid variants has resulted in the identification of variants with increased transduction efficiency compared to normal AAV serotypes. One such variant is AAV-PHP.B, which demonstrated a 40-fold greater efficiency in the CNS compared to an equivalent AAV9 vector following adult administration (Deverman et al., 2016). This particular variant also had the added advantage of increased efficiency in human neurons compared to AAV9 *in vitro*, however ultimate clinical translation with this capsid variant will be an additional challenge, as unlike rAAV9

vectors, AAV-PHP.B has not previously been administered into humans and so may require to be tested in non-human primates.

## 7.8 Conclusion

Taken together, the work presented in this thesis signals that AAV-mediated gene therapy has significant therapeutic potential for treating Niemann-Pick Type C disease and warrants further investigation. We have verified that the human *NPC1* cDNA can viably be incorporated into a functional rAAV construct to produce functional and fully packaged AAV9-hNPC1 vectors, which were validated *in vivo* to confirm overexpression of NPC1 in transduced neurons. A series of crucial proof of concept experiments and preclinical survival studies in a well-characterised murine model of NP-C demonstrated that a single ICV administration of an efficient and neuronal-selective AAV9-hNPC1 vector directly into the CSF of neonatal mice can increase the lifespan of *Npc1*<sup>-/-</sup> mice by 120%. Improvements in weight were accompanied with the long-term normalisation of locomotor and coordination activity, significant and long-term neuronal protection in monitored brain regions and a likely deceleration of lipid accumulation within AAV9-hNPC1 treated brains. The therapeutic efficacy of this gene therapy study on *Npc1*<sup>-/-</sup> mice was also placed in the context of other competing therapies in the NP-C arena, with AAV9-hNPC1 treatment demonstrating a significant improvement in average lifespan compared to the only currently licenced drug for NP-C patients, without the associated adverse side effects.

Although more work needs to be done to determine the importance of non-neuronal transduction for longer-term survival and whether these results will translate through to adult mice or larger animal models, it is hoped that this work represents an important step towards the development of an effective gene therapy treatment for NP-C disease. The translation of preclinical gene therapy studies to successful clinical trials for neurodegenerative conditions very similar to NP-C, and the current interest in commercialisation of gene therapy means that this is an opportune

moment and climate in which to continue the pursuit towards development of gene therapy for NP-C.

# 8 Supplementary Data

**Mouse NPC1 CCDS29064.1 cDNA** 1 ATGGGTGGCAACACCCGGCCCTGGCCCTGCTGCTGCTGCTGTGTGCCCTGCGCAGGTGTTTTGCAATCTCTGT 75  
**Human NPC1 CCDS 11878.1 cDNA** 1 ATGACCGCTGGGGCCTGGCCCTGGCCCTGCTGCTGCTGCTGTGTGCCAGCGCAGGTGTTTTGCAATCTCTGT 75  
 ATGRSYGCKRCRSRCYGGCCCTYGGCCCTSCTGCTGCTGCTGTGTGTCWGGCGAGGTGTTTTCRCACTCTGT

**Mouse NPC1 CCDS29064.1 cDNA** 76 GTTTGGTATGGAGAGTGTGGAATGGACTGGAGATAAGAGGTACAACCTGTAATATTTGCCCCACAAAACCC 150  
**Human NPC1 CCDS 11878.1 cDNA** 76 GTTTGGTATGGAGAGTGTGGAATGGATAATGGAGATAAGAGGTACAACCTGTAATATTTGCCCCACAAAACCA 150  
 GTTTGGTATGGAGAGTGTGGAATGCRWMTGGRGAYAAAGAGGTACAAYTYRAATATTTGCCCCACAAAACCM

**Mouse NPC1 CCDS29064.1 cDNA** 151 CTCCCAAAGGACGGCTATGACTTAGTGCAGGAACCTGTCCAGGACTCTTCTTTGCAATGTCAGTCTCTGCTGT 225  
**Human NPC1 CCDS 11878.1 cDNA** 151 TTCCCAAAGGATGGCTATGACTTAGTGCAGGAACCTGTCCAGGACTCTTCTTTGCAATGTCAGTCTCTGCTGT 225  
 YTSCCAAAGGAYGGMATGACTTAGTGCAGGAACCTGTCCAGGAYTCTTCTTTGCAATGTCAGTCTCTGCTGT

**Mouse NPC1 CCDS29064.1 cDNA** 226 GACATTCACAGCTTCAGACCTGAAAGTAACTGCAGCTGCCCTGCAGTTCCTGTCCAGGTGTCGCTCATGT 300  
**Human NPC1 CCDS 11878.1 cDNA** 226 GATGTTCCAGCTTCAGACCTGAAAGTAACTGCAGCTGCCCTGCAGTTCCTGTCCAGATGTCCTCATCTGT 300  
 GAYRTTCRCAGCTTCAGACCTRAARRRYAACCTGCAGCTGCCCTGCAGTTCCTGTCCAGRTGTCCTCTGT

**Mouse NPC1 CCDS29064.1 cDNA** 301 TTTTATAACCTAATGACCTGTTTTGTGAGCTAACATGTAGCCCTGACAGAGTCAGTTTGAATGTTACAGCA 375  
**Human NPC1 CCDS 11878.1 cDNA** 301 TTTTATAACCTACTGACCTGTTTTGTGAGCTAACATGTAGCCCTGACAGAGTCAGTTTGAATGTTACAGCT 375  
 TTTTATAACCTAMTGAMCCTGTTTTGTGAGCTRACATGTAGCCWCRCAGAGTCAGTTTYGAATGTTKACAGCW

**Mouse NPC1 CCDS29064.1 cDNA** 376 ACTGAGGATTATTTGATCCTAAGACACAGGAGATAAAACAAATGTAAAGGAAATGACTACTTTGTCGGACAG 450  
**Human NPC1 CCDS 11878.1 cDNA** 376 ACTGAGGATTATTTGATCCTTACAAACAGACGAAACAAATGTAAAGGAAATGACTACTTTGTCGGACAG 450  
 ACTGARGATTATKTTGATCCTRWKACAMASSAGAMKAAAACAAATGTRARARGRTASARTACTWYGTCCGACAG

**Mouse NPC1 CCDS29064.1 cDNA** 451 AGCTTCGCAATGCGATGTACAATGCCTGCCCTGATGTGGAGGGCCCTTCCAGTAAAGGAAAGGCTTGGACTC 525  
**Human NPC1 CCDS 11878.1 cDNA** 451 AGTTTTGCAATGCAATGTACAATGCCTGCCCGGATGTGGAGGGCCCTTCCAGTAAAGGAAAGGCTTGGACTC 525  
 AGYTTYGCSAATGCRATGTACAATGCCTGCCGKATGTGGAGGSCCYTCMAGTAAYGASAAGGCCYTRGGACTC

**Mouse NPC1 CCDS29064.1 cDNA** 526 TTGTGTGGGAGGGATGCCCTGCCCTCAATGCCACCAACTGGATTGATACATGTTCAATAAGACAAACGGACA 600  
**Human NPC1 CCDS 11878.1 cDNA** 526 CTGTGTGGGAGGGACCTGCACCCCTTAATGCCACCAACTGGATTGATACATGTTCAATAAGGACAAACGGACA 600  
 YTGTGTGGGARGGAYGCYSRYGCTGYAATGCCACCAACTGGATTGARTACATGTTCAATAARGACAAYGGACAR

**Mouse NPC1 CCDS29064.1 cDNA** 601 GGCCGATTTACCATCACTCCTGTGTTTTGAGATCTTTCAATCCTTGGGATGGAGCCCATGAAATGCCACCAA 675  
**Human NPC1 CCDS 11878.1 cDNA** 601 GGACCTTTACCATCACTCCTGTGTTTTGAGATCTTTCAATCCTTGGGATGGAGCCCATGAAATGCCACCAA 675  
 GRCRCWTTTACCATCACTCCTGTGTTTTGAGATCTTYCARTCCWTGGGATGGAGCCCATGARMATGCCACCAA

**Mouse NPC1 CCDS29064.1 cDNA** 676 GGCTGCAATGAGTCTGTGATGAGGTCAGGGCCATGTAGCTGCCAGSACTGCTCATCTGCTCGGCCCAAG 750  
**Human NPC1 CCDS 11878.1 cDNA** 676 GGCTGTGACAGTCTGTGATGAGGTCAGACCCATGTAGCTGCCAASACTGCTCATCTGCTCGGCCCAAG 750  
 GGCTGYRAYGAGTCTGTRGATGAGGTCACRGRCCATGTAGCTGCCARGACTGCTCYATYGTCTYGGCCCAAG

**Mouse NPC1 CCDS29064.1 cDNA** 751 CCCCAGCCCCACCCCTCCTATGCCCTGGAGGATCTGGGGCTGGATGCCATGTATGTCATCATGTGGTCCACC 825  
**Human NPC1 CCDS 11878.1 cDNA** 751 CCCCAGCCCCACCCCTCCTGCTCCCTGGAGGATCTGGGGCTGGATGCCATGTATGTCATCATGTGGATCACC 825  
 CCCCAGCCCCACCYCTCCTRYKCCCTGGAGGATCYKGGCTTGGAYGCCATGTATGTCATCATGTGGRTACC

**Mouse NPC1 CCDS29064.1 cDNA** 826 TACCTGGCATTTCTGTTTGTGTTTTTTGGAGCACTTTGGCAGTGTGGTGCACAGAAAGCGGTACTTTGTCTCT 900  
**Human NPC1 CCDS 11878.1 cDNA** 826 TACATGGCTTTTCTGTTTGTGTTTTTTGGAGCATTTTGGCAGTGTGGTGCACAGAAAGCGGTACTTTGTCTCT 900  
 TACRTGGCRTTTTYGYTTGTGTTTTTTGGAGCACTTTKGCAGTGTGGTGCYACAGAARRCGGTAYTTTGTSTCY

**Mouse NPC1 CCDS29064.1 cDNA** 901 GAGTACACTCCCATGACAGTAAATAGCTTTTCTGTTAAATAGCAGTGACAAAGGGGAGGCTCATGCTGTGAC 975  
**Human NPC1 CCDS 11878.1 cDNA** 901 GAGTACACTCCCATGATAGCAATATAGCTTTTCTGTTAATGCAAGTGACAAAGGGAGAGGCTCTGCTGTGAC 975  
 GAGTACACTCCCATYGAYAGYAAATMGCTTTTTCTGTTAAATRSAGTGACAAAGGRGARGCSTCMCTGCTGTGAC

**Mouse NPC1 CCDS29064.1 cDNA** 976 CCACITGCTGCAGCATTGATGACTGCTGAGGCGCATGTTACAAAGTGGGGGCTTCTCTGTGCCGAAATCC 1050  
**Human NPC1 CCDS 11878.1 cDNA** 976 CCTGTGAGCCAGCATTGAGGCTGCTGAGGCGCATGTTACAAAGTGGGGGCTTCTCTGTGCCGAAATCC 1050  
 CCWSTYRGYGACGATTTGAKGRCTGYTGGGCGSMTGTTACAMRSTGGGGGCTTCTCTGTGCCGAAAYCCY

**Mouse NPC1 CCDS29064.1 cDNA** 1051 AACTGCATCATTTTCTCTCATGGCCCTCACTACTGTTGCTCTCTGGCCTGGTATTTGTCCAGGTCAACACC 1125  
**Human NPC1 CCDS 11878.1 cDNA** 1051 GGCTGTGCATTTTCTCTCTGCTGGCTCTTCACTACTGCTGTTGCTCTCTGGCCTGGTATTTGTCCAGGTCAACACC 1125  
 RSCGTGYRTCATTTTCTCTCTRYTGGYCTTCATYACTGYGTGTYCKTCWGGCTGGRTTTGTCCRGGTCACMACC

**Mouse NPC1 CCDS29064.1 cDNA** 1126 AATCCGTGAGACTCTGGTCAAGCCCTCACTGAGGCGCGGTGGAAAAAGAGTACTTTGACAAAGCACTTTGG 1200  
**Human NPC1 CCDS 11878.1 cDNA** 1126 AATCCAGTTGACTCTGGTCAAGCCCTCACTGAGGCGCGGTGGAAAAAGAGTACTTTGACAAAGCACTTTGG 1200  
 AATCCWGTWASCTCTGGTCAAGCCCYMRCAGYAGGCGYCGYTGAAAAARGAGTACTTTGACMAGCACTTTGGG

**Mouse NPC1 CCDS29064.1 cDNA** 1201 CCTTTCTTTCGACGGAGCAGCTTATCATCCAGGCCCCAAACACAGTGTTCATATCTACGAAACCGTACCCTCC 1275  
**Human NPC1 CCDS 11878.1 cDNA** 1201 CCTTTCTTTCGACGGAGCAGCTTATCATCCAGGCCCTCTCACTGACAAAACATTTACCGGCAATACCCTTCC 1275  
 CCTTTCTTYCGSACGGAGCAGCTYATCATCCRGGCCCCYMWACYRRYRWWCAYATYACARSRCRTACCCYKCR

**Mouse NPC1 CCDS29064.1 cDNA** 1276 GGAGCCGATGTGCCCTTGGGCTCCATTGAACAAAGAGATCTGCACCAGGTTCTGGACTTACAGATTCGCCATT 1350  
**Human NPC1 CCDS 11878.1 cDNA** 1276 GGAGCTGATGTAACCTTTGGGCTCCGCTGACATACAGATCTGCACCAGGTTCTGACTTACAAATAGCCCATC 1350  
 GGAGCYGATGTRCCCTTYGGRCTCCRYTKRACAWASAGATWCTGCACCAGGTTCTGACTTACARATMGCCATY

Mouse NPC1 CCDS29064.1 cDNA 1351 GAAAGCATCACCGAATCTTACAAACAATGAAACCGTGACACTGCAGGACATCTGTGGGCCCCCTCTCCATAC 1425  
 Human NPC1 CCDS 11878.1 cDNA 1351 GAAAACATTAAGTCCCTTATGACAATGAGACTGTGACACTTCAAAGACATCTGTGGGCCCTCTTCCACCTAT 1425  
 GAAARCATYACYGCMCTCTAYRACAATGARACYGTGACACTKCARGACATCTGYKTGGCCCCYCTYTCWCRRATY

Mouse NPC1 CCDS29064.1 cDNA 1426 AACAAAGAACTGCACCATTATGAGTGTGTTAAATTAATCTCCAGAACAGCCATGCGGTGCTGGACAGCCAGTAGTGGC 1500  
 Human NPC1 CCDS 11878.1 cDNA 1426 AACACGAAGCTGCACCATTATGAGTGTGTTAAATTAATCTCCAGAACAGCCATGCGGTGCTGGACAGCCAGGAAAGGG 1500  
 AACAMGAAGTGCACCATTWTGAGTGTGTTAAATTAATCTCCAGAACAGCCATKCSGTGCTGGACMRCMARRWAGGS

Mouse NPC1 CCDS29064.1 cDNA 1501 GACGACTTCTATATCTACGCTGATTACCACACACACTTTCTGTACTGTGTACGGGCTCCCGCCTCTTGAATGAT 1575  
 Human NPC1 CCDS 11878.1 cDNA 1501 GACGACTTCTTCTGCTATGCGATTACCACACGCACTTTCTGTACTGTGTACGGGCTCCCGCCTCTTGAATGAT 1575  
 GACGACTTCTWTRTSTAYGCGATTACCACACRCACCTTTCTGTACTGTGTACGGGCTCCYGCCTCYTGAATGAT

Mouse NPC1 CCDS29064.1 cDNA 1576 ACAGATTGCTCCACCGTCCCTTCTGGGTACATTTGGAGGACCGTGTGCCCGTGGCTGTGTGGGTGGGTAT 1650  
 Human NPC1 CCDS 11878.1 cDNA 1576 ACAAGTTGCTCCATGACCCCTTCTGGGTACATTTGGTGGACAGTGTGCCCGTGGCTGTGTGGGTGGGTAT 1650  
 ACRAGTTGCTCCAYGRYCCCTGYCTGGGTACTTTGGWGGACCRGTGTGCCCGTGGCTGTGTGGGTGGGTAT

Mouse NPC1 CCDS29064.1 cDNA 1651 GATGATCAGAACTACAAACATGCCACCGGCTGTGTGATCACCTTCCCGTGAATAATTACTACAATGACACAGAG 1725  
 Human NPC1 CCDS 11878.1 cDNA 1651 GATGATCAAACTACAAATAACCGCACTGCCCTTGTGATCACCTTCCCGTGAATAATTACTACAATGATACAGAG 1725  
 GATGATCARAACTACAAYAYGCCACYGCSCTTGTGATYACCTTCCCYGTSAAATAATTACTAYAATGAYACAGAG

Mouse NPC1 CCDS29064.1 cDNA 1726 AGCTCCAGAGGGCCCTGGCCCTGGGAGAAAGAGTTTATTAGTTTGTGAAAACTACAAGAATCCCAATCTGACC 1800  
 Human NPC1 CCDS 11878.1 cDNA 1726 AAAGCTCCAGAGGGCCCAAGCCCTGGGAGAAAGAGTTTATTAGTTTGTGAAAACTACAAGAATCCCAATCTGACC 1800  
 ARGCTCCAGAGGGCCYRGGCCCTGGGARAAAGAGTTTATTARTTTTGTGAAAACTACAAGAATCCMAATCTGACC

Mouse NPC1 CCDS29064.1 cDNA 1801 ATTTCTTCACTGCTGAGCGAAGCATCGAAGATGAGCTCAATCGGAAAGTAAACAGTGAACGTTTCCACCGTCACT 1875  
 Human NPC1 CCDS 11878.1 cDNA 1801 ATTTCTTCACTGCTGAGCGAAGCATCGAAGATGAGCTCAATCGGAAAGTAAACAGTGAACGTTTCCACCGTCACT 1875  
 ATTTCTTCACTGCTGARGAAGYATYGAAGATGARCTMAATCGKAAAGTRACAGTGAATGTTCCACCGTYRTM

Mouse NPC1 CCDS29064.1 cDNA 1876 ATCAGCTACCTCTGATGTTTCTGTACATTTCCCTCGCCCTGGGTACATCCAGCTCCAGCAGGCTCTGGTG 1950  
 Human NPC1 CCDS 11878.1 cDNA 1876 ATTAGCTATGCCATCTGTTCTATATATTTCCCTAGCCTTGGGGCACATGAAAGCTCTCCAGGCTCTGGTG 1950  
 ATYAGCTAYGYCRTSATGTTTCTRTAYATTTCCCTMGCCYTGKKCACATSMARAGCTGYMGAGGCTCTGGTG

Mouse NPC1 CCDS29064.1 cDNA 1951 GATTCCTAAGATCTCGCTGGCATTGCGGGGATCTGATCGTGTAGCTCGGTGGCTGCTCTGGGCATCTTC 2025  
 Human NPC1 CCDS 11878.1 cDNA 1951 GATTCCTAAGCTCTCACTAGGCATCGCGGCATCTGATCGTGTAGCTCGGTGGCTGCTCTGGGTCTCTTC 2025  
 GATTCCTAAGRTCTCRCTRGGCATTGCGGGSATCYTGATCGTGTAGCTCGGTGGCTGCTCTGGGTCTCTTC

Mouse NPC1 CCDS29064.1 cDNA 2026 AGCTACATGGGATGGCCCTGACCCTCATCTGATTGAGSTCATCCCAATCTGGTGTGGTGTGGGTTGGAC 2100  
 Human NPC1 CCDS 11878.1 cDNA 2026 AGCTACATGGGATGGCCCTGACCCTCATCTGATTGAGSTCATCCCAATCTGGTGTGGTGTGGGTTGGAC 2100  
 AGCTACATKGGWTTGCCSYTGACCCTCATYGTSAATTGARGTCACTCCRTCTCTGGTGTGGTGTGGTGTGGTGGAC

Mouse NPC1 CCDS29064.1 cDNA 2101 AACATCTTCAATCTAGTGCAGACCTACCAGAGAGATGAGCGTCTTCAAGAGGAAAGCTGGATCAGCAGCTGGGC 2175  
 Human NPC1 CCDS 11878.1 cDNA 2101 AACATCTTCAATCTAGTGCAGACCTACCAGAGAGATGAGCGTCTTCAAGAGGAAAGCTGGATCAGCAGCTGGGC 2175  
 AACATCTTCAATCTRGTGCAGRCCCTACCAGAGAGATGARCGTCTTCARGRGAAACCTGGATCAGCAGCTGGGC

Mouse NPC1 CCDS29064.1 cDNA 2176 AGGATCCTTGGAGAAGTGGCCCGGACCATGTTCCCTTTCATCCTTTTCTGAGACTCAGCATTTTTCTTTGGGGG 2250  
 Human NPC1 CCDS 11878.1 cDNA 2176 AGGATCCTTGGAGAAGTGGCCCGGACCATGTTCCCTTTCATCCTTTTCTGAGACTCAGCATTTTTCTTTGGGGG 2250  
 AGGRTCTTGGAGAAGTGGCCSASATGTTCCCTKTCATCCTTTTCTGAGACYKAGCATTTTTTCTTGGGRCR

Mouse NPC1 CCDS29064.1 cDNA 2251 CTGTCTCGATGCCAGCTGTGCACACCTTCTCTCTTTTGGGGAAATGGCCCTCCATATTGACTTCTCTCTCAG 2325  
 Human NPC1 CCDS 11878.1 cDNA 2251 TTGTCTCGATGCCAGCTGTGCACACCTTCTCTCTTTTGGGGAAATGGCACTCTCATATTGACTTCTCTCTCAG 2325  
 YTGTCCKYGATGCCAGCYGTGCACACCTTCTCTCTTTTGGGGAAWTGGCMGTYCATTGACTTCTCTCTCAG

Mouse NPC1 CCDS29064.1 cDNA 2326 ATTACCTGCTTTGTGAGCTGTGTGGGGTTAGATATTAAGAGGCAAGAGAAAAACCATCTGGACATCTTGTGCT 2400  
 Human NPC1 CCDS 11878.1 cDNA 2326 ATTACCTGCTTTGTGAGCTGTGTGGGGTTAGACATTAAGAGGCAAGAGAAAAATGGCTAGACATCTTGTGCT 2400  
 ATTACCTGYTTYGTGAGYCTSTTGGGGTTAGAYATTAARMGKCAAGAGAAAAAYCRKTRGACATCYTKTGCTGT

Mouse NPC1 CCDS29064.1 cDNA 2401 GTCAGAGGCTGCTGAGCAGGACAAAGTAGCCACCGCCTCCGAAAGTACCTGTTTCGCTTCTTCAAAAACATCTTT 2475  
 Human NPC1 CCDS 11878.1 cDNA 2401 GTCAGAGGCTGCTGAGGATGGAACAAGCGTCCAGCCCTCAGAGCTGTTGTTTCGCTTCTTCAAAAACATCTTT 2475  
 GTCAGAGGCTGAMGAYGGAMMARGYRKCASGCCTCMGARAGCTRYTGTTCGCTTCTTCAAAAACCTMCTWT

Mouse NPC1 CCDS29064.1 cDNA 2476 GCGCCCTTCTGCTGAAGGACTGGCTGAGGCCAATTGTGGTAGCGGTGTTGTGGGCTTCTGTGCATTGAGTGT 2550  
 Human NPC1 CCDS 11878.1 cDNA 2476 TCTCCACTTCTGCTGAAGGACTGGATGAGACCAATTGTGATAGCAAAATTTGTGGGCTTCTGTGCATTGAGTGT 2550  
 KYCCMCTTCTGCTRAAGGACTGGMTGAGRCAAAATGTGRTAGCRTRTTTGTGGYGTCTGTGCATTGAGYRTY

Mouse NPC1 CCDS29064.1 cDNA 2551 GCGGTGGTGAACAAAGTAGACATCGGGTTGGATCAGTCTCTCTCAATGCCAAACGATGCGTATGCTGATGACTAT 2625  
 Human NPC1 CCDS 11878.1 cDNA 2551 GCGGTGGTGAACAAAGTAGATATGATTTGGATCAGTCTCTCTCAATGCCAAACGATGCGTATGCTGATGACTAT 2625  
 GCRGTSSTGAACAAAGTAGAYATYGRRTGGATCAGTCTCTYTCRATGCCARAYGAYTCSAYTRGRKAYTAT

Mouse NPC1 CCDS29064.1 cDNA 2626 TTCAAATCACTGCTCAGTACCTGCACTGGGGCCACCCSTGTACTTTGTCCTGGAGGAAGGCTTAATACTACAGT 2700  
 Human NPC1 CCDS 11878.1 cDNA 2626 TTCAAATCACTGCTCAGTACCTGCACTGGGGCCACCCSTGTACTTTGTCCTGGAGGAAGGCTTAATACTACAGT 2700  
 TTCAAATCMTRSTCAGTACCTGCAYKCGGGYCCRCYGTGACTTTGTCCTGGAGGAAGGSYAYRACTACAST

Mouse NPC1 CCDS29064.1 cDNA 2701 TCACGCAAGGGCAGAACATGGTGTGCGGGCGGCATGGGCTGTGACAATGATCCCTGGTGCAGCAGATATTTAAC 2775  
 Human NPC1 CCDS 11878.1 cDNA 2701 TCTTCCAAAGGGCAGAACATGGTGTGCGGGCGGCATGGGCTGTGACAATGATCCCTGGTGCAGCAGATATTTAAC 2775  
 TCWYSCAARGGGCAGAACATGGTGTGCGGGCGGCATGGGCTGYRACAATGAYTCCCTGGTGCAGCAGATATTTAAC

Mouse NPC1 CCDS29064.1 cDNA 2776 GCAAGCTGAGCTGGACACTACACCCGATAGGCTTCGCCCCCTCGTCTGGATCGATGACTACTTTGACTGGGT 2850  
 Human NPC1 CCDS 11878.1 cDNA 2776 GCGGCGAGCTGGACACTATACCCGATAGGCTTCGCCCCCTCGTCTGGATCGATGACTACTTTGACTGGGT 2850  
 GCRGCKSAGCTGGACAMCTAYACCCGARTAGGCTTCGCCCCCTCGTCTGGATCGAYGAYTAYTTYGACTGGGT

**Mouse NPC1 CCDS29064.1 cDNA** 2926 TGTGTCCGCTGCAGACCTCTGACTCCAGAGGGTAAACAGAGGCCCTCAGGGGAAAGAAATTCATGAAATTCCTGCC 3000  
**Human NPC1 CCDS 11878.1 cDNA** 2926 TGCCTTCGCTGCAGGCTCTGACTCCGGAGGCAACAGAGGCCCTCAGGGGGAGAGCTTCATGAAATTCCTGCC 3000  
 TGYGYCGCTGCAGRCCTCTGACTCCRGARGGYAAACAGAGGCCCTCAGGGRRRAGAMTTCATGARATTCCTGCC

**Mouse NPC1 CCDS29064.1 cDNA** 3001 ATGTTCCCTTTCGATAAACCCTAACCCCAAGTGGCCAAAGGGGGACATGCTGCTTACCGSTTACGCTGTTAACAT 3075  
**Human NPC1 CCDS 11878.1 cDNA** 3001 ATGTTCCCTTTCGATAAACCCTAACCCCAAGTGGCCAAAGGGGGACATGCTGCTTACCGSTTACGCTGTTAACAT 3075  
 ATGTTCCCTTTCGATAAACCCTAACCCCAAGTGGCCAAAGGGGGACATGCTGCTTACCGSTTACGCTGTTAACAT

**Mouse NPC1 CCDS29064.1 cDNA** 3076 GTG--GGAGATGACACTTACATTTGGGGCCACTTACTTTCATGACCTACCACACCATTACTTAAGACCTCCGCTGAC 3147  
**Human NPC1 CCDS 11878.1 cDNA** 3076 CTCCTTGGCCATGGCACAGGGTGGGAGCCAGTACTTTCATGACCTACCACACCATTACTTAAGACCTCCGCTGAC 3150  
 STSCTTGGMSATGRCACYWRSRYTGGRGCCACKTACTTTCATGACCTACCACACCRTCTKMGACCTCYGCTGAC

**Mouse NPC1 CCDS29064.1 cDNA** 3148 TATACTGATGCCATGAAGAAAGCTCGGCTAATAGCCAGTAAATCACCAGAAACCATGCCCTTCTAAGGGGAGTGA 3222  
**Human NPC1 CCDS 11878.1 cDNA** 3151 TTTATTTGACCTCTGAAGAAAGCCGACTTATAGCCAGTAAATCACCAGAAACCATGCCCATTAACGGGAGTGC 3225  
 TWTAYTGAYGCMYTAGAAGAAAGCYCGRCTWATAGCCAGTAAAYRTCACSGAAACCATGSGYWYTAASGGGAGTGM

**Mouse NPC1 CCDS29064.1 cDNA** 3223 TACCGCGTATTCCCTTACAGTGTGTTCTACTGCTTCTATGAACAGTACCTGACCATTATTGATGACACCATCTTT 3297  
**Human NPC1 CCDS 11878.1 cDNA** 3226 TACCGAGTATTCCCTTACAGTGTGTTTATGCTTCTACTGAACAGTACCTGACCATTATTGATGACACCATCTTT 3300  
 TACCGMGATTTTCCTTACAGTGTGTTTAYGTCTTCTATGAACAGTACCTGACCATYATTGAYGACACYATCTTY

**Mouse NPC1 CCDS29064.1 cDNA** 3298 AACCTCACTGTGTCTCTGGGCTCCATATTCTGGTGACCTTGGTGGTCTGGGCTGTGAGCTTGGTCTGGCGT 3372  
**Human NPC1 CCDS 11878.1 cDNA** 3301 AACCTCACTGTGTCTCTGGGCTCCATATTCTGGTGACCTTGGTGGTCTGGGCTGTGAGCTTGGTCTGGAGTC 3375  
 AACCTCRGTGTCTCTGGGCKSATATTTCTGGTGACCTTGGTGGTCTGGGCTGTGAGCTTGGTCTGCRGTC

**Mouse NPC1 CCDS29064.1 cDNA** 3373 ATCATGTGTATCACCATAGCCATGATCCCTGGTCAACATGTTCCGGTTCATGTGGCTGTGGGCATCAGTCTGAAT 3447  
**Human NPC1 CCDS 11878.1 cDNA** 3376 ATCATGTGTATCACCATAGCCATGATCCCTGGTCAACATGTTCCGGTTCATGTGGCTGTGGGCATCAGTCTGAAC 3450  
 ATCATGTGTATCACCATAGCCATGATCCCTGGTCAACATGTTCCGGTTCATGTGGCTGTGGGCATCAGTCTGAAC

**Mouse NPC1 CCDS29064.1 cDNA** 3448 GCGGTCCTCCTTGGTCAACTTGGTGATGAGCTCGGCCATTTCTGTGGAGTTCTGCAGCCATATAACAGAGGCAATC 3522  
**Human NPC1 CCDS 11878.1 cDNA** 3451 GCTGTAATCCTTGGTCAACTTGGTGATGAGCTCGGCCATTTCTGTGGAGTTCTGCAGCCATATAACAGAGGCAATC 3525  
 GCKGTMTCCTTGGTCAACTTGGTGATGAGCTCGGCCATTTCTGTGGAGTTCTGCAGCCAYATAACAGAGGCAATC

**Mouse NPC1 CCDS29064.1 cDNA** 3523 ACCATGAGTACCAAAAGGAGCCGAGTGGAGCCGGCGGGAAGAGGCACTGCCACATGGGTAGTCTGTAATTCAGT 3597  
**Human NPC1 CCDS 11878.1 cDNA** 3526 ACGGTGAGCATCAAAAGGAGCCGAGTGGAGCCGGCGGGAAGAGGCACTGCCACATGGGTAGTCTGTAATTCAGT 3600  
 ACSRTGAGYAYSAAAAGGAGCCGAGTGGAGCCGGCGGGAAGAGGCACTGCCACATGGGYAGYTCYGRFTTCAGT

**Mouse NPC1 CCDS29064.1 cDNA** 3598 GGAATCACACTTACGAAATTTGGAGGATCTGGTGTTAGCCCTTTGCCAAATCTCAAATTTTTCAGATATTTTAC 3672  
**Human NPC1 CCDS 11878.1 cDNA** 3601 GGAATCACACTTACGAAATTTGGAGGATTTGGTGTTAGCCCTTTGCCAAATCTCAAATTTTTCAGATATTTTAC 3675  
 GGAATCACACTTACGAAATTTGGAGGATYGTGGTGTTRGCYTTTGCCAAATCTCAAATTTTYSAGATATTTTAC

**Mouse NPC1 CCDS29064.1 cDNA** 3673 TTCAGGATGTAATTTGCCATGGTCTTACTCGGAGCCACTCATGACTAATATTTCTCCGCTTACTCAGTTAC 3747  
**Human NPC1 CCDS 11878.1 cDNA** 3676 TTCAGGATGTAATTTGCCATGGTCTTACTCGGAGCCACTCATGACTAATATTTCTCCGCTTACTCAGTTAC 3750  
 TTCAGGATGTAATTTGCCATGGTCTTACTCGGAGCCACTCAYGGAYTAATATTTCTCYCCYGTCTTACTCAGTTAC

**Mouse NPC1 CCDS29064.1 cDNA** 3748 ATAGGGCCGTCGGTGAATAAAGCTAAAAGACACACCCTTACGAGCCCTACAGAGGCACAGAGAGAGACGGCTC 3822  
**Human NPC1 CCDS 11878.1 cDNA** 3751 ATAGGGCCATCAATTAATAAAGCAAAAGTTGTGCCACTGAAAGAGCCATACAGAGGCACAGAGCCGCAACGGCTC 3825  
 ATAGGGCCRTCRGTRAATAAAGCYAAAAGWYRYRCCACTKAMGAGCGMTACARAGGRACAGAGMGMAACGGCTY

**Mouse NPC1 CCDS29064.1 cDNA** 3823 CTC AATTTTAG 3834  
**Human NPC1 CCDS 11878.1 cDNA** 3826 CTAAATTTTAG 3837  
 CTMAATTTYTAG

### Supplementary Figure S1: Human *NPC1* and murine *Npc1* cDNA homology

Alignment of human NPC1 (CCDS11878.1) and murine *Npc1* (CCDS29064.1) cDNA coding sequences sourced from the CCDS Database (<https://www.ncbi.nlm.nih.gov/CCDS/CcdsBrowse.cgi>), resulting in a 83.4% sequence homology.

```

Human NPC1 NP_000262.2 Protein 1 MARGLALGILLLLCPAQVFSQSCVWYEGCGIAYGDKRYNCEYSGPPKPLPKDGYDLVQELCPG 65
Mouse NPC1 NP_032746.2Protein 1 MGAHHPALGILLLLCPAQVFSQSCVWYEGCGIATGDKRYNCRMSGPPKPLPKDGYDLVQELCPG 65
M A ALGILLLLCPAQVFSQSCVWYEGCGIA GDKRYNC YSGPPKPLPKDGYDLVQELCPG

Human NPC1 NP_000262.2 Protein 66 EFFCNVSLCCDVRQLQTLKDNLQLPLQLSRCPSCFYNNLNFCELTCSPRQSQFLNVTATEDYV 130
Mouse NPC1 NP_032746.2Protein 66 EFFDNVSLCCDIQQLQTLKSNLQLPLQLSRCPSCFYNNLNFCELTCSPHQSQFLNVTATEDYF 130
FF NVSLCCD QLQTLK NLQLPLQLSRCPSCFYNL LFCELTCSQ SQSFLNVTATEDY

Human NPC1 NP_000262.2 Protein 131 DPVTNQT KTNVKELQYVVGQSFANAMYACRDVEAPSSNDKALGLLCGKDADACNATNWIEYMFN 195
Mouse NPC1 NP_032746.2Protein 131 DEKIQENKTNVKELEYFVGQSFANAMYACRDVEAPSSNEKALGLLCGRDAFACNATNWIEYMFN 195
DP T KTNVKEL Y VQGSFANAMYACRDVEAPSSN KALGLLCC DA ACNATNWIEYMFN

Human NPC1 NP_000262.2 Protein 196 KDNQAPFTIIPVFSDFEFGMEPMNATKGCDESVDEVTA PCSCQDCSIVCGPKPQPPPPAPW 260
Mouse NPC1 NP_032746.2Protein 196 KDNQAPFTIIPVFSDLILGMEPMNATKGCDESVDEVTA PCSCQDCSIVCGPKPQPPPPAPW 260
KDNQAPFTI PVFSD GMEPM NATKGC ESVDEVTA PCSCQDCSIVCGPKPQPPPP PW

Human NPC1 NP_000262.2 Protein 261 TILGLDAMYVIMWITYMAFLLVFFGAFFAVWCYRKYFVSEYTPIDSNIAFSVNSDKGEASCCD 325
Mouse NPC1 NP_032746.2Protein 261 RILGLDAMYVIMWVYVAFLVFFGALLAVWCRRRYFVSEYTPIDSNIAFSVNSDKGEASCCD 325
I GLDAMYVIMW TY AFL VFFGA AVWC R RYFVSEYTPIDSNIAFSVN SDKGEASCCD

Human NPC1 NP_000262.2 Protein 326 PVSAAFFCCLRRRLFTRWCSFCVRNPGCVIFFSLVITACSSGLVVFVVTNTPVDLWSAPSSQARL 390
Mouse NPC1 NP_032746.2Protein 326 PLGAAFDDCLRRMFTKWGAFQVRNFTCIIFSLAFITVCSGLVVFVQVTTNPVELWSAPHSQARL 390
P AAF CLRR FT WG FCVRNP C IFFSL FIT CSSGLVVFV VTNTPV LWSAP SQARL

Human NPC1 NP_000262.2 Protein 391 EKEYFDHFHGFPPFRTEQLIIAPLTLKHIIYEPYSGADVPFGPPLDILHQVLDLQIAIENITA 455
Mouse NPC1 NP_032746.2Protein 391 EKEYFDHFHGFPPFRTEQLIIQAENISVHIYEPYPAGADVFPFPPIKELHQVLDLQIAIESITA 455
EKEYFD HFGPPFRTEQLII AP T HIY PYP GADVFPFPPL ILHQVLDLQIAIE ITA

Human NPC1 NP_000262.2 Protein 456 SYDNETVTLQDICLAPLSPYNNCTILSVLNYFQNSHVLDDHKKGDDFFVYADYHHTFLYCVRAP 520
Mouse NPC1 NP_032746.2Protein 456 SYDNETVTLQDICVAPLSPYNNCTILSVLNYFQNSHAVLDSVGGDDFFVYADYHHTFLYCVRAP 520
SY NETVTLQDIC APLSPYN NCTI SVLNYFQNSH VLD GDDF YADYHHTFLYCVRAP

Human NPC1 NP_000262.2 Protein 521 ASLNDTSLHHPCLGTFGGVPVFWLVGGYDDQNYNNATALVITFPVNNYNDTEKLQRAQAWEK 585
Mouse NPC1 NP_032746.2Protein 521 ASLNDTSLHHPCLGTFGGVPVFWLVGGYDDQNYNNATALVITFPVNNYNDTERLQRAQAWEK 585
ASLNDTSLH PCLGTFGGVPVFWLVGGYDDQNYNNATALVITFPVNNYNDTE LQRA AWEK

Human NPC1 NP_000262.2 Protein 586 EFINFVKYKPNLTISFTAERSIEDELNRESDSVFTVVISYAIMFLYISLALGHMKSCRLLV 650
Mouse NPC1 NP_032746.2Protein 586 EFINFVKYKPNLTISFTAERSIEDELNRESDSVFTVVISYVVMFLYISLALGHQSCSRLLV 650
EFI FVKYKPNLTISFTAERSIEDELNRES SDVFTV ISY MFLYISLALGH SC RLLV

Human NPC1 NP_000262.2 Protein 651 DSKVSLGIAGLIVLSSVACSLGVFSYIGLPLTLIVIEVIPFLVLAVGVDNIFILVQAYQRDERL 715
Mouse NPC1 NP_032746.2Protein 651 DSKISLGIAGLIVLSSVACSLGIFSYMPLTLIVIEVIPFLVLAVGVDNIFILVQAYQRDERL 715
DSK SLGIAGLIVLSSVACSLG FSY G PLTLIVIEVIPFLVLAVGVDNIFILVQ YQRDERL

Human NPC1 NP_000262.2 Protein 716 QEBTLDQQLGRVLGEVAPMFLSSFSSETVAFFGALSMPAVHTFSLFAGLAVIDFLLQITCFV 780
Mouse NPC1 NP_032746.2Protein 716 QEBTLDQQLGRILGEVAPMFLSSFSSETVAFFGALSMPAVHTFSLFAGLAVIDFLLQITCFV 780
Q ETLDQQLGR LGEVAP MFLSSFSSET AFF GALS MPAVHTFSLFAG AV IDFLLQITCFV

Human NPC1 NP_000262.2 Protein 781 SLLGLDIKRQEKNRDLDFCCVRGAEDGTSVQASESLFRFFKNYSPELLLKDWRPIVIAFVGV 845
Mouse NPC1 NP_032746.2Protein 781 SLLGLDIKRQEKNRDLDFCCVRGADDGQGSASESYLFRFFKNYFAPLLLKDWRPIVIAFVGV 845
SLLGLDIKRQEKN LDI CVRGA DG ASES LFRFFKN PLLLKDWR PIVIA FVGV

Human NPC1 NP_000262.2 Protein 846 LSFSAVAVNKVDIGLDQSLMPPDSYMDYFYSQYLHAGPPVYFVLEEGYDYSKQNMVCG 910
Mouse NPC1 NP_032746.2Protein 846 LSFSAVAVNKVDIGLDQSLMPPDSYVIDYFYSQYLHAGPPVYFVLEEGYDYSKQNMVCG 910
LSFS AV NKVDIGLDQSLMPP DSY DYFYS QYLH GPPVYFVLEEG Y S KQNMVCG

Human NPC1 NP_000262.2 Protein 911 GMGCDNDSLVQOIFNAALDNYTRIGFAPSSWIDDYFDWVQSSCCRNITDQFCNASVVDPA 975
Mouse NPC1 NP_032746.2Protein 911 GMGCDNDSLVQOIFNAALDYTRIGFAPSSWIDDYFDWVQSSCCRNITDQFCNASVVDPA 975
GMGC NDSLVQOIFNAAL D YTR GFAPSSWIDDYFDWV QSSCCRNIT DQFCNASV VDP

Human NPC1 NP_000262.2 Protein 976 CVRCRPLTPEGKQRPQGGDFMRFLPMFLSDNPNPKCGKGGHAAYSAVNIILGCHGTRV GATYFMT 1040
Mouse NPC1 NP_032746.2Protein 976 CVRCRPLTPEGKQRPQGGDFEMKFLPMFLSDNPNPKCGKGGHAAYGSAVNIIVGDDTYIGATYFMT 1039
CVRCRPLTPEGKQRPQ G FM FLMFLSDNPNPKCGKGGHAAY SAVNI G T GATYFMT

Human NPC1 NP_000262.2 Protein 1041 YHTVLTQTSADFIDALKKARLIASNVTETMGINGSAYRVFPYSVFYVFYEQYLTIIDDTIFNLV 1105
Mouse NPC1 NP_032746.2Protein 1040 YHTILKTSADYDAKARLIASNITETMRSGSDYRVFPYSVFYVFYEQYLTIIDDTIFNLV 1104
YHT L TSAD DA KKARLIASN TETM GS YRVFPYSVFYVFYEQYLTIIDDTIFNL VS

Human NPC1 NP_000262.2 Protein 1106 LGAIFLVTMVLGCELWSAVIMCATIAMVLNMFVGMWLVGISLNAVSLVNLVMSCGISVEFCSH 1170
Mouse NPC1 NP_032746.2Protein 1105 LGSIFLVTLVVLGCELWSAVIMCITIAMVLNMFVGMWLVGISLNAVSLVNLVMSCGISVEFCSH 1169
LG IFLVT V LGCELWSAVIMC TIAM LVNMFVGMWLVGISLNAVSLVNLVMSCGISVEFCSH

Human NPC1 NP_000262.2 Protein 1171 ITRAFVSMKGSRVERAEALAHMGSSVFGITTLTKFGGIVVLAFAKSIQIFIFFRMYLAMVLL 1235
Mouse NPC1 NP_032746.2Protein 1170 ITRAFVSMKGSRVERAEALAHMGSSVFGITTLTKFGGIVVLAFAKSIQIFIFFRMYLAMVLL 1234
ITRAFT S KGSRV RAEALAHMGSSVFGITTLTKFGGIVVLAFAKSIQIF IFFRMYLAMVLL

Human NPC1 NP_000262.2 Protein 1236 GATHGLIFLPVLLSYIGPSVNKAKSCATEERYKGTERRERLLNF 1278
Mouse NPC1 NP_032746.2Protein 1235 GATHGLIFLPVLLSYIGPSVNKAKRHTEERYKGTERRERLLNF 1277
GATHGLIFLPVLLSYIGPSVNKAK T ERY KGTERRERLLNF

```

### Supplementary Figure S2: Human and murine NPC1 protein homology

Alignment of human NPC1 (NP\_000262.2) and murine NPC1 (NP\_032746.2) amino acid sequences.

5'

ATGACCGCTCGCGGCCTGGCCCTTGGCCCTCCTCCTGCTGCTACTGTGTCCA  
GCGCAGGTGTTTTACAGTCTGTGTTTGGTATGGAGAGTGTGGAATTGCA  
TATGGGGACAAGAGGTACAATTGCGAATATTCTGGCCCACCAAACCATT  
GCCAAAGGATGGATATGACTTAGTGCAGGAACTCTGTCCAGGATTCTTCTT  
TGGCAATGTCAGTCTCTGTTGTGATGTTTCGGCAGCTTCAGACACTAAAAGA  
CAACCTGCAGCTGCCTCTACAGTTTCTGTCCAGATGTCCATCCTGTTTTAT  
AACCTACTGAACCTGTTTTGTGAGCTGACATGTAGCCCTCGACAGAGTCAG  
TTTTTGAATGTTACAGTACTGAAGATTATGTTGATCCTGTTACAAACCAG  
ACGAAAACAAATGTGAAAGAGTTACAATACTACGTTCGGACAGAGTTTTGC  
CAATGCAATGTACAATGCCTGCCGGGATGTGGAGGCCCCCTCAAGTAATG  
ACAAGGCCCTGGGACTCCTGTGTGGGAAGGACGCTGACGCCTGTAATGCC  
ACCAACTGGATTGAATACATGTTCAATAAGGACAATGGACAGGCACCTTT  
TACCATCACTCCTGTGTTTTAGATTTTCCAGTCCATGGGATGGAGCCCAT  
GAACAATGCCACCAAAGGCTGTGACGAGTCTGTGGATGAGGTCACAGCAC  
CATGTAGCTGCCAAGACTGCTCTATTGTCTGTGGCCCAAGCCCCAGCCCC  
CACCTCCTCCTGCTCCCTGGACGATCCTTGGCTTGGACGCCATGTATGTCA  
TCATGTGGATCACCTACATGGCGTTTTTGTCTGTGTTTTTTGGAGCATTTTT  
TGCAGTGTGGTGTACAGAAAACGGTATTTTGTCTCCGAGTAACTCCCAT  
CGATAGCAATATAGCTTTTTCTGTTAATGCAAGTGACAAAGGAGAGGCGT  
CCTGCTGTGACCCTGTCAGCGCAGCATTGAGGGCTGCTTGAAGCGGCTGT  
TCACACGCTGGGGGTCTTTCTGCGTCCGAAACCCTGGCTGTGTCATTTTCTT  
CTCGCTGGTCTTCATTACTGCGTGTTTCGTGAGCCCTGGTGTGTTGTCCGGGTC  
ACAACCAATCCAGTTGACCTCTGGTCAGCCCCAGCAGCCAGGCTCGCCT  
GGAAAAGAGTACTTTGACCAGCACTTTGGGCCTTTCTTCCGGACGGAGC  
AGCTCATCATCCGGGCCCTCTCACTGACAAACACATTTACCAGCCATAACC  
CTTCGGGAGCTGATGTACCCTTTGGACCTCCGCTTACATACAGATACTGC  
ACCAGGTTCTTGACTTACAAATAGCCATCGAAAACATTACTGCCTCTTATG  
ACAATGAGACTGTGACACTTCAAGACATCTGCTTGGCCCCCTTTTACCCTG  
ATAACACGAACTGCACCATTTTGAAGTGTGTTAAATTAATTTCCAGAACAGCC  
ATCCCGTGTGACCACAAGAAAGGGGACGACTTCTTTGTGTATGCCGATT  
ACCACACGCACTTTCTGTACTGCGTACGGGCTCCTGCCTCTCTGAATGATA  
CAAGTTTGCTCCATGACCCTTGTCTGGGTACGTTTGGTGGACCAGTGTTCC  
CGTGGCTTGTGTTGGGAGGCTATGATGATCAAAACTACAATAACGCCACT  
GCCCTTGTGATTACCTTCCCTGTCAATAATTACTATAATGATACAGAGAAG  
CTCCAGAGGGCCCAGGCCTGGGAAAAAGAGTTTATTAATTTTGTGAAAAA  
CTACAAGAATCCCAATCTGACCATTTCCCTTCACTGCTGAACGAAGTATTGA  
AGATGAACTAAATCGTGAAAGTGACAGTGTGCTTACCCTTGTAAATTA  
GCTATGCCATCATGTTTCTATATATTTCCCTAGCCTTGGGGCACATGAAAA  
GCTGTGCGCAGGCTTCTGGTGGATTGAAAGTCTCACTAGGCATCGCGGGC  
ATCTTGATCGTGCTGAGCTCGGTGGCTTGGCTCCTTGGGTGTCTTACGCTAC  
ATTGGGTTGCCCTTACCCTCATTGTGATTGAAGTCATCCCGTTCCCTGGTG  
CTGGCTGTTGGAGTGGACAACATCTTCATTCTGGTGCAGGCCTACCAGAGA  
GATGAACGTCTTCAAGGGGAAACCCTGGATCAGCAGCTGGGCAGGGTCTT  
AGGAGAAGTGGCTCCCAGTATGTTCTGTGATCCTTTTCTGAGACTGTAGC  
ATTTTTCTTAGGAGCATTGTCCGTGATGCCAGCCGTGCACACCTTCTCTCTC  
TTTGGCGGATTGGCAGTCTTCATTGACTTTCTTCTGCAGATTACCTGTTTCG  
TGAGTCTCTTGGGGTTAGACATTAACGTCAAGAGAAAAATCGGCTAGAC  
ATCTTTTGTGTGTCAGAGGTGCTGAAGATGGAACAAGCGTCCAGGCCTC  
AGAGAGCTGTTTGTTCGCTTCTTCAAAAACCTCCTATTCTCCACTTCTGCTA  
AAGGACTGGATGAGACCAATTGTGATAGCAATATTTGTGGGTGTTCTGTCA  
TTCAGCATCGCAGTCTGAACAAAGTAGATATTGGATTGGATCAGTCTCTT  
TCGATGCCAGATGACTCCTACATGGTGGATTATTTCAAATCCATCAGTCAG  
TACCTGCATGCGGGTCCGCCTGTGTACTTTGTCTGGAGGAAGGGCACGAC  
TAACTTCTTCAAAGGGGCAGAACATGGTGTGCGGCGGCATGGGCTGCAA

CAATGATTCCCTGGTGCAGCAGATATTTAACGCGGCGCAGCTGGACA  
ACTATACCCGAATAGGCTTCGCCCCCTCGTCCTGGATCGACGATTATTT  
CGACTGGGTGAAGCCACAGTCGTCTTGCTGTGAGTGGACAATATCACT  
GACCAGTTCTGCAATGCTTCAGTGGTTGACCCTGCCTGCGTTCGCTGC  
AGGCCTCTGACTCCGGAAGGCAAACAGAGGCCTCAGGGGGGAGACTT  
CATGAGATTCCCTGCCATGTTCCTTTCGGATAACCCTAACCCCAAGT  
GTGGCAAAGGGGGACATGCTGCCTATAGTTCTGCAGTTAACATCCT  
CCTTGGCCATGGCACCAGGGTCGGAGCCACGTACTTCATGACCTACC  
ACACCGTGCTGCAGACCTCTGCTGACTTTATTGACGCTCTGAAGAA  
AGCCCGACTTATAGCCAGTAATGTCACCGAAACCATGGGCATTAAC  
GGCAGTGCCTACCGAGTATTTCCTTACAGTGTGTTTATGTCTTCT  
ACGAACAGTACCTGACCATCATTGACGACACTATCTTCAACCTCGG  
TGTGCCCTGGGCGCGATATTTCTGGTGACCATGGTCCTCCTGGG  
CTGTGAGCTCTGGTCTGCAGTCATCATGTGTGCCACCATCGCCAT  
GGTCTTGGTCAACATGTTTGGAGTTATGTGGCTCTGGGGCATCAGT  
CTGAACGCTGTATCCTTGGTCAACCTGGTGATGAGCTGTGGCATCT  
CCGTGGAGTTCTGCA GCCACATAACCAGAGCGTTCACGGTGAGCAT  
GAAAGGCAGCCGCGTGGAGCGCGCGGAAGAGGCACTTGCCACAT  
GGGCAGCTCCGTGTTCA GTGGAATCACACTTACAAAATTTGGAG  
GGATTGTGGTGTGGCTTTTGCCAAATCTCA AATTTTCCAGATAT  
TCTACTTCAGGATGTATTTGGCCATGGTCTTACTGGGAGCCACT  
CACGGATTAATATTTCTCCCTGTCTTACTCAGTTACATAGGGCC  
ATCAGTAAATAAAGCCAAAAGTTGTGCCACTGAAGAGCGATACAA  
AGGAACAGAGCGCGAACGGCTTCTAAATTTCTAG 3'

**Supplementary Figure S3: Human NPC1 cDNA**

Complete human NPC1 cDNA sequence used in this study.

# References

- ABEDIA.COM. 2017. *GENE THERAPY CLINICAL TRIALS WORLDWIDE* [Online]. Journal of Gene Medicine: Wiley. Available: <http://www.abedia.com/wiley/vectors.php> [Accessed 6 Jan 2017].
- ACHORD, D. T., BROT, F. E., BELL, C. E. & SLY, W. S. 1978. Human beta-glucuronidase: in vivo clearance and in vitro uptake by a glycoprotein recognition system on reticuloendothelial cells. *Cell*, 15, 269-78.
- ADRIOUCH, S., FRANCK, E., DROUOT, L., BONNEAU, C., JOLINON, N., SALVETTI, A. & BOYER, O. 2011. Improved Immunological Tolerance Following Combination Therapy with CTLA-4/Ig and AAV-Mediated PD-L1/2 Muscle Gene Transfer. *Front Microbiol*, 2, 199.
- AIUTI, A., BIASCO, L., SCARAMUZZA, S., FERRUA, F., CICALESE, M. P., BARICORDI, C., DIONISIO, F., CALABRIA, A., GIANNELLI, S., CASTIELLO, M. C., BOSTICARDO, M., EVANGELIO, C., ASSANELLI, A., CASIRAGHI, M., DI NUNZIO, S., CALLEGARO, L., BENATI, C., RIZZARDI, P., PELLIN, D., DI SERIO, C., SCHMIDT, M., VON KALLE, C., GARDNER, J., MEHTA, N., NEDUVA, V., DOW, D. J., GALY, A., MINIERO, R., FINOCCHI, A., METIN, A., BANERJEE, P. P., ORANGE, J. S., GALIMBERTI, S., VALSECCHI, M. G., BIFFI, A., MONTINI, E., VILLA, A., CICERI, F., RONCAROLO, M. G. & NALDINI, L. 2013. Lentiviral hematopoietic stem cell gene therapy in patients with Wiskott-Aldrich syndrome. *Science*, 341, 1233151.
- AKLI, S., CAILLAUD, C., VIGNE, E., STRATFORD-PERRICAUDET, L. D., POENARU, L., PERRICAUDET, M., KAHN, A. & PESCHANSKI, M. R. 1993. Transfer of a foreign gene into the brain using adenovirus vectors. *Nat Genet*, 3, 224-8.

- AL-DOSARI, M. S. & GAO, X. 2009. Nonviral gene delivery: principle, limitations, and recent progress. *AAPS J*, 11, 671-81.
- ALEXANDER, B. L., ALI, R. R., ALTON, E. W., BAINBRIDGE, J. W., BRAUN, S., CHENG, S. H., FLOTTE, T. R., GASPAR, H. B., GREZ, M., GRIESENBACH, U., KAPLITT, M. G., OTT, M. G., SEGER, R., SIMONS, M., THRASHER, A. J., THRASHER, A. Z. & YLA-HERTTUALA, S. 2007. Progress and prospects: gene therapy clinical trials (part 1). *Gene Ther*, 14, 1439-47.
- ALLOCCA, M., DORIA, M., PETRILLO, M., COLELLA, P., GARCIA-HOYOS, M., GIBBS, D., KIM, S. R., MAGUIRE, A., REX, T. S., DI VICINO, U., CUTILLO, L., SPARROW, J. R., WILLIAMS, D. S., BENNETT, J. & AURICCHIO, A. 2008. Serotype-dependent packaging of large genes in adeno-associated viral vectors results in effective gene delivery in mice. *J Clin Invest*, 118, 1955-64.
- ALVELIUS, G., HJALMARSON, O., GRIFFITHS, W. J., BJORKHEM, I. & SJOVALL, J. 2001. Identification of unusual 7-oxygenated bile acid sulfates in a patient with Niemann-Pick disease, type C. *J Lipid Res*, 42, 1571-7.
- APAOLAZA, P. S., DEL POZO-RODRIGUEZ, A., TORRECILLA, J., RODRIGUEZ-GASCON, A., RODRIGUEZ, J. M., FRIEDRICH, U., WEBER, B. H. & SOLINIS, M. A. 2015. Solid lipid nanoparticle-based vectors intended for the treatment of X-linked juvenile retinoschisis by gene therapy: In vivo approaches in Rs1h-deficient mouse model. *J Control Release*, 217, 273-83.
- APPLEDORN, D. M., PATIAL, S., MCBRIDE, A., GODBEHERE, S., VAN ROOIJEN, N., PARAMESWARAN, N. & AMALFITANO, A. 2008. Adenovirus vector-induced innate inflammatory mediators, MAPK signaling, as well as adaptive immune responses are dependent upon both TLR2 and TLR9 in vivo. *J Immunol*, 181, 2134-44.

- ARIZA, L., GIMENEZ-LLORT, L., CUBIZOLLE, A., PAGES, G., GARCIA-LAREU, B., SERRATRICE, N., COTS, D., THWAITE, R., CHILLON, M., KREMER, E. J. & BOSCH, A. 2014. Central nervous system delivery of helper-dependent canine adenovirus corrects neuropathology and behavior in mucopolysaccharidosis type VII mice. *Hum Gene Ther*, 25, 199-211.
- ARNBERG, N. 2012. Adenovirus receptors: implications for targeting of viral vectors. *Trends Pharmacol Sci*, 33, 442-8.
- ASOKAN, A., SCHAFFER, D. V. & SAMULSKI, R. J. 2012. The AAV vector toolkit: poised at the clinical crossroads. *Mol Ther*, 20, 699-708.
- ATCHISON, R. W., CASTO, B. C. & HAMMON, W. M. 1965. Adenovirus-Associated Defective Virus Particles. *Science*, 149, 754-6.
- BALAKRISHNAN, B. & JAYANDHARAN, G. R. 2014. Basic biology of adeno-associated virus (AAV) vectors used in gene therapy. *Curr Gene Ther*, 14, 86-100.
- BARCIA, C., JIMENEZ-DALMARONI, M., KROEGER, K. M., PUNTEL, M., RAPAPORT, A. J., LAROCQUE, D., KING, G. D., JOHNSON, S. A., LIU, C., XIONG, W., CANDOLFI, M., MONDKAR, S., NG, P., PALMER, D., CASTRO, M. G. & LOWENSTEIN, P. R. 2007. One-year expression from high-capacity adenoviral vectors in the brains of animals with pre-existing anti-adenoviral immunity: clinical implications. *Mol Ther*, 15, 2154-63.
- BARNHAM, K. J. & BUSH, A. I. 2008. Metals in Alzheimer's and Parkinson's diseases. *Curr Opin Chem Biol*, 12, 222-8.
- BASTIANELLI, E. 2003. Distribution of calcium-binding proteins in the cerebellum. *Cerebellum*, 2, 242-62.
- BAUER, P., KNOBLICH, R., BAUER, C., FINCKH, U., HUFEN, A., KROPP, J., BRAUN, S., KUSTERMANN-KUHN, B., SCHMIDT, D., HARZER, K. &

- ROLFS, A. 2002. NPC1: Complete genomic sequence, mutation analysis, and characterization of haplotypes. *Hum Mutat*, 19, 30-8.
- BECERRA, S. P., KOCZOT, F., FABISCH, P. & ROSE, J. A. 1988. Synthesis of adeno-associated virus structural proteins requires both alternative mRNA splicing and alternative initiations from a single transcript. *J Virol*, 62, 2745-54.
- BELLETTATO, C. M. & SCARPA, M. 2010. Pathophysiology of neuropathic lysosomal storage disorders. *J Inherit Metab Dis*, 33, 347-62.
- BELMATOUG, N., BURLINA, A., GIRALDO, P., HENDRIKSZ, C. J., KUTER, D. J., MENGEL, E. & PASTORES, G. M. 2011. Gastrointestinal disturbances and their management in miglustat-treated patients. *J Inherit Metab Dis*, 34, 991-1001.
- BENJAMIN, E. R., KHANNA, R., SCHILLING, A., FLANAGAN, J. J., PELLEGRINO, L. J., BRIGNOL, N., LUN, Y., GUILLEN, D., RANES, B. E., FRASCELLA, M., SOSKA, R., FENG, J., DUNGAN, L., YOUNG, B., LOCKHART, D. J. & VALENZANO, K. J. 2012. Co-administration with the pharmacological chaperone AT1001 increases recombinant human alpha-galactosidase A tissue uptake and improves substrate reduction in Fabry mice. *Mol Ther*, 20, 717-26.
- BERNS, K. I. & ADLER, S. 1972. Separation of two types of adeno-associated virus particles containing complementary polynucleotide chains. *J Virol*, 9, 394-6.
- BESSIS, N., GARCIACOZAR, F. J. & BOISSIER, M. C. 2004. Immune responses to gene therapy vectors: influence on vector function and effector mechanisms. *Gene Ther*, 11 Suppl 1, S10-7.
- BETT, A. J., PREVEC, L. & GRAHAM, F. L. 1993. Packaging capacity and stability of human adenovirus type 5 vectors. *J Virol*, 67, 5911-21.

- BEVAN, A. K., DUQUE, S., FOUST, K. D., MORALES, P. R., BRAUN, L., SCHMELZER, L., CHAN, C. M., MCCRATE, M., CHICOINE, L. G., COLEY, B. D., PORENSKY, P. N., KOLB, S. J., MENDELL, J. R., BURGHESE, A. H. & KASPAR, B. K. 2011. Systemic gene delivery in large species for targeting spinal cord, brain, and peripheral tissues for pediatric disorders. *Mol Ther*, 19, 1971-80.
- BIFFI, A. 2016. Gene therapy for lysosomal storage disorders: a good start. *Hum Mol Genet*, 25, R65-75.
- BIFFI, A., DE PALMA, M., QUATTRINI, A., DEL CARRO, U., AMADIO, S., VISIGALLI, I., SESSA, M., FASANO, S., BRAMBILLA, R., MARCHESINI, S., BORDIGNON, C. & NALDINI, L. 2004. Correction of metachromatic leukodystrophy in the mouse model by transplantation of genetically modified hematopoietic stem cells. *J Clin Invest*, 113, 1118-29.
- BIFFI, A., MONTINI, E., LORIOLI, L., CESANI, M., FUMAGALLI, F., PLATI, T., BALDOLI, C., MARTINO, S., CALABRIA, A., CANALE, S., BENEDICENTI, F., VALLANTI, G., BIASCO, L., LEO, S., KABBARA, N., ZANETTI, G., RIZZO, W. B., MEHTA, N. A., CICALESE, M. P., CASIRAGHI, M., BOELEN, J. J., DEL CARRO, U., DOW, D. J., SCHMIDT, M., ASSANELLI, A., NEDUVA, V., DI SERIO, C., STUPKA, E., GARDNER, J., VON KALLE, C., BORDIGNON, C., CICERI, F., ROVELLI, A., RONCAROLO, M. G., AIUTI, A., SESSA, M. & NALDINI, L. 2013. Lentiviral hematopoietic stem cell gene therapy benefits metachromatic leukodystrophy. *Science*, 341, 1233-1238.
- BLOM, T. S., LINDER, M. D., SNOW, K., PIHKO, H., HESS, M. W., JOKITALO, E., VECKMAN, V., SYVANEN, A. C. & IKONEN, E. 2003. Defective endocytic trafficking of NPC1 and NPC2 underlying infantile Niemann-Pick type C disease. *Hum Mol Genet*, 12, 257-72.
- BOADO, R. J., LU, J. Z., HUI, E. K., SUMBRIA, R. K. & PARDRIDGE, W. M. 2013. Pharmacokinetics and brain uptake in the rhesus monkey of a fusion

protein of arylsulfatase a and a monoclonal antibody against the human insulin receptor. *Biotechnol Bioeng*, 110, 1456-65.

BONEKAMP, N. A., VOLKL, A., FAHIMI, H. D. & SCHRADER, M. 2009. Reactive oxygen species and peroxisomes: struggling for balance. *Biofactors*, 35, 346-55.

BOUSTANY, R. M. 2013. Lysosomal storage diseases--the horizon expands. *Nat Rev Neurol*, 9, 583-98.

BRANTLY, M. L., CHULAY, J. D., WANG, L., MUELLER, C., HUMPHRIES, M., SPENCER, L. T., ROUHANI, F., CONLON, T. J., CALCEDO, R., BETTS, M. R., SPENCER, C., BYRNE, B. J., WILSON, J. M. & FLOTTE, T. R. 2009. Sustained transgene expression despite T lymphocyte responses in a clinical trial of rAAV1-AAT gene therapy. *Proc Natl Acad Sci U S A*, 106, 16363-8.

BREMOVA, T., MALINOVA, V., AMRAOUI, Y., MENGEL, E., REINKE, J., KOLNIKOVA, M. & STRUPP, M. 2015. Acetyl-dl-leucine in Niemann-Pick type C: A case series. *Neurology*, 85, 1368-75.

BREOUS, E., SOMANATHAN, S., VANDENBERGHE, L. H. & WILSON, J. M. 2009. Hepatic regulatory T cells and Kupffer cells are crucial mediators of systemic T cell tolerance to antigens targeting murine liver. *Hepatology*, 50, 612-21.

BROEKMAN, M. L., BAEK, R. C., COMER, L. A., FERNANDEZ, J. L., SEYFRIED, T. N. & SENA-ESTEVEZ, M. 2007. Complete correction of enzymatic deficiency and neurochemistry in the GM1-gangliosidosis mouse brain by neonatal adeno-associated virus-mediated gene delivery. *Mol Ther*, 15, 30-7.

BROOKS, A. I., STEIN, C. S., HUGHES, S. M., HETH, J., MCCRAY, P. M., JR., SAUTER, S. L., JOHNSTON, J. C., CORY-SLECHTA, D. A., FEDEROFF,

- H. J. & DAVIDSON, B. L. 2002. Functional correction of established central nervous system deficits in an animal model of lysosomal storage disease with feline immunodeficiency virus-based vectors. *Proc Natl Acad Sci U S A*, 99, 6216-21.
- BROOKS, A. R., HARKINS, R. N., WANG, P., QIAN, H. S., LIU, P. & RUBANYI, G. M. 2004. Transcriptional silencing is associated with extensive methylation of the CMV promoter following adenoviral gene delivery to muscle. *J Gene Med*, 6, 395-404.
- BROWN, D. E., THRALL, M. A., WALKLEY, S. U., WENGER, D. A., MITCHELL, T. W., SMITH, M. O., ROYALS, K. L., MARCH, P. A. & ALLISON, R. W. 1994. Feline Niemann-Pick disease type C. *Am J Pathol*, 144, 1412-5.
- BROWN, M. S. & GOLDSTEIN, J. L. 1986. A receptor-mediated pathway for cholesterol homeostasis. *Science*, 232, 34-47.
- BU, J., ASHE, K. M., BRINGAS, J., MARSHALL, J., DODGE, J. C., CABRERA-SALAZAR, M. A., FORSAYETH, J., SCHUCHMAN, E. H., BANKIEWICZ, K. S., CHENG, S. H., SHIHABUDDIN, L. S. & PASSINI, M. A. 2012. Merits of combination cortical, subcortical, and cerebellar injections for the treatment of Niemann-Pick disease type A. *Mol Ther*, 20, 1893-901.
- BULLER, R. M., JANIK, J. E., SEBRING, E. D. & ROSE, J. A. 1981. Herpes simplex virus types 1 and 2 completely help adenovirus-associated virus replication. *J Virol*, 40, 241-7.
- BURGERT, H. G., RUZSICS, Z., OBERMEIER, S., HILGENDORF, A., WINDHEIM, M. & ELSING, A. 2002. Subversion of host defense mechanisms by adenoviruses. *Curr Top Microbiol Immunol*, 269, 273-318.

- BURNS, J. C., FRIEDMANN, T., DRIEVER, W., BURRASCANO, M. & YEE, J. K. 1993. Vesicular stomatitis virus G glycoprotein pseudotyped retroviral vectors: concentration to very high titer and efficient gene transfer into mammalian and nonmammalian cells. *Proc Natl Acad Sci U S A*, 90, 8033-7.
- BUSTOS, R., KOLEN, E. R., BRAITERMAN, L., BAINES, A. J., GORELICK, F. S. & HUBBARD, A. L. 2001. Synapsin I is expressed in epithelial cells: localization to a unique trans-Golgi compartment. *J Cell Sci*, 114, 3695-704.
- BYRNE, B. J., FALK, D. J., CLEMENT, N. & MAH, C. S. 2012. Gene therapy approaches for lysosomal storage disease: next-generation treatment. *Hum Gene Ther*, 23, 808-15.
- CACHON-GONZALEZ, M. B., WANG, S. Z., LYNCH, A., ZIEGLER, R., CHENG, S. H. & COX, T. M. 2006. Effective gene therapy in an authentic model of Tay-Sachs-related diseases. *Proc Natl Acad Sci U S A*, 103, 10373-8.
- CALCEDO, R., MORIZONO, H., WANG, L., MCCARTER, R., HE, J., JONES, D., BATSHAW, M. L. & WILSON, J. M. 2011. Adeno-associated virus antibody profiles in newborns, children, and adolescents. *Clin Vaccine Immunol*, 18, 1586-8.
- CALCEDO, R., VANDENBERGHE, L. H., GAO, G., LIN, J. & WILSON, J. M. 2009. Worldwide epidemiology of neutralizing antibodies to adeno-associated viruses. *J Infect Dis*, 199, 381-90.
- CAO, Y., ESPINOLA, J. A., FOSSALE, E., MASSEY, A. C., CUERVO, A. M., MACDONALD, M. E. & COTMAN, S. L. 2006. Autophagy is disrupted in a knock-in mouse model of juvenile neuronal ceroid lipofuscinosis. *J Biol Chem*, 281, 20483-93.

- CAPILLA-GONZALEZ, V., LAVELL, E., QUINONES-HINOJOSA, A. & GUERRERO-CAZARES, H. 2015. Regulation of subventricular zone-derived cells migration in the adult brain. *Adv Exp Med Biol*, 853, 1-21.
- CARSTEA, E. D., MORRIS, J. A., COLEMAN, K. G., LOFTUS, S. K., ZHANG, D., CUMMINGS, C., GU, J., ROSENFELD, M. A., PAVAN, W. J., KRIZMAN, D. B., NAGLE, J., POLYMEROPOULOS, M. H., STURLEY, S. L., IOANNOU, Y. A., HIGGINS, M. E., COMLY, M., COONEY, A., BROWN, A., KANESKI, C. R., BLANCHETTE-MACKIE, E. J., DWYER, N. K., NEUFELD, E. B., CHANG, T. Y., LISCUM, L., STRAUSS, J. F., 3RD, OHNO, K., ZEIGLER, M., CARMİ, R., SOKOL, J., MARKIE, D., O'NEILL, R. R., VAN DIGGELEN, O. P., ELLEDER, M., PATTERSON, M. C., BRADY, R. O., VANIER, M. T., PENTCHEV, P. G. & TAGLE, D. A. 1997. Niemann-Pick C1 disease gene: homology to mediators of cholesterol homeostasis. *Science*, 277, 228-31.
- CASTO, B. C., ATCHISON, R. W. & HAMMON, W. M. 1967. Studies on the relationship between adeno-associated virus type I (AAV-1) and adenoviruses. I. Replication of AAV-1 in certain cell cultures and its effect on helper adenovirus. *Virology*, 32, 52-9.
- CAVAZZANA-CALVO, M., HACEIN-BEY, S., DE SAINT BASILE, G., GROSS, F., YVON, E., NUSBAUM, P., SELZ, F., HUE, C., CERTAIN, S., CASANOVA, J. L., BOUSSO, P., DEIST, F. L. & FISCHER, A. 2000. Gene therapy of human severe combined immunodeficiency (SCID)-X1 disease. *Science*, 288, 669-72.
- CEARLEY, C. N. & WOLFE, J. H. 2007. A single injection of an adeno-associated virus vector into nuclei with divergent connections results in widespread vector distribution in the brain and global correction of a neurogenetic disease. *J Neurosci*, 27, 9928-40.

- CHAMBERLAIN, K., RIYAD, J. M. & WEBER, T. 2016. Expressing Transgenes That Exceed the Packaging Capacity of Adeno-Associated Virus Capsids. *Hum Gene Ther Methods*, 27, 1-12.
- CHANDLER, R. J., LAFAVE, M. C., VARSHNEY, G. K., TRIVEDI, N. S., CARRILLO-CARRASCO, N., SENAC, J. S., WU, W., HOFFMANN, V., ELKAHLOUN, A. G., BURGESS, S. M. & VENDITTI, C. P. 2015. Vector design influences hepatic genotoxicity after adeno-associated virus gene therapy. *J Clin Invest*, 125, 870-80.
- CHANDLER, R. J., WILLIAMS, I. M., GIBSON, A. L., DAVIDSON, C. D., INCAO, A. A., HUBBARD, B. T., PORTER, F. D., PAVAN, W. J. & VENDITTI, C. P. 2016. Systemic AAV9 gene therapy improves the lifespan of mice with Niemann-Pick disease, type C1. *Hum Mol Genet*.
- CHANG, M., COOPER, J. D., SLEAT, D. E., CHENG, S. H., DODGE, J. C., PASSINI, M. A., LOBEL, P. & DAVIDSON, B. L. 2008. Intraventricular enzyme replacement improves disease phenotypes in a mouse model of late infantile neuronal ceroid lipofuscinosis. *Mol Ther*, 16, 649-56.
- CHARMAN, M., KENNEDY, B. E., OSBORNE, N. & KARTEN, B. 2010. MLN64 mediates egress of cholesterol from endosomes to mitochondria in the absence of functional Niemann-Pick Type C1 protein. *J Lipid Res*, 51, 1023-34.
- CHENG, S. H. 2014. Gene therapy for the neurological manifestations in lysosomal storage disorders. *J Lipid Res*, 55, 1827-38.
- CHOI, J. H., YU, N. K., BAEK, G. C., BAKES, J., SEO, D., NAM, H. J., BAEK, S. H., LIM, C. S., LEE, Y. S. & KAANG, B. K. 2014. Optimization of AAV expression cassettes to improve packaging capacity and transgene expression in neurons. *Mol Brain*, 7, 17.

- CHOUDHURY, S. R., HUDRY, E., MAGUIRE, C. A., SENA-ESTEVEZ, M., BREAKFIELD, X. O. & GRANDI, P. 2016. Viral vectors for therapy of neurologic diseases. *Neuropharmacology*.
- COLOGNA, S. M., CLUZEAU, C. V., YANJANIN, N. M., BLANK, P. S., DAIL, M. K., SIEBEL, S., TOTH, C. L., WASSIF, C. A., LIEBERMAN, A. P. & PORTER, F. D. 2014. Human and mouse neuroinflammation markers in Niemann-Pick disease, type C1. *J Inherit Metab Dis*, 37, 83-92.
- CONSIGLIO, A., QUATTRINI, A., MARTINO, S., BENSADOUN, J. C., DOLCETTA, D., TROJANI, A., BENAGLIA, G., MARCHESINI, S., CESTARI, V., OLIVERIO, A., BORDIGNON, C. & NALDINI, L. 2001. In vivo gene therapy of metachromatic leukodystrophy by lentiviral vectors: correction of neuropathology and protection against learning impairments in affected mice. *Nat Med*, 7, 310-6.
- COUGNOUX, A., CLUZEAU, C., MITRA, S., LI, R., WILLIAMS, I., BURKERT, K., XU, X., WASSIF, C. A., ZHENG, W. & PORTER, F. D. 2016. Necroptosis in Niemann-Pick disease, type C1: a potential therapeutic target. *Cell Death Dis*, 7, e2147.
- COUTINHO, M. F., LACERDA, L. & ALVES, S. 2012. Glycosaminoglycan storage disorders: a review. *Biochem Res Int*, 2012, 471325.
- COX, T., LACHMANN, R., HOLLAK, C., AERTS, J., VAN WEELY, S., HREBICEK, M., PLATT, F., BUTTERS, T., DWEK, R., MOYSES, C., GOW, I., ELSTEIN, D. & ZIMRAN, A. 2000. Novel oral treatment of Gaucher's disease with N-butyldeoxynojirimycin (OGT 918) to decrease substrate biosynthesis. *Lancet*, 355, 1481-5.
- COX, T. M. & CACHON-GONZALEZ, M. B. 2012. The cellular pathology of lysosomal diseases. *J Pathol*, 226, 241-54.

- CRESSANT, A., DESMARIS, N., VEROT, L., BREJOT, T., FROISSART, R., VANIER, M. T., MAIRE, I. & HEARD, J. M. 2004. Improved behavior and neuropathology in the mouse model of Sanfilippo type IIIB disease after adeno-associated virus-mediated gene transfer in the striatum. *J Neurosci*, 24, 10229-39.
- CRUMLING, M. A., LIU, L., THOMAS, P. V., BENSON, J., KANICKI, A., KABARA, L., HALSEY, K., DOLAN, D. & DUNCAN, R. K. 2012. Hearing loss and hair cell death in mice given the cholesterol-chelating agent hydroxypropyl-beta-cyclodextrin. *PLoS One*, 7, e53280.
- CUNNINGHAM, S. C., DANE, A. P., SPINOULAS, A., LOGAN, G. J. & ALEXANDER, I. E. 2008. Gene delivery to the juvenile mouse liver using AAV2/8 vectors. *Mol Ther*, 16, 1081-8.
- DAHMS, N. M. 1996. Insulin-like growth factor II/cation-independent mannose 6-phosphate receptor and lysosomal enzyme recognition. *Biochem Soc Trans*, 24, 136-41.
- DAMDINDORJ, L., KARNAN, S., OTA, A., HOSSAIN, E., KONISHI, Y., HOSOKAWA, Y. & KONISHI, H. 2014. A comparative analysis of constitutive promoters located in adeno-associated viral vectors. *PLoS One*, 9, e106472.
- DAVIDSON, B. L., ALLEN, E. D., KOZARSKY, K. F., WILSON, J. M. & ROESSLER, B. J. 1993. A model system for in vivo gene transfer into the central nervous system using an adenoviral vector. *Nat Genet*, 3, 219-23.
- DAVIDSON, C. D., ALI, N. F., MICSENYI, M. C., STEPHNEY, G., RENAULT, S., DOBRENIS, K., ORY, D. S., VANIER, M. T. & WALKLEY, S. U. 2009. Chronic cyclodextrin treatment of murine Niemann-Pick C disease ameliorates neuronal cholesterol and glycosphingolipid storage and disease progression. *PLoS One*, 4, e6951.

- DAYA, S. & BERNS, K. I. 2008. Gene therapy using adeno-associated virus vectors. *Clin Microbiol Rev*, 21, 583-93.
- DAYTON, R. D., WANG, D. B. & KLEIN, R. L. 2012. The advent of AAV9 expands applications for brain and spinal cord gene delivery. *Expert Opin Biol Ther*, 12, 757-66.
- DEGENNARO, L. J., KANAZIR, S. D., WALLACE, W. C., LEWIS, R. M. & GREENGARD, P. 1983. Neuron-specific phosphoproteins as models for neuronal gene expression. *Cold Spring Harb Symp Quant Biol*, 48 Pt 1, 337-45.
- DEL POZO-RODRIGUEZ, A., SOLINIS, M. A. & RODRIGUEZ-GASCON, A. 2016. Applications of lipid nanoparticles in gene therapy. *Eur J Pharm Biopharm*, 109, 184-193.
- DEMAIS, V., BARTHELEMY, A., PERRAUT, M., UNGERER, N., KEIME, C., REIBEL, S. & PFRIEGER, F. W. 2016. Reversal of Pathologic Lipid Accumulation in NPC1-Deficient Neurons by Drug-Promoted Release of LAMP1-Coated Lamellar Inclusions. *J Neurosci*, 36, 8012-25.
- DESNICK, R. J. & SCHUCHMAN, E. H. 2012. Enzyme replacement therapy for lysosomal diseases: lessons from 20 years of experience and remaining challenges. *Annu Rev Genomics Hum Genet*, 13, 307-35.
- DEVERMAN, B. E., PRAVDO, P. L., SIMPSON, B. P., KUMAR, S. R., CHAN, K. Y., BANERJEE, A., WU, W. L., YANG, B., HUBER, N., PASCA, S. P. & GRADINARU, V. 2016. Cre-dependent selection yields AAV variants for widespread gene transfer to the adult brain. *Nat Biotechnol*, 34, 204-9.
- DIROSARIO, J., DIVERS, E., WANG, C., ETTER, J., CHARRIER, A., JUKKOLA, P., AUER, H., BEST, V., NEWSOM, D. L., MCCARTY, D. M. & FU, H. 2009. Innate and adaptive immune activation in the brain of MPS IIIB mouse model. *J Neurosci Res*, 87, 978-90.

- DISMUKE, D. J., TENENBAUM, L. & SAMULSKI, R. J. 2013. Biosafety of recombinant adeno-associated virus vectors. *Curr Gene Ther*, 13, 434-52.
- DODGE, J. C., CLARKE, J., SONG, A., BU, J., YANG, W., TAKSIR, T. V., GRIFFITHS, D., ZHAO, M. A., SCHUCHMAN, E. H., CHENG, S. H., O'RIORDAN, C. R., SHIHABUDDIN, L. S., PASSINI, M. A. & STEWART, G. R. 2005. Gene transfer of human acid sphingomyelinase corrects neuropathology and motor deficits in a mouse model of Niemann-Pick type A disease. *Proc Natl Acad Sci U S A*, 102, 17822-7.
- DODGE, J. C., CLARKE, J., TRELEAVEN, C. M., TAKSIR, T. V., GRIFFITHS, D. A., YANG, W., FIDLER, J. A., PASSINI, M. A., KAREY, K. P., SCHUCHMAN, E. H., CHENG, S. H. & SHIHABUDDIN, L. S. 2009. Intracerebroventricular infusion of acid sphingomyelinase corrects CNS manifestations in a mouse model of Niemann-Pick A disease. *Exp Neurol*, 215, 349-57.
- DONG, J. Y., FAN, P. D. & FRIZZELL, R. A. 1996. Quantitative analysis of the packaging capacity of recombinant adeno-associated virus. *Hum Gene Ther*, 7, 2101-12.
- DONSANTE, A., MCEACHIN, Z., RILEY, J., LEUNG, C. H., KANZ, L., O'CONNOR, D. M. & BOULIS, N. M. 2016. Intracerebroventricular delivery of self-complementary adeno-associated virus serotype 9 to the adult rat brain. *Gene Ther*, 23, 401-7.
- DONSANTE, A., MILLER, D. G., LI, Y., VOGLER, C., BRUNT, E. M., RUSSELL, D. W. & SANDS, M. S. 2007. AAV vector integration sites in mouse hepatocellular carcinoma. *Science*, 317, 477.
- DUBRIDGE, R. B., TANG, P., HSIA, H. C., LEONG, P. M., MILLER, J. H. & CALOS, M. P. 1987. Analysis of mutation in human cells by using an Epstein-Barr virus shuttle system. *Mol Cell Biol*, 7, 379-87.

- DUNBAR, C. E., KOHN, D. B., SCHIFFMANN, R., BARTON, N. W., NOLTA, J. A., ESPLIN, J. A., PENSIERO, M., LONG, Z., LOCKEY, C., EMMONS, R. V., CSIK, S., LEITMAN, S., KREBS, C. B., CARTER, C., BRADY, R. O. & KARLSSON, S. 1998. Retroviral transfer of the glucocerebrosidase gene into CD34+ cells from patients with Gaucher disease: in vivo detection of transduced cells without myeloablation. *Hum Gene Ther*, 9, 2629-40.
- DUQUE, S., JOUSSEMET, B., RIVIERE, C., MARAIS, T., DUBREIL, L., DOUAR, A. M., FYFE, J., MOULLIER, P., COLLE, M. A. & BARKATS, M. 2009. Intravenous administration of self-complementary AAV9 enables transgene delivery to adult motor neurons. *Mol Ther*, 17, 1187-96.
- ELLIGER, S. S., ELLIGER, C. A., AGUILAR, C. P., RAJU, N. R. & WATSON, G. L. 1999. Elimination of lysosomal storage in brains of MPS VII mice treated by intrathecal administration of an adeno-associated virus vector. *Gene Ther*, 6, 1175-8.
- ELRICK, M. J., PACHECO, C. D., YU, T., DADGAR, N., SHAKKOTTAI, V. G., WARE, C., PAULSON, H. L. & LIEBERMAN, A. P. 2010. Conditional Niemann-Pick C mice demonstrate cell autonomous Purkinje cell neurodegeneration. *Hum Mol Genet*, 19, 837-47.
- ENQUIST, I. B., LO BIANCO, C., OOKA, A., NILSSON, E., MANSSON, J. E., EHINGER, M., RICHTER, J., BRADY, R. O., KIRIK, D. & KARLSSON, S. 2007. Murine models of acute neuronopathic Gaucher disease. *Proc Natl Acad Sci U S A*, 104, 17483-8.
- ERTEKIN, C. & AYDOGDU, I. 2003. Neurophysiology of swallowing. *Clin Neurophysiol*, 114, 2226-44.
- FAGONE, P., WRIGHT, J. F., NATHWANI, A. C., NIENHUIS, A. W., DAVIDOFF, A. M. & GRAY, J. T. 2012. Systemic errors in quantitative polymerase chain reaction titration of self-complementary adeno-associated

viral vectors and improved alternative methods. *Hum Gene Ther Methods*, 23, 1-7.

FAN, M., SIDHU, R., FUJIWARA, H., TORTELLI, B., ZHANG, J., DAVIDSON, C., WALKLEY, S. U., BAGEL, J. H., VITE, C., YANJANIN, N. M., PORTER, F. D., SCHAFFER, J. E. & ORY, D. S. 2013. Identification of Niemann-Pick C1 disease biomarkers through sphingolipid profiling. *J Lipid Res*, 54, 2800-14.

FEDERICI, T., TAUB, J. S., BAUM, G. R., GRAY, S. J., GRIEGER, J. C., MATTHEWS, K. A., HANDY, C. R., PASSINI, M. A., SAMULSKI, R. J. & BOULIS, N. M. 2012. Robust spinal motor neuron transduction following intrathecal delivery of AAV9 in pigs. *Gene Ther*, 19, 852-9.

FENSOM, A. H., GRANT, A. R., STEINBERG, S. J., WARD, C. P., LAKE, B. D., LOGAN, E. C. & HULMAN, G. 1999. An adult with a non-neuronopathic form of Niemann-Pick C disease. *J Inherit Metab Dis*, 22, 84-6.

FERLA, R., CLAUDIANI, P., COTUGNO, G., SACCONI, P., DE LEONIBUS, E. & AURICCHIO, A. 2014. Similar therapeutic efficacy between a single administration of gene therapy and multiple administrations of recombinant enzyme in a mouse model of lysosomal storage disease. *Hum Gene Ther*, 25, 609-18.

FILOCAMO, M. & MORRONE, A. 2011. Lysosomal storage disorders: molecular basis and laboratory testing. *Hum Genomics*, 5, 156-69.

FITZGERALD, M. & SHENK, T. 1981. The sequence 5'-AAUAAA-3' forms parts of the recognition site for polyadenylation of late SV40 mRNAs. *Cell*, 24, 251-60.

FOUST, K. D., NURRE, E., MONTGOMERY, C. L., HERNANDEZ, A., CHAN, C. M. & KASPAR, B. K. 2009. Intravascular AAV9 preferentially targets neonatal neurons and adult astrocytes. *Nat Biotechnol*, 27, 59-65.

- FRATANTONI, J. C., HALL, C. W. & NEUFELD, E. F. 1968. Hurler and Hunter syndromes: mutual correction of the defect in cultured fibroblasts. *Science*, 162, 570-2.
- FRIEDLAND, N., LIOU, H. L., LOBEL, P. & STOCK, A. M. 2003. Structure of a cholesterol-binding protein deficient in Niemann-Pick type C2 disease. *Proc Natl Acad Sci U S A*, 100, 2512-7.
- FU, H., DIROSARIO, J., KILLEDAR, S., ZARASPE, K. & MCCARTY, D. M. 2011. Correction of neurological disease of mucopolysaccharidosis IIIB in adult mice by rAAV9 trans-blood-brain barrier gene delivery. *Mol Ther*, 19, 1025-33.
- FU, R., YANJANIN, N. M., BIANCONI, S., PAVAN, W. J. & PORTER, F. D. 2010. Oxidative stress in Niemann-Pick disease, type C. *Mol Genet Metab*, 101, 214-8.
- FUKUDA, T., ROBERTS, A., AHEARN, M., ZAAL, K., RALSTON, E., PLOTZ, P. H. & RABEN, N. 2006. Autophagy and lysosomes in Pompe disease. *Autophagy*, 2, 318-20.
- GAGE, F. H. 2000. Mammalian neural stem cells. *Science*, 287, 1433-8.
- GAO, C., SANDS, M. S., HASKINS, M. E. & PONDER, K. P. 2000. Delivery of a retroviral vector expressing human beta-glucuronidase to the liver and spleen decreases lysosomal storage in mucopolysaccharidosis VII mice. *Mol Ther*, 2, 233-44.
- GAO, G., ALVIRA, M. R., SOMANATHAN, S., LU, Y., VANDENBERGHE, L. H., RUX, J. J., CALCEDO, R., SANMIGUEL, J., ABBAS, Z. & WILSON, J. M. 2003. Adeno-associated viruses undergo substantial evolution in primates during natural infections. *Proc Natl Acad Sci U S A*, 100, 6081-6.

- GAO, G., VANDENBERGHE, L. H., ALVIRA, M. R., LU, Y., CALCEDO, R., ZHOU, X. & WILSON, J. M. 2004. Clades of Adeno-associated viruses are widely disseminated in human tissues. *J Virol*, 78, 6381-8.
- GAUDET, D., METHOT, J., DERY, S., BRISSON, D., ESSIEMBRE, C., TREMBLAY, G., TREMBLAY, K., DE WAL, J., TWISK, J., VAN DEN BULK, N., SIER-FERREIRA, V. & VAN DEVENTER, S. 2013. Efficacy and long-term safety of alipogene tiparvovec (AAV1-LPLS447X) gene therapy for lipoprotein lipase deficiency: an open-label trial. *Gene Ther*, 20, 361-9.
- GENTNER, B., VISIGALLI, I., HIRAMATSU, H., LECHMAN, E., UNGARI, S., GIUSTACCHINI, A., SCHIRA, G., AMENDOLA, M., QUATTRINI, A., MARTINO, S., ORLACCHIO, A., DICK, J. E., BIFFI, A. & NALDINI, L. 2010. Identification of hematopoietic stem cell-specific miRNAs enables gene therapy of globoid cell leukodystrophy. *Sci Transl Med*, 2, 58ra84.
- GIESE, A. K., MASCHER, H., GRITTNER, U., EICHLER, S., KRAMP, G., LUKAS, J., TE VRUCHTE, D., AL EISA, N., CORTINA-BORJA, M., PORTER, F. D., PLATT, F. M. & ROLFS, A. 2015. A novel, highly sensitive and specific biomarker for Niemann-Pick type C1 disease. *Orphanet J Rare Dis*, 10, 78.
- GINN, S. L., ALEXANDER, I. E., EDELSTEIN, M. L., ABEDI, M. R. & WIXON, J. 2013. Gene therapy clinical trials worldwide to 2012 - an update. *J Gene Med*, 15, 65-77.
- GLICK, D., BARTH, S. & MACLEOD, K. F. 2010. Autophagy: cellular and molecular mechanisms. *J Pathol*, 221, 3-12.
- GOLDIN, E., ROFF, C. F., MILLER, S. P., RODRIGUEZ-LAFRASSE, C., VANIER, M. T., BRADY, R. O. & PENTCHEV, P. G. 1992. Type C Niemann-Pick disease: a murine model of the lysosomal cholesterol lipidosis

- accumulates sphingosine and sphinganine in liver. *Biochim Biophys Acta*, 1127, 303-11.
- GOLDMAN, S. D. & KRISE, J. P. 2010. Niemann-Pick C1 functions independently of Niemann-Pick C2 in the initial stage of retrograde transport of membrane-impermeable lysosomal cargo. *J Biol Chem*, 285, 4983-94.
- GOLDSTEIN, J. L., DANA, S. E., FAUST, J. R., BEAUDET, A. L. & BROWN, M. S. 1975. Role of lysosomal acid lipase in the metabolism of plasma low density lipoprotein. Observations in cultured fibroblasts from a patient with cholesteryl ester storage disease. *J Biol Chem*, 250, 8487-95.
- GONDRE-LEWIS, M. C., MCGLYNN, R. & WALKLEY, S. U. 2003. Cholesterol accumulation in NPC1-deficient neurons is ganglioside dependent. *Curr Biol*, 13, 1324-9.
- GRAY, S. J., FOTI, S. B., SCHWARTZ, J. W., BACHABOINA, L., TAYLOR-BLAKE, B., COLEMAN, J., EHLERS, M. D., ZYLKA, M. J., MCCOWN, T. J. & SAMULSKI, R. J. 2011a. Optimizing promoters for recombinant adeno-associated virus-mediated gene expression in the peripheral and central nervous system using self-complementary vectors. *Hum Gene Ther*, 22, 1143-53.
- GRAY, S. J., MATAGNE, V., BACHABOINA, L., YADAV, S., OJEDA, S. R. & SAMULSKI, R. J. 2011b. Preclinical differences of intravascular AAV9 delivery to neurons and glia: a comparative study of adult mice and nonhuman primates. *Mol Ther*, 19, 1058-69.
- GRAY, S. J., NAGABHUSHAN KALBURGI, S., MCCOWN, T. J. & JUDE SAMULSKI, R. 2013. Global CNS gene delivery and evasion of anti-AAV-neutralizing antibodies by intrathecal AAV administration in non-human primates. *Gene Ther*, 20, 450-9.

- GRIFFIN, L. D., GONG, W., VEROT, L. & MELLON, S. H. 2004. Niemann-Pick type C disease involves disrupted neurosteroidogenesis and responds to allopregnanolone. *Nat Med*, 10, 704-11.
- GROUP, N.-C. G. W., WRAITH, J. E., BAUMGARTNER, M. R., BEMBI, B., COVANIS, A., LEVADE, T., MENGEL, E., PINEDA, M., SEDEL, F., TOPCU, M., VANIER, M. T., WIDNER, H., WIJBURG, F. A. & PATTERSON, M. C. 2009. Recommendations on the diagnosis and management of Niemann-Pick disease type C. *Mol Genet Metab*, 98, 152-65.
- GUNDERSEN, H. J., JENSEN, E. B., KIEU, K. & NIELSEN, J. 1999. The efficiency of systematic sampling in stereology--reconsidered. *J Microsc*, 193, 199-211.
- HABERLAND, M., MONTGOMERY, R. L. & OLSON, E. N. 2009. The many roles of histone deacetylases in development and physiology: implications for disease and therapy. *Nat Rev Genet*, 10, 32-42.
- HACEIN-BEY-ABINA, S., GARRIGUE, A., WANG, G. P., SOULIER, J., LIM, A., MORILLON, E., CLAPPIER, E., CACCAVELLI, L., DELABESSE, E., BELDJORD, K., ASNAFI, V., MACINTYRE, E., DAL CORTIVO, L., RADFORD, I., BROUSSE, N., SIGAUX, F., MOSHOUS, D., HAUER, J., BORKHARDT, A., BELOHRADSKY, B. H., WINTERGERST, U., VELEZ, M. C., LEIVA, L., SORENSEN, R., WULFFRAAT, N., BLANCHE, S., BUSHMAN, F. D., FISCHER, A. & CAVAZZANA-CALVO, M. 2008. Insertional oncogenesis in 4 patients after retrovirus-mediated gene therapy of SCID-X1. *J Clin Invest*, 118, 3132-42.
- HACEIN-BEY-ABINA, S., VON KALLE, C., SCHMIDT, M., MCCORMACK, M. P., WULFFRAAT, N., LEBOULCH, P., LIM, A., OSBORNE, C. S., PAWLIUK, R., MORILLON, E., SORENSEN, R., FORSTER, A., FRASER, P., COHEN, J. I., DE SAINT BASILE, G., ALEXANDER, I., WINTERGERST, U., FREBOURG, T., AURIAS, A., STOPPA-LYONNET, D., ROMANA, S., RADFORD-WEISS, I., GROSS, F., VALENSI, F.,

- DELABESSE, E., MACINTYRE, E., SIGAUX, F., SOULIER, J., LEIVA, L. E., WISSLER, M., PRINZ, C., RABBITTS, T. H., LE DEIST, F., FISCHER, A. & CAVAZZANA-CALVO, M. 2003. LMO2-associated clonal T cell proliferation in two patients after gene therapy for SCID-X1. *Science*, 302, 415-9.
- HAHN, C. N., DEL PILAR MARTIN, M., ZHOU, X. Y., MANN, L. W. & D'AZZO, A. 1998. Correction of murine galactosialidosis by bone marrow-derived macrophages overexpressing human protective protein/cathepsin A under control of the colony-stimulating factor-1 receptor promoter. *Proc Natl Acad Sci U S A*, 95, 14880-5.
- HARA, T., NAKAMURA, K., MATSUI, M., YAMAMOTO, A., NAKAHARA, Y., SUZUKI-MIGISHIMA, R., YOKOYAMA, M., MISHIMA, K., SAITO, I., OKANO, H. & MIZUSHIMA, N. 2006. Suppression of basal autophagy in neural cells causes neurodegenerative disease in mice. *Nature*, 441, 885-9.
- HAREENDRAN, S., BALAKRISHNAN, B., SEN, D., KUMAR, S., SRIVASTAVA, A. & JAYANDHARAN, G. R. 2013. Adeno-associated virus (AAV) vectors in gene therapy: immune challenges and strategies to circumvent them. *Rev Med Virol*, 23, 399-413.
- HARRISON, F., YEAGY, B. A., ROCCA, C. J., KOHN, D. B., SALOMON, D. R. & CHERQUI, S. 2013. Hematopoietic stem cell gene therapy for the multisystemic lysosomal storage disorder cystinosis. *Mol Ther*, 21, 433-44.
- HARUI, A., SUZUKI, S., KOCHANNEK, S. & MITANI, K. 1999. Frequency and stability of chromosomal integration of adenovirus vectors. *J Virol*, 73, 6141-6.
- HAURIGOT, V., MARCO, S., RIBERA, A., GARCIA, M., RUZO, A., VILLACAMPA, P., AYUSO, E., ANOR, S., ANDALUZ, A., PINEDA, M., GARCIA-FRUCTUOSO, G., MOLAS, M., MAGGIONI, L., MUNOZ, S., MOTAS, S., RUBERTE, J., MINGOZZI, F., PUMAROLA, M. & BOSCH,

- F. 2013. Whole body correction of mucopolysaccharidosis IIIA by intracerebrospinal fluid gene therapy. *J Clin Invest*.
- HIGGINS, M. E., DAVIES, J. P., CHEN, F. W. & IOANNOU, Y. A. 1999. Niemann-Pick C1 is a late endosome-resident protein that transiently associates with lysosomes and the trans-Golgi network. *Mol Genet Metab*, 68, 1-13.
- HINDERER, C., BELL, P., GURDA, B. L., WANG, Q., LOUBOUTIN, J. P., ZHU, Y., BAGEL, J., O'DONNELL, P., SIKORA, T., RUANE, T., WANG, P., HASKINS, M. E. & WILSON, J. M. 2014. Intrathecal gene therapy corrects CNS pathology in a feline model of mucopolysaccharidosis I. *Mol Ther*, 22, 2018-27.
- HINDERER, C., BELL, P., LOUBOUTIN, J. P., ZHU, Y., YU, H., LIN, G., CHOA, R., GURDA, B. L., BAGEL, J., O'DONNELL, P., SIKORA, T., RUANE, T., WANG, P., TARANTAL, A. F., CASAL, M. L., HASKINS, M. E. & WILSON, J. M. 2015. Neonatal Systemic AAV Induces Tolerance to CNS Gene Therapy in MPS I Dogs and Nonhuman Primates. *Mol Ther*, 23, 1298-307.
- HINDERER, C., KATZ, N., LOUBOUTIN, J. P., BELL, P., YU, H., NAYAL, M., KOZARSKY, K., O'BRIEN, W. T., GOODE, T. & WILSON, J. M. 2016. Delivery of an Adeno-Associated Virus Vector into Cerebrospinal Fluid Attenuates Central Nervous System Disease in Mucopolysaccharidosis Type II Mice. *Hum Gene Ther*, 27, 906-915.
- HIRSCH, M. L., WOLF, S. J. & SAMULSKI, R. J. 2016. Delivering Transgenic DNA Exceeding the Carrying Capacity of AAV Vectors. *Methods Mol Biol*, 1382, 21-39.
- HOLOPAINEN, J. M., SAARIKOSKI, J., KINNUNEN, P. K. & JARVELA, I. 2001. Elevated lysosomal pH in neuronal ceroid lipofuscinoses (NCLs). *Eur J Biochem*, 268, 5851-6.

- HORDEAUX, J., DUBREIL, L., DENIAUD, J., IACOBELLI, F., MOREAU, S., LEDEVIN, M., LE GUINER, C., BLOUIN, V., LE DUFF, J., MENDES-MADEIRA, A., ROLLING, F., CHEREL, Y., MOULLIER, P. & COLLE, M. A. 2015. Efficient central nervous system AAVrh10-mediated intrathecal gene transfer in adult and neonate rats. *Gene Ther*, 22, 316-24.
- HOWE, C. L., GRANGER, B. L., HULL, M., GREEN, S. A., GABEL, C. A., HELENIUS, A. & MELLMAN, I. 1988. Derived protein sequence, oligosaccharides, and membrane insertion of the 120-kDa lysosomal membrane glycoprotein (lgp120): identification of a highly conserved family of lysosomal membrane glycoproteins. *Proc Natl Acad Sci U S A*, 85, 7577-81.
- HUANG, X., SUYAMA, K., BUCHANAN, J., ZHU, A. J. & SCOTT, M. P. 2005. A *Drosophila* model of the Niemann-Pick type C lysosome storage disease: *dnpcl1a* is required for molting and sterol homeostasis. *Development*, 132, 5115-24.
- HUNG, Y. H., FAUX, N. G., KILLILEA, D. W., YANJANIN, N., FIRNKES, S., VOLITAKIS, I., GANIO, G., WALTERFANG, M., HASTINGS, C., PORTER, F. D., ORY, D. S. & BUSH, A. I. 2014. Altered transition metal homeostasis in Niemann-Pick disease, type C1. *Metallomics*, 6, 542-53.
- IKONEN, E. 2008. Cellular cholesterol trafficking and compartmentalization. *Nat Rev Mol Cell Biol*, 9, 125-38.
- INFANTE, R. E., RADHAKRISHNAN, A., ABI-MOSLEH, L., KINCH, L. N., WANG, M. L., GRISHIN, N. V., GOLDSTEIN, J. L. & BROWN, M. S. 2008a. Purified NPC1 protein: II. Localization of sterol binding to a 240-amino acid soluble luminal loop. *J Biol Chem*, 283, 1064-75.
- INFANTE, R. E., WANG, M. L., RADHAKRISHNAN, A., KWON, H. J., BROWN, M. S. & GOLDSTEIN, J. L. 2008b. NPC2 facilitates bidirectional

transfer of cholesterol between NPC1 and lipid bilayers, a step in cholesterol egress from lysosomes. *Proc Natl Acad Sci U S A*, 105, 15287-92.

JACKSON, K. L., DAYTON, R. D., DEVERMAN, B. E. & KLEIN, R. L. 2016. Better Targeting, Better Efficiency for Wide-Scale Neuronal Transduction with the Synapsin Promoter and AAV-PHP.B. *Front Mol Neurosci*, 9, 116.

JIANG, X., SIDHU, R., PORTER, F. D., YANJANIN, N. M., SPEAK, A. O., TE VRUCHTE, D. T., PLATT, F. M., FUJIWARA, H., SCHERRER, D. E., ZHANG, J., DIETZEN, D. J., SCHAFFER, J. E. & ORY, D. S. 2011. A sensitive and specific LC-MS/MS method for rapid diagnosis of Niemann-Pick C1 disease from human plasma. *J Lipid Res*, 52, 1435-45.

JIN, L., ZENG, X., LIU, M., DENG, Y. & HE, N. 2014. Current progress in gene delivery technology based on chemical methods and nano-carriers. *Theranostics*, 4, 240-55.

JOLLY, R. D., DALEFIELD, R. R. & PALMER, D. N. 1993. Ceroid, lipofuscin and the ceroid-lipofuscinoses (Batten disease). *J Inherit Metab Dis*, 16, 280-3.

JONES, E. A. & WEISSENBORN, K. 1997. Neurology and the liver. *J Neurol Neurosurg Psychiatry*, 63, 279-93.

JOOSS, K. & CHIRMULE, N. 2003. Immunity to adenovirus and adeno-associated viral vectors: implications for gene therapy. *Gene Ther*, 10, 955-63.

KAKKIS, E., MCENTEE, M., VOGLER, C., LE, S., LEVY, B., BELICHENKO, P., MOBLEY, W., DICKSON, P., HANSON, S. & PASSAGE, M. 2004. Intrathecal enzyme replacement therapy reduces lysosomal storage in the brain and meninges of the canine model of MPS I. *Mol Genet Metab*, 83, 163-74.

KAPLAN, A., ACHORD, D. T. & SLY, W. S. 1977. Phosphohexosyl components of a lysosomal enzyme are recognized by pinocytosis receptors on human fibroblasts. *Proc Natl Acad Sci U S A*, 74, 2026-30.

- KAZANTSEV, A. G. & THOMPSON, L. M. 2008. Therapeutic application of histone deacetylase inhibitors for central nervous system disorders. *Nat Rev Drug Discov*, 7, 854-68.
- KELLY, D. A., PORTMANN, B., MOWAT, A. P., SHERLOCK, S. & LAKE, B. D. 1993. Niemann-Pick disease type C: diagnosis and outcome in children, with particular reference to liver disease. *J Pediatr*, 123, 242-7.
- KENNY, G. D., BIENEMANN, A. S., TAGALAKIS, A. D., PUGH, J. A., WELSER, K., CAMPBELL, F., TABOR, A. B., HAILES, H. C., GILL, S. S., LYTHGOE, M. F., MCLEOD, C. W., WHITE, E. A. & HART, S. L. 2013. Multifunctional receptor-targeted nanocomplexes for the delivery of therapeutic nucleic acids to the brain. *Biomaterials*, 34, 9190-200.
- KIELAR, C., MADDOX, L., BIBLE, E., PONTIKIS, C. C., MACAULEY, S. L., GRIFFEY, M. A., WONG, M., SANDS, M. S. & COOPER, J. D. 2007. Successive neuron loss in the thalamus and cortex in a mouse model of infantile neuronal ceroid lipofuscinosis. *Neurobiol Dis*, 25, 150-62.
- KIM, I., RODRIGUEZ-ENRIQUEZ, S. & LEMASTERS, J. J. 2007. Selective degradation of mitochondria by mitophagy. *Arch Biochem Biophys*, 462, 245-53.
- KIM, J. Y., GRUNKE, S. D., LEVITES, Y., GOLDE, T. E. & JANKOWSKY, J. L. 2014. Intracerebroventricular viral injection of the neonatal mouse brain for persistent and widespread neuronal transduction. *J Vis Exp*, 51863.
- KING, J. A., DUBIELZIG, R., GRIMM, D. & KLEINSCHMIDT, J. A. 2001. DNA helicase-mediated packaging of adeno-associated virus type 2 genomes into preformed capsids. *EMBO J*, 20, 3282-91.
- KIRKEGAARD, T., GRAY, J., PRIESTMAN, D. A., WALLOM, K. L., ATKINS, J., OLSEN, O. D., KLEIN, A., DRNDARSKI, S., PETERSEN, N. H., INGEMANN, L., SMITH, D. A., MORRIS, L., BORNAES, C.,

- JORGENSEN, S. H., WILLIAMS, I., HINSBY, A., ARENZ, C., BEGLEY, D., JAATTELA, M. & PLATT, F. M. 2016. Heat shock protein-based therapy as a potential candidate for treating the sphingolipidoses. *Sci Transl Med*, 8, 355ra118.
- KIRKEGAARD, T., ROTH, A. G., PETERSEN, N. H., MAHALKA, A. K., OLSEN, O. D., MOILANEN, I., ZYLICZ, A., KNUDSEN, J., SANDHOFF, K., ARENZ, C., KINNUNEN, P. K., NYLANDSTED, J. & JAATTELA, M. 2010. Hsp70 stabilizes lysosomes and reverts Niemann-Pick disease-associated lysosomal pathology. *Nature*, 463, 549-53.
- KLEIN, R., RUTTKOWSKI, B., KNAPP, E., SALMONS, B., GUNZBURG, W. H. & HOHENADL, C. 2006. WPRE-mediated enhancement of gene expression is promoter and cell line specific. *Gene*, 372, 153-61.
- KLINKE, G., ROHRBACH, M., GIUGLIANI, R., BURDA, P., BAUMGARTNER, M. R., TRAN, C., GAUTSCHI, M., MATHIS, D. & HERSBERGER, M. 2015. LC-MS/MS based assay and reference intervals in children and adolescents for oxysterols elevated in Niemann-Pick diseases. *Clin Biochem*, 48, 596-602.
- KNOWLES, R. B., SABRY, J. H., MARTONE, M. E., DEERINCK, T. J., ELLISMAN, M. H., BASSELL, G. J. & KOSIK, K. S. 1996. Translocation of RNA granules in living neurons. *J Neurosci*, 16, 7812-20.
- KO, D. C., MILENKOVIC, L., BEIER, S. M., MANUEL, H., BUCHANAN, J. & SCOTT, M. P. 2005. Cell-autonomous death of cerebellar purkinje neurons with autophagy in Niemann-Pick type C disease. *PLoS Genet*, 1, 81-95.
- KOCZOT, F. J., CARTER, B. J., GARON, C. F. & ROSE, J. A. 1973. Self-complementarity of terminal sequences within plus or minus strands of adenovirus-associated virus DNA. *Proc Natl Acad Sci U S A*, 70, 215-9.

- KOHLBRENNER, E., HENCKAERTS, E., RAPTI, K., GORDON, R. E., LINDEN, R. M., HAJJAR, R. J. & WEBER, T. 2012. Quantification of AAV particle titers by infrared fluorescence scanning of coomassie-stained sodium dodecyl sulfate-polyacrylamide gels. *Hum Gene Ther Methods*, 23, 198-203.
- KOMATSU, M., WAGURI, S., CHIBA, T., MURATA, S., IWATA, J., TANIDA, I., UENO, T., KOIKE, M., UCHIYAMA, Y., KOMINAMI, E. & TANAKA, K. 2006. Loss of autophagy in the central nervous system causes neurodegeneration in mice. *Nature*, 441, 880-4.
- KORNFELD, S. 1992. Structure and function of the mannose 6-phosphate/insulinlike growth factor II receptors. *Annu Rev Biochem*, 61, 307-30.
- KOTIN, R. M., LINDEN, R. M. & BERNS, K. I. 1992. Characterization of a preferred site on human chromosome 19q for integration of adeno-associated virus DNA by non-homologous recombination. *EMBO J*, 11, 5071-8.
- KOZAK, M. 2005. Regulation of translation via mRNA structure in prokaryotes and eukaryotes. *Gene*, 361, 13-37.
- KREMER, E. J., BOUTIN, S., CHILLON, M. & DANOS, O. 2000. Canine adenovirus vectors: an alternative for adenovirus-mediated gene transfer. *J Virol*, 74, 505-12.
- KRUTH, H. S., COMLY, M. E., BUTLER, J. D., VANIER, M. T., FINK, J. K., WENGER, D. A., PATEL, S. & PENTCHEV, P. G. 1986. Type C Niemann-Pick disease. Abnormal metabolism of low density lipoprotein in homozygous and heterozygous fibroblasts. *J Biol Chem*, 261, 16769-74.
- KUMAR, M., KELLER, B., MAKALOU, N. & SUTTON, R. E. 2001. Systematic determination of the packaging limit of lentiviral vectors. *Hum Gene Ther*, 12, 1893-905.

- KUWABARA, P. E. & LABOUESSE, M. 2002. The sterol-sensing domain: multiple families, a unique role? *Trends Genet*, 18, 193-201.
- KWON, H. J., ABI-MOSLEH, L., WANG, M. L., DEISENHOFER, J., GOLDSTEIN, J. L., BROWN, M. S. & INFANTE, R. E. 2009. Structure of N-terminal domain of NPC1 reveals distinct subdomains for binding and transfer of cholesterol. *Cell*, 137, 1213-24.
- LACHMANN, R. H., TE VRUCHTE, D., LLOYD-EVANS, E., REINKENSMEIER, G., SILLENCE, D. J., FERNANDEZ-GUILLEN, L., DWEK, R. A., BUTTERS, T. D., COX, T. M. & PLATT, F. M. 2004. Treatment with miglustat reverses the lipid-trafficking defect in Niemann-Pick disease type C. *Neurobiol Dis*, 16, 654-8.
- LAI, Y., YUE, Y. & DUAN, D. 2010. Evidence for the failure of adeno-associated virus serotype 5 to package a viral genome  $\geq 8.2$  kb. *Mol Ther*, 18, 75-9.
- LEIMIG, T., MANN, L., MARTIN MDEL, P., BONTEN, E., PERSONS, D., KNOWLES, J., ALLAY, J. A., CUNNINGHAM, J., NIENHUIS, A. W., SMEYNE, R. & D'AZZO, A. 2002. Functional amelioration of murine galactosialidosis by genetically modified bone marrow hematopoietic progenitor cells. *Blood*, 99, 3169-78.
- LEINEKUGEL, P., MICHEL, S., CONZELMANN, E. & SANDHOFF, K. 1992. Quantitative correlation between the residual activity of beta-hexosaminidase A and arylsulfatase A and the severity of the resulting lysosomal storage disease. *Hum Genet*, 88, 513-23.
- LEWEN, A., MATZ, P. & CHAN, P. H. 2000. Free radical pathways in CNS injury. *J Neurotrauma*, 17, 871-90.
- LEWITT, P. A., REZAI, A. R., LEEHEY, M. A., OJEMANN, S. G., FLAHERTY, A. W., ESKANDAR, E. N., KOSTYK, S. K., THOMAS, K., SARKAR, A., SIDDIQUI, M. S., TATTER, S. B., SCHWALB, J. M., POSTON, K. L.,

- HENDERSON, J. M., KURLAN, R. M., RICHARD, I. H., VAN METER, L., SAPAN, C. V., DURING, M. J., KAPLITT, M. G. & FEIGIN, A. 2011. AAV2-GAD gene therapy for advanced Parkinson's disease: a double-blind, sham-surgery controlled, randomised trial. *Lancet Neurol*, 10, 309-19.
- LI, C., GOUDY, K., HIRSCH, M., ASOKAN, A., FAN, Y., ALEXANDER, J., SUN, J., MONAHAN, P., SEIBER, D., SIDNEY, J., SETTE, A., TISCH, R., FRELINGER, J. & SAMULSKI, R. J. 2009. Cellular immune response to cryptic epitopes during therapeutic gene transfer. *Proc Natl Acad Sci U S A*, 106, 10770-4.
- LI, C., HE, Y., NICOLSON, S., HIRSCH, M., WEINBERG, M. S., ZHANG, P., KAFRI, T. & SAMULSKI, R. J. 2013. Adeno-associated virus capsid antigen presentation is dependent on endosomal escape. *J Clin Invest*, 123, 1390-401.
- LI, X., WANG, J., COUTAVAS, E., SHI, H., HAO, Q. & BLOBEL, G. 2016. Structure of human Niemann-Pick C1 protein. *Proc Natl Acad Sci U S A*, 113, 8212-7.
- LIANG, S. B., YOSHIMITSU, M., POEPPL, A., RASAIHAH, V. I., CAI, J., FOWLER, D. H. & MEDIN, J. A. 2007. Multiple reduced-intensity conditioning regimens facilitate correction of Fabry mice after transplantation of transduced cells. *Mol Ther*, 15, 618-27.
- LISOWSKI, L., DANE, A. P., CHU, K., ZHANG, Y., CUNNINGHAM, S. C., WILSON, E. M., NYGAARD, S., GROMPE, M., ALEXANDER, I. E. & KAY, M. A. 2014. Selection and evaluation of clinically relevant AAV variants in a xenograft liver model. *Nature*, 506, 382-6.
- LISOWSKI, L., TAY, S. S. & ALEXANDER, I. E. 2015. Adeno-associated virus serotypes for gene therapeutics. *Curr Opin Pharmacol*, 24, 59-67.
- LIU, B., TURLEY, S. D., BURNS, D. K., MILLER, A. M., REPA, J. J. & DIETSCHY, J. M. 2009. Reversal of defective lysosomal transport in NPC

disease ameliorates liver dysfunction and neurodegeneration in the npc1<sup>-/-</sup> mouse. *Proc Natl Acad Sci U S A*, 106, 2377-82.

LIU, G., MARTINS, I., WEMMIE, J. A., CHIORINI, J. A. & DAVIDSON, B. L. 2005a. Functional correction of CNS phenotypes in a lysosomal storage disease model using adeno-associated virus type 4 vectors. *J Neurosci*, 25, 9321-7.

LIU, Y., XU, L., HENNIG, A. K., KOVACS, A., FU, A., CHUNG, S., LEE, D., WANG, B., HERATI, R. S., MOSINGER OGILVIE, J., CAI, S. R. & PARKER PONDER, K. 2005b. Liver-directed neonatal gene therapy prevents cardiac, bone, ear, and eye disease in mucopolysaccharidosis I mice. *Mol Ther*, 11, 35-47.

LLOYD-EVANS, E. & HASLETT, L. J. 2016. The lysosomal storage disease continuum with ageing-related neurodegenerative disease. *Ageing Res Rev*, 32, 104-121.

LLOYD-EVANS, E., MORGAN, A. J., HE, X., SMITH, D. A., ELLIOT-SMITH, E., SILLENCE, D. J., CHURCHILL, G. C., SCHUCHMAN, E. H., GALIONE, A. & PLATT, F. M. 2008. Niemann-Pick disease type C1 is a sphingosine storage disease that causes deregulation of lysosomal calcium. *Nat Med*, 14, 1247-55.

LLOYD-EVANS, E. & PLATT, F. M. 2010. Lipids on trial: the search for the offending metabolite in Niemann-Pick type C disease. *Traffic*, 11, 419-28.

LLOYD-EVANS, E. & PLATT, F. M. 2011. Lysosomal Ca<sup>2+</sup> homeostasis: role in pathogenesis of lysosomal storage diseases. *Cell Calcium*, 50, 200-5.

LLOYD-EVANS, E., WALLER-EVANS, H., PETERNEVA, K. & PLATT, F. M. 2010. Endolysosomal calcium regulation and disease. *Biochem Soc Trans*, 38, 1458-64.

- LOCK, M., ALVIRA, M., VANDENBERGHE, L. H., SAMANTA, A., TOELEN, J., DEBYSER, Z. & WILSON, J. M. 2010. Rapid, simple, and versatile manufacturing of recombinant adeno-associated viral vectors at scale. *Hum Gene Ther*, 21, 1259-71.
- LOFTUS, S. K., ERICKSON, R. P., WALKLEY, S. U., BRYANT, M. A., INCAO, A., HEIDENREICH, R. A. & PAVAN, W. J. 2002. Rescue of neurodegeneration in Niemann-Pick C mice by a prion-promoter-driven *Npc1* cDNA transgene. *Hum Mol Genet*, 11, 3107-14.
- LOFTUS, S. K., MORRIS, J. A., CARSTEAD, E. D., GU, J. Z., CUMMINGS, C., BROWN, A., ELLISON, J., OHNO, K., ROSENFELD, M. A., TAGLE, D. A., PENTCHEV, P. G. & PAVAN, W. J. 1997. Murine model of Niemann-Pick C disease: mutation in a cholesterol homeostasis gene. *Science*, 277, 232-5.
- LOPEZ, M. E., KLEIN, A. D., DIMBIL, U. J. & SCOTT, M. P. 2011. Anatomically defined neuron-based rescue of neurodegenerative Niemann-Pick type C disorder. *J Neurosci*, 31, 4367-78.
- LOPEZ, M. E., KLEIN, A. D. & SCOTT, M. P. 2012. Complement is dispensable for neurodegeneration in Niemann-Pick disease type C. *J Neuroinflammation*, 9, 216.
- LOPEZ, M. E. & SCOTT, M. P. 2013. Genetic dissection of a cell-autonomous neurodegenerative disorder: lessons learned from mouse models of Niemann-Pick disease type C. *Dis Model Mech*, 6, 1089-100.
- LOWENTHAL, A. C., CUMMINGS, J. F., WENGER, D. A., THRALL, M. A., WOOD, P. A. & DE LAHUNTA, A. 1990. Feline sphingolipidosis resembling Niemann-Pick disease type C. *Acta Neuropathol*, 81, 189-97.
- LUND, T. C. 2013. Hematopoietic stem cell transplant for lysosomal storage diseases. *Pediatr Endocrinol Rev*, 11 Suppl 1, 91-8.

- LYSENG-WILLIAMSON, K. A. 2014. Miglustat: a review of its use in Niemann-Pick disease type C. *Drugs*, 74, 61-74.
- MA, X., LIU, Y., TITTIGER, M., HENNIG, A., KOVACS, A., POPELKA, S., WANG, B., HERATI, R., BIGG, M. & PONDER, K. P. 2007. Improvements in mucopolysaccharidosis I mice after adult retroviral vector-mediated gene therapy with immunomodulation. *Mol Ther*, 15, 889-902.
- MAARUP, T. J., CHEN, A. H., PORTER, F. D., FARHAT, N. Y., ORY, D. S., SIDHU, R., JIANG, X. & DICKSON, P. I. 2015. Intrathecal 2-hydroxypropyl-beta-cyclodextrin in a single patient with Niemann-Pick C1. *Mol Genet Metab*, 116, 75-9.
- MAGUIRE, A. M., SIMONELLI, F., PIERCE, E. A., PUGH, E. N., JR., MINGOZZI, F., BENNICELLI, J., BANFI, S., MARSHALL, K. A., TESTA, F., SURACE, E. M., ROSSI, S., LYUBARSKY, A., ARRUDA, V. R., KONKLE, B., STONE, E., SUN, J., JACOBS, J., DELL'OSSO, L., HERTLE, R., MA, J. X., REDMOND, T. M., ZHU, X., HAUCK, B., ZELENIAIA, O., SHINDLER, K. S., MAGUIRE, M. G., WRIGHT, J. F., VOLPE, N. J., MCDONNELL, J. W., AURICCHIO, A., HIGH, K. A. & BENNETT, J. 2008. Safety and efficacy of gene transfer for Leber's congenital amaurosis. *N Engl J Med*, 358, 2240-8.
- MALATHI, K., HIGAKI, K., TINKELENBERG, A. H., BALDERES, D. A., ALMANZAR-PARAMIO, D., WILCOX, L. J., ERDENIZ, N., REDICAN, F., PADAMSEE, M., LIU, Y., KHAN, S., ALCANTARA, F., CARSTEA, E. D., MORRIS, J. A. & STURLEY, S. L. 2004. Mutagenesis of the putative sterol-sensing domain of yeast Niemann Pick C-related protein reveals a primordial role in subcellular sphingolipid distribution. *J Cell Biol*, 164, 547-56.
- MANGO, R. L., XU, L., SANDS, M. S., VOGLER, C., SEILER, G., SCHWARZ, T., HASKINS, M. E. & PONDER, K. P. 2004. Neonatal retroviral vector-

mediated hepatic gene therapy reduces bone, joint, and cartilage disease in mucopolysaccharidosis VII mice and dogs. *Mol Genet Metab*, 82, 4-19.

MANNO, C. S., PIERCE, G. F., ARRUDA, V. R., GLADER, B., RAGNI, M., RASKO, J. J., OZELO, M. C., HOOTS, K., BLATT, P., KONKLE, B., DAKE, M., KAYE, R., RAZAVI, M., ZAJKO, A., ZEHNDER, J., RUSTAGI, P. K., NAKAI, H., CHEW, A., LEONARD, D., WRIGHT, J. F., LESSARD, R. R., SOMMER, J. M., TIGGES, M., SABATINO, D., LUK, A., JIANG, H., MINGOZZI, F., COUTO, L., ERTL, H. C., HIGH, K. A. & KAY, M. A. 2006. Successful transduction of liver in hemophilia by AAV-Factor IX and limitations imposed by the host immune response. *Nat Med*, 12, 342-7.

MARSHALL, E. 1999. Gene therapy death prompts review of adenovirus vector. *Science*, 286, 2244-5.

MATRAI, J., CHUAH, M. K. & VANDENDRIESSCHE, T. 2010. Recent advances in lentiviral vector development and applications. *Mol Ther*, 18, 477-90.

MATSUO, M., TOGAWA, M., HIRABARU, K., MOCHINAGA, S., NARITA, A., ADACHI, M., EGASHIRA, M., IRIE, T. & OHNO, K. 2013. Effects of cyclodextrin in two patients with Niemann-Pick Type C disease. *Mol Genet Metab*, 108, 76-81.

MAUE, R. A., BURGESS, R. W., WANG, B., WOOLEY, C. M., SEBURN, K. L., VANIER, M. T., ROGERS, M. A., CHANG, C. C., CHANG, T. Y., HARRIS, B. T., GRABER, D. J., PENATTI, C. A., PORTER, D. M., SZWERGOLD, B. S., HENDERSON, L. P., TOTENHAGEN, J. W., TROUARD, T. P., BORBON, I. A. & ERICKSON, R. P. 2012. A novel mouse model of Niemann-Pick type C disease carrying a D1005G-Npc1 mutation comparable to commonly observed human mutations. *Hum Mol Genet*, 21, 730-50.

- MCFARLAND, T. J., ZHANG, Y., ATCHANEYASKUL, L. O., FRANCIS, P., STOUT, J. T. & APPUKUTTAN, B. 2006. Evaluation of a novel short polyadenylation signal as an alternative to the SV40 polyadenylation signal. *Plasmid*, 56, 62-7.
- MCGOVERN, M. M., WASSERSTEIN, M. P., GIUGLIANI, R., BEMBI, B., VANIER, M. T., MENGEL, E., BRODIE, S. E., MENDELSON, D., SKLOOT, G., DESNICK, R. J., KURIYAMA, N. & COX, G. F. 2008. A prospective, cross-sectional survey study of the natural history of Niemann-Pick disease type B. *Pediatrics*, 122, e341-9.
- MCINTOSH, J. H., COCHRANE, M., COBBOLD, S., WALDMANN, H., NATHWANI, S. A., DAVIDOFF, A. M. & NATHWANI, A. C. 2012. Successful attenuation of humoral immunity to viral capsid and transgenic protein following AAV-mediated gene transfer with a non-depleting CD4 antibody and cyclosporine. *Gene Ther*, 19, 78-85.
- MCKAY BOUNFORD, K. & GISSEN, P. 2014. Genetic and laboratory diagnostic approach in Niemann Pick disease type C. *J Neurol*, 261 Suppl 2, S569-75.
- MCLEAN, J. R., SMITH, G. A., ROCHA, E. M., HAYES, M. A., BEAGAN, J. A., HALLETT, P. J. & ISACSON, O. 2014. Widespread neuron-specific transgene expression in brain and spinal cord following synapsin promoter-driven AAV9 neonatal intracerebroventricular injection. *Neurosci Lett*, 576, 73-8.
- MECHTLER, T. P., STARY, S., METZ, T. F., DE JESUS, V. R., GREBER-PLATZER, S., POLLAK, A., HERKNER, K. R., STREUBEL, B. & KASPER, D. C. 2012. Neonatal screening for lysosomal storage disorders: feasibility and incidence from a nationwide study in Austria. *Lancet*, 379, 335-41.
- MEIKLE, P. J., HOPWOOD, J. J., CLAGUE, A. E. & CAREY, W. F. 1999. Prevalence of lysosomal storage disorders. *JAMA*, 281, 249-54.

- MENGEL, E., KLUNEMANN, H. H., LOURENCO, C. M., HENDRIKSZ, C. J., SEDEL, F., WALTERFANG, M. & KOLB, S. A. 2013. Niemann-Pick disease type C symptomatology: an expert-based clinical description. *Orphanet J Rare Dis*, 8, 166.
- MEYER, K., FERRAIUOLO, L., SCHMELZER, L., BRAUN, L., MCGOVERN, V., LIKHTE, S., MICHELS, O., GOVONI, A., FITZGERALD, J., MORALES, P., FOUST, K. D., MENDELL, J. R., BURGHESE, A. H. & KASPAR, B. K. 2015. Improving single injection CSF delivery of AAV9-mediated gene therapy for SMA: a dose-response study in mice and nonhuman primates. *Mol Ther*, 23, 477-87.
- MILLARD, E. E., GALE, S. E., DUDLEY, N., ZHANG, J., SCHAFFER, J. E. & ORY, D. S. 2005. The sterol-sensing domain of the Niemann-Pick C1 (NPC1) protein regulates trafficking of low density lipoprotein cholesterol. *J Biol Chem*, 280, 28581-90.
- MILLARD, E. E., SRIVASTAVA, K., TRAUB, L. M., SCHAFFER, J. E. & ORY, D. S. 2000. Niemann-pick type C1 (NPC1) overexpression alters cellular cholesterol homeostasis. *J Biol Chem*, 275, 38445-51.
- MINGOZZI, F. & HIGH, K. A. 2011. Therapeutic in vivo gene transfer for genetic disease using AAV: progress and challenges. *Nat Rev Genet*, 12, 341-55.
- MINGOZZI, F., MAUS, M. V., HUI, D. J., SABATINO, D. E., MURPHY, S. L., RASKO, J. E., RAGNI, M. V., MANNO, C. S., SOMMER, J., JIANG, H., PIERCE, G. F., ERTL, H. C. & HIGH, K. A. 2007. CD8(+) T-cell responses to adeno-associated virus capsid in humans. *Nat Med*, 13, 419-22.
- MINGOZZI, F., MEULENBERG, J. J., HUI, D. J., BASNER-TSCHAKARJAN, E., HASBROUCK, N. C., EDMONSON, S. A., HUTNICK, N. A., BETTS, M. R., KASTELEIN, J. J., STROES, E. S. & HIGH, K. A. 2009. AAV-1-mediated gene transfer to skeletal muscle in humans results in dose-dependent activation of capsid-specific T cells. *Blood*, 114, 2077-86.

- MIYOSHI, H., BLOMER, U., TAKAHASHI, M., GAGE, F. H. & VERMA, I. M. 1998. Development of a self-inactivating lentivirus vector. *J Virol*, 72, 8150-7.
- MOCHIZUKI, H., SCHWARTZ, J. P., TANAKA, K., BRADY, R. O. & REISER, J. 1998. High-titer human immunodeficiency virus type 1-based vector systems for gene delivery into nondividing cells. *J Virol*, 72, 8873-83.
- MONTINI, E., CESANA, D., SCHMIDT, M., SANVITO, F., PONZONI, M., BARTHOLOMAE, C., SERGI SERGI, L., BENEDICENTI, F., AMBROSI, A., DI SERIO, C., DOGLIONI, C., VON KALLE, C. & NALDINI, L. 2006. Hematopoietic stem cell gene transfer in a tumor-prone mouse model uncovers low genotoxicity of lentiviral vector integration. *Nat Biotechnol*, 24, 687-96.
- MORGAN, A. J., PLATT, F. M., LLOYD-EVANS, E. & GALIONE, A. 2011. Molecular mechanisms of endolysosomal Ca<sup>2+</sup> signalling in health and disease. *Biochem J*, 439, 349-74.
- MUCHOWSKI, P. J. & WACKER, J. L. 2005. Modulation of neurodegeneration by molecular chaperones. *Nat Rev Neurosci*, 6, 11-22.
- MULDOON, L. L., ALVAREZ, J. I., BEGLEY, D. J., BOADO, R. J., DEL ZOPPO, G. J., DOOLITTLE, N. D., ENGELHARDT, B., HALLENBECK, J. M., LONER, R. R., OHLFEST, J. R., PRAT, A., SCARPA, M., SMEYNE, R. J., DREWES, L. R. & NEUWELT, E. A. 2013. Immunologic privilege in the central nervous system and the blood-brain barrier. *J Cereb Blood Flow Metab*, 33, 13-21.
- NAKAI, H., YANT, S. R., STORM, T. A., FUESS, S., MEUSE, L. & KAY, M. A. 2001. Extrachromosomal recombinant adeno-associated virus vector genomes are primarily responsible for stable liver transduction in vivo. *J Virol*, 75, 6969-76.

- NAKASONE, N., NAKAMURA, Y. S., HIGAKI, K., OUMI, N., OHNO, K. & NINOMIYA, H. 2014. Endoplasmic reticulum-associated degradation of Niemann-Pick C1: evidence for the role of heat shock proteins and identification of lysine residues that accept ubiquitin. *J Biol Chem*, 289, 19714-25.
- NAKATOGAWA, H., SUZUKI, K., KAMADA, Y. & OHSUMI, Y. 2009. Dynamics and diversity in autophagy mechanisms: lessons from yeast. *Nat Rev Mol Cell Biol*, 10, 458-67.
- NATHWANI, A. C., GRAY, J. T., NG, C. Y., ZHOU, J., SPENCE, Y., WADDINGTON, S. N., TUDDENHAM, E. G., KEMBALL-COOK, G., MCINTOSH, J., BOON-SPIJKER, M., MERTENS, K. & DAVIDOFF, A. M. 2006. Self-complementary adeno-associated virus vectors containing a novel liver-specific human factor IX expression cassette enable highly efficient transduction of murine and nonhuman primate liver. *Blood*, 107, 2653-61.
- NATHWANI, A. C., TUDDENHAM, E. G., RANGARAJAN, S., ROSALES, C., MCINTOSH, J., LINCH, D. C., CHOWDARY, P., RIDDELL, A., PIE, A. J., HARRINGTON, C., O'BEIRNE, J., SMITH, K., PASI, J., GLADER, B., RUSTAGI, P., NG, C. Y., KAY, M. A., ZHOU, J., SPENCE, Y., MORTON, C. L., ALLAY, J., COLEMAN, J., SLEEP, S., CUNNINGHAM, J. M., SRIVASTAVA, D., BASNER-TSCHAKARJAN, E., MINGOZZI, F., HIGH, K. A., GRAY, J. T., REISS, U. M., NIENHUIS, A. W. & DAVIDOFF, A. M. 2011. Adenovirus-associated virus vector-mediated gene transfer in hemophilia B. *N Engl J Med*, 365, 2357-65.
- NAUMER, M., SONNTAG, F., SCHMIDT, K., NIETO, K., PANKE, C., DAVEY, N. E., POPA-WAGNER, R. & KLEINSCHMIDT, J. A. 2012. Properties of the adeno-associated virus assembly-activating protein. *J Virol*, 86, 13038-48.

- NAURECKIENE, S., SLEAT, D. E., LACKLAND, H., FENSOM, A., VANIER, M. T., WATTIAUX, R., JADOT, M. & LOBEL, P. 2000. Identification of HE1 as the second gene of Niemann-Pick C disease. *Science*, 290, 2298-301.
- NEUFELD, E. B., WASTNEY, M., PATEL, S., SURESH, S., COONEY, A. M., DWYER, N. K., ROFF, C. F., OHNO, K., MORRIS, J. A., CARSTEADT, E. D., INCARDONA, J. P., STRAUSS, J. F., 3RD, VANIER, M. T., PATTERSON, M. C., BRADY, R. O., PENTCHEV, P. G. & BLANCHETTE-MACKIE, E. J. 1999. The Niemann-Pick C1 protein resides in a vesicular compartment linked to retrograde transport of multiple lysosomal cargo. *J Biol Chem*, 274, 9627-35.
- NEVILLE, D. C., COQUARD, V., PRIESTMAN, D. A., TE VRUCHTE, D. J., SILLENCE, D. J., DWEK, R. A., PLATT, F. M. & BUTTERS, T. D. 2004. Analysis of fluorescently labeled glycosphingolipid-derived oligosaccharides following ceramide glycanase digestion and anthranilic acid labeling. *Anal Biochem*, 331, 275-82.
- NIA, S. 2014. Psychiatric signs and symptoms in treatable inborn errors of metabolism. *J Neurol*, 261 Suppl 2, S559-68.
- NIXON, R. A., YANG, D. S. & LEE, J. H. 2008. Neurodegenerative lysosomal disorders: a continuum from development to late age. *Autophagy*, 4, 590-9.
- NONNENMACHER, M. & WEBER, T. 2012. Intracellular transport of recombinant adeno-associated virus vectors. *Gene Ther*, 19, 649-58.
- OGAWA, K., YOSHIHASHI, H., SUZUKI, Y., KAMEI, S. & MIZUTANI, T. 2010. Clinical study of the responsible lesion for dysarthria in the cerebellum. *Intern Med*, 49, 861-4.
- OHGAMI, N., KO, D. C., THOMAS, M., SCOTT, M. P., CHANG, C. C. & CHANG, T. Y. 2004. Binding between the Niemann-Pick C1 protein and a

- photoactivatable cholesterol analog requires a functional sterol-sensing domain. *Proc Natl Acad Sci U S A*, 101, 12473-8.
- OSTEDGAARD, L. S., ROKHLINA, T., KARP, P. H., LASHMIT, P., AFIONE, S., SCHMIDT, M., ZABNER, J., STINSKI, M. F., CHIORINI, J. A. & WELSH, M. J. 2005. A shortened adeno-associated virus expression cassette for CFTR gene transfer to cystic fibrosis airway epithelia. *Proc Natl Acad Sci U S A*, 102, 2952-7.
- PACHECO, C. D., KUNKEL, R. & LIEBERMAN, A. P. 2007. Autophagy in Niemann-Pick C disease is dependent upon Beclin-1 and responsive to lipid trafficking defects. *Hum Mol Genet*, 16, 1495-503.
- PALMER, D. J. & NG, P. 2005. Helper-dependent adenoviral vectors for gene therapy. *Hum Gene Ther*, 16, 1-16.
- PAPANDREOU, A. & GISSEN, P. 2016. Diagnostic workup and management of patients with suspected Niemann-Pick type C disease. *Ther Adv Neurol Disord*, 9, 216-29.
- PARENTI, G., ANDRIA, G. & BALLABIO, A. 2015. Lysosomal storage diseases: from pathophysiology to therapy. *Annu Rev Med*, 66, 471-86.
- PARENTI, G., MORACCI, M., FECAROTTA, S. & ANDRIA, G. 2014. Pharmacological chaperone therapy for lysosomal storage diseases. *Future Med Chem*, 6, 1031-45.
- PARK, W. D., O'BRIEN, J. F., LUNDQUIST, P. A., KRAFT, D. L., VOCKLEY, C. W., KARNES, P. S., PATTERSON, M. C. & SNOW, K. 2003. Identification of 58 novel mutations in Niemann-Pick disease type C: correlation with biochemical phenotype and importance of PTC1-like domains in NPC1. *Hum Mutat*, 22, 313-25.
- PARRA, J., KLEIN, A. D., CASTRO, J., MORALES, M. G., MOSQUEIRA, M., VALENCIA, I., CORTES, V., RIGOTTI, A. & ZANLUNGO, S. 2011. Npc1

deficiency in the C57BL/6J genetic background enhances Niemann-Pick disease type C spleen pathology. *Biochem Biophys Res Commun*, 413, 400-6.

PASSINI, M. A., WATSON, D. J., VITE, C. H., LANDSBURG, D. J., FEIGENBAUM, A. L. & WOLFE, J. H. 2003. Intraventricular brain injection of adeno-associated virus type 1 (AAV1) in neonatal mice results in complementary patterns of neuronal transduction to AAV2 and total long-term correction of storage lesions in the brains of beta-glucuronidase-deficient mice. *J Virol*, 77, 7034-40.

PASTORES, G. M. 2010. *Lysosomal storage disorders : principles and practice*, Singapore ; Hackensack, N.J., World Scientific Chapter 4.

PATTERSON, M. 1993. Niemann-Pick Disease Type C. *In*: PAGON, R. A., ADAM, M. P., ARDINGER, H. H., WALLACE, S. E., AMEMIYA, A., BEAN, L. J. H., BIRD, T. D., FONG, C. T., MEFFORD, H. C., SMITH, R. J. H. & STEPHENS, K. (eds.) *GeneReviews(R)*. Seattle (WA).

PATTERSON, M. C., HENDRIKSZ, C. J., WALTERFANG, M., SEDEL, F., VANIER, M. T., WIJBURG, F. & GROUP, N.-C. G. W. 2012. Recommendations for the diagnosis and management of Niemann-Pick disease type C: an update. *Mol Genet Metab*, 106, 330-44.

PATTERSON, M. C., VECCHIO, D., JACKLIN, E., ABEL, L., CHADHABOREHAM, H., LUZY, C., GIORGINO, R. & WRAITH, J. E. 2010. Long-term miglustat therapy in children with Niemann-Pick disease type C. *J Child Neurol*, 25, 300-5.

PATTERSON, M. C., VECCHIO, D., PRADY, H., ABEL, L. & WRAITH, J. E. 2007. Miglustat for treatment of Niemann-Pick C disease: a randomised controlled study. *Lancet Neurol*, 6, 765-72.

- PENCEA, V., BINGAMAN, K. D., FREEDMAN, L. J. & LUSKIN, M. B. 2001. Neurogenesis in the subventricular zone and rostral migratory stream of the neonatal and adult primate forebrain. *Exp Neurol*, 172, 1-16.
- PENTCHEV, P. G. 2004. Niemann-Pick C research from mouse to gene. *Biochim Biophys Acta*, 1685, 3-7.
- PENTCHEV, P. G., BOOTHE, A. D., KRUTH, H. S., WEINTROUB, H., STIVERS, J. & BRADY, R. O. 1984. A genetic storage disorder in BALB/C mice with a metabolic block in esterification of exogenous cholesterol. *J Biol Chem*, 259, 5784-91.
- PENTCHEV, P. G., COMLY, M. E., KRUTH, H. S., VANIER, M. T., WENGER, D. A., PATEL, S. & BRADY, R. O. 1985. A defect in cholesterol esterification in Niemann-Pick disease (type C) patients. *Proc Natl Acad Sci U S A*, 82, 8247-51.
- PENTCHEV, P. G., GAL, A. E., BOOTH, A. D., OMODEO-SALE, F., FOUKS, J., NEUMEYER, B. A., QUIRK, J. M., DAWSON, G. & BRADY, R. O. 1980. A lysosomal storage disorder in mice characterized by a dual deficiency of sphingomyelinase and glucocerebrosidase. *Biochim Biophys Acta*, 619, 669-79.
- PEREIRA, V. G., GAZARINI, M. L., RODRIGUES, L. C., DA SILVA, F. H., HAN, S. W., MARTINS, A. M., TERSARIOL, I. L. & D'ALMEIDA, V. 2010. Evidence of lysosomal membrane permeabilization in mucopolysaccharidosis type I: rupture of calcium and proton homeostasis. *J Cell Physiol*, 223, 335-42.
- PERSAUD-SAWIN, D. A. & BOUSTANY, R. M. 2005. Cell death pathways in juvenile Batten disease. *Apoptosis*, 10, 973-85.
- PIGUET, F., SONDHI, D., PIRAUD, M., FOUQUET, F., HACKETT, N. R., AHOANSOU, O., VANIER, M. T., BIECHE, I., AUBOURG, P.,

- CRYSTAL, R. G., CARTIER, N. & SEVIN, C. 2012. Correction of brain oligodendrocytes by AAVrh.10 intracerebral gene therapy in metachromatic leukodystrophy mice. *Hum Gene Ther*, 23, 903-14.
- PINEDA, M., WRAITH, J. E., MENGEL, E., SEDEL, F., HWU, W. L., ROHRBACH, M., BEMBI, B., WALTERFANG, M., KORENKE, G. C., MARQUARDT, T., LUZY, C., GIORGINO, R. & PATTERSON, M. C. 2009. Miglustat in patients with Niemann-Pick disease Type C (NP-C): a multicenter observational retrospective cohort study. *Mol Genet Metab*, 98, 243-9.
- PIPER, R. C. & LUZIO, J. P. 2004. CUPpling calcium to lysosomal biogenesis. *Trends Cell Biol*, 14, 471-3.
- PITHA, J., IRIE, T., SKLAR, P. B. & NYE, J. S. 1988. Drug solubilizers to aid pharmacologists: amorphous cyclodextrin derivatives. *Life Sci*, 43, 493-502.
- PLATT, F. M. 2014. Sphingolipid lysosomal storage disorders. *Nature*, 510, 68-75.
- PLATT, F. M., BOLAND, B. & VAN DER SPOEL, A. C. 2012. The cell biology of disease: lysosomal storage disorders: the cellular impact of lysosomal dysfunction. *J Cell Biol*, 199, 723-34.
- PLATT, F. M., NEISES, G. R., DWEK, R. A. & BUTTERS, T. D. 1994. N-butyldeoxynojirimycin is a novel inhibitor of glycolipid biosynthesis. *J Biol Chem*, 269, 8362-5.
- PLATT, F. M., WASSIF, C., COLACO, A., DARDIS, A., LLOYD-EVANS, E., BEMBI, B. & PORTER, F. D. 2014. Disorders of cholesterol metabolism and their unanticipated convergent mechanisms of disease. *Annu Rev Genomics Hum Genet*, 15, 173-94.
- PLATT, N., SPEAK, A. O., COLACO, A., GRAY, J., SMITH, D. A., WILLIAMS, I. M., WALLOM, K. L. & PLATT, F. M. 2016. Immune dysfunction in Niemann-Pick disease type C. *J Neurochem*, 136 Suppl 1, 74-80.

- PLOTKIN, J. B. & KUDLA, G. 2011. Synonymous but not the same: the causes and consequences of codon bias. *Nat Rev Genet*, 12, 32-42.
- POLTEN, A., FLUHARTY, A. L., FLUHARTY, C. B., KAPPLER, J., VON FIGURA, K. & GIESELMANN, V. 1991. Molecular basis of different forms of metachromatic leukodystrophy. *N Engl J Med*, 324, 18-22.
- PONTIKIS, C. C., DAVIDSON, C. D., WALKLEY, S. U., PLATT, F. M. & BEGLEY, D. J. 2013. Cyclodextrin alleviates neuronal storage of cholesterol in Niemann-Pick C disease without evidence of detectable blood-brain barrier permeability. *J Inherit Metab Dis*, 36, 491-8.
- PORTER, F. D., SCHERRER, D. E., LANIER, M. H., LANGMADE, S. J., MOLUGU, V., GALE, S. E., OLZESKI, D., SIDHU, R., DIETZEN, D. J., FU, R., WASSIF, C. A., YANJANIN, N. M., MARSO, S. P., HOUSE, J., VITE, C., SCHAFFER, J. E. & ORY, D. S. 2010. Cholesterol oxidation products are sensitive and specific blood-based biomarkers for Niemann-Pick C1 disease. *Sci Transl Med*, 2, 56ra81.
- POUPETOVA, H., LEDVINOVA, J., BERNA, L., DVORAKOVA, L., KOZICH, V. & ELLEDER, M. 2010. The birth prevalence of lysosomal storage disorders in the Czech Republic: comparison with data in different populations. *J Inherit Metab Dis*, 33, 387-96.
- PRAGGASTIS, M., TORTELLI, B., ZHANG, J., FUJIWARA, H., SIDHU, R., CHACKO, A., CHEN, Z., CHUNG, C., LIEBERMAN, A. P., SIKORA, J., DAVIDSON, C., WALKLEY, S. U., PIPALIA, N. H., MAXFIELD, F. R., SCHAFFER, J. E. & ORY, D. S. 2015. A murine Niemann-Pick C1 I1061T knock-in model recapitulates the pathological features of the most prevalent human disease allele. *J Neurosci*, 35, 8091-106.
- PRESSEY, S. N., SMITH, D. A., WONG, A. M., PLATT, F. M. & COOPER, J. D. 2012. Early glial activation, synaptic changes and axonal pathology in the

thalamocortical system of Niemann-Pick type C1 mice. *Neurobiol Dis*, 45, 1086-100.

PRIESTMAN, D. A., VAN DER SPOEL, A. C., BUTTERS, T. D., DWEK, R. A. & PLATT, F. M. 2008. N-butyldeoxynojirimycin causes weight loss as a result of appetite suppression in lean and obese mice. *Diabetes Obes Metab*, 10, 159-66.

PRINETTI, A., PRIONI, S., CHIRICOZZI, E., SCHUCHMAN, E. H., CHIGORNO, V. & SONNINO, S. 2011. Secondary alterations of sphingolipid metabolism in lysosomal storage diseases. *Neurochem Res*, 36, 1654-68.

QIU, J. & PINTEL, D. 2008. Processing of adeno-associated virus RNA. *Front Biosci*, 13, 3101-15.

QUINN, P. J. 2013. Structure of sphingomyelin bilayers and complexes with cholesterol forming membrane rafts. *Langmuir*, 29, 9447-56.

QUINN, P. J. 2014. Sphingolipid symmetry governs membrane lipid raft structure. *Biochim Biophys Acta*, 1838, 1922-30.

RABINOWITZ, J. E., ROLLING, F., LI, C., CONRATH, H., XIAO, W., XIAO, X. & SAMULSKI, R. J. 2002. Cross-packaging of a single adeno-associated virus (AAV) type 2 vector genome into multiple AAV serotypes enables transduction with broad specificity. *J Virol*, 76, 791-801.

RADIN, N. S. 1996. Treatment of Gaucher disease with an enzyme inhibitor. *Glycoconj J*, 13, 153-7.

RAHIM, A. A., WONG, A. M., AHMADI, S., HOEFER, K., BUCKLEY, S. M., HUGHES, D. A., NATHWANI, A. N., BAKER, A. H., MCVEY, J. H., COOPER, J. D. & WADDINGTON, S. N. 2012. In utero administration of Ad5 and AAV pseudotypes to the fetal brain leads to efficient, widespread and long-term gene expression. *Gene Ther*, 19, 936-46.

- RAMAMOORTH, M. & NARVEKAR, A. 2015. Non viral vectors in gene therapy-an overview. *J Clin Diagn Res*, 9, GE01-6.
- REHMAN, Z., ZUHORN, I. S. & HOEKSTRA, D. 2013. How cationic lipids transfer nucleic acids into cells and across cellular membranes: recent advances. *J Control Release*, 166, 46-56.
- REMENOVA, T., MORAND, O., AMATO, D., CHADHA-BOREHAM, H., TSURUTANI, S. & MARQUARDT, T. 2015. A double-blind, randomized, placebo-controlled trial studying the effects of *Saccharomyces boulardii* on the gastrointestinal tolerability, safety, and pharmacokinetics of miglustat. *Orphanet J Rare Dis*, 10, 81.
- REUNERT, J., FOBKER, M., KANNENBERG, F., DU CHESNE, I., PLATE, M., WELLHAUSEN, J., RUST, S. & MARQUARDT, T. 2016. Rapid Diagnosis of 83 Patients with Niemann Pick Type C Disease and Related Cholesterol Transport Disorders by Cholestantriol Screening. *EBioMedicine*, 4, 170-175.
- RIBERA, A., HAURIGOT, V., GARCIA, M., MARCO, S., MOTAS, S., VILLACAMPA, P., MAGGIONI, L., LEON, X., MOLAS, M., SANCHEZ, V., MUNOZ, S., LEBORGNE, C., MOLL, X., PUMAROLA, M., MINGOZZI, F., RUBERTE, J., ANOR, S. & BOSCH, F. 2015. Biochemical, histological and functional correction of mucopolysaccharidosis type IIIB by intra-cerebrospinal fluid gene therapy. *Hum Mol Genet*, 24, 2078-95.
- RODRIGUEZ-LAFRASSE, C., ROUSSON, R., PENTCHEV, P. G., LOUISOT, P. & VANIER, M. T. 1994. Free sphingoid bases in tissues from patients with type C Niemann-Pick disease and other lysosomal storage disorders. *Biochim Biophys Acta*, 1226, 138-44.
- ROSENBAUM, A. I., ZHANG, G., WARREN, J. D. & MAXFIELD, F. R. 2010. Endocytosis of beta-cyclodextrins is responsible for cholesterol reduction in Niemann-Pick type C mutant cells. *Proc Natl Acad Sci U S A*, 107, 5477-82.

- ROVELLI, A. M. 2008. The controversial and changing role of haematopoietic cell transplantation for lysosomal storage disorders: an update. *Bone Marrow Transplant*, 41 Suppl 2, S87-9.
- RUZO, A., MARCO, S., GARCIA, M., VILLACAMPA, P., RIBERA, A., AYUSO, E., MAGGIONI, L., MINGOZZI, F., HAURIGOT, V. & BOSCH, F. 2012. Correction of pathological accumulation of glycosaminoglycans in central nervous system and peripheral tissues of MPSIIIA mice through systemic AAV9 gene transfer. *Hum Gene Ther*, 23, 1237-46.
- SACK, B. K. & HERZOG, R. W. 2009. Evading the immune response upon in vivo gene therapy with viral vectors. *Curr Opin Mol Ther*, 11, 493-503.
- SACK, B. K., HERZOG, R. W., TERHORST, C. & MARKUSIC, D. M. 2014. Development of Gene Transfer for Induction of Antigen-specific Tolerance. *Mol Ther Methods Clin Dev*, 1, 14013.
- SALEGIO, E. A., KELLS, A. P., RICHARDSON, R. M., HADACZEK, P., FORSAYETH, J., BRINGAS, J., SARDI, S. P., PASSINI, M. A., SHIHABUDDIN, L. S., CHENG, S. H., FIANDACA, M. S. & BANKIEWICZ, K. S. 2010. Magnetic resonance imaging-guided delivery of adeno-associated virus type 2 to the primate brain for the treatment of lysosomal storage disorders. *Hum Gene Ther*, 21, 1093-103.
- SALEGIO, E. A., SAMARANCH, L., KELLS, A. P., MITTERMAYER, G., SAN SEBASTIAN, W., ZHOU, S., BEYER, J., FORSAYETH, J. & BANKIEWICZ, K. S. 2013. Axonal transport of adeno-associated viral vectors is serotype-dependent. *Gene Ther*, 20, 348-52.
- SALSANO, E., UMEH, C., RUFA, A., PAREYSON, D. & ZEE, D. S. 2012. Vertical supranuclear gaze palsy in Niemann-Pick type C disease. *Neurol Sci*, 33, 1225-32.

- SAMARANCH, L., SALEGIO, E. A., SAN SEBASTIAN, W., KELLS, A. P., FOUST, K. D., BRINGAS, J. R., LAMARRE, C., FORSAYETH, J., KASPAR, B. K. & BANKIEWICZ, K. S. 2012. Adeno-associated virus serotype 9 transduction in the central nervous system of nonhuman primates. *Hum Gene Ther*, 23, 382-9.
- SANDS, M. S. & DAVIDSON, B. L. 2006. Gene therapy for lysosomal storage diseases. *Mol Ther*, 13, 839-49.
- SANO, R., ANNUNZIATA, I., PATTERSON, A., MOSHIACH, S., GOMERO, E., OPFERMAN, J., FORTE, M. & D'AZZO, A. 2009. GM1-ganglioside accumulation at the mitochondria-associated ER membranes links ER stress to Ca(2+)-dependent mitochondrial apoptosis. *Mol Cell*, 36, 500-11.
- SANTOS-LOZANO, A., VILLAMANDOS GARCIA, D., SANCHIS-GOMAR, F., FIUZA-LUCES, C., PAREJA-GALEANO, H., GARATACHEA, N., NOGALES GADEA, G. & LUCIA, A. 2015. Niemann-Pick disease treatment: a systematic review of clinical trials. *Ann Transl Med*, 3, 360.
- SARAIVA, J., NOBRE, R. J. & PEREIRA DE ALMEIDA, L. 2016. Gene therapy for the CNS using AAVs: The impact of systemic delivery by AAV9. *J Control Release*, 241, 94-109.
- SARKAR, S., CARROLL, B., BUGANIM, Y., MAETZEL, D., NG, A. H., CASSADY, J. P., COHEN, M. A., CHAKRABORTY, S., WANG, H., SPOONER, E., PLOEGH, H., GSPONER, J., KOROLCHUK, V. I. & JAENISCH, R. 2013. Impaired autophagy in the lipid-storage disorder Niemann-Pick type C1 disease. *Cell Rep*, 5, 1302-15.
- SARNA, J. R., LAROUCHE, M., MARZBAN, H., SILLITOE, R. V., RANCOURT, D. E. & HAWKES, R. 2003. Patterned Purkinje cell degeneration in mouse models of Niemann-Pick type C disease. *J Comp Neurol*, 456, 279-91.

- SCHEDIN, S., SINDELAR, P. J., PENTCHEV, P., BRUNK, U. & DALLNER, G. 1997. Peroxisomal impairment in Niemann-Pick type C disease. *J Biol Chem*, 272, 6245-51.
- SCHRODER, A. R., SHINN, P., CHEN, H., BERRY, C., ECKER, J. R. & BUSHMAN, F. 2002. HIV-1 integration in the human genome favors active genes and local hotspots. *Cell*, 110, 521-9.
- SCHUCHMAN, E. H. & WASSERSTEIN, M. P. 2015. Types A and B Niemann-Pick disease. *Best Pract Res Clin Endocrinol Metab*, 29, 237-47.
- SCHULTZ, M. L., KRUS, K. L. & LIEBERMAN, A. P. 2016. Lysosome and endoplasmic reticulum quality control pathways in Niemann-Pick type C disease. *Brain Res*, 1649, 181-188.
- SCHULTZ, M. L., TECEDOR, L., CHANG, M. & DAVIDSON, B. L. 2011. Clarifying lysosomal storage diseases. *Trends Neurosci*, 34, 401-10.
- SCHWARZWAELDER, K., HOWE, S. J., SCHMIDT, M., BRUGMAN, M. H., DEICHMANN, A., GLIMM, H., SCHMIDT, S., PRINZ, C., WISSLER, M., KING, D. J., ZHANG, F., PARSLEY, K. L., GILMOUR, K. C., SINCLAIR, J., BAYFORD, J., PERAJ, R., PIKE-OVERZET, K., STAAL, F. J., DE RIDDER, D., KINNON, C., ABEL, U., WAGEMAKER, G., GASPAR, H. B., THRASHER, A. J. & VON KALLE, C. 2007. Gammaretrovirus-mediated correction of SCID-X1 is associated with skewed vector integration site distribution in vivo. *J Clin Invest*, 117, 2241-9.
- SCHWEND, T., LOUCKS, E. J., SNYDER, D. & AHLGREN, S. C. 2011. Requirement of Npc1 and availability of cholesterol for early embryonic cell movements in zebrafish. *J Lipid Res*, 52, 1328-44.
- SCOTT, J. E. & WILLETT, I. H. 1966. Binding of cationic dyes to nucleic acids and their biological polyanions. *Nature*, 209, 985-7.

- SECHI, A., DARDIS, A., ZAMPIERI, S., RABACCHI, C., ZANONI, P., CALANDRA, S., DE MAGLIO, G., PIZZOLITTO, S., MARUOTTI, V., DI MUZIO, A., PLATT, F. & BEMBI, B. 2014. Effects of miglustat treatment in a patient affected by an atypical form of Tangier disease. *Orphanet J Rare Dis*, 9, 143.
- SENA-ESTEVEZ, M., TEBBETS, J. C., STEFFENS, S., CROMBLEHOLME, T. & FLAKE, A. W. 2004. Optimized large-scale production of high titer lentivirus vector pseudotypes. *J Virol Methods*, 122, 131-9.
- SERGIJENKO, A., LANGFORD-SMITH, A., LIAO, A. Y., PICKFORD, C. E., MCDERMOTT, J., NOWINSKI, G., LANGFORD-SMITH, K. J., MERRY, C. L., JONES, S. A., WRAITH, J. E., WYNN, R. F., WILKINSON, F. L. & BIGGER, B. W. 2013. Myeloid/Microglial driven autologous hematopoietic stem cell gene therapy corrects a neuronopathic lysosomal disease. *Mol Ther*, 21, 1938-49.
- SETTEMBRE, C., FRALDI, A., JAHREISS, L., SPAMPANATO, C., VENTURI, C., MEDINA, D., DE PABLO, R., TACCHETTI, C., RUBINSZTEIN, D. C. & BALLABIO, A. 2008. A block of autophagy in lysosomal storage disorders. *Hum Mol Genet*, 17, 119-29.
- SEVIN, C., BENRAISS, A., VAN DAM, D., BONNIN, D., NAGELS, G., VEROT, L., LAURENDEAU, I., VIDAUD, M., GIESELMANN, V., VANIER, M., DE DEYN, P. P., AUBOURG, P. & CARTIER, N. 2006. Intracerebral adeno-associated virus-mediated gene transfer in rapidly progressive forms of metachromatic leukodystrophy. *Hum Mol Genet*, 15, 53-64.
- SEVIN, M., LESCA, G., BAUMANN, N., MILLAT, G., LYON-CAEN, O., VANIER, M. T. & SEDEL, F. 2007. The adult form of Niemann-Pick disease type C. *Brain*, 130, 120-33.
- SHERIDAN, C. 2011. Gene therapy finds its niche. *Nat Biotechnol*, 29, 121-8.

- SHEVTSOVA, Z., MALIK, J. M., MICHEL, U., BAHR, M. & KUGLER, S. 2005. Promoters and serotypes: targeting of adeno-associated virus vectors for gene transfer in the rat central nervous system in vitro and in vivo. *Exp Physiol*, 90, 53-9.
- SIEGEL, D. A. & WALKLEY, S. U. 1994. Growth of ectopic dendrites on cortical pyramidal neurons in neuronal storage diseases correlates with abnormal accumulation of GM2 ganglioside. *J Neurochem*, 62, 1852-62.
- SILLENCE, D. J. 2013. Glucosylceramide modulates endolysosomal pH in Gaucher disease. *Mol Genet Metab*, 109, 194-200.
- SIMONARO, C. M., GE, Y., ELIYAHU, E., HE, X., JEPSEN, K. J. & SCHUCHMAN, E. H. 2010. Involvement of the Toll-like receptor 4 pathway and use of TNF-alpha antagonists for treatment of the mucopolysaccharidoses. *Proc Natl Acad Sci U S A*, 107, 222-7.
- SKOCAJ, M., RESNIK, N., GRUNDNER, M., OTA, K., ROJKO, N., HODNIK, V., ANDERLUH, G., SOBOTA, A., MACEK, P., VERANIC, P. & SEPCIC, K. 2014. Tracking cholesterol/sphingomyelin-rich membrane domains with the osteolysin A-mCherry protein. *PLoS One*, 9, e92783.
- SLEAT, D. E., WISEMAN, J. A., EL-BANNA, M., PRICE, S. M., VEROT, L., SHEN, M. M., TINT, G. S., VANIER, M. T., WALKLEY, S. U. & LOBEL, P. 2004. Genetic evidence for nonredundant functional cooperativity between NPC1 and NPC2 in lipid transport. *Proc Natl Acad Sci U S A*, 101, 5886-91.
- SMITH, D., WALLOM, K. L., WILLIAMS, I. M., JEYAKUMAR, M. & PLATT, F. M. 2009. Beneficial effects of anti-inflammatory therapy in a mouse model of Niemann-Pick disease type C1. *Neurobiol Dis*, 36, 242-51.
- SNYDER, B. R., GRAY, S. J., QUACH, E. T., HUANG, J. W., LEUNG, C. H., SAMULSKI, R. J., BOULIS, N. M. & FEDERICI, T. 2011. Comparison of

adeno-associated viral vector serotypes for spinal cord and motor neuron gene delivery. *Hum Gene Ther*, 22, 1129-35.

SOLOMON, D., WINKELMAN, A. C., ZEE, D. S., GRAY, L. & BUTTNER-ENNEVER, J. 2005. Niemann-Pick type C disease in two affected sisters: ocular motor recordings and brain-stem neuropathology. *Ann N Y Acad Sci*, 1039, 436-45.

SOMERS, K. L., ROYALS, M. A., CARSTEAN, E. D., RAFI, M. A., WENGER, D. A. & THRALL, M. A. 2003. Mutation analysis of feline Niemann-Pick C1 disease. *Mol Genet Metab*, 79, 99-103.

SOUDAIS, C., SKANDER, N. & KREMER, E. J. 2004. Long-term in vivo transduction of neurons throughout the rat CNS using novel helper-dependent CAV-2 vectors. *FASEB J*, 18, 391-3.

SOUWEIDANE, M. M., FRASER, J. F., ARKIN, L. M., SONDHI, D., HACKETT, N. R., KAMINSKY, S. M., HEIER, L., KOSOFSKY, B. E., WORGALL, S., CRYSTAL, R. G. & KAPLITT, M. G. 2010. Gene therapy for late infantile neuronal ceroid lipofuscinosis: neurosurgical considerations. *J Neurosurg Pediatr*, 6, 115-22.

SPAMPANATO, C., DE LEONIBUS, E., DAMA, P., GARGIULO, A., FRALDI, A., SORRENTINO, N. C., RUSSO, F., NUSCO, E., AURICCHIO, A., SURACE, E. M. & BALLABIO, A. 2011. Efficacy of a combined intracerebral and systemic gene delivery approach for the treatment of a severe lysosomal storage disorder. *Mol Ther*, 19, 860-9.

SPENCE, M. W. & CALLAHAN, J. W. 1989. Sphingomyelin-cholesterol lipidoses: the Niemann-Pick group of diseases. *The metabolic basis of inherited disease*. McGraw-Hill, New York.

SPIEGEL, R., RAAS-ROTHSCHILD, A., REISH, O., REGEV, M., MEINER, V., BARGAL, R., SURY, V., MEIR, K., NADJARI, M., HERMANN, G.,

- IANCU, T. C., SHALEV, S. A. & ZEIGLER, M. 2009. The clinical spectrum of fetal Niemann-Pick type C. *Am J Med Genet A*, 149A, 446-50.
- STEIN, C. S., PEMBERTON, J. L., VAN ROOIJEN, N. & DAVIDSON, B. L. 1998. Effects of macrophage depletion and anti-CD40 ligand on transgene expression and redosing with recombinant adenovirus. *Gene Ther*, 5, 431-9.
- STEIN, V. M., CROOKS, A., DING, W., PROCIUK, M., O'DONNELL, P., BRYAN, C., SIKORA, T., DINGEMANSE, J., VANIER, M. T., WALKLEY, S. U. & VITE, C. H. 2012. Miglustat improves purkinje cell survival and alters microglial phenotype in feline Niemann-Pick disease type C. *J Neuropathol Exp Neurol*, 71, 434-48.
- STORCH, J. & XU, Z. 2009. Niemann-Pick C2 (NPC2) and intracellular cholesterol trafficking. *Biochim Biophys Acta*, 1791, 671-8.
- STRECK, C. J., DICKSON, P. V., NG, C. Y., ZHOU, J., HALL, M. M., GRAY, J. T., NATHWANI, A. C. & DAVIDOFF, A. M. 2006. Antitumor efficacy of AAV-mediated systemic delivery of interferon-beta. *Cancer Gene Ther*, 13, 99-106.
- STROES, E. S., NIERMAN, M. C., MEULENBERG, J. J., FRANSSSEN, R., TWISK, J., HENNY, C. P., MAAS, M. M., ZWINDERMAN, A. H., ROSS, C., ARONICA, E., HIGH, K. A., LEVI, M. M., HAYDEN, M. R., KASTELEIN, J. J. & KUIVENHOVEN, J. A. 2008. Intramuscular administration of AAV1-lipoprotein lipase S447X lowers triglycerides in lipoprotein lipase-deficient patients. *Arterioscler Thromb Vasc Biol*, 28, 2303-4.
- STRUPP, M., TEUFEL, J., HABS, M., FEUERECKER, R., MUTH, C., VAN DE WARRENBURG, B. P., KLOPSTOCK, T. & FEIL, K. 2013. Effects of acetyl-DL-leucine in patients with cerebellar ataxia: a case series. *J Neurol*, 260, 2556-61.

- SUROSKY, R. T., URABE, M., GODWIN, S. G., MCQUISTON, S. A., KURTZMAN, G. J., OZAWA, K. & NATSOULIS, G. 1997. Adeno-associated virus Rep proteins target DNA sequences to a unique locus in the human genome. *J Virol*, 71, 7951-9.
- SYM, M., BASSON, M. & JOHNSON, C. 2000. A model for niemann-pick type C disease in the nematode *Caenorhabditis elegans*. *Curr Biol*, 10, 527-30.
- TAGALAKIS, A. D., GROSSE, S. M., MENG, Q. H., MUSTAPA, M. F., KWOK, A., SALEHI, S. E., TABOR, A. B., HAILES, H. C. & HART, S. L. 2011. Integrin-targeted nanocomplexes for tumour specific delivery and therapy by systemic administration. *Biomaterials*, 32, 1370-6.
- TANG, H., KUHEN, K. L. & WONG-STAAAL, F. 1999. Lentivirus replication and regulation. *Annu Rev Genet*, 33, 133-70.
- TARDIEU, M., ZERAH, M., HUSSON, B., DE BOURNONVILLE, S., DEIVA, K., ADAMSBAUM, C., VINCENT, F., HOCQUEMILLER, M., BROISSAND, C., FURLAN, V., BALLABIO, A., FRALDI, A., CRYSTAL, R. G., BAUGNON, T., ROUJEAU, T., HEARD, J. M. & DANOS, O. 2014. Intracerebral administration of adeno-associated viral vector serotype rh.10 carrying human SGSH and SUMF1 cDNAs in children with mucopolysaccharidosis type IIIA disease: results of a phase I/II trial. *Hum Gene Ther*, 25, 506-16.
- TE VRUCHTE, D., LLOYD-EVANS, E., VELDMAN, R. J., NEVILLE, D. C., DWEK, R. A., PLATT, F. M., VAN BLITTERSWIJK, W. J. & SILLENCE, D. J. 2004. Accumulation of glycosphingolipids in Niemann-Pick C disease disrupts endosomal transport. *J Biol Chem*, 279, 26167-75.
- TESSITORE, A., DEL, P. M. M., SANO, R., MA, Y., MANN, L., INGRASSIA, A., LAYWELL, E. D., STEINDLER, D. A., HENDERSHOT, L. M. & D'AZZO, A. 2004. GM1-ganglioside-mediated activation of the unfolded protein

response causes neuronal death in a neurodegenerative gangliosidosis. *Mol Cell*, 15, 753-66.

TIAN, J., XU, Z., SMITH, J. S., HOFHERR, S. E., BARRY, M. A. & BYRNES, A. P. 2009. Adenovirus activates complement by distinctly different mechanisms in vitro and in vivo: indirect complement activation by virions in vivo. *J Virol*, 83, 5648-58.

TJIONG, H. B., SENG, P. N., DEBUCH, H. & WIEDEMANN, H. R. 1973. Brain lipids of a case of juvenile Niemann-Pick disease. *J Neurochem*, 21, 1475-85.

TRAPANI, I., COLELLA, P., SOMMELLA, A., IODICE, C., CESI, G., DE SIMONE, S., MARROCCO, E., ROSSI, S., GIUNTI, M., PALFI, A., FARRAR, G. J., POLISHCHUK, R. & AURICCHIO, A. 2014. Effective delivery of large genes to the retina by dual AAV vectors. *EMBO Mol Med*, 6, 194-211.

VALENZANO, K. J., KHANNA, R., POWE, A. C., BOYD, R., LEE, G., FLANAGAN, J. J. & BENJAMIN, E. R. 2011. Identification and characterization of pharmacological chaperones to correct enzyme deficiencies in lysosomal storage disorders. *Assay Drug Dev Technol*, 9, 213-35.

VAN TIL, N. P., STOK, M., AERTS KAYA, F. S., DE WAARD, M. C., FARAHBAKHSIAN, E., VISSER, T. P., KROOS, M. A., JACOBS, E. H., WILLART, M. A., VAN DER WEGEN, P., SCHOLTE, B. J., LAMBRECHT, B. N., DUNCKER, D. J., VAN DER PLOEG, A. T., REUSER, A. J., VERSTEGEN, M. M. & WAGEMAKER, G. 2010. Lentiviral gene therapy of murine hematopoietic stem cells ameliorates the Pompe disease phenotype. *Blood*, 115, 5329-37.

VANCE, J. E. 2012. Dysregulation of cholesterol balance in the brain: contribution to neurodegenerative diseases. *Dis Model Mech*, 5, 746-55.

- VANCE, J. E. & KARTEN, B. 2014. Niemann-Pick C disease and mobilization of lysosomal cholesterol by cyclodextrin. *J Lipid Res*, 55, 1609-21.
- VANIER, M. T. 1983. Biochemical studies in Niemann-Pick disease. I. Major sphingolipids of liver and spleen. *Biochim Biophys Acta*, 750, 178-84.
- VANIER, M. T. 1999. Lipid changes in Niemann-Pick disease type C brain: personal experience and review of the literature. *Neurochem Res*, 24, 481-9.
- VANIER, M. T. 2010. Niemann-Pick disease type C. *Orphanet J Rare Dis*, 5, 16.
- VANIER, M. T. 2013. Niemann-Pick diseases. *Handb Clin Neurol*, 113, 1717-21.
- VANIER, M. T. 2015. Complex lipid trafficking in Niemann-Pick disease type C. *J Inherit Metab Dis*, 38, 187-99.
- VANIER, M. T., GISSEN, P., BAUER, P., COLL, M. J., BURLINA, A., HENDRIKSZ, C. J., LATOUR, P., GOIZET, C., WELFORD, R. W., MARQUARDT, T. & KOLB, S. A. 2016. Diagnostic tests for Niemann-Pick disease type C (NP-C): A critical review. *Mol Genet Metab*, 118, 244-54.
- VANIER, M. T. & LATOUR, P. 2015. Laboratory diagnosis of Niemann-Pick disease type C: the filipin staining test. *Methods Cell Biol*, 126, 357-75.
- VANIER, M. T., WENGER, D. A., COMLY, M. E., ROUSSON, R., BRADY, R. O. & PENTCHEV, P. G. 1988. Niemann-Pick disease group C: clinical variability and diagnosis based on defective cholesterol esterification. A collaborative study on 70 patients. *Clin Genet*, 33, 331-48.
- VARGAS, J., JR., GUSELLA, G. L., NAJFELD, V., KLOTMAN, M. E. & CARA, A. 2004. Novel integrase-defective lentiviral episomal vectors for gene transfer. *Hum Gene Ther*, 15, 361-72.

- VAZQUEZ, M. C., BALBOA, E., ALVAREZ, A. R. & ZANLUNGO, S. 2012. Oxidative stress: a pathogenic mechanism for Niemann-Pick type C disease. *Oxid Med Cell Longev*, 2012, 205713.
- VAZQUEZ, M. C., DEL POZO, T., ROBLEDO, F. A., CARRASCO, G., PAVEZ, L., OLIVARES, F., GONZALEZ, M. & ZANLUNGO, S. 2011. Alteration of gene expression profile in Niemann-Pick type C mice correlates with tissue damage and oxidative stress. *PLoS One*, 6, e28777.
- VICTOR, S., COULTER, J. B., BESLEY, G. T., ELLIS, I., DESNICK, R. J., SCHUCHMAN, E. H. & VELLODI, A. 2003. Niemann-Pick disease: sixteen-year follow-up of allogeneic bone marrow transplantation in a type B variant. *J Inherit Metab Dis*, 26, 775-85.
- VIITALA, J., CARLSSON, S. R., SIEBERT, P. D. & FUKUDA, M. 1988. Molecular cloning of cDNAs encoding lamp A, a human lysosomal membrane glycoprotein with apparent Mr approximately equal to 120,000. *Proc Natl Acad Sci U S A*, 85, 3743-7.
- VISIGALLI, I., DELAI, S., POLITI, L. S., DI DOMENICO, C., CERRI, F., MRAK, E., D'ISA, R., UNGARO, D., STOK, M., SANVITO, F., MARIANI, E., STASZEWSKY, L., GODI, C., RUSSO, I., CECERE, F., DEL CARRO, U., RUBINACCI, A., BRAMBILLA, R., QUATTRINI, A., DI NATALE, P., PONDER, K., NALDINI, L. & BIFFI, A. 2010. Gene therapy augments the efficacy of hematopoietic cell transplantation and fully corrects mucopolysaccharidosis type I phenotype in the mouse model. *Blood*, 116, 5130-9.
- VITE, C. H., BAGEL, J. H., SWAIN, G. P., PROCIUK, M., SIKORA, T. U., STEIN, V. M., O'DONNELL, P., RUANE, T., WARD, S., CROOKS, A., LI, S., MAULDIN, E., STELLAR, S., DE MEULDER, M., KAO, M. L., ORY, D. S., DAVIDSON, C., VANIER, M. T. & WALKLEY, S. U. 2015. Intracisternal cyclodextrin prevents cerebellar dysfunction and Purkinje cell death in feline Niemann-Pick type C1 disease. *Sci Transl Med*, 7, 276ra26.

- VITE, C. H., DING, W., BRYAN, C., O'DONNELL, P., CULLEN, K., ALEMAN, D., HASKINS, M. E. & VAN WINKLE, T. 2008. Clinical, electrophysiological, and serum biochemical measures of progressive neurological and hepatic dysfunction in feline Niemann-Pick type C disease. *Pediatr Res*, 64, 544-9.
- VITNER, E. B., PLATT, F. M. & FUTERMAN, A. H. 2010. Common and uncommon pathogenic cascades in lysosomal storage diseases. *J Biol Chem*, 285, 20423-7.
- VOIKAR, V., RAUVALA, H. & IKONEN, E. 2002. Cognitive deficit and development of motor impairment in a mouse model of Niemann-Pick type C disease. *Behav Brain Res*, 132, 1-10.
- WAKABAYASHI, T., SHIMADA, Y., AKIYAMA, K., HIGUCHI, T., FUKUDA, T., KOBAYASHI, H., ETO, Y., IDA, H. & OHASHI, T. 2015. Hematopoietic Stem Cell Gene Therapy Corrects Neuropathic Phenotype in Murine Model of Mucopolysaccharidosis Type II. *Hum Gene Ther*, 26, 357-66.
- WALKLEY, S. U. 1995. Pyramidal neurons with ectopic dendrites in storage diseases exhibit increased GM2 ganglioside immunoreactivity. *Neuroscience*, 68, 1027-35.
- WALKLEY, S. U. 2007. Pathogenic mechanisms in lysosomal disease: a reappraisal of the role of the lysosome. *Acta Paediatr*, 96, 26-32.
- WALKLEY, S. U., SIKORA, J., MICSENYI, M., DAVIDSON, C. & DOBRENIS, K. 2010. Lysosomal compromise and brain dysfunction: examining the role of neuroaxonal dystrophy. *Biochem Soc Trans*, 38, 1436-41.
- WALKLEY, S. U. & SUZUKI, K. 2004. Consequences of NPC1 and NPC2 loss of function in mammalian neurons. *Biochim Biophys Acta*, 1685, 48-62.

- WALKLEY, S. U. & VANIER, M. T. 2009. Secondary lipid accumulation in lysosomal disease. *Biochim Biophys Acta*, 1793, 726-36.
- WALTERFANG, M., CHIEN, Y. H., IMRIE, J., RUSHTON, D., SCHUBIGER, D. & PATTERSON, M. C. 2012. Dysphagia as a risk factor for mortality in Niemann-Pick disease type C: systematic literature review and evidence from studies with miglustat. *Orphanet J Rare Dis*, 7, 76.
- WALTERFANG, M., PATENAUDE, B., ABEL, L. A., KLUENEMANN, H., BOWMAN, E. A., FAHEY, M. C., DESMOND, P., KELSO, W. & VELAKOULIS, D. 2013. Subcortical volumetric reductions in adult Niemann-Pick disease type C: a cross-sectional study. *AJNR Am J Neuroradiol*, 34, 1334-40.
- WANG, C., LIU, F., LIU, Y. Y., ZHAO, C. H., YOU, Y., WANG, L., ZHANG, J., WEI, B., MA, T., ZHANG, Q., ZHANG, Y., CHEN, R., SONG, H. & YANG, Z. 2011. Identification and characterization of neuroblasts in the subventricular zone and rostral migratory stream of the adult human brain. *Cell Res*, 21, 1534-50.
- WARD, S., O'DONNELL, P., FERNANDEZ, S. & VITE, C. H. 2010. 2-hydroxypropyl-beta-cyclodextrin raises hearing threshold in normal cats and in cats with Niemann-Pick type C disease. *Pediatr Res*, 68, 52-6.
- WASSERSTEIN, M. P., JONES, S. A., SORAN, H., DIAZ, G. A., LIPPA, N., THURBERG, B. L., CULM-MERDEK, K., SHAMIYEH, E., INGUILIZIAN, H., COX, G. F. & PUGA, A. C. 2015. Successful within-patient dose escalation of olipudase alfa in acid sphingomyelinase deficiency. *Mol Genet Metab*, 116, 88-97.
- WASSERSTEIN, M. P. & SCHUCHMAN, E. H. 1993. Acid Sphingomyelinase Deficiency. *In*: PAGON, R. A., ADAM, M. P., ARDINGER, H. H., WALLACE, S. E., AMEMIYA, A., BEAN, L. J. H., BIRD, T. D., FONG, C.

- T., MEFFORD, H. C., SMITH, R. J. H. & STEPHENS, K. (eds.) *GeneReviews(R)*. Seattle (WA).
- WASSERSTEIN, M. P. & SCHUCHMAN, E. H. 2015. Acid Sphingomyelinase Deficiency. *In*: PAGON, R. A., ADAM, M. P., ARDINGER, H. H., WALLACE, S. E., AMEMIYA, A., BEAN, L. J. H., BIRD, T. D., FONG, C. T., MEFFORD, H. C., SMITH, R. J. H. & STEPHENS, K. (eds.) *GeneReviews(R)*. Seattle (WA).
- WASSIF, C. A., CROSS, J. L., IBEN, J., SANCHEZ-PULIDO, L., COUGNOUX, A., PLATT, F. M., ORY, D. S., PONTING, C. P., BAILEY-WILSON, J. E., BIESECKER, L. G. & PORTER, F. D. 2016. High incidence of unrecognized visceral/neurological late-onset Niemann-Pick disease, type C1, predicted by analysis of massively parallel sequencing data sets. *Genet Med*, 18, 41-8.
- WATARI, H., BLANCHETTE-MACKIE, E. J., DWYER, N. K., WATARI, M., NEUFELD, E. B., PATEL, S., PENTCHEV, P. G. & STRAUSS, J. F., 3RD 1999. Mutations in the leucine zipper motif and sterol-sensing domain inactivate the Niemann-Pick C1 glycoprotein. *J Biol Chem*, 274, 21861-6.
- WATSON, G., BASTACKY, J., BELICHENKO, P., BUDDHIKOT, M., JUNGLES, S., VELLARD, M., MOBLEY, W. C. & KAKKIS, E. 2006. Intrathecal administration of AAV vectors for the treatment of lysosomal storage in the brains of MPS I mice. *Gene Ther*, 13, 917-25.
- WEITZMAN, M. D. & LINDEN, R. M. 2011. Adeno-associated virus biology. *Methods Mol Biol*, 807, 1-23.
- WELFORD, R. W., GARZOTTI, M., MARQUES LOURENCO, C., MENGEL, E., MARQUARDT, T., REUNERT, J., AMRAOUI, Y., KOLB, S. A., MORAND, O. & GROENEN, P. 2014. Plasma lysosphingomyelin demonstrates great potential as a diagnostic biomarker for Niemann-Pick disease type C in a retrospective study. *PLoS One*, 9, e114669.

- WENGER, D. A., BARTH, G. & GITHENS, J. H. 1977. Nine cases of sphingomyelin lipidosis, a new variant in Spanish-American Children. Juvenile variant of Niemann-Pick Disease with foamy and sea-blue histiocytes. *Am J Dis Child*, 131, 955-61.
- WEST, M. J., SLOMIANKA, L. & GUNDERSEN, H. J. 1991. Unbiased stereological estimation of the total number of neurons in the subdivisions of the rat hippocampus using the optical fractionator. *Anat Rec*, 231, 482-97.
- WHITE, J. D., THESIER, D. M., SWAIN, J. B., KATZ, M. G., TOMASULO, C., HENDERSON, A., WANG, L., YARNALL, C., FARGNOLI, A., SUMAROKA, M., ISIDRO, A., PETROV, M., HOLT, D., NOLEN-WALSTON, R., KOCH, W. J., STEDMAN, H. H., RABINOWITZ, J. & BRIDGES, C. R. 2011. Myocardial gene delivery using molecular cardiac surgery with recombinant adeno-associated virus vectors in vivo. *Gene Ther*, 18, 546-52.
- WHITNEY, E. R., KEMPER, T. L., ROSENE, D. L., BAUMAN, M. L. & BLATT, G. J. 2008. Calbindin-D28k is a more reliable marker of human Purkinje cells than standard Nissl stains: a stereological experiment. *J Neurosci Methods*, 168, 42-7.
- WIJBURG, F. A., SEDEL, F., PINEDA, M., HENDRIKSZ, C. J., FAHEY, M., WALTERFANG, M., PATTERSON, M. C., WRAITH, J. E. & KOLB, S. A. 2012. Development of a suspicion index to aid diagnosis of Niemann-Pick disease type C. *Neurology*, 78, 1560-7.
- WILLIAMS, I. M., WALLOM, K. L., SMITH, D. A., AL EISA, N., SMITH, C. & PLATT, F. M. 2014. Improved neuroprotection using miglustat, curcumin and ibuprofen as a triple combination therapy in Niemann-Pick disease type C1 mice. *Neurobiol Dis*, 67, 9-17.
- WIRTH, T., PARKER, N. & YLA-HERTTUALA, S. 2013. History of gene therapy. *Gene*, 525, 162-9.

- WORGALL, S., SONDHI, D., HACKETT, N. R., KOSOFSKY, B., KEKATPURE, M. V., NEYZI, N., DYKE, J. P., BALLON, D., HEIER, L., GREENWALD, B. M., CHRISTOS, P., MAZUMDAR, M., SOUWEIDANE, M. M., KAPLITT, M. G. & CRYSTAL, R. G. 2008. Treatment of late infantile neuronal ceroid lipofuscinosis by CNS administration of a serotype 2 adeno-associated virus expressing CLN2 cDNA. *Hum Gene Ther*, 19, 463-74.
- WOS, M., SZCZEPANOWSKA, J., PIKULA, S., TYLKI-SZYMANSKA, A., ZABLOCKI, K. & BANDOROWICZ-PIKULA, J. 2016. Mitochondrial dysfunction in fibroblasts derived from patients with Niemann-Pick type C disease. *Arch Biochem Biophys*, 593, 50-9.
- WRAITH, J. E. 2002. Lysosomal disorders. *Semin Neonatol*, 7, 75-83.
- WRAITH, J. E., SEDEL, F., PINEDA, M., WIJBURG, F. A., HENDRIKSZ, C. J., FAHEY, M., WALTERFANG, M., PATTERSON, M. C., CHADHA-BOREHAM, H. & KOLB, S. A. 2014. Niemann-Pick type C Suspicion Index tool: analyses by age and association of manifestations. *J Inherit Metab Dis*, 37, 93-101.
- WRAITH, J. E., VECCHIO, D., JACKLIN, E., ABEL, L., CHADHA-BOREHAM, H., LUZY, C., GIORGINO, R. & PATTERSON, M. C. 2010. Miglustat in adult and juvenile patients with Niemann-Pick disease type C: long-term data from a clinical trial. *Mol Genet Metab*, 99, 351-7.
- WU, Y. P., MIZUKAMI, H., MATSUDA, J., SAITO, Y., PROIA, R. L. & SUZUKI, K. 2005. Apoptosis accompanied by up-regulation of TNF-alpha death pathway genes in the brain of Niemann-Pick type C disease. *Mol Genet Metab*, 84, 9-17.
- WU, Z., YANG, H. & COLOSI, P. 2010. Effect of genome size on AAV vector packaging. *Mol Ther*, 18, 80-6.

- WYATT, K., HENLEY, W., ANDERSON, L., ANDERSON, R., NIKOLAOU, V., STEIN, K., KLINGER, L., HUGHES, D., WALDEK, S., LACHMANN, R., MEHTA, A., VELLODI, A. & LOGAN, S. 2012. The effectiveness and cost-effectiveness of enzyme and substrate replacement therapies: a longitudinal cohort study of people with lysosomal storage disorders. *Health Technol Assess*, 16, 1-543.
- XIE, C., GONG, X. M., LUO, J., LI, B. L. & SONG, B. L. 2017. Intracardiac injection of AAV9-NPC1 significantly ameliorates Purkinje cell death and behavioral abnormalities in mouse Niemann-Pick type C disease. *J Lipid Res*.
- XIE, Z. & KLIONSKY, D. J. 2007. Autophagosome formation: core machinery and adaptations. *Nat Cell Biol*, 9, 1102-9.
- XU, S., BENOFF, B., LIOU, H. L., LOBEL, P. & STOCK, A. M. 2007. Structural basis of sterol binding by NPC2, a lysosomal protein deficient in Niemann-Pick type C2 disease. *J Biol Chem*, 282, 23525-31.
- YANEZ-MUNOZ, R. J., BALAGGAN, K. S., MACNEIL, A., HOWE, S. J., SCHMIDT, M., SMITH, A. J., BUCH, P., MACLAREN, R. E., ANDERSON, P. N., BARKER, S. E., DURAN, Y., BARTHOLOMAE, C., VON KALLE, C., HECKENLIVELY, J. R., KINNON, C., ALI, R. R. & THRASHER, A. J. 2006. Effective gene therapy with nonintegrating lentiviral vectors. *Nat Med*, 12, 348-53.
- YANG, Y., JOOSS, K. U., SU, Q., ERTL, H. C. & WILSON, J. M. 1996. Immune responses to viral antigens versus transgene product in the elimination of recombinant adenovirus-infected hepatocytes in vivo. *Gene Ther*, 3, 137-44.
- YU, T., SHAKKOTTAI, V. G., CHUNG, C. & LIEBERMAN, A. P. 2011. Temporal and cell-specific deletion establishes that neuronal Npc1 deficiency is sufficient to mediate neurodegeneration. *Hum Mol Genet*, 20, 4440-51.

- YU, W., GONG, J. S., KO, M., GARVER, W. S., YANAGISAWA, K. & MICHIKAWA, M. 2005. Altered cholesterol metabolism in Niemann-Pick type C1 mouse brains affects mitochondrial function. *J Biol Chem*, 280, 11731-9.
- ZAISS, A. K., LIU, Q., BOWEN, G. P., WONG, N. C., BARTLETT, J. S. & MURUVE, D. A. 2002. Differential activation of innate immune responses by adenovirus and adeno-associated virus vectors. *J Virol*, 76, 4580-90.
- ZERVAS, M., DOBRENIS, K. & WALKLEY, S. U. 2001a. Neurons in Niemann-Pick disease type C accumulate gangliosides as well as unesterified cholesterol and undergo dendritic and axonal alterations. *J Neuropathol Exp Neurol*, 60, 49-64.
- ZERVAS, M., SOMERS, K. L., THRALL, M. A. & WALKLEY, S. U. 2001b. Critical role for glycosphingolipids in Niemann-Pick disease type C. *Curr Biol*, 11, 1283-7.
- ZHANG, H., YANG, B., MU, X., AHMED, S. S., SU, Q., HE, R., WANG, H., MUELLER, C., SENA-ESTEVEZ, M., BROWN, R., XU, Z. & GAO, G. 2011. Several rAAV vectors efficiently cross the blood-brain barrier and transduce neurons and astrocytes in the neonatal mouse central nervous system. *Mol Ther*, 19, 1440-8.
- ZHANG, J. & LIU, Q. 2015. Cholesterol metabolism and homeostasis in the brain. *Protein Cell*, 6, 254-64.
- ZIEGLER, R. J., LONNING, S. M., ARMENTANO, D., LI, C., SOUZA, D. W., CHERRY, M., FORD, C., BARBON, C. M., DESNICK, R. J., GAO, G., WILSON, J. M., PELUSO, R., GODWIN, S., CARTER, B. J., GREGORY, R. J., WADSWORTH, S. C. & CHENG, S. H. 2004. AAV2 vector harboring a liver-restricted promoter facilitates sustained expression of therapeutic levels of alpha-galactosidase A and the induction of immune tolerance in Fabry mice. *Mol Ther*, 9, 231-40.

ZUFFEREY, R., DONELLO, J. E., TRONO, D. & HOPE, T. J. 1999. Woodchuck hepatitis virus posttranscriptional regulatory element enhances expression of transgenes delivered by retroviral vectors. *J Virol*, 73, 2886-92.

ZUFFEREY, R., DULL, T., MANDEL, R. J., BUKOVSKY, A., QUIROZ, D., NALDINI, L. & TRONO, D. 1998. Self-inactivating lentivirus vector for safe and efficient in vivo gene delivery. *J Virol*, 72, 9873-80.